Modeling and Simulation in Science,
Engineering and Technology

Livio Gibelli
Editor

Crowd Dynamics, Volume 2

Theory, Models, and Applications

Birkhäuser

Modeling and Simulation in Science, Engineering and Technology

More information about this series at http://www.springer.com/series/4960

Livio Gibelli
Editor

Crowd Dynamics, Volume 2

Theory, Models, and Applications

Birkhäuser

Editor
Livio Gibelli
Institute for Multiscale Thermofluids
University of Edinburgh
Edinburgh, UK

ISSN 2164-3679 ISSN 2164-3725 (electronic)
Modeling and Simulation in Science, Engineering and Technology
ISBN 978-3-030-50449-6 ISBN 978-3-030-50450-2 (eBook)
https://doi.org/10.1007/978-3-030-50450-2

Mathematics Subject Classification: 34H05, 35Q93, 90B20, 91B99, 93A30

This book is published under the imprint Birkäuser, www.birkhauser-science.com by the registered company Springer Nature Switzerland AG
The registered company address is: Gewerbestrasse 11, 6330 Cham, Switzerland

Preface

The study of human crowds is a challenging interdisciplinary field, which combines ideas and techniques from different disciplines, ranging from mathematics and physics to informatics and psychology.

This area of research has attracted enormous attention in recent years not only for its theoretical interest but also for its potential societal benefits. Indeed, computational models of crowd movement can lead to more efficient transportation planning, a key driver of sustainability, thus reducing the cost of transportation and pollution and improving the population's quality of life.

Another timely application, motivated by the recent outbreak of Covid-19, is about controlling the spread of contagious diseases. This target may be achieved by coupling a contagion model with simulations of human crowds that take into account the change of the pedestrians' behaviour due to social distancing measures.

This book is the second of a series, which aims at presenting the state of the art, challenges, and future research perspectives in the area of modeling and simulation of human crowds as well as at providing practical guidelines for crowd management. The topics are covered from different perspectives, thus providing a comprehensive overview on the works carried out in this challenging research area.

The present edited book comprises nine chapters with contributions from leading experts in the field. The focus is on three main areas, namely pedestrian interactions, multiscale modeling, and dynamics in complex environments. Chapter 1 is an introductory chapter, which highlights insights presented in the following chapters and gives an overview of the book.

While this edited book does not cover all the possible topics, it leads the reader to a deeper understanding of pedestrians, dynamics and to envisioning the future research directions. A forthcoming *Crowd Dynamics* Volume 3 will continue chasing the new trends in this area.

Edinburgh, UK
September 2018

Livio Gibelli

Contents

Behavioral Human Crowds

Nicola Bellomo, Livio Gibelli, and Damian Knopoff

Abstract This chapter provides an introduction to the contents of Gibelli (in Crowd Dynamics, Volume 2—Theory, Models, and Safety Problems. Modeling and Simulation in Science, Engineering, and Technology, Birkhäuser, New York, 2020) and a general critical analysis on modeling, simulation, and control of human crowds with emphasis on research perspectives. The contents are organized in three parts: firstly, three key topics are stated which will be probably the focus of future research; Subsequently, the contents of Chaps. "Artificial Neural Networks for the Estimation of Pedestrian Interaction Forces–Mixed Traffic Simulation of Cars and Pedestrians for Transportation Policy Assessment" are summarized by setting them in the context of the aforementioned key research topics; finally, some promising research directions are presented and discussed.

1 Plan of the Chapter

The study of human crowds is a challenging interdisciplinary research field which requires contributions from different disciplines, ranging from technology, which is needed to detect the main features of crowds, to mathematics and computational sciences, which allow one to derive models of crowds and to simulate their dynamics, respectively.

N. Bellomo
University of Granada, Granada, Spain
IMATI CNR, Pavia, Italy
e-mail: bellomo@imati.cnr.it

L. Gibelli (✉)
School of Engineering, University of Edinburgh, Edinburgh, UK
e-mail: livio.gibelli@ed.ac.uk

D. A. Knopoff
University of Cordoba and CONICET, Cordoba, Argentina
e-mail: damian.knopoff@unc.edu.ar

L. Gibelli (ed.), *Crowd Dynamics, Volume 2*, Modeling and Simulation in Science, Engineering and Technology, https://doi.org/10.1007/978-3-030-50450-2_1

Human psychology can also significantly contribute to crowd modeling, especially if one attempts to capture the pedestrian's behavior in crisis situations, like a rapid evacuation due to incidents or when the crowd includes groups of activists that confront with each other [23]. In all these applications, the pedestrian's dynamics is strongly influenced by social interactions [1, 22, 29] which contribute to spread out unusual behaviors through the crowd.

This area of research has attracted enormous attention in recent years not only for its theoretical interest but also for the potential societal benefits. As an example, computational models of crowd movement can lead to more efficient transportation planning, a key driver of sustainability, thus reducing the cost of transportation, pollution, and improving the population's quality of life. Furthermore, these tools can contribute to city security and safety in that pedestrians/vehicles may be used as sensors to identify threats that compromise the safety of persons and infrastructures (e.g. in natural disasters or acts of terrorism).

This introductory chapter presents an overview of the edited book [25] which addresses various aspects of modeling, simulations, and control of the dynamics of human crowds. A key reference is Volume 1 which provided important contributions on the same research areas [26].

We start by briefly presenting three key topics which will probably form the focus of future research. These topics are selected according to our own bias and, although they do not encompass all the current open problems, their discussion paves the way to a deeper understanding of the contents of this edited book and it may help in foreseeing the future directions in this challenging research field.

Key Topic 1: *As all systems of self-propelled particles, the collective motion of human crowds is driven by interactions at the microscopic scale. The modeling should account for behavioral walking strategy of pedestrians which, in turn, has its roots in pedestrians' psychology. The nonlocality and nonlinear nature of interactions between pedestrians cannot be overlooked.*

Key Topic 2: *Pedestrians generally move in complex environments constituted by a network of interconnected areas, each of them with different geometrical features. The study of crowd dynamics should account for this complexity so as to provide tools which may support urban planners and crisis managers in dealing with problems of practical interest.*

Key Topic 3: *Crowd dynamics is usually studied by means of individual based models, kinetic models, and hydrodynamic models. Accordingly, the focus is either on the behavior of single pedestrian, on the crowd as a whole, or a combination of the two. However, the modeling approach should account for the multiscale features inherent in the dynamics of crowds rather than being limited to a specific scale of description.*

The rest of the chapter is organized as follows:

Section 2 outlines the contents of Chapters 2–9 of [25], setting them in the context of the key research challenges presented in this section.

Section 3 proposes some perspective reasoning on the research activity that should be carried out to make seminal contributions in this challenging research field.

2 On the Contents of the Edited Book

The contents of the edited book [25] deal with front-edge research topics in the modeling, simulation, and control of crowd dynamics. Although they bring important contributions to this research field, many problems are still left open, as we will discuss in the last section.

The next chapters cover a broad range of areas (i.e. from mathematics to engineering and psychology) but we can roughly group them based on which *Key Topic* they mainly contribute to. A graphical index is shown in Fig. 1.

The contributions to *Key Topic 1* are Chaps. "Artificial Neural Networks for the Estimation of Pedestrian Interaction Forces, High-Statistics Modeling of Complex Pedestrian Avoidance Scenarios, and Modeling Collective Behavior: Insights and Applications from Crowd Psychology."

Chapter "Artificial Neural Networks for the Estimation of Pedestrian Interaction Forces" [28] shows how artificial neural networks can be used to fit the unknown interaction forces between pedestrians who enter in the celebrated social force model [31]. The artificial neural network is trained simultaneously with other parameters arising in the model by using a tailored cost function and stochastic gradient techniques. The approach is tested by using real data sets for the unidirectional and bidirectional flow in corridors. The potential applications involve the management of emergency situations [30, 32].

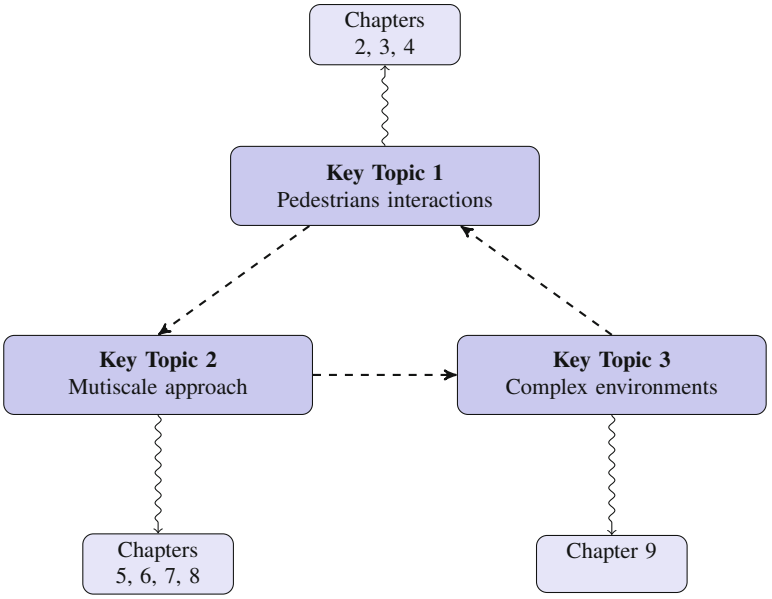

Fig. 1 Graphical index of the edited book

Chapter "High-Statistics Modeling of Complex Pedestrian Avoidance Scenarios" [21] aims at providing a detailed description of interactions between pedestrians. The main focus is the quantitative modeling of the dynamics of a single pedestrian in a way which is deeply connected with the physics of flowing active matter, see also [20]. The authors enlighten the statistical features of the pedestrian's trajectories as given by high-statistics pedestrian dynamics measurements collected in real-life conditions. The study is both on the undisturbed motion, namely in the absence of interactions with other pedestrians, and on the avoidance dynamics triggered by a pedestrian incoming in the opposite direction. This kind of investigation can contribute to get a more fundamental understanding of the self-organization ability of crowds, e.g. lanes of uniform walking direction in pedestrians counter flows [9, 27].

Chapter "Modeling Collective Behavior: Insights and Applications from Crowd Psychology" [37] discusses how preestablished and emerging social identities can affect the pedestrian behavior in crowds. This is a key process which occurs in a broad variety of circumstances, e.g. the commuters on a train which breaks down, the pedestrians in an emergency evacuation, and so forth. In all these cases, people start seeing each other as sharing the same fate and identity and modify their walking strategy accordingly. This study contributes to understand which psychological features of pedestrians should be included into the mathematical modeling of crowd dynamics. A similar investigation has been carried out in [34].

The contributions to *Key Topic 2* are Chaps. "Crowd Dynamics through Conservation Laws, The Fokker–Planck Framework in the Modeling of Pedestrians' Motion, Recent Developments in Controlled Crowd Dynamics, and Mathematical Models and Methods for Crowd Dynamics Control."

Chapter "Crowd Dynamics through Conservation Laws" [18] develops a sharp qualitative analysis of a variety of crowd dynamics models with nonlocal terms. These terms are obtained by convolutions with smooth functions and are deemed to reproduce the visual horizon of each pedestrian. Models are classified according to the physical domain, to the terms affected by the nonlocal operators, and to the number of different populations composing the crowd.

Chapter "The Fokker–Planck Framework in the Modeling of Pedestrians' Motion" [15] deals with control problems in crowd dynamics models. In more detail, the chapter presents a modeling approach by stochastic drift-diffusion processes and the related Fokker–Planck equations. The predictive ability of these models is carefully studied and different control strategies are discussed. The dynamics of a single pedestrian subject to perturbations and collision avoidance maneuvers is studied based on the formulation of a Fokker–Planck Nash game. In addition, a critical analysis on the mean-field approach to crowd motion is proposed providing pointers to relevant models.

Chapter "Recent Developments in Controlled Crowd Dynamics" [7] provides a survey of recent results on the theory and applications of sparse control methods to many fields, ranging from crowd dynamics to opinion formation and wealth models. The challenges and approaches in mean-field/hydrodynamic limits are also

discussed. The techniques are applied to an elementary particle model to illustrate the basic methods but the extension to nonlinear models is also briefly addressed.

Chapter "Mathematical Models and Methods for Crowd Dynamics Control" [3] presents a detailed analysis of two specific control strategies: The first strategy refers to the use of special agents, called leaders, to steer the crowd toward the desired direction. This strategy relies on the strength of the social influence (herding effect), namely the natural tendency of people to follow group mates in situations of emergency or doubt. The second strategy consists in modifying the walking area by adding obstacles optimally shaped and placed. The mathematical models are discussed at different observation and modeling scales within a general multiscale framework.

The contributions to *Key Topic 3* are Chap. "Mixed Traffic Simulation of Cars and Pedestrians for Transportation Policy Assessment."

Chapter "Mixed Traffic Simulation of Cars and Pedestrians for Transportation Policy Assessment" [24] sets out a new vision of the simulation of mixed traffic consisting of cars, trams, and pedestrians, as a practical tool to assess different transportation policies. A major issue is the modeling of interactions between heterogeneous agents and the capability to fully capture the geometrical complexity of the network where the dynamics is studied. In this chapter, the empirical data and mathematical models are combined to develop a simulator which turns out to be an important tool for urban planners.

3 A Forward Look to Research Perspectives

The topics presented in the chapters of this edited book stimulate to a forward look at some research perspectives in the area of crowd modeling and simulations. The emerging idea is that the future research activity will be addressed, more and more, to provide practical tools which may bring benefits to our society. More specifically, computational models should be developed within a systems approach to contribute either to optimize the overall flow of vehicles over networks of roads in cities or to help crisis managers in dealing with safety problems such as emergency evacuations, in complex situations like the one depicted in Fig. 2.

Accordingly, future research programs should tackle the key topics listed in Sect. 1 as a whole, rather than viewing them as objectives to be achieved independently one from the other. In addition, it is worth stressing that the aforementioned topics generate challenging analytic and computational problems which definitely deserve attention and may stimulate fundamental research activity as well.

Bearing all the above in mind, the following thoughts are brought to the reader's attention along with some bibliographic indications.

Detailed Modeling of Pedestrians Interactions The derivation of models consistent with the objectives of the aforementioned systems approach requires fundamental understanding of the dynamics of interactions whose modeling at different scales

Fig. 2 Snapshot of pedestrians and vehicles along a congested road

should follow the same principles [5]. This is closely related to *Key Topic 2* and *Key Topic 3*.

The modeling approach should preliminary group the interacting entities in different populations, characterizing their heterogeneity and interaction rules. As an example, this strategy has been proposed in [5] for a crowd in a domain with boundaries, internal obstacles, and inlet–outlet doors. However, it is worth stressing that a more comprehensive modeling approach requires to also account for the heterogeneity of the walking areas as well as, more in general, the complex dynamics studied in [24].

Note that the modeling approach must fulfill two important additional requirements, especially with respect to the management of crisis situations. Firstly, the computational effort required for numerically solving the model should be kept as small as possible since the real-time simulations of the crowd are needed. Secondly, one should account for emotional states which can drive the crowd far from rational behaviors as those studied in [6, 35]. An interesting approach to propagation of stress by contagion has been proposed in [11, 39], while the development in [13] derives models from the study of interactions at the individual based scale corresponding to consensus dynamics. These papers have shown how flow patterns are modified by the propagation of stress. These pioneer studies on the spreading of emotional states prompt to further investigations, which might also be related to control problems [2].

Multiscale Approach to Crowd Dynamics The modeling of pedestrians crowds needs a multiscale approach since a single observation and representation scale

cannot fully capture the collective dynamics of living systems. Indeed, the dynamics at the microscopic scale defines the conceptual basis toward the derivation of models at the mesoscopic scale. In turn, the hydrodynamic models, corresponding to observable macroscopic quantities, can be obtained from kinetic models by letting the distance between individuals tend to zero.

A more general discussion has been elaborated in [5]. Therein, it is shown that models can be derived at each scale through common assumptions on the walking strategy and using the same parameters. The described approach includes the spreading of emotional states which is a recent contribution in the literature on crowd dynamics [13, 39]. Chapters "Modeling Collective Behavior: Insights and Applications from Crowd Psychology, Recent Developments in Controlled Crowd Dynamics, and Mathematical Models and Methods for Crowd Dynamics Control" provide a survey of results, where macroscopic models are derived from the underlying description at the microscale by local averaging tools and from kinetic models by mean-field averaging, see also [14, 16]. Perturbation methods in terms of a small parameter corresponding to the distance between walkers have been developed in [8], while a general methodology on the derivation of diffusion models has been proposed in [17] by a technique somehow inspired by the Hilbert sixth problem [33].

However, it is plain that this research topic is only at an initial stage and further activity has to be carried out to account for the broad variety of the dynamics of emotional states as well as for the system heterogeneity.

A System Approach to Crowd Dynamics The chapter [24] has proposed an attractive approach to modeling the dynamics of heterogeneous agents, from pedestrians to vehicles moving over networks in large cities. The same modeling approach may be developed for dealing with emergency evacuation from environments described as complex networks whose branches have specific features. As an example, the heterogeneity of walking areas should be fully taken into account [19, 36].

The adoption of this systems approach is fundamental for designing a simulation platform to support urban planners and/or crisis managers. Such a platform may offer a virtual and augmented-reality environment which permits one to optimize the flow of vehicles in road networks, improve the management of safety problems and/or the design of buildings [38]. Furthermore, crisis managers can be trained by allowing them to explore different scenarios triggered by the possible actions that can be taken in emergency conditions. Some perspective ideas are proposed in [12] toward the development of machine learning devices to select optimal safety actions based on the sharp analysis of a database repository of a large number of simulations corresponding to different external actions.

Finally, let us mention that the derivation and application of the models pose challenging analytic problems. These include:

(i) Qualitative analysis, namely existence and regularity of solutions of initial-boundary value problems;

(ii) Asymptotic analysis toward the derivation of models at the higher scale from the underlying description at the lower scale;
(iii) Development of suitable computational methods, as models at different scales have different differential structures, which requires a specific numerical treatment.

Chapter "High-Statistics Modeling of Complex Pedestrian Avoidance Scenarios" [18] provides, as an example of the topic mentioned in (i), a sharp study of models at the macroscopic scale. This topic has already been treated in the contributions included in [26], in particular [4] and [35], for models at the macroscopic scale, while a qualitative analysis of kinetic theory models has been developed in [10]. However, the preceding sections have enlightened how the complexity of models has been rapidly increasing to refer to urban environments and complex venues in general. The above literature refers to models at the macroscopic scale, while less studied is the case of kinetic type models [10].

The multiscale vision for modeling crowd dynamics has already generated problems, presenting challenging analytic difficulties, examples are [3, 8, 16]. The hint of [5] suggests to develop models at each scale according to the same principles and using the same parameters. This rationale has been applied to some specific models, see, for instance, [3, 8], while the development of a multiscale vision for a dynamics over complex networks remains a challenging open problem.

References

1. G. Ajmone Marsan, N. Bellomo, L. Gibelli, Stochastic evolutionary differential games toward a systems theory of behavioral social dynamics. Math. Models Methods Appl. Sci. **26**, 1051–1093 (2016)
2. G. Albi, M. Bongini, E. Cristiano, D. Kalise, Invisible control of self-organizing agents leaving unknown environments. SIAM J. Appl. Math. **76**(4), 1683–1710 (2016)
3. G. Albi, E. Cristiani, L. Pareschi, D. Peri, Mathematical models and methods for crowd dynamics control, in *Crowd Dynamics, Volume 2 - Theory, Models, and Safety Problems*. Modeling and Simulation in Science, Engineering, and Technology, chap. 8 (Birkhäuser, New York, 2020)
4. B. Andreianov, C. Donatello, U. Razafison, M. D. Rosini, One-dimensional conservation laws with nonlocal point constraints on the flux, in *Crowd Dynamics, Volume 2 - Theory, Models, and Safety Problems*. Modeling and Simulation in Science, Engineering, and Technology (Birkhäuser, New York, 2018), pp. 103–135
5. B. Aylaj, N. Bellomo, L. Gibelli, A. Reali, On a unified multiscale vision of behavioral crowds. Math. Models Methods Appl. Sci. **30**(1), 1–22 (2020)
6. R. Bailo, J.A. Carrillo, P. Degond, Pedestrian models based on rational behaviour, in *Crowd Dynamics, Volume 1 - Theory, Models, and Safety Problems*. Modeling and Simulation in Science, Engineering, and Technology (Birkhäuser, New York, 2018)
7. M.K. Banda, M. Herty, T. Trimborn, Recent developments in controlled crowd dynamics, in *Crowd Dynamics, Volume 2 - Theory, Models, and Safety Problems*. Modeling and Simulation in Science, Engineering, and Technology, chap. 7 (Birkhäuser, New York, 2020)
8. N. Bellomo, A. Bellouquid, On multiscale models of pedestrian crowds from mesoscopic to macroscopic. Commun. Math. Sci. **13**(7), 1649–1664 (2015)

9. N. Bellomo, L. Gibelli, Toward a mathematical theory of behavioral-social dynamics for pedestrian crowds. Math. Models Methods Appl. Sci. **25**(13), 2417–2437 (2015).
10. N. Bellomo, A. Bellouquid, D. Knopoff, From the micro-scale to collective crowd dynamics. Multiscale Model. Simul. **11**, 943–963 (2013)
11. A.L. Bertozzi, J. Rosado, M.B. Short, L. Wang, Contagion shocks in one dimension. J. Stat. Phys. **158**, 647–664 (2015)
12. N. Bellomo, D. Clarke, L. Gibelli, P. Townsend, B.J. Vreugdenhil, Human behaviours in evacuation crowd dynamics: from modeling to "big data" toward crisis management. Phys. Life Rev. **18**, 1–21 (2016)
13. N. Bellomo, L. Gibelli, N. Outada, On the interplay between behavioral dynamics and social interactions in human crowds. Kinetic Relat. Models **12**, 397–409 (2019)
14. R. Borsche, A. Klar, F. Schneider, Numerical methods for mean-field and moment models for pedestrian flow, in *Crowd Dynamics, Volume 1 - Theory, Models, and Safety Problems*. Modeling and Simulation in Science, Engineering, and Technology, chap. 7 (Birkhäuser, New York, 2018)
15. A. Borzì The Fokker-Planck framework in the modeling of pedestrians' motion, in *Crowd Dynamics, Volume 2 - Theory, Models, and Safety Problems*. Modeling and Simulation in Science, Engineering, and Technology, chap. 6 (Birkhäuser, New York, 2020)
16. M. Burger, P. Markowich, J.F. Pietschmann, Continuous limit of a crowd motion and herding model: analysis and numerical simulations. Kinetic Relat. Models **4**(4), 1025–1047 (2011)
17. D. Burini, N. Chouhad, Hilbert method toward a multiscale analysis from kinetic to macroscopic models for active particles. Math. Models Methods Appl. Sci. **27**, 1327–1353 (2017)
18. R.M. Colombo, M. Lecureux–Mercier, M. Garavello, Crowd dynamics through conservation laws, in *Crowd Dynamics, Volume 2 - Theory, Models, and Safety Problems*. Modeling and Simulation in Science, Engineering, and Technology, chap. 9 (Birkhäuser, New York, 2020)
19. M. Colangeli, A. Muntean, O. Richardson, T. Thieu, Modeling interactions between active and passive agents moving through heterogeneous environments, in *Crowd Dynamics, Volume 1 - Theory, Models, and Safety Problems*. Modeling and Simulation in Science, Engineering, and Technology (Birkhäuser, New York, 2018), pp. 211–258
20. A. Corbetta, A. Mountean, K. Vafayi, Parameter estimation of social forces in pedestrian dynamics models via probabilistic method. Math. Biosci. Eng. **12**, 337–356 (2015)
21. A. Corbetta, L. Schilders, F. Toschi, High-statistics modeling of complex pedestrian avoidance scenarios, in *Crowd Dynamics, Volume 2 - Theory, Models, and Safety Problems*. Modeling and Simulation in Science, Engineering, and Technology, chap. 4 (Birkhäuser, New York, 2018)
22. E. Cristiani, F.S. Priuli, A. Tosin, Modeling rationality to control self-organization of crowds: an environmental approach. SIAM J. Appl. Math. **75**(2), 605–629 (2015)
23. J.-M. Epstein, Modeling civil violence: an agent based computational approach. Proc. Natl. Acad. Sci. **99**, 7243–7250 (2002)
24. H. Fujii, H. Uchida, T. Yamada, S. Yoshimura, Mixed traffic simulation of cars and pedestrians for transportation policy assessment, in *Crowd Dynamics, Volume 2 - Theory, Models, and Safety Problems*. Modeling and Simulation in Science, Engineering, and Technology, chap. 2 (Birkhäuser, New York, 2020)
25. L. Gibelli, in *Crowd Dynamics, Volume 2 - Theory, Models, and Safety Problems*. Modeling and Simulation in Science, Engineering, and Technology (Birkhäuser, New York, 2020)
26. L. Gibelli, N. Bellomo, in *Crowd Dynamics, Volume 1 - Theory, Models, and Safety Problems*. Modeling and Simulation in Science, Engineering, and Technology (Birkhäuser, New York, 2018), pp. 1–14
27. G.H. Goldsztein, Self-organization when pedestrians move in opposite directions. Multi-lane circular track model. Appl. Sci. **10**, 563 (2020). https://doi.org/10.3390/app10020563

28. S. Göttlich, S. Knapp, Artificial neural networks for the estimation of pedestrian interaction forces, in *Crowd Dynamics, Volume 2 - Theory, Models, and Safety Problems*. Modeling and Simulation in Science, Engineering, and Technology, chap. 3 (Birkhäuser, New York, 2020)
29. M. Haghani, M. Sarvi, Social dynamics in emergency evacuations: disentangling crowds attraction and repulsion effects. Phys. A **475**, 24–34 (2017)
30. D. Helbing, A. Johansson, *Pedestrian Crowd and Evacuation Dynamics*. Encyclopedia of Complexity and System Science (Springer, Berlin, 2009), pp. 6476–6495
31. D. Helbing, P. Molnár, Social force model for pedestrian dynamics. Phys. Rev. E **51**, 4282–4286 (1995)
32. D. Helbing, A. Johansson, H.-Z. Al-Abideen, Dynamics of crowd disasters: an empirical study. Phys. Rev. E **75**, 046109 (2007)
33. D. Hilbert, Mathematical problems. Bullet. Am. Math. Soc. **8**(10), 437–479 (1902)
34. M. Kinateder, T.D. Wirth, W.H. Warren, Crowd dynamics in virtual reality, in *Crowd Dynamics, Volume 1 - Theory, Models, and Safety Problems*, ed. by L. Gibelli, N. Bellomo. Modeling and Simulation in Science, Engineering, and Technology (Birkhäuser, New York, 2018), pp. 15–36
35. B. Piccoli, F. Rossi, Measure-theoretic models for crowd dynamics, in *Crowd Dynamics, Volume 1 - Theory, Models, and Safety Problems*. Modeling and Simulation in Science, Engineering, and Technology (Birkhäuser, New York, 2018)
36. E. Ronchi, D. Nilsson, Pedestrian movement in smoke: theory, data and modeling approaches, in *Crowd Dynamics, Volume 1 - Theory, Models, and Safety Problems*. Modeling and Simulation in Science, Engineering, and Technology, chap. 3 (Birkhäuser, New York, 2018)
37. A. Templeton, Inserire il titolo in *Crowd Dynamics, Volume 2 - Theory, Models, and Safety Problems*, ed. by L. Gibelli. Modeling and Simulation in Science, Engineering, and Technology, chap. 5 (Birkhäuser, New York, 2020)
38. H. Vermuyten, J. Belien, L. De Boeck, G. Reniers, T. Wauters, A review of optimisation models for pedestrian evacuation and design problems. Saf. Sci. **87**, 167–178 (2016)
39. L. Wang, M.B. Short, A.L. Bertozzi, Efficient numerical methods for multiscale crowd dynamics with emotional contagion. Math. Models Methods Appl. Sci. **27**, 205–230 (2017)

Artificial Neural Networks for the Estimation of Pedestrian Interaction Forces

Simone Göttlich and Stephan Knapp

Abstract We present a data fitting approach for the social force model by Helbing and Molnár using artificial neural networks. The latter are used as a universal approximation for the unknown interaction forces between pedestrians. We train the artificial neural network simultaneously with other parameters arising in the model by utilizing a tailored cost function and stochastic gradient techniques. We test our approach using real data sets for the unidirectional and bidirectional flow in corridors and point out the advantages and drawbacks of the proposed approach.

1 Introduction

The modeling of crowd dynamics provides a useful tool for the evacuation or capacity planning problem. A good overview of existing literature on pedestrian flow models can be found in [2, 3, 8, 13], where mainly two classes of modeling approaches, i.e. microscopic and macroscopic models, are distinguished. Microscopic pedestrian models typically rely on Newton-type dynamics, e.g. in [8, 19, 26] or cellular automata, e.g. in [6, 23, 29], while macroscopic models can be either derived via limiting processes [8, 10, 15, 24] or phenomenologically, see e.g. [18, 21, 26, 27]. Starting from a microscopic level, model extensions include, for example, vision cones [11], shortest-path information [12], and stochastic velocities [10, 31, 32].

In fact, all kinds of models are typically based on information about the pedestrians' behavior such as their maximal acceleration, comfort velocity, interaction with other pedestrians, and obstacles. If these parameters are well-known, the models can be used to predict reliably the movements of pedestrians. The latter is an important issue for analyzing capacities of buildings and the detection of safe escape routes.

S. Göttlich (✉) · S. Knapp
Department of Mathematics, University of Mannheim, Mannheim, Germany
e-mail: goettlich@uni-mannheim.de; stknapp@mail.uni-mannheim.de

L. Gibelli (ed.), *Crowd Dynamics, Volume 2*, Modeling and Simulation in Science, Engineering and Technology, https://doi.org/10.1007/978-3-030-50450-2_2

Unluckily, it is hard to obtain good approximations of the modeling parameters and the parameters should be estimated using real data from studies about pedestrian dynamics.[1] Real data should be used carefully since behavior of humans may additionally depend on further influences, i.e. cultural aspects or panic. A good overview of issues concerning parameter estimation can be found in [1, 22, 30].

In this contribution, we aim to estimate the pedestrian interaction forces for the unidirectional and bidirectional flow in corridors for a microscopic pedestrian model. In contrast to [7, 14], where a Bayesian probabilistic method has been applied for the estimation, we focus on artificial neural networks [4]. In a very recent result by Tordeux [33], artificial neural networks have been used for the estimation of pedestrian speed in corridors and bottleneck situations. In our case, the artificial neural network is a building block in a physically motivated model, the so-called social force model, and is used as a function approximation. The application is non-classical in the sense that we do not intend to match a given input with the outcome of the artificial neural network. More precisely, the compared output depends on unknown parameters which we aim to find during the training of the model. Due to this structure, we have to deal with a non-classical cost function and the parameter identification gets more involved. Since parameter estimation for pedestrian flow models is an emerging research area, in particular in combination with real data, it opens new challenging questions from a theoretical and computational viewpoint. We try to address those while presenting our numerical results.

2 Parameter Estimation

This section is devoted to the application of artificial neural networks for parameter estimation in the pedestrian flow model by Helbing and Molnár. To do so, we first introduce the modeling details and explain the mathematical framework of the artificial neural network. Since our intention is to estimate the interaction between pedestrians, the crucial point will be the computation of weights for the artificial neural network.

Inspired by the social force model [19], our investigations are based on Newton-type microscopic equations which describe the movement and acceleration of every pedestrian due to obstacles, destinations, and interaction forces. Let us consider $i = 1, \dots, N$, $N \in \mathbb{N}$, pedestrians having positions $X_i(t) \in \mathbb{R}^2$ and velocities $V_i(t) \in \mathbb{R}^2$ at time $t \geq 0$. This means that we look from top on to pedestrians, which are represented by their center of mass $X_i(t)$ and their direction of movement $V_i(t)$. In general, the model can be written as

$$\begin{aligned} \frac{d}{dt} X_i(t) &= V_i(t), \\ \frac{d}{dt} V_i(t) &= \frac{1}{\tau}(D_i(X_i(t))v_c - V_i(t)) + F(X_i(t), V_i(t), \mathbf{X}_{-i}(t), \mathbf{V}_{-i}(t)) \\ &\quad + F^w(X_i(t), V_i(t)), \end{aligned} \tag{1}$$

[1] http://ped.fz-juelich.de/database/.

where $\tau > 0$ denotes a relaxation time describing how fast pedestrians achieve their comfort velocity, D_i is the unit vector towards the destination, and $v_c > 0$ is the comfort velocity. The forces F and F^w describe the acceleration caused by interaction with other pedestrians, where $z_{-i} = (z_1, \ldots, z_{i-1}, z_{i+1}, \ldots, z_N)$, and the acceleration caused by walls or obstacles, respectively.

The component $D_i(X_i(t))v_c$ describes the desired velocity vector given that there are no pedestrians and walls around pedestrian i. Hence, $\frac{1}{\tau}(D_i(X_i(t))v_c - V_i(t))$ is an acceleration along the direction of the desired velocity vector of pedestrian i. Assuming that $D_i(X_i(t)) = D_i$ is independent of the position then, in the absence of other pedestrians and walls, we get

$$\frac{d}{dt}V_i(t) = \frac{1}{\tau}(D_i v_c - V_i(t)) \tag{2}$$

with solution $V_i(t) = D_i v_c + e^{-\frac{t}{\tau}}(V_i(0) - D_i v_c)$. That means, $\frac{1}{\tau}$ is the decay rate of the initial deviation away from the desired velocity vector $v_c D_i$. Regarding the interaction acceleration function F, it seems unpromising estimating this high dimensional function, i.e. for large N, by using data. Therefore, we assume the following structure of F:

$$F(X_i(t), V_i(t), \mathbf{X}_{-i}(t), \mathbf{V}_{-i}(t)) = \sum_{k=1, k\neq i}^{N} G(X_i(t) - X_k(t), V_i(t) - V_k(t)). \tag{3}$$

In fact, this means that we assume identical reactions of every single pedestrian given the other pedestrians. Common choices for G in the literature are potentials [15, 28] equipped with a vision cone [11]. In [28], the repulsive forces are given by a parameterized (Morse-type) potential and the parameters are estimated using data to solve a minimization problem with quadratic costs. Reasonable assumptions are made but the shape of the function G has to be proposed. However, we will assume that Eq. (3) holds and our goal is to recover $G\colon \mathbb{R}^4 \to \mathbb{R}^2$ using data for an artificial neural network as an approximation tool.

The acceleration at boundaries given by the function F^w is crucial since obstacles and walls can be assumed as solid objects and these objects represent a reflective boundary. This fact can be only incorporated into F^w by considering unbounded accelerations, which makes the system (1) very hard to solve. One way out of this has been introduced in [15], where the boundary is incorporated by manipulating the realized velocity $\frac{d}{dt}X_i(t) = \mathcal{V}(X_i(t), V_i(t))$. Then, $V_i(t)$ can be interpreted as the desired, but maybe not realized, velocity in the presence of obstacles. For this reason, we neglect the wall forces in the rest of this manuscript and comment on boundary treatment individually in examples.

Summarizing, we need a general tool to fit the function G appropriately. If we assume a potential again, e.g. a Morse potential, and try to find the parameters, we assume too much and could be wrong. Therefore, we choose an artificial neural network as function approximation for the function G. For completeness, we introduce artificial neural networks in the following and state relevant results for our purpose.

2.1 Artificial Neural Network as Universal Function Approximation

Unlike existing contributions for the parameter estimation in pedestrian models [7, 14, 28], we focus on artificial neural networks for the parameter estimation. Motivated by recent works for neural networks applied to ordinary differential equations [5, 16], we will now embed our parameter estimation problem into this context.

2.2 Setting Up an Artificial Neural Network

We consider feed forward artificial neural networks here, which means that the input given into the input layer is fed forward through the network only, i.e. there exists no connections backwards. More detailed, let L be the number of layers including the input and hidden layer (Fig. 1).

The value of the so-called neurons $a_k^{(l)}$ in layer l and neuron k is computed as follows:

Input Layer

$$a_1^{(1)} = 1, \quad a_k^{(1)} = x_{k-1} \tag{4}$$

for $k \in \{2, \dots, n^{(1)} + 1\}$, where $x \in \mathbb{R}^{n^{(1)}}$ is the input (feature) and $n^{(1)}$ is the number of neurons without the bias unit $a_1^{(1)}$.

Hidden Layers

$$a_1^{(l)} = 1, \quad a_k^{(l)} = g^{(l)} \left(\sum_{\tilde{k}=1}^{n^{(l-1)}+1} \theta_{\tilde{k},k}^{(l-1)} a_{\tilde{k}}^{(l-1)} \right) \tag{5}$$

for $l \in \{2, \dots, L-1\}$ and $k \in \{2, \dots, n^{(l)} + 1\}$.

Output Layer

$$a_k^{(L)} = g^{(L)}\left(\sum_{\tilde{k}=1}^{n^{(L-1)}+1} \theta_{\tilde{k},k}^{(L-1)} a_{\tilde{k}}^{(L-1)}\right) \tag{6}$$

for $k \in \{1, \ldots, n^{(L)}\}$. One has to recognize that the output layer does not contain a bias unit, i.e. where a fixed value is set to 1. The entry $\theta_{i,j}^{(l)}$ of the matrices $\theta^{(l)} \in \mathbb{R}^{n^{(l-1)} \times n^{(l)}}$ describes the weight from neuron $a_i^{(l-1)}$ to the value of the neuron $a_j^{(l)}$.

Example 1 We consider the case of a single hidden layer in this example, i.e. $L = 3$. Further, we assume an output layer size of $n^{(L)} = 1$ here. Then, we can write

$$\begin{aligned} a^{(3)} &= g^{(3)}\left(\sum_{\tilde{k}=1}^{n^{(2)}+1} \theta_{\tilde{k},1}^{(2)} a_{\tilde{k}}^{(2)}\right) \\ &= g^{(3)}\left(\sum_{\tilde{k}=1}^{n^{(2)}+1} \theta_{\tilde{k},1}^{(2)} g^{(1)}\left(\sum_{s=1}^{n^{(1)}+1} \theta_{s\tilde{k}}^{(1)} a_s^{(1)}\right)\right) \\ &= g^{(3)}\left(\theta_{1,1}^{(2)} + \sum_{\tilde{k}=2}^{n^{(2)}+1} \theta_{\tilde{k},1}^{(2)} g^{(1)}\left(\theta_{1,\tilde{k}}^{(1)} + \sum_{s=2}^{n^{(1)}+1} \theta_{s\tilde{k}}^{(1)} x_{s-1}\right)\right). \end{aligned}$$

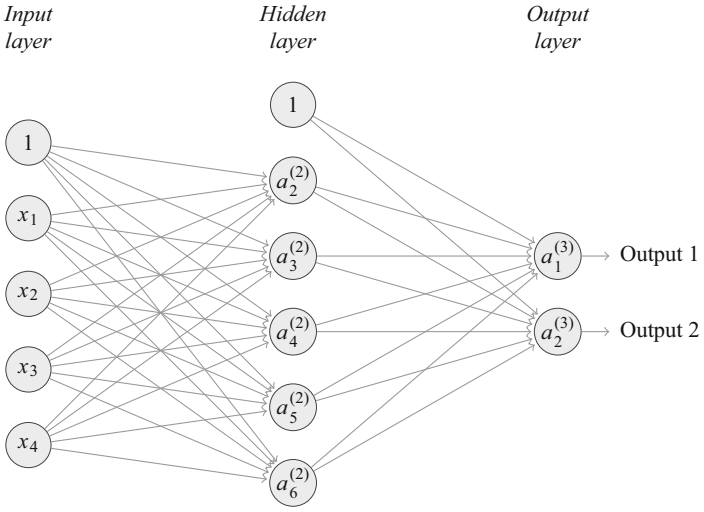

Fig. 1 Graphical representation of a feed forward artificial neural network with one hidden layer

Hence, the output a^3 is a nested sum of weighted evaluations of functions of the input x. A quite common choice is $g^{(L)}(z) = z$ as the identity. This representation allows for an increasing size of the hidden layer $n^{(2)}$ that we can profit from a special class of approximation functions. Indeed, this is the result of the so-called universal approximation theorems:

Theorem 1 ([9, 20])

1. *Let f be a continuous function on $[0,1]^{n^{(1)}}$ and $\epsilon > 0$ as well as the activation function $g^{(1)}$ is assumed to be a continuous sigmoid function, i.e. $\lim_{t\to\infty} g^{(1)}(t) = 1$ and $\lim_{t\to-\infty} g^{(1)}(t) = 0$. Then, there exists an artificial neural network in the form of*

$$a^{(3)}(x) = \sum_{\tilde{k}=2}^{n^{(2)}+1} \theta^2_{\tilde{k},1} g^{(1)}\left(\theta^{(1)}_{1,\tilde{k}} + \sum_{s=2}^{n^{(1)}+1} \theta^1_{s\tilde{k}} x_{s-1}\right)$$

such that

$$\|a^{(3)} - f\|_\infty < \epsilon.$$

2. *Let $f \in L^p(\mu)$, where μ is a finite measure on $\mathbb{R}^{n^{(1)}}$ and $\epsilon > 0$ as well as the activation function $g^{(1)}$ is assumed to be unbounded and nonconstant. Then, there exists an artificial neural network in the form of*

$$a^{(3)}(x) = \sum_{\tilde{k}=2}^{n^{(2)}+1} \theta^2_{\tilde{k},1} g^{(1)}\left(\theta^{(1)}_{1,\tilde{k}} + \sum_{s=2}^{n^{(1)}+1} \theta^1_{s\tilde{k}} x_{s-1}\right)$$

such that

$$\left(\int_{\mathbb{R}^{n^{(1)}}} |a^{(3)}(x) - f(x)|^p \mu(dx)\right)^{\frac{1}{p}} < \epsilon.$$

Theorem 1 implies that we can find an artificial neural network with one single hidden layer such that a function is approximated appropriately in this way.

In order to obtain the weights for approximating functions we use a minimization problem. To do so, let $h_\theta(x) = (a_k^{(L)})$ be the output of the network for a given input x. Then, we define the cost function as

$$J(\theta) = \frac{1}{m}\left(\sum_{i=1}^{m} C(h_\theta(x^{(i)}), y^{(i)}) + \lambda \mathcal{R}(\theta)\right), \tag{7}$$

where $C\colon \mathbb{R}^{n^{(L)}} \times \mathbb{R}^{n^{(L)}} \to \mathbb{R}$ describes the cost of the difference between the feature value $x^{(i)}$ and the measured output $y^{(i)}$, $\lambda \geq 0$, and $\mathcal{R}\colon \mathbb{R}^{(n^{(1)}+1)\times(n^{(2)}+1)} \times \cdots \times \mathbb{R}^{n^{(L-1)+1}\times n^{(L)}} \to \mathbb{R}$ is a regularization of the parameters θ.

Typical choices are quadratic costs

$$C(z, y) = \frac{1}{2}\|z - y\|_2^2$$

and

$$\mathcal{R}(\theta) = \frac{1}{2}\sum_{l=1}^{L-1}\sum_{i=2}^{n^{(l)}+1}\sum_{j=1}^{n^{(l+1)}+1}\left(\theta_{i,j}^{(l)}\right)^2, \tag{8}$$

where the bias units $\theta_{1,j}^{(l)}$ are not considered in the regularization $\mathcal{R}(\theta)$.

In order to obtain an approximation for a given function $f\colon \mathbb{R}^{n^{(1)}} \to \mathbb{R}^{n^{(L)}}$, we use a training set $x^{(i)} \in \mathbb{R}^{n^{(1)}}$, $i \in \{1, \ldots, m\}$ with $m \in \mathbb{N}$ samples and define the output as $y^{(i)} = f(x^{(i)})$. Then, we solve

$$\min_{\theta} J(\theta)$$

to obtain an optimal value θ^* such that the artificial neural network approximates the function f well in the sense of the costs J. It is clear that the cost function J might have several local minima leading to difficulties in finding the global solution.

We briefly comment on the choice of activation functions $g^{(l)}$. Although there exist various choices, it is quite common to choose $g^{(L)}(z) = z$ as the identity and the other $g^{(l)}$ as the sigmoid function $g^{(l)}(z) = \frac{1}{1+e^{-z}}$, as the rectified linear unit (ReLU) $g^{(l)}(z) = \max(z, 0)$ or as the smoothed version of the latter, i.e. the softplus or SmoothReLU function $g^{(l)}(z) = \ln(1 + e^z)$. The identity $g^{(L)}(z) = z$ in the last layer allows the space $\mathbb{R}$ as the image of the artificial neural network because the output is then given as linear combination of the previous layer. Sigmoid activation functions $g^{(l)}(z) = \frac{1}{1+e^{-z}}$ can be basically used to mimic decisions (true or false) due to their shape. The rectified linear unit $g^{(l)}(z) = \max(z, 0)$ is bio-inspired, see e.g. [17] and has been used successfully in artificial neural networks for a faster training of the network. Due to the lack of differentiability at $z = 0$ smoothed versions like the SmoothReLU mentioned above are common alternatives.

2.2.1 Gradient Descent and Related Algorithms

In order to minimize the cost function (7), we use a descent gradient approach. Let us denote by $\alpha \in \mathbb{R}^K$ the K parameters to fit and we assume a general cost function J in the form of

$$J(\alpha) = \frac{1}{m}\left(\sum_{i=1}^{m} Q_i(\alpha)\right), \tag{9}$$

where $Q_i(\alpha)$ denotes the cost of sample i associated with the parameters α. The negative gradient $-\nabla J(\alpha)$ indicates the steepest descent of J at the point α and minimizing J can be therefore achieved by "walking" into the latter direction of the steepest descent. Let $\eta > 0$ be a parameter scaling of the step size and $\alpha_0 \in \mathbb{R}^k$ be given, then

$$\alpha_{k+1} = \alpha_k - \eta \nabla J(\alpha_k)$$

provides an iteration α_k, which might end up in a local minimum of the cost function J. Here, we face several problems:

- the computation time of $\nabla J(\alpha_k)$ is too high, which is caused by a large number m of samples or a costly computation of ∇Q,
- the iteration α_k might not converge,
- the algorithm ends up in a local minimum.

The first item can be tackled by considering the so-called stochastic gradient or mini batch gradient descent schemes. The idea is as follows: Starting with a randomly chosen subset I_k of $\{1, \ldots, m\}$ containing $\tilde{m} \leq m$ elements, we adapt the iteration of the gradient descent in the following way:

$$\begin{aligned}\alpha_{k+1} &= \alpha_k - \eta \frac{1}{\tilde{m}}\left(\sum_{i \in I_k} \nabla Q_i(\alpha_k)\right) \\ &=: \alpha_k - \eta \nabla J_k^{\tilde{m}}(\alpha_k).\end{aligned}$$

If we choose $\tilde{m} = m$, then we obtain the so-called full batch gradient descent, which is the classical gradient descent algorithm.

A very crucial parameter is the step size, or so-called learning rate η. If η is chosen too large, the iteration might diverge and, in contrast, if η is too small, it takes a large amount of iterations to reach some local minimum. Therefore, efficient heuristics have been developed to choose and update the learning rate. A brief overview can be found in e.g. [35] as well as in.[2] A first step is the use of ADAGRAD, which assumes an individual learning rate for every parameter, i.e.

[2] https://ruder.io/optimizing-gradient-descent/index.html#visualizationofalgorithms.

$$\alpha_{k+1,i} = \alpha_{k,i} - \frac{\eta}{\sqrt{\sum_{l=0}^{k}(\nabla J_l^{\tilde{m}}(\alpha_l)_i)^2}} \nabla J_k^{\tilde{m}}(\alpha_k)_i$$

for $i = 1, \ldots, m$. This means that the learning rates decay fast in the presence of high gradients and cannot increase anymore. Thus, as soon as a direction has a very small learning rate, the algorithm cannot improve this direction appropriately. To overcome this issue, the algorithm ADAGRAD has been developed in [35] by considering a finite accumulate over window. Let $E[g^2]_k$ satisfy $E[g^2]_{k+1} = \rho E[g^2]_k + (1-\rho)(\nabla J_k^{\tilde{m}}(\alpha_k))^2$ for $E[g^2]_0 = 0$ and $\rho \in (0, 1)$. Then $E[g^2]_k$ adapts to the squared gradient information iteratively with rate ρ. The latter resolves the problem of always decaying learning rates but does not explain how to choose η in a proper way. We define $\Delta\alpha_k = \alpha_{k+1} - \alpha_k$ and the ADADELTA algorithm reads then as follows

$$\begin{aligned} E[g^2]_k &= \rho E[g^2]_{k-1} + (1-\rho)(\nabla J_{k-1}^{\tilde{m}}(\alpha_{k-1}))^2, \\ \Delta\alpha_k &= -\frac{\sqrt{E[\Delta\alpha^2]_{k-1} + \epsilon}}{\sqrt{E[g^2]_k + \epsilon}} \nabla J_k^{\tilde{m}}(\alpha_k), \\ E[\Delta\alpha^2]_k &= \rho E[\Delta\alpha^2]_{k-1} + (1-\rho)\Delta\alpha_k^2, \end{aligned}$$

where $\epsilon > 0$ is a chosen parameter to avoid singular values by division by zero and initially $E[\Delta\alpha^2]_0 = 0$.

Since the presented algorithm only uses local information, it might converge to a local minimum in the presence of several minima, which is often the case considering artificial neural networks. In [25], an additive noise has been added to the gradient, which is damped to zero as the number of iterations increases. This allows for a probability to escape from local minima. Because this is a relevant and non-difficult issue, there is recent research considering multiplicative noise or more advanced noises to improve the probability of escaping a local minimum, see, for example, [34, 36]. In our formulas, we replace the gradient $\nabla J_k^{\tilde{m}}(\alpha_k)$ by $\nabla J_k^{\tilde{m}}(\alpha_k) + N_k$, where $N_k \sim \mathcal{N}(0, \Sigma_k)$ is a multivariate normal distributed random vector with zero mean and covariance matrix Σ_k. According to [25], we choose $(\Sigma_k)_{ii} = \frac{\eta_1}{(1+k)^{\eta_2}}$ for some constants $\eta_1, \eta_2 > 0$ and $(\Sigma)_{ij} = 0$ whenever $i \neq j$.

We briefly comment about the calculation of the gradient of the cost function. An artificial neural network is simply speaking a chain of functions and to obtain the gradient with respect to the parameters θ, the chain rule needs to be applied. This can be done by backpropagation through the network, i.e. starting with the output layer the derivatives are computed according to the chain rule backwards to the first hidden layer. For more information about backpropagation, or computation of the gradient, we recommend [4].

2.3 Parameter Estimation and Cost Function in Pedestrian Flow Model

We go back now to the initial motivation that we want to recover the interaction function G between pedestrians from real data. In order to recover the interaction function G, we also need to estimate the remaining parameters τ, v_c simultaneously, which makes the setting different to classical artificial neural network applications. From the data point of view, we will have the measured positions $X_i^k \in \mathbb{R}^2$ at discrete times t_k, where $t_0 < t_1 < \cdots < t_m$. We first discretize the microscopic pedestrian model in the following way:

$$V_i(t_k) = \frac{d}{dt} X_i(t_k) \approx \frac{X_i(t_{k+1}) - X_i(t_{k-1})}{t_{k+1} - t_{k-1}},$$
$$S_i(t_k) = \frac{d}{dt} V_i(t_k) \approx \frac{X_i(t_{k+1}) - 2X_i(t_k) + X_i(t_{k-1})}{\Delta t_k \Delta t_{k-1}},$$

where $\Delta t_k = t_{k+1} - t_k$. Therefore, we use $V_i^k = V_i(t_k)$ and $S_i^k = S_i(t_k)$ as approximations of the velocity and acceleration of pedestrian i at time t_k.

If we estimate all D_i, i.e. the destination of pedestrian i, the number of parameters increases significantly and cannot expect good estimations. Therefore, we perform a "pre-processing" and identify the destination by identifying pedestrians destination from trajectories. We will explain the used approximation more detailed while discussing the application examples.

The main difference to the classical learning and application of the artificial neural network is here that we do not have the classical input–output structure. More precisely, we can use the trajectories but have no explicit outputs given. Therefore, we introduce the following cost function, where we denote by $\alpha = (\tau, v_c, \theta)$ the collection of all parameters which we want to estimate from data. The cost function reads as follows:

$$\mathcal{J}(\alpha) = \frac{1}{m}\frac{1}{2}\sum_{k=1}^{m}\Big[\sum_{i=1}^{N^k}\Big|\tau S_i^k - (D_i^k v_c - V_i^k) - \tau \sum_{j=1, j\neq i}^{N^k} h_\theta(X_i^k - X_j^k, V_i^k - V_j^k)\Big|^2 + \mathcal{R}(\theta)\Big].$$

First of all, we observe the classical structure of the cost function as in (7) that allows for using the toolbox of the stochastic gradient descent algorithms. The regularization $\mathcal{R}$ is the one introduced in (8), which regularizes the parameters θ that do not originate from a bias unit. The first part of the cost function simply results from the ODE system of the trajectories and shows that we want to satisfy the second equation (equation for the acceleration) as good as possible. Here, we multiply the equation for the acceleration by τ to avoid divisions by zero and more stable gradients with respect to this parameter.

2.3.1 Data and Preprocessing of Data

In this last part of the section we comment on the preprocessing of the data. We use the data from the data archive of experimental data from studies about pedestrian dynamics,[3] where next to the videos of the experiments one obtains trajectory data. More precisely, we focus on the corridor unidirectional and bidirectional flow data.[4] The main contents of the trajectory data are

- x and y coordinates at every frame number,
- personal ID identifying the corresponding individual as time evolves,
- the frame rate.

One significant difficulty is that the number of pedestrians and also the set of personal IDs change over time, which is clear since pedestrians enter and leave the corridor. Since we need approximations of the time derivative of the trajectory data, we need at least data of a pedestrian i in frame $k-1$, k, and $k+1$. We first cleaned them out and assigned the corresponding velocity and acceleration values.

In a next step, we identify the destination of each pedestrian by taking the normalized mean velocity direction. To avoid too many different destination directions, we round the latter values, since pedestrians in this scenario have to walk through the corridor and should not change their main direction.

3 Computational Results

First we introduce the setting and parameter used throughout this section. We randomly choose 60% from the data, i.e. from the frames, as the training set. The remaining 40% are used as test set. The initial parameters are $\alpha_0 = (\tau_0, v_{C,0}, \theta_0)$ with $\tau_0 = 0.1$, $v_{C,0}$ as the average norm of the velocities from the test set and θ_0 are uniformly distributed randomly chosen from $[-1, 1]$ with exception of the parameters originating from the last hidden bias unit, which are set to zero. As activation functions in the hidden layer we use smooth rectifier units (softplus) $g^{(2)}(x) = \ln(1 + e^x)$ with derivative $(g^{(2)})'(x) = \frac{1}{1+e^{-x}}$, which is the logistic function. The output layer activation function is given as the identity $g^{(3)}(x) = x$ in our case and we assume the parameter $\lambda = 10^{-2}$ for the regularization.

In the stochastic gradient descent algorithm we use the gradient noise with the parameters $\eta_1 = 0.5$ and $\eta_2 = 0.25$ as proposed in [25]. And according to [35], we use $\rho = 0.95$ and $\epsilon = 10^{-6}$ in the ADADELTA algorithm. The batch sizes will be varied in the examples as well as the size of the hidden layer of the artificial neural network.

[3] http://ped.fz-juelich.de/database/.

[4] https://doi.org/10.34735/ped.2013.5, https://doi.org/10.34735/ped.2013.6.

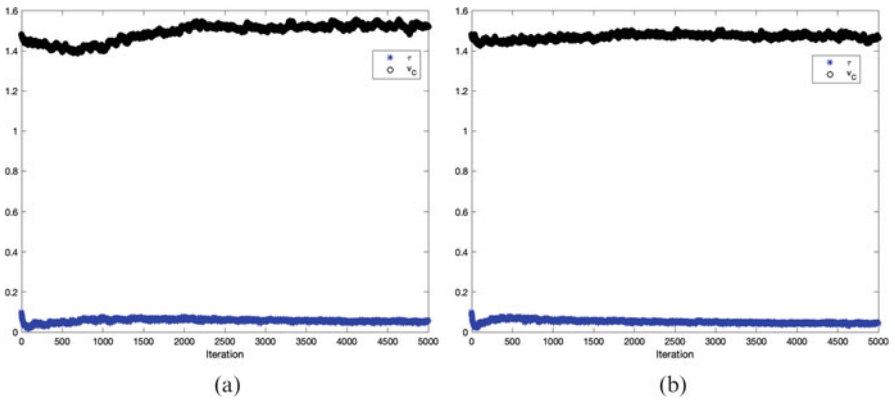

(a) (b)

Fig. 2 Value of τ (blue star) and v_c (black circle) during iteration. (**a**) 4 neurons in hidden layer. (**b**) 40 neurons in hidden layer

3.1 Unidirectional Flow in Corridor

We use the data `trajUNICORR50001` from database[5] in the following. It contains the trajectory data for pedestrians walking from the right to the left in a corridor. As one can observe from the video, which can be found also there, we do not have a high amount of interaction between the pedestrians as well as we expect almost no acceleration influences from the data. For this reason, we choose $\tau_0 = 0.1$ here. We choose the configurations of the artificial neural network as $n^{(1)} = 4$, $n^{(3)} = 2$ and $n^{(2)} \in \{4, 40\}$ here.

In Fig. 2 the values of τ and v_c during the stochastic gradient are shown indicating that our initial guess of both parameters is close to the values during the iterations. Also, we observe no severe difference between the case of 4 hidden neurons (Fig. 2a) and 40 hidden neurons (Fig. 2b). Since the calculation of the full batch costs, i.e. the cost function evaluated on the complete training or test set, is very costly from the computational point of view, we only computed the cost function for the initial guess and the guess after 5000 iterations of the stochastic gradient algorithm. In Table 1 the relaxation time τ^* and comfort velocity v_c^* after 5000 stochastic gradient iterations are shown. They are reasonable since v_c^* are around 5–6 km/h. As mentioned before, we do not observe much acceleration in the data such that a small value of τ^* is reasonable as the comfort velocity is achieved very quickly. In the case of 4 neurons in the hidden layer, i.e. $5 \cdot 4 + 5 \cdot 2 = 30$ parameters for G, we have a decrease in the cost function on both, the training and test set. Surprisingly, in the case of 40 neurons in the hidden layer ($5 \cdot 40 + 41 \cdot 2 = 282$ parameters) the cost function increases. This might be due to not enough iterations, small batch size, or a wrong regularization parameter.

[5] https://doi.org/10.34735/ped.2013.6.

Table 1 τ^* and v_c^* after training and cost function evaluated on the test and training set for initial parameter set and after 5000 stochastic gradient iterations with a batch size of 1

	τ^*	v_c^*	$J_{train}(\alpha_0)$	$J_{test}(\alpha_0)$	$J_{train}(\alpha^*)$	$J_{test}(\alpha^*)$
4 neurons	0.0564	1.5210	517.29	530.08	449.23	451.05
40 neurons	0.0409	1.4650	568.12	578.49	857.89	908.53

Figures 3 and 4 show the approximated function G, which is essentially the artificial neural network. Since the dimension of the input is of dimension 4 and the output's dimension is 2, we have drawn the mappings $(x, y) \mapsto G_1((x, y), v)$ and $(x, y) \mapsto G_2((x, y), v)$ for some fixed $v \in \mathbb{R}^2$ separately. We recover the intuition of G again: G_1 is the attraction or repulsion (depending on the sign) in the x direction whereas G_2 describes the same in the y direction. The inputs of G are the difference in the position, i.e. $X_i - X_k$, which corresponds to the values (x, y) and the difference of the velocities $V_i - V_k$ corresponding to v here. Let us assume pedestrian i is at x position $X_{i,1}(t) > X_{k,1}(t)$ but in y direction they are the same position, i.e. $X_{i,2}(t) = X_{k,2}(t)$, which implies $x > 0$ and $y = 0$. Pedestrians in this experiment walk from the right to the left and we imply by the latter assumption that pedestrian i walks behind pedestrian k. If $v_i = (-2, 0)$ and $v_k = (-1, 0)$, i.e. pedestrian i walks faster, then $v = (-1, 0)$. This situation is shown in Fig. 3 in the left first corners of the subfigures. We observe that the force decreases with x increasing, which is reasonable. One could worry about the values being always negative here but that is a problem of parameter identification since we only have single direction interactions in the data (all walk from right to the left). The plots corresponding to $v = (1, 0)$ show exactly the opposite, i.e. pedestrian i walks slower than pedestrian k. To understand the graphics with $v = (0, -1)$ and $v = (0, 1)$ we consider the following situation:

Let pedestrians i and k stay at the same x position but the y coordinate of i is assumed to be greater than the coordinate of k. If $v_i = (-1, -1)$ and $v_k = (-1, 1)$ that means they might run into each other, we obtain $v = (0, -2)$, or normalized $v = (0, -1)$. We see that for fixed $x = 0$ the value of G in x-direction (G_1) increases in y in Fig. 3a. In y-direction (b) it is the opposite as one would expect.

In Fig. 4 the behavior is different. One can observe that the function behaves more nonlinear and also covers an increasing and decreasing behavior as the distance $\|(x, y)\|$ changes. In order to obtain a better result in terms of the cost function, one has to use larger batch sizes as well as more iterations.

Since Figs. 3 and 4 indicate that 4 neurons are too less and 40 need a long time to converge in the stochastic gradient algorithm, we take 10 neurons and work with a batch size of 9. Figure 5 shows the result for G, which looks much better now although we reduced the number of iterations to 2500. Table 2 shows that we have a decreasing cost function again and the optimal values are close to the values in Table 1. A big difference can be seen in Fig. 5, where the shape of the function G fits better to the intuitions stated before. We also see that the x-direction has been learned better than the y-direction, which is clear from the data.

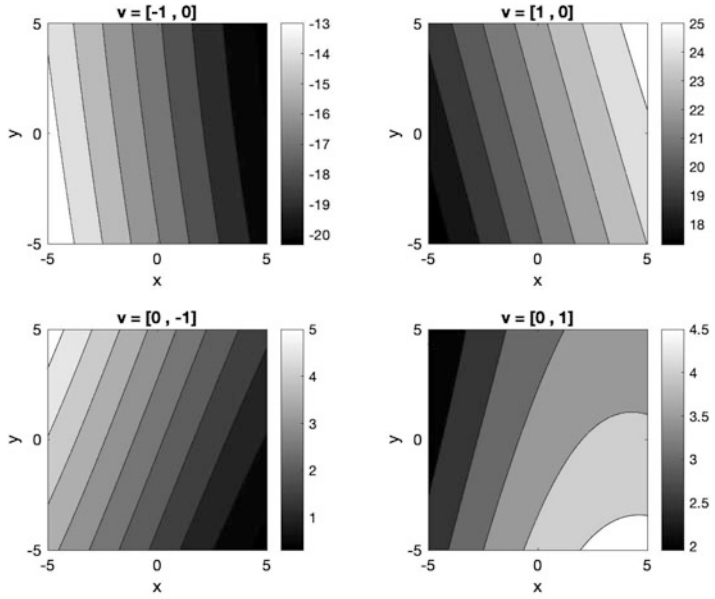

(a)

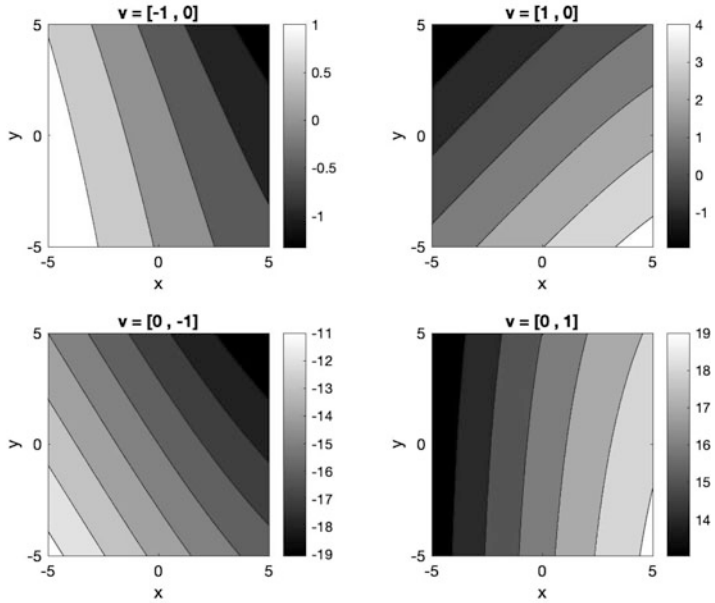

(b)

Fig. 3 Approximated function $G((x, y), (v_1, v_2))$. (**a**) x-direction with 4 neurons in hidden layer. (**b**) y-direction with 4 neurons in hidden layer

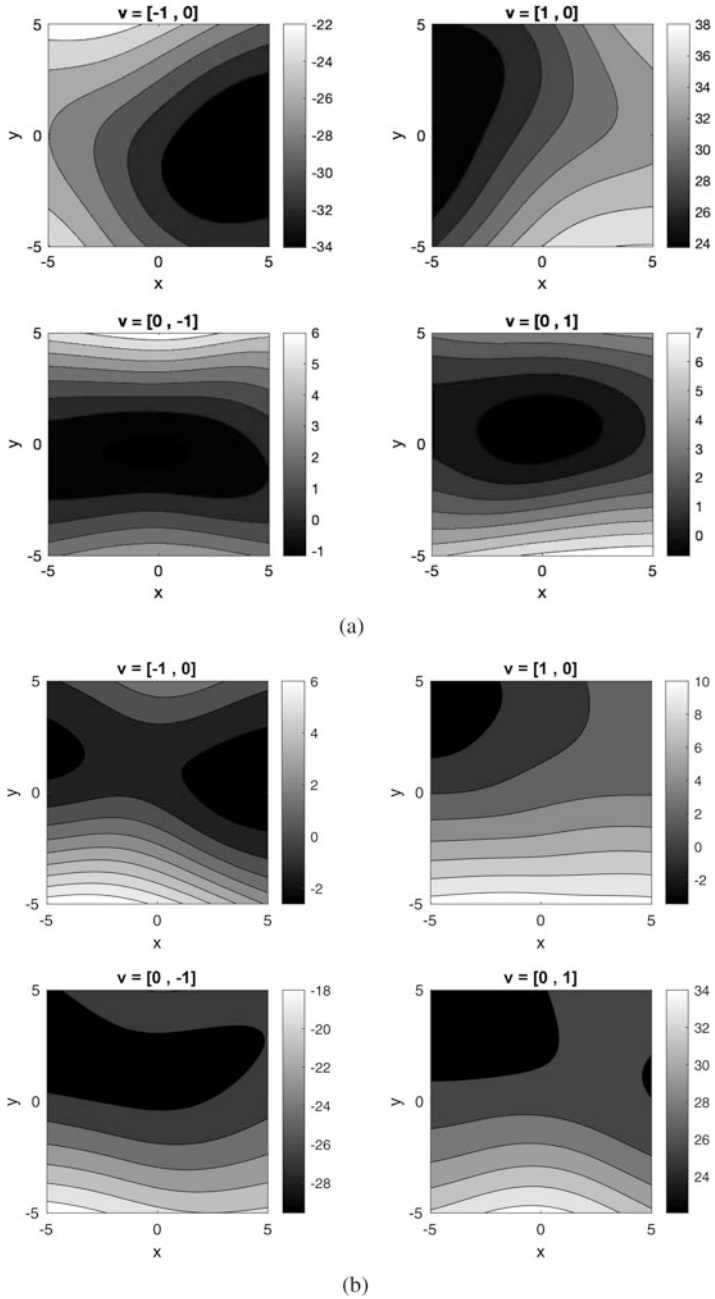

Fig. 4 Approximated function $G((x, y), (v_1, v_2))$. (**a**) x-direction with 40 neurons in hidden layer. (**b**) y-direction with 40 neurons in hidden layer

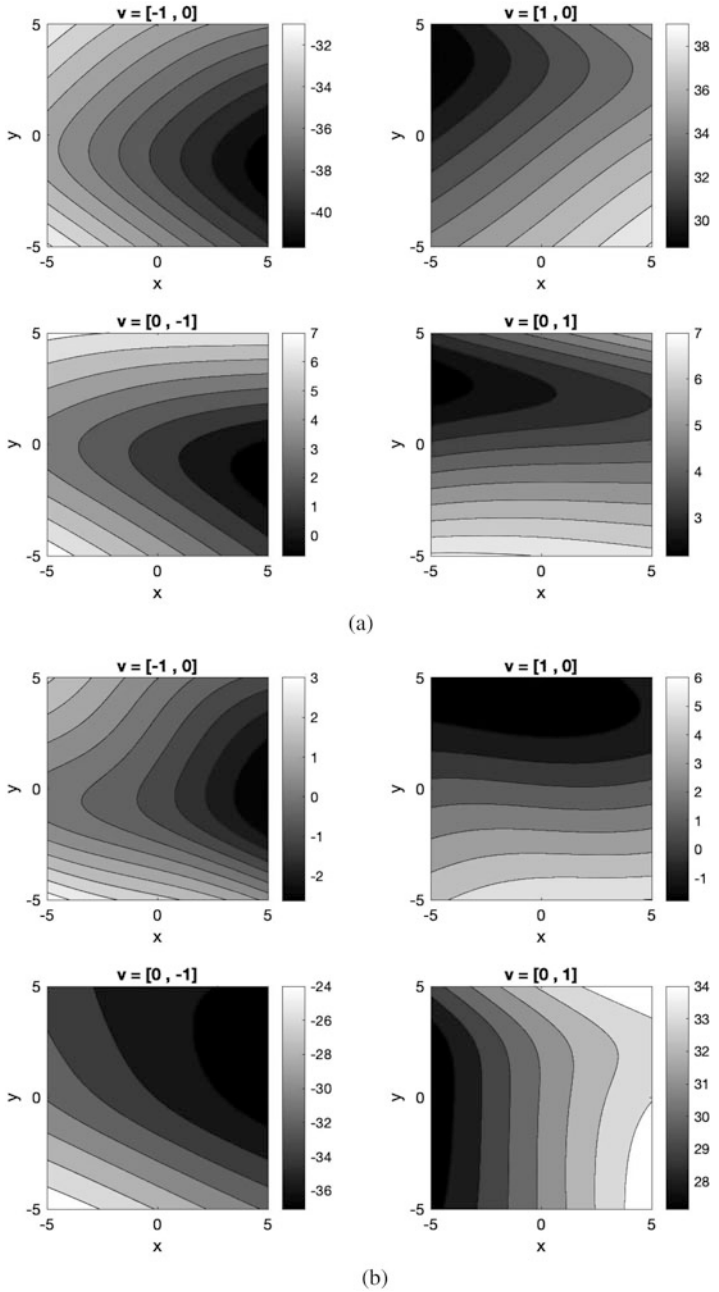

Fig. 5 Approximated function $G((x, y), (v_1, v_2))$. (**a**) x-direction with 10 neurons in hidden layer. (**b**) y-direction with 10 neurons in hidden layer

Table 2 τ^* and v_c^* after training and cost function evaluated on the test and training set for initial parameter set and after 2500 stochastic gradient iterations with a batch size of 9

	τ^*	v_c^*	$J_{train}(\alpha_0)$	$J_{test}(\alpha_0)$	$J_{train}(\alpha^*)$	$J_{test}(\alpha^*)$
10 neurons	0.0391	1.4683	556.61	567.52	493.79	502.09

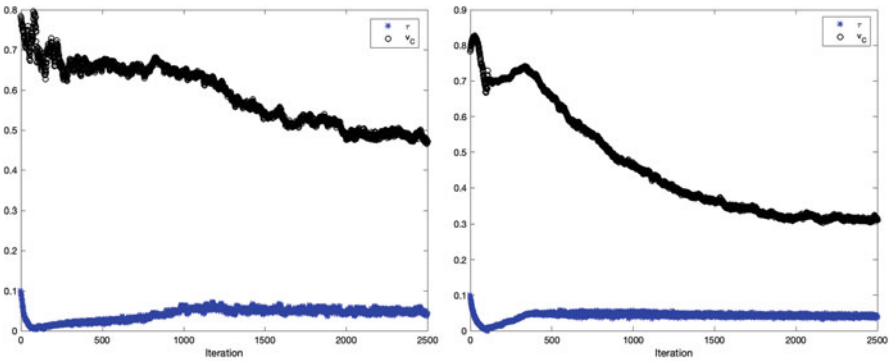

Fig. 6 Value of τ (blue star) and v_c (black circle) during iteration. (a) 4 neurons in hidden layer and batch size 1. (**b**) 10 neurons in hidden layer and batch size 9

3.2 Bidirectional Flow in Corridor

We also have a look at a second data set called `BICORR400A1`.[6] Here, two groups of pedestrian run against each other in a corridor, i.e. we have pedestrians walking to the right and to the left. As before, we use a batch size of one for the stochastic gradient algorithm and 4 neurons in the hidden layer. Due to computational limitations, we restrict on 2500 iterations here. Figure 6 shows the evolution of the parameters τ and v_c during the stochastic gradient, where left 4 neurons and a batch size of 1 have been used and on the right 10 neurons and a batch size of 9. The values for τ do not change significantly anymore and the values of v_c tend to being flat as well.

Table 3 contains the values for τ and v_c after the iterations. Since the number of pedestrians in the corridor is high, we have a lower average speed, which implies a lower v_c^*. The cost function value is lower for α^* than for the initial configuration α_0 and Fig. 7 indicates that the function G has been fitted in a better way. More detailed, we always have the increasing or decreasing behavior in x direction.

Considering the interaction function G for 10 neurons and using a larger batch size of 9, we see again a more nonlinear behavior, see Fig. 8. More detailed, Fig. 8a indicates that the interaction in x-direction, i.e. G_1 depends strongly on y compared to Fig. 7a. This is based on the data since the pedestrians form two walking blocks of

[6] https://doi.org/10.34735/ped.2013.6.

Table 3 τ^* and v_c^* after training and cost function evaluated on the test and training set for initial parameter set and after 2500 stochastic gradient iterations with a batch size of 9

	τ^*	v_c^*	$J_{train}(\alpha_0)$	$J_{test}(\alpha_0)$	$J_{train}(\alpha^*)$	$J_{test}(\alpha^*)$
4 neurons	0.0438	0.4715	500.68	513.71	449.23.71	451.05.09
10 neurons	0.0373	0.3112	–	–	–	–

groups: one walking to the left and one walking to the right and almost no mixture in the corridor. Figure 8 shows a quite similar behavior as it is the case for 4 neurons.

Summarizing, the choice of the number of neurons severely affects the results as one would expect. Also the type of data strongly influences the results. This is due to effects, which are or are not covered in the data.

4 Conclusion

We have derived a data fit setting for the social force model, where the interaction is based on an artificial neural network. In addition, we have introduced the numerical treatment, including stochastic gradient descent heuristics and data preprocessing. The quality of the data fit severely depends on the number of artificial neurons and the number of stochastic gradient iterations as we have seen in results based on real data sets. Due to computational restrictions one cannot significantly increase the number of artificial neurons and the number of iterations simultaneously. From the results we also conclude that the interaction strongly depends on the velocity of both interacting pedestrians as well as their distance from each other.

In terms of computation time, the minimization of the cost function took about 2–3 h in the case of 4 neurons and a batch size of one, whereas the batch size of 9 and 10 neurons required 12 h (unidirectional) and 3 days (bidirectional) to reach the number of iterations on a standard desktop computer. The computation time also depends strongly on the number of pedestrians, which are present in a sample since the number of evaluations increases quadratically in the number of pedestrians. One possible way out of the computational restrictions might be the use of well-developed artificial neural network implementations and embed them into the presented model.

Summarizing, there is a recent trend to carry out data-driven approaches to estimate parameters in crowd models. So far, the Bayesian probabilistic approach [7, 14] and the artificial neural networks approach [33] are the most common tools in the literature. Both approaches are characterized by the computational evaluation of special optimization problems with differential equations as constraints and are therefore computationally costly. Furthermore, the choice of other problem-specific parameters and a reasonable initial guess might be crucial to numerically compute reasonable solutions. From a theoretical point of view, it seems that the Bayesian

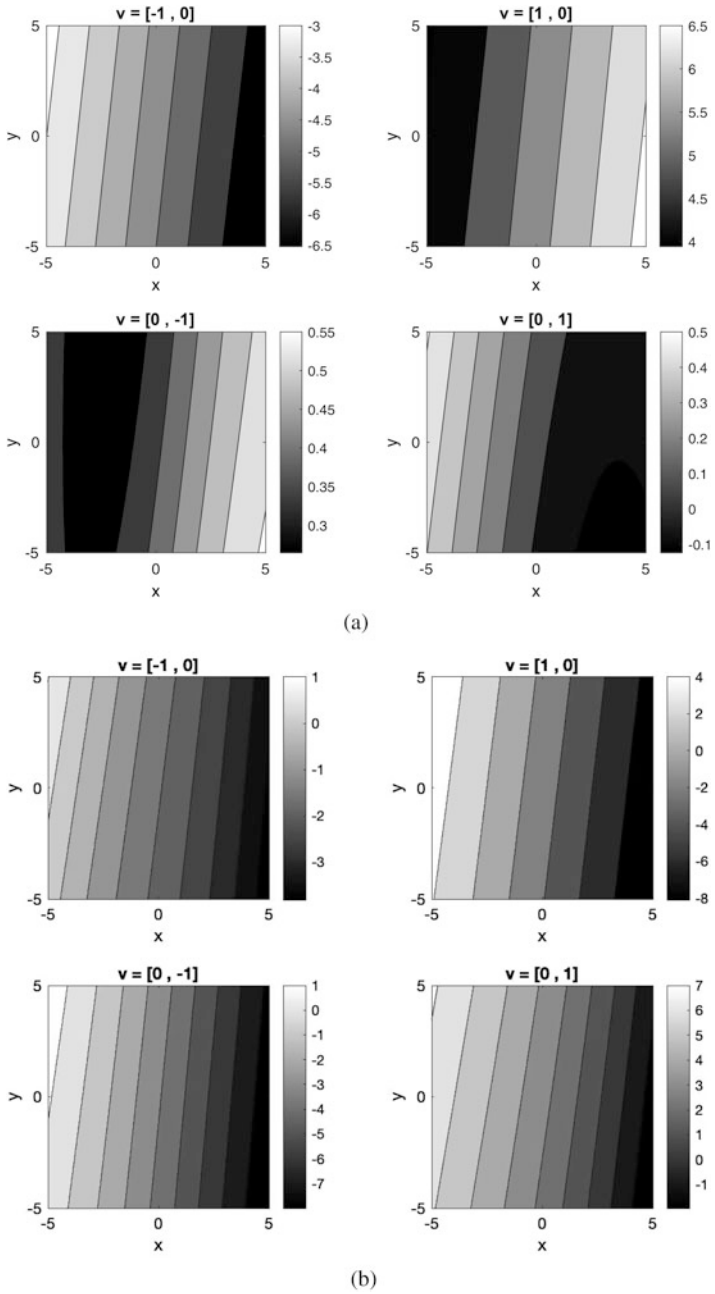

Fig. 7 Approximated function $G((x, y), (v_1, v_2))$. (**a**) x-direction with 4 neurons in hidden layer. (**b**) y-direction with 4 neurons in hidden layer

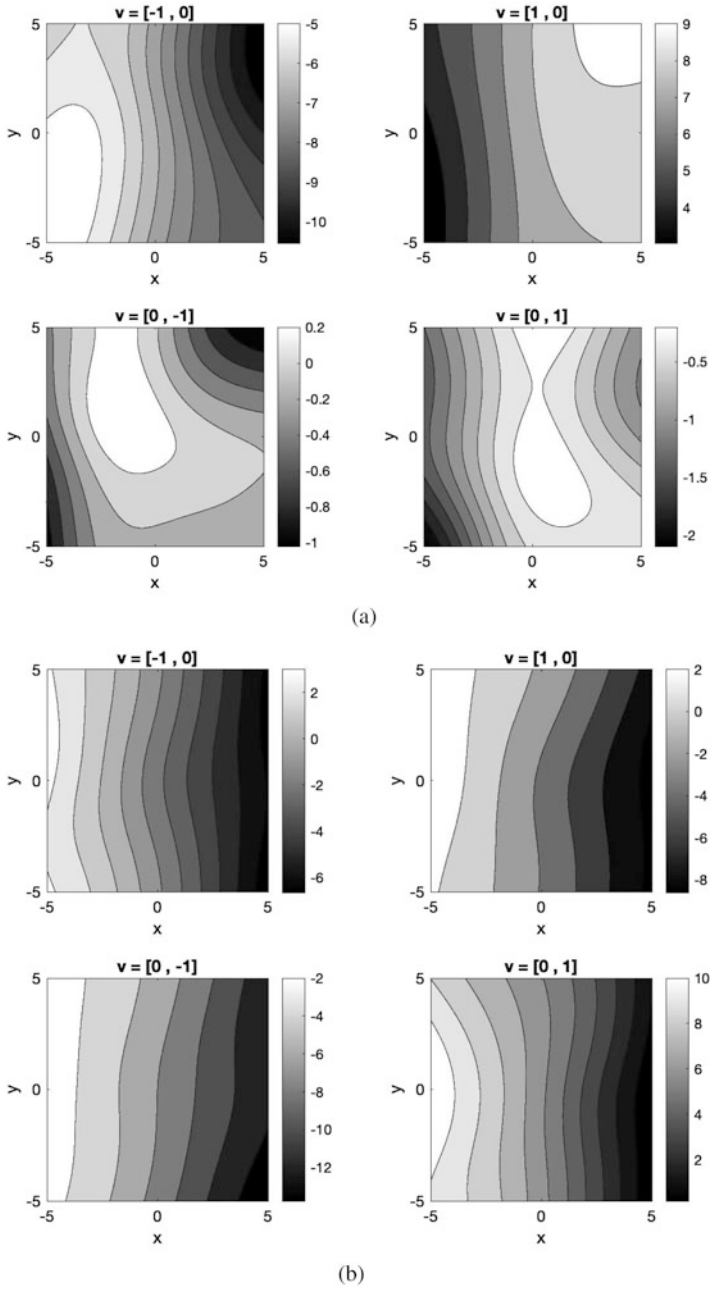

Fig. 8 Approximated function $G((x, y), (v_1, v_2))$. (**a**) x-direction with 10 neurons in hidden layer. (**b**) y-direction with 10 neurons in hidden layer

approach can rely on more results, while the theory on artificial neural network is rather in the early stages. However, a direct comparison of both approaches based on the same setting is still missing.

Acknowledgments This work was supported by DFG grants No. GO 1920/7-1, GO 1920/10-1 and the DAAD project "Stochastic dynamics for complex networks and systems" (Project-ID 57444394).

References

1. R.C. Aster, B. Borchers, C.H. Thurber, *Parameter Estimation and Inverse Problems*, 2nd edn. (Elsevier/Academic Press, Amsterdam, 2013)
2. N. Bellomo, C. Dogbe, On the modeling of traffic and crowds: a survey of models, speculations, and perspectives. SIAM Rev. **53**, 409–463 (2011)
3. N. Bellomo, C. Bianca, V. Coscia, On the modeling of crowd dynamics: an overview and research perspectives. SeMA J. **54**, 25–46 (2011)
4. C.M. Bishop, Pattern Recognition and Machine Learning. Information Science and Statistics (Springer, New York, 2006)
5. R.T.Q. Chen, Y. Rubanova, J. Bettencourt, D. Duvenaud, Neural ordinary differential equations (2018). arXiv:1806.07366
6. A. Chertock, A. Kurganov, A. Polizzi, I. Timofeyev, Pedestrian flow models with slowdown interactions. Math. Models Methods Appl. Sci. **24**, 249–275 (2014)
7. A. Corbetta, A. Muntean, K. Vafayi, Parameter estimation of social forces in pedestrian dynamics models via a probabilistic method. Math. Biosci. Eng. **12**, 337–356 (2015)
8. E. Cristiani, B. Piccoli, A. Tosin, *Multiscale Modeling of Pedestrian Dynamics*. Modeling, Simulation and Applications, vol. 12 (Springer, Cham, 2014)
9. G. Cybenko, Approximation by superpositions of a sigmoidal function. Math. Control Signals Syst. **2**, 303–314 (1989)
10. P. Degond, C. Appert-Rolland, M. Moussaïd, J. Pettré, G. Theraulaz, A hierarchy of heuristic-based models of crowd dynamics. J. Stat. Phys. **152**, 1033–1068 (2013)
11. P. Degond, C. Appert-Rolland, J. Pettré, G. Theraulaz, Vision-based macroscopic pedestrian models. Kinet. Relat. Models **6**, 809–839 (2013)
12. R. Etikyala, S. Göttlich, A. Klar, S. Tiwari, Particle methods for pedestrian flow models: from microscopic to nonlocal continuum models. Math. Models Methods Appl. Sci. **24**, 2503–2523 (2014)
13. L. Gibelli, N. Bellomo, (eds.), *Crowd Dynamics. Vol. 1. Theory, Models, and Safety Problems*. Modeling and Simulation in Science, Engineering and Technology (Birkhäuser/Springer, Cham, 2018)
14. S.N. Gomes, A.M. Stuart, M.-T. Wolfram, Parameter estimation for macroscopic pedestrian dynamics models from microscopic data. SIAM J. Appl. Math. **79**, 1475–1500 (2019)
15. S. Göttlich, S. Knapp, P. Schillen, A pedestrian flow model with stochastic velocities: microscopic and macroscopic approaches. Kinet. Relat. Models **11**, 1333–1358 (2018)
16. E. Haber, L. Ruthotto, Stable architectures for deep neural networks. Inverse Problems **34**, 014004 (2017)
17. R.H.R. Hahnloser, R. Sarpeshkar, M.A. Mahowald, R.J. Douglas, H.S. Seung, Digital selection and analogue amplification coexist in a cortex-inspired silicon circuit. Nature **405**, 947–951 (2000)
18. D. Helbing, A fluid dynamic model for the movement of pedestrians. Complex Syst. **6**, 391–415 (1992)

19. D. Helbing, P. Molnár, Social force model for pedestrian dynamics. Phys. Rev. E **51**, 4282–4286 (1995)
20. K. Hornik, Approximation capabilities of multilayer feedforward networks. Neural Netw. **4**, 251–257 (1991)
21. R.L. Hughes, A continuum theory for the flow of pedestrians. Transp. Res. B **36**, 507–535 (2002)
22. J. Kaipio, E. Somersalo, *Statistical and Computational Inverse Problems*. Applied Mathematical Sciences, vol. 160 (Springer, New York, 2005)
23. A. Kirchner, A. Schadschneider, Cellular automaton simulations of pedestrian dynamics and evacuation processes, in *Traffic and Granular Flow'01*, ed. by M. Fukui, Y. Sugiyama, M. Schreckenberg, D.E. Wolf (Springer, Berlin, 2003), pp. 531–536
24. A. Klar, F. Schneider, O. Tse, Approximate models for stochastic dynamic systems with velocities on the sphere and associated Fokker-Planck equations. Kinet. Relat. Models **7**, 509–529 (2014)
25. A. Neelakantan, L. Vilnis, Q.V. Le, I. Sutskever, L. Kaiser, K. Kurach, J. Martens, Adding gradient noise improves learning for very deep networks (2015). http://arxiv.org/abs/1511.06807v1
26. B. Piccoli, A. Tosin, Pedestrian flows in bounded domains with obstacles. Contin. Mech. Thermodyn. **21**, 85–107 (2009)
27. B. Piccoli, A. Tosin, Time-evolving measures and macroscopic modeling of pedestrian flow. Arch. Ration. Mech. Anal. **199**, 707–738 (2011)
28. C. Rudloff, T. Matyus, S. Seer, D. Bauer, Can walking behavior be predicted? Analysis of calibration and fit of pedestrian models. Transp. Res. Rec. J. Transp. Res. Board **2264**, 101–109 (2011)
29. M. Schultz, *Stochastic Transition Model for Pedestrian Dynamics* (Springer, Cham, 2014), pp. 971–987
30. A. Tarantola, *Inverse Problem Theory and Methods for Model Parameter Estimation* (Society for Industrial and Applied Mathematics (SIAM), Philadelphia, 2005)
31. A. Tordeux, A. Schadschneider, *A Stochastic Optimal Velocity Model for Pedestrian Flow* (Springer, Cham, 2016), pp. 528–538
32. A. Tordeux, A. Schadschneider, White and relaxed noises in optimal velocity models for pedestrian flow with stop-and-go waves. J. Phys. A **49**, 185101 (2016)
33. A. Tordeux, M. Chraibi, A. Seyfried, A. Schadschneider, Prediction of pedestrian speed with artificial neural networks, in *Traffic and Granular Flow'17*, ed. by S.H. Hamdar (Springer, Cham, 2019), pp. 327–335
34. J. Wu, W. Hu, H. Xiong, J. Huan, Z. Zhu, The multiplicative noise in stochastic gradient descent: data-dependent regularization, continuous and discrete approximation (2019). http://arxiv.org/abs/1906.07405v1.
35. M.D. Zeiler, ADADELTA: an adaptive learning rate method (2012). http://arxiv.org/abs/1212.5701v1
36. Z. Zhu, J. Wu, B. Yu, L. Wu, J. Ma, The anisotropic noise in stochastic gradient descent: its behavior of escaping from sharp minima and regularization effects. http://arxiv.org/abs/1803.00195v5

High-Statistics Modeling of Complex Pedestrian Avoidance Scenarios

Alessandro Corbetta, Lars Schilders, and Federico Toschi

Abstract Modeling the behavior of pedestrians walking in crowds is an outstanding fundamental challenge, deeply connected with the physics of flowing active matter. The strong societal relevance of the topic, for its relations with individual safety and comfort, sparked vast modeling efforts from multiple scientific communities. Yet, likely because of the technical difficulties in acquiring experimental data, models quantitatively reproducing (statistical) features of pedestrian flows are scarce. This contribution has a twofold aim. First, we consider a pedestrian dynamics modeling approach previously proposed by some of the authors and based on Langevin equations. We review the approach and show that in the undisturbed and in the pairwise avoidance regimes (i.e., in absence of interactions between pedestrians and in case of avoidance of a single individual walking in the opposite direction) the model is in quantitative agreement with real-life high-statistics measurements. Second, moving towards the final goal of quantitative and generic crowd dynamics models, we consider the more complex case of a single individual walking through a dense crowd advancing in the opposite direction. We analyze the challenges connected to treating such dynamics and extend the Langevin model to reproduce quantitatively selected observed features.

A. Corbetta (✉) · L. Schilders
Department of Applied Physics, Eindhoven University of Technology, Eindhoven, The Netherlands
e-mail: a.corbetta@tue.nl

F. Toschi
Department of Applied Physics, Eindhoven University of Technology, Eindhoven, The Netherlands

Department of Mathematics and Computer Science, Eindhoven University of Technology, Eindhoven, The Netherlands

CNR-IAC, Rome, Italy

L. Gibelli (ed.), *Crowd Dynamics, Volume 2*, Modeling and Simulation in Science, Engineering and Technology, https://doi.org/10.1007/978-3-030-50450-2_3

1 Introduction

The quantitative understanding of the motion of pedestrians walking in public shared spaces is an outstanding issue of increasing societal urgency. The scientific challenges associated with the understanding and modeling of human dynamics share deep connections with the physics of active matter and with fluid dynamics [1, 17, 18, 20]. Growing urbanization yields higher and higher loads of users on public infrastructures such as station hubs, airports, or museums. This translates into more complex, high-density, crowd flow conditions, and poses increasing management challenges when it comes to ensuring individual safety and comfort. Achieving a quantitative comprehension and developing reliable models for the crowd motion may help, for instance, in the design of facilities or for optimizing crowd management.

Many among the proposed physical models for crowd dynamics rely on the analogy between pedestrians and active particles [13]. Either at the micro-, meso- or macro-scopic scale [1], pedestrians are usually represented as self-propelling particles whose dynamics is regulated by *ad-hoc* social interaction potentials (cf. reviews [8, 10]). While many features of crowd dynamics have been qualitatively captured by such modeling strategies (e.g., negative correlation between crowd density and average walking velocity, intermittent behavior at bottlenecks, formation of lanes in presence of opposing crowd flows [11, 23]), our quantitative understanding remains scarce, especially in comparison with other active matter systems [15]. This likely connects with the difficulty of acquiring high-quality data with sufficient statistical resolution to resolve the high variability exhibited by pedestrian behavior. Such variability includes, for instance, different choice of paths, fluctuations in velocity, rare events, as stopping or turning around [5]. Underlying a quantitative comprehension is the capability of explaining and modeling a given pedestrian dynamics scenario, including the variability that is measurable across many statistically independent realizations, which, ultimately, enables one to estimate the statistics of, e.g. permanence and evacuation times, positions, fluxes, Level-of-Service [9] and tackle questions as "which are the common behaviors in a given facility? Which rare (and potentially dangerous) events can occur? How likely are they?"

In this chapter we discuss the challenges connected to the quantitative modeling of a relevant and ubiquitous—yet conceptually simple—crowd dynamics scenario which involves one pedestrian, onward referred to as the *target pedestrian*, walking in a crowd of N other pedestrians that are going in the opposite direction. We shall identify this scenario as 1 vs. N, of which, in Fig. 1, we report four consecutive snapshots taken from real-life recordings. Our analysis employs unique measurements collected through a months-long, 24/7, real-life experimental campaign that targeted a section of the main walkway of Eindhoven train station, in the Netherlands. Thanks to state-of-the-art automated pedestrian tracking technologies, fully developed in house [3–6, 14], we collected millions of high-resolution pedestrian trajectories including hundreds of occurrences of 1 vs. N scenarios.

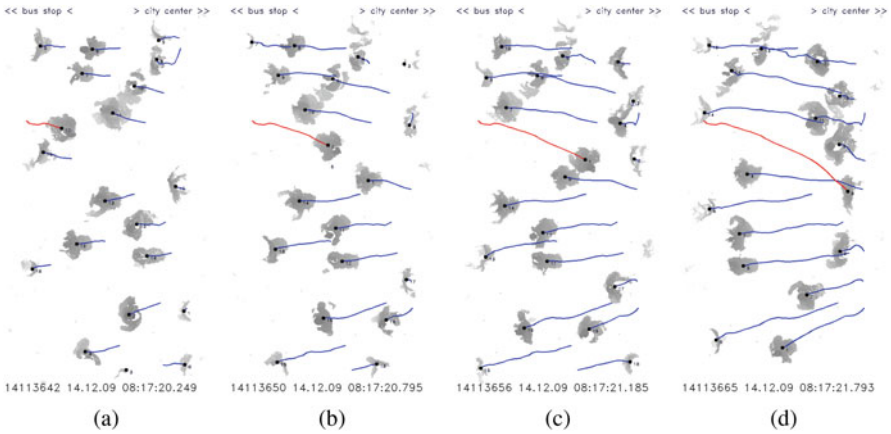

Fig. 1 Avoidance scenario, 1 vs. N, involving the target pedestrian walking towards the right (red trajectory), while a crowd of pedestrians proceeds in opposite direction (blue trajectories). We report four snapshots in chronological order. The target pedestrian escapes collisions by walking diagonally with respect to the longitudinal axis of the corridor (the most likely, in some sense "natural," walking direction that, in this figure, corresponds to the horizontal direction). In the scenario considered, N is the number of pedestrians walking in opposition to the target that have appeared in the field of view of our sensors in the time window when the target was present. Furthermore, we restrict to scenarios in which no person walking in the same direction of the target is present

In previous works, we explored such conditions in the low density limit. In particular, we proposed quantitative models for the case of a pedestrian walking undisturbed (1 vs. 0) [5] and for the case of a pedestrian avoiding a single individual coming in the opposite direction (1 vs.1) [6]. This contribution addresses the complexity, from the modeling and from the data analytic points of view, arising when dealing with the 1 vs. N generalization. Let $z_1(t) = (x_1(t), x_p(t))$ be the state of the target pedestrian, which includes his/her instantaneous position, $x_1(t)$, and, with abuse of notation, his/her *desired path*, $x_p(t)$ (in the following, the desired path will be a coordinate parameterizing the straight line that a pedestrian aims at maintaining; this could be generalized to include, e.g. a target destination).

Our final model, assuming a superposition of pair-wise interactions having the form proposed in [6], involves the Newton-like dynamics

$$\ddot{z}_1 = F(\dot{z}_1) + \mathcal{N}(\{K(z_1, x_i), i = 2, \ldots, N+1\}) + \sigma \dot{W}, \tag{1}$$

where the $\{x_i\}$'s ($i = 2, \ldots, N$) are the positions of the opposing pedestrians, $F(\dot{z_1})$ is an active term regulating the onward motion of the target pedestrian, $K(z_1, x_i)$ is the pair-wise social interaction force between the target and the i-th individual, $\mathcal{N}(\cdot)$ is a (non-linear) superposition rule for the pair-wise forces. Finally, a white Gaussian noise term $\dot{W}$, with intensity σ, provides for stochastic fluctuations.

The present analysis shows, on the basis of high statistics measurements, how simplifying hypotheses based on symmetry made for the 1 vs. 0 and 1 vs. 1 cases [5, 6] do not hold in the general 1 vs. N case (as could have been expected, since the influence of the boundary becomes relevant). Furthermore, we discuss how the interplay of the propulsion dynamics, determined by $F(\dot{z}_1)$, and the presence of many interaction forces, determined by the term $\mathcal{N}(\cdot)$, may yield nonphysical effects. We present therefore some modifications to Eq. (1) that enable to recover features of the observed dynamics at the "operational level" (e.g., local collision avoidance movements, cf. [12] for a reference). This will open the discussion on how to perform data acquisition and how to achieve quantitative modeling to address the dynamics at the, so-called, "tactical level," in which broader-scale individual decisions are taken. These include, for instance, the definition of a preferred path, selected by each individual within the current room/building, to reach a desired destination.

This chapter is structured as follows: in Sect. 2 we introduce our real-life pedestrian tracking setup; in Sect. 3 we review our previous quantitative model for pedestrians walking in diluted conditions; in Sect. 4 we discuss through physical observables the more generic 1 vs. N scenario, and introduce some of the complexities connected to its analysis and modeling; in Sect. 5 we address generalizations of our previous model to such case. A final discussion in Sect. 6 closes the chapter.

2 Measurement Setup and 1 vs. N Avoidance Scenario

In this section, we briefly review the measurement campaign and the technique employed to collect the data that we consider throughout this chapter. Relevant references for the details of the campaign and of the measurement technique are also supplied. Then we provide a formal definition which unambiguously identifies 1 vs. N scenarios.

The pedestrian dynamics data considered have been collected in the period October 2014–March 2015 in a 24/7 pedestrian trajectory acquisition campaign in the main walkway of Eindhoven train station [4] (see Fig. 2). The measurements were collected through a state-of-the-art pedestrian tracking system, built in-house, and based on an array of overhead depth sensors (Microsoft Kinect™ [16]). The sensor view-cones were in partial overlap and allowed us to acquire data from a full transversal section of the walkway; our observation window had a size of about 9 m in the transversal direction and of 3 m in the longitudinal direction.

Depth sensors provide depth maps at a regular frame rate (in our case 15 Hz), i.e. the distance field between a point and the camera plane. Examples of depth maps (with superimposed tracking data) are reported in Fig. 1. Notably, depth maps are non-privacy intrusive: no features allowing individual recognition are acquired. Nevertheless, depth maps enable accurate pedestrian localization algorithms (see [2, 3, 21] for general conceptual papers about the technique, [4] for technical details

Fig. 2 Picture of the pedestrian tracking setup in the main walkway of Eindhoven train station where the data described here were collected. We overlay a sketch of the measurement area, reported at the floor level, and of the initial part of the view-cones of the four depth sensors used to acquire raw depth data. As the sensors had overlapping view, we could acquire (after appropriate data fusion) continuous depth maps of the full measurement area, as those in Fig. 1 (the picture is taken facing the city center, i.e. the observer is walking a trajectory analogous to that of the target pedestrian in Fig. 1). The axes corresponding to the physical coordinates (ξ, η) are also sketched (the canonical (x, y) coordinates are here reserved for the position of a pedestrian in reference to their preferred path)

about this campaign, and [14] for a more recent, highly accurate, machine learning-based localization approach).

Our measurement location was crossed daily by several tens of thousands people and, depending on weekday and hour, the site underwent different crowd loads. Pedestrians could often walk undisturbed at night hours or, more rarely, during off-peak times (i.e., late morning and early afternoon). Else, our sensors could measure highly variable crowding conditions ranging from uni-directional to bi-directional flows with varying density levels.

We consider here scenarios that involve exactly one target pedestrian walking to either of the two possible directions, while other N individuals are walking towards the opposite side. This means that in accordance to our recording, the trajectory of the target pedestrian has been perturbed exclusively by these further N, and no other pedestrian walking in the direction of the target was observed simultaneously (and thus in the neighborhood). In [6] we proposed a graph-based approach to describe these conditions and to efficiently find them within large databases of Lagrangian data.

3 Physics and Modeling of the Diluted Dynamics (1 vs. 0 and 1 vs.1)

In this section we review the model for diluted pedestrian motion and pairwise interactions that we proposed in our previous papers [5] and [6]. We consider a crowd scenario to be diluted whenever the target pedestrian can move freely from the influence of other peer pedestrians (e.g., incoming, or moving close by, i.e. 1 vs. 0 condition) or they are just minimally affected (1 vs.1).

In diluted conditions, individuals crossing a corridor typically move following (and fluctuating around) preferred paths that develop as approximately straight trajectories. Preferred paths belong to the tactical level of movement planning, in other words, changes in preferred paths are connected to individual choices performed at level overarching fine scale navigation movements (operational level). Without loss of generality, we consider a coordinate system such that the state of a pedestrian can be described through three position-like variables, $z = (x, y, y_p)$, and relative velocities (in the following indicated, respectively, with u, v, and $\dot{y}_p$). In particular, y_p parameterizes the preferred path (that we assume parallel to the x-axis) and (x, y) identifies the instantaneous pedestrian position.

In this reference system, as x varies, individuals approach (or, conversely, get farther apart from) their destinations. In the transversal direction, fluctuations of amplitude $\tilde{y} = y - y_p$ occur around the center of the preferred path, y_p. In absence of avoidance interactions with other pedestrians, we expect $\dot{y}_p = 0$, at least on the tactical time-scale. Conversely, we expect that the need of avoiding a pedestrian incoming with opposite velocity will be reflected in a dynamics for y_p.

Following [6], we model the motion of a target pedestrian in a 1 vs.1 condition with a Langevin dynamics as

$$\frac{\mathrm{d}x}{\mathrm{d}t} = u(t) \tag{2}$$

$$\frac{\mathrm{d}y}{\mathrm{d}t} = v(t) \tag{3}$$

$$\frac{\mathrm{d}u}{\mathrm{d}t} = -4\alpha_i u(u^2 - u_{p,i}^2) + \sigma \dot{W}_x - e_x F_{short} \tag{4}$$

$$\frac{\mathrm{d}v}{\mathrm{d}t} = -2\lambda v - 2\beta(y - y_p) + \sigma \dot{W}_y - e_y F_{short} + F_{vision}, \tag{5}$$

$$\frac{\mathrm{d}y_p}{\mathrm{d}t} = \dot{y_p}(t) \tag{6}$$

$$\frac{\mathrm{d}\dot{y}_p}{\mathrm{d}t} = F_{vision} - 2\mu \dot{y}_p. \tag{7}$$

In the remainder of this section we detail the expressions and the modeling ideas underlying the preferred velocities, $u_{p,i}$, the friction terms, $-2\lambda v$ and $-\mu \dot{y}_p$, and the social forces F_{short} and F_{vision}. We anticipate that F_{short} and F_{vision} are

Table 1 Parameters for the model in Eqs. (2)–(7)

1 vs. 0 and 1 vs.1		1 vs.1 only	
Desired walking speed		*Vision f. inter. scale*	
$u_{p,w}$ (walkers)	$1.29\,\mathrm{ms}^{-1}$	R	2.4 m
Desired running speed		*Contact-av f. inter. scale*	
$u_{p,r}$ (runners)	$2.70\,\mathrm{ms}^{-1}$	r	0.6 m
Coeff. $U(u)$, *walkers*		*Desired path friction*	
α_w	$0.037\,\mathrm{m}^{-2}\mathrm{s}$	μ	$1.0\,\mathrm{s}^{-1}$
Coeff. $U(u)$, *runners*		*Vision f. intensity*	
α_r (runners)	$0.0015\,\mathrm{m}^{-2}\mathrm{s}$	A	$1.5\,\mathrm{ms}^{-2}$
Noise intensity		*Contact-av f. intensity*	
σ	$0.25\ \mathrm{ms}^{-3/2}$	B	$0.7\,\mathrm{ms}^{-2}$
Transv. confinement		*Vision f. angular dep.*	
β	$1.765\ \mathrm{m}^{-2}\mathrm{s}$	χ_{vision} (threshold)	20°
Transv. friction		*Contact-av f. angular dep.*	
λ	$0.297\,\mathrm{s}^{-1}$	χ_{short} (threshold)	90°
Runner % in 1 vs. 0	4.02%	Runner % in 1 vs.1	0.2%

exponentially decaying social interaction forces depending on the distance between the target pedestrian and the other individual. Consistently, they vanish in the case of a pedestrian walking undisturbed, thus, in such case, $\dot{y}_p = 0$ holds, and the model restricts to that considered in [5]. For the sake of brevity, in Eqs. (2)–(7) we omitted the subscript "1" for the target pedestrian variables as in the notation in Eq. (1), as in the current case there is no ambiguity (i.e., x should be written as x_1, and similarly for the other variables. However, the position variables of the second pedestrian, like x_2, are in fact hidden in the social force terms).

The second-order dynamics in Eqs. (2)–(7) includes the interplay of activity, fluctuations, and interactions. In [5] we showed that, in absence of interactions, the motion of a pedestrian is characterized by small and frequent Gaussian velocity fluctuations around a preferred and stable velocity state, $(u, v) = (\pm u_p, 0)$. Large fluctuations can be observed as well, although rarely: for a narrow corridor, the prominent case is the transition between the two stable velocity states $u \to -u$, which comes with a direction inversion. The simplest conceivable velocity potential, $U = U(u)$, allowing for this phenomenology is a symmetric polynomial double well with minima at $u = \pm u_p$, i.e. $U(u) \sim (u^2 - u_p^2)^2$, from which one has the force term $-\partial_u U(u) \sim -u(u^2 - u_p^2)$ in Eq. (4). In combination with a small Gaussian noise (term $\sigma \dot{W}_x$), this yields small-scale Gaussian fluctuations and rare Poisson-distributed inversion events (see also [7] for a path-integral based derivation of the event statistics), both in excellent agreement with the data (cf. [5]). In Eq. (4), we included the subscript i on the preferred velocity and on the force intensity coefficient, respectively $u_{p,i}$ and α_i, to allow independent "populations" of pedestrians having different moving features (e.g., walking vs. running) combined in different percentages (see Table 1). In Fig. 3a we report a comparison of the

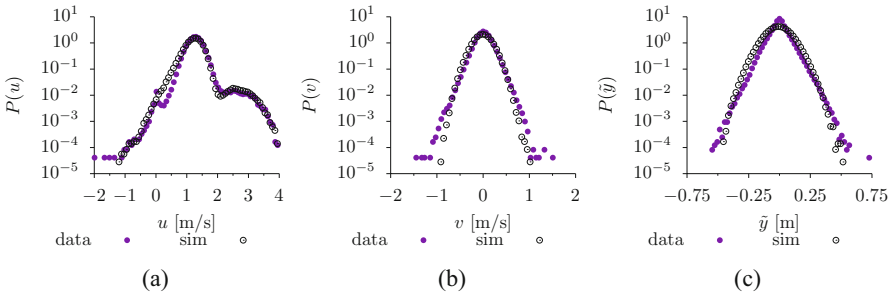

Fig. 3 Probability distribution functions of walking velocity and positions for pedestrians walking undisturbed 1 vs. 0: comparison between measurements (purple dots) and simulations of Eqs. (2)–(7) in absence of interaction forces (circle markers, simulation parameters in Table 1). The panels contain, respectively, (**a**) longitudinal velocities (u), (**b**) transversal velocities (v), (**c**) transversal positions with respect to the preferred path ($\tilde{y} = y - y_p$). Pedestrians walk most frequently at around 1.29 m/s (cf. (**a**)). Besides, we observe a small fraction of running pedestrians, about 4%, contributing to the hump at above 2 m/s and pedestrians turning back, providing negative velocities contributions. (**b**) Transversal fluctuations in velocity appear to be well approximated by a Gaussian distribution, while (**c**) transversal positions exhibit small deviations from a Gaussian behavior. The model captures quantitatively the complete longitudinal velocity statistics including the running hump as well as the inversion events. The transversal dynamics is also well approximated as a stochastic damped harmonic oscillator (Eqs. (3) and (5))

probability distribution function of the longitudinal velocity u for undisturbed pedestrians in case of measurements and simulated data and a good agreement is apparent.

We treat the transversal dynamics as a damped stochastic harmonic oscillator centered at y_p, respectively, via the friction force $-2v\lambda$, the Gaussian noise $\sigma \dot{W}_y$, and the harmonic confinement $-2\beta(y - y_p)$. This yields Gaussian fluctuations of v and $\tilde{y}$, which are also in very good agreement with the measurements, Fig. 3b, c. For both the longitudinal and transversal components we employ white in time (i.e., δ-correlated) and mutually uncorrelated Gaussian noise forcing ($\dot{W}_x$, $\dot{W}_y$), with equal intensity (σ), as validated in [5]. Our hypotheses on the noise structure are guided by simplicity, yet they are somehow arbitrary and not mandatory [20].

Interactions enrich the system of social force-based coupling terms and of a second-order deterministic dynamics for y_p (Eqs. (6)–(7)). We consider two conceptually different coupling forces:

- a long-range, vision-based, avoidance force

$$F_{vision}(x_1, y_1, x_2, y_2) = -\text{sign}(e_y) A \exp(-d^2/R^2) \chi_{vision}(\tilde{\theta}), \tag{8}$$

where e_y is the y component of the unit vector pointing from (x_1, y_1) to (x_2, y_2) (i.e., the unit vector $(e_x, e_y) = (x_2 - x_1, y_2 - y_1)/d$, d being the Euclidean distance between the positions of the pedestrians, $d = ||(x_2 - x_1, y_2 - y_1)||_2$), $\tilde{\theta}$ is the angle between the x-axis and the distance vector $(x_2 - x_1, y_2 - y_1)$,

$\chi_{vision}(\tilde{\theta})$ is the indicator function that is equal to 1 if $|\tilde{\theta}| \leq 20°$ and vanishing otherwise, A and R are an amplitude and a scale parameter.

- a short-range contact avoidance force

$$F_{short}(x_1, y_1, x_2, y_2) = B \exp(-d^2/r^2)\chi_{short}(\tilde{\theta}), \tag{9}$$

where $\chi_{short}(\tilde{\theta})$ is an indicator function that is equal to 1 if $|\tilde{\theta}| \leq 90°$ and vanishing otherwise, B and r are an amplitude and a scale parameter.

Note that F_{vision} operates on the transversal direction only and appears both in Eqs. (5) and (7). In other words, it influences the dynamics of $\tilde{y}$ only through $\dot{y}_p$. In fact, combining Eqs. (5) and (7), the evolution of $\tilde{y}$ satisfies

$$\frac{d^2\tilde{y}}{dt^2} = -2\lambda\frac{d\tilde{y}}{dt} - 2(\mu - \lambda)\dot{y}_p - 2\beta\tilde{y} + \sigma\dot{W}_y - e_y F_{short}. \tag{10}$$

Vision and contact avoidance forces allow to reproduce the overall avoidance dynamics. We analyze this by considering how the pedestrian distance, projected on the y direction, transversal to the motion, changes during the avoidance maneuvers. In particular, we consider three projected distances:

1. Δy_i: the absolute value of the transversal distance, as the pedestrians appear in our observation window;
2. Δy_s: the absolute value of the transversal distance, at the instant of minimum total distance between the pedestrians;
3. Δy_e: the absolute value of the transversal distance when the pedestrians leave our observation window.

In Fig. 4, we report the conditioned averages of these distance, comparing measurements and simulations. In particular, Fig. 4a contains the average transversal distance when the two pedestrians are closest (i.e., side-by-side, $e(\Delta y_s)$), conditioned to their entrance distance (Δy_i). We observe that for $\Delta y_i \lessapprox 1.4$ m avoidance maneuvers start and pedestrians move laterally to prevent collisions. In case of pedestrians entering facing each other ($\Delta y_i \approx 0$), on average they establish a mutual transversal distance of about 75 cm. As experience suggests, for large transversal distances no concrete influence is measured. In Fig. 4b, we report the average transversal distance as the two pedestrians leave the observation area ($e(\Delta y_e)$) conditioned to the transversal distance at the moment of minimum distance (Δy_s). We observe that, on average, the mutual distance remains unchanged. This means that the act of avoidance impacts on the preferred path, which drifts laterally as collision is avoided and then is not restored. We can read this as an operational-level dynamics (avoidance gesture), that impacts on the coarser-scale tactical-level dynamics, as the preferred path gets changed. Remarkably, the model is capable of quantitatively recovering these features. We refer the interested reader to [6] where we additionally discuss the full conditioned probability distributions of

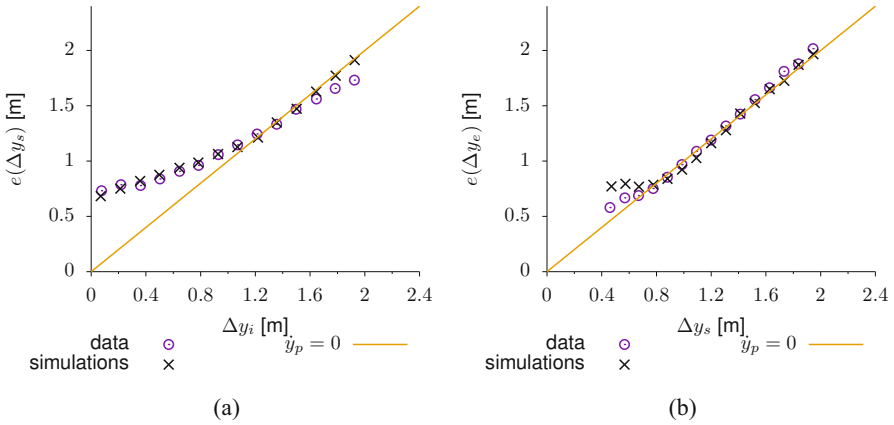

Fig. 4 Average conditioned transversal distance between two pedestrians in a 1 vs.1 condition: comparison between data and simulations. (**a**) Average, $e(|\Delta y_s|)$, of absolute lateral distance when at the closest point (side-by-side, y-axis) conditioned to the absolute lateral distance when at the entrance (Δy_i, x-axis). (**b**) Average, $e(|\Delta y_e|)$, of absolute lateral distance when at the exit (y-axis), conditioned to the absolute lateral distance when side-by-side ($|\Delta y_s|$, x-axis). The diagonal line identifies cases in which the transversal distance between the pedestrians has not changed from one measurement point to the next, which can be interpreted as a preferred path that remained unchanged as pedestrian crossed the observation window. The model in Eqs. (2)–(7) reproduces with high accuracy the avoidance dynamics

the transversal distances plus other statistical observables such as pre- and post-encounter speed and collision counts.

Note that both scenarios considered so far, 1 vs. 0 and 1 vs.1, feature a translational symmetry in the transversal direction, i.e. the dynamics is unchanged by rigid translations: $y \to y + c$, $y_p \to y_p + c$.

4 Observables of the 1 vs. N Scenario

As a target pedestrian walks avoiding an increasing number of other individuals moving in the opposite direction (i.e., 1 vs. N, $N > 1$), his or her trajectory acquires a richer and more fluctuating dynamics. In Fig. 5, we compare trajectories of pedestrians moving towards the city center (i.e., from left to right) in case of undisturbed pedestrians (1 vs. 0, Fig. 5a) and in case 1 vs. 10^+ (i.e., $N \geq 10$, Fig. 5b). Note that the trajectories are reported in the physical coordinate system, (ξ, η), where the first component is parallel to the span of the corridor and the second component is in the transversal direction. These coordinates must not be confused with (x, y, y_p) which are instead aligned with the individual preferred paths. In this random sample of trajectories, it is already visible that in the case of individual pedestrians the absence of incoming "perturbations" allows less

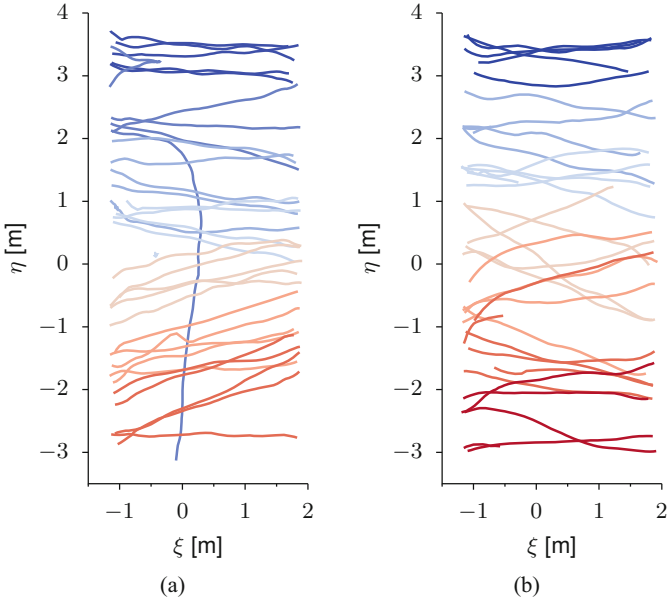

Fig. 5 Random selection of trajectories of pedestrians walking from the bus station side of the train station toward the city center (from left to right in this reference), in case (**a**) of pedestrians walking alone (i.e., 1 vs. 0) or (**b**) in case 1 vs. 10. In case of pedestrians walking alone (**a**), the trajectories are mostly rectilinear, superimposing small fluctuations to an intended path. In rare cases we observe large deviations, as, for instance, inversions or drastic trajectory changes. In case of target pedestrians facing a crowd (**b**), the trajectories exhibit ample deviations following the need of avoiding incoming individuals. Avoidance maneuvers effectively increase fluctuations, direction changes along the path, and dispersion in the position in which the pedestrian leaves the observation zone. The trajectories are here reported in physical coordinates (ξ, η) (cf. Fig. 2)

pronounced fluctuations that, in most of the cases occur around well-defined straight paths, i.e. by definition, the preferred paths. It must be noticed that these preferred paths are not, generally, parallel to the ξ-axis. Rare largely deviating trajectories also appear, in the figure it is reported a case of trajectory inversion. Conversely, the presence of incoming pedestrians, in addition to enhancing small-scale fluctuations, frequently yields curved or S-like trajectories for the target individual, as an effect of successive avoidance maneuvers.

An incoming crowd enhances the tendency of the target pedestrian to keep the right-hand side. In Fig. 6a we report the probability distribution function of transversal positions (in the corridor reference, i.e., $pdf(\eta)$). As the number of incoming pedestrians increases, the η distribution increasingly peaks on the right-hand side, remaining focused in the close proximity of the wall. Out of the bulk and close to a wall, avoidance remains easiest and straight trajectories can be followed, see Fig. 5b.

On the opposite, avoidance maneuvers are strongest in the bulk, and of magnitude increasing with the number of incoming pedestrians, N, at least up to a threshold.

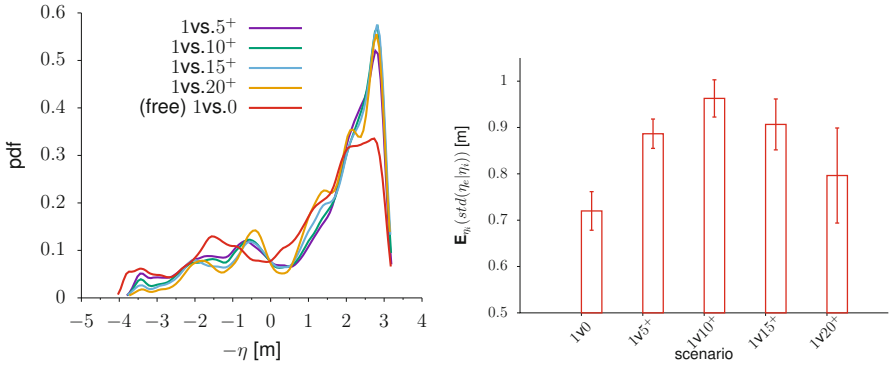

Fig. 6 (**a**) Probability distribution function of traversal positions, η, for target pedestrians in free flow (1 vs. 0) vs. an increasing number of incoming pedestrians (note that the η axis is flipped to $-\eta$ with respect to the reference in Fig. 2 such that the right side of the plot coincides with the right side of the corridor for an observer located as in Fig. 2). Although the corridor is rectangular, the position distribution is not uniform. We believe that this possibly connects both to cultural biases and to the geometry upstream with respect to the observed areas. The entrance area is, in fact, asymmetric and wider on its right end. As the incoming pedestrians increase in number, so does the tendency to choose for the right side of the corridor. (**b**) Aggregated statistics of the outlet position dispersion conditioned to inlet location and incoming flow. The inlet distribution in (**a**) maps to an articulated outlet distribution with dependency on inlet and flow conditions. We report it in aggregated form by averaging the conditioned standard deviation of the outlet position, $std(\eta_e|\eta_i)$, over the inlet position η_i, (hence, no further dependency on η_i remains). The evaluation is restricted to the bulk of the flow, $-1.5\,\text{m} \leq \eta_i \leq 3.1\,\text{m}$, i.e. measurements within half a meter from the left wall and from the right-side peak are neglected. Error bars report the standard error on the average. As the incoming crowd grows, and up to the case of 10 incoming pedestrians, so it grows the variance in the outlet position distribution. In other words, the need of avoidance induces larger and larger deviations from the average trajectory. Further increments of the number of incoming pedestrians yield a reduction in dispersion. This likely connects with the fact that the target pedestrian remains "funneled" by the incoming crowd. According to (**a**) this happens with highest probability in proximity of the right-hand side wall

In Fig. 6b we report the aggregated measurement of the dispersion in the transversal position as the target pedestrian leaves our observation window, η_e, conditioned to their entrance position, η_i. Specifically we report the average, computed over η_i, of the standard deviation of η_e conditioned to η_i, in formulas $\mathbf{E}_{\eta_i}(std(\eta_e|\eta_i))$. In other words, for each entrance location (considered after a binning of the area, $-1.5\,\text{m} \leq \eta_i \leq 3.1\,\text{m}$, into 20 uniformly spaced sub-regions), we consider the conditioned standard deviation of exit location(s). As this aims at measuring the "point-dispersion" from each individual entrance site, we average all these point-dispersion measurements. We notice that the average point-dispersion increases by 20% from scenario 1 vs. 0 to 1 vs. 5^+ and by a further 10% when restricting to 1 vs. 10^+. If we restrict to a larger number of incoming pedestrians, the average dispersion starts reducing. This is likely a consequence of the fact that, in many

cases, the target pedestrian remains "funneled" in a narrow space left by the incoming crowd.

Considering the increment in the variability and in the fluctuations of the trajectories for the generic 1 vs. N case, for large N, and the relative shortness of our observation window (about 3 m), contrarily to the 1 vs. 0 and 1 vs.1 cases, our data only allows us to evaluate operational-level movements. In other words, within our observation window we can collect statistics about the fine scale avoidance but not on the way the preferred path gets modified on a longer time-scale. On this bases, in the next section we present a model for the 1 vs. N scenario.

5 Modeling 1 vs. N Dynamics via Superposition of Interactions

In this section we address the generalization of the model in Eqs. (2)–(7) (cf. Sect. 3) as the number of incoming pedestrians increases. Our underlying hypothesis is the existence of a superposition rule for the pairwise vision-based and contact avoidance forces in presence of more than one opposing pedestrian. In the next equations, we indicate these as $\mathcal{N}_{short}(\{\cdot\})$ and $\mathcal{N}_{vision}(\{\cdot\})$. To emphasize the generality of the superposition, we set the argument of these functions to the whole set of pairwise forces, in general referred to as $\{f_i\}$. The linear superposition rule (or linear superposition of effects, i.e. $\mathcal{N}(\{f_i\}) = \sum_i f_i$), ubiquitous in classical physics, has been widely considered in pedestrian dynamics (e.g., [8, 11]), but also it has been criticized (e.g., [19]). Notably, in a context of linear superposition of forces, the total force intensity may diverge in presence of a large crowd. Most importantly, however, it is likely that the individual reactions are dependent on a (weighted) selection of surrounding stimuli rather than on their blunt linear combination [19]. In formulas, we consider the following dynamics:

$$\frac{dx_1}{dt} = u_1 \tag{11}$$

$$\frac{du_1}{dt} = F(u_1) - \mathcal{N}_{short}(\{e_{x,i} F_{short,i}\}) + \sigma_x \dot{W}_x \tag{12}$$

$$\frac{dy_1}{dt} = v_1 \tag{13}$$

$$\frac{dv_1}{dt} = -2\lambda v_1 - 2\beta(y_1 - y_p) - \mathcal{N}_{short}(\{e_{y,i} F_{short,i}\}) + \mathcal{N}_{vision}(\{F_{vision,i}\}) + \sigma_y \dot{W}_y \tag{14}$$

$$\frac{dy_{p,1}}{dt} = \dot{y}_{p,1} \tag{15}$$

$$\frac{d\dot{y}_{p,1}}{dt} = -2\mu \dot{y}_{p,1} + \mathcal{N}_{vision}(\{F_{vision,i}\}), \tag{16}$$

here the subscripts "1" and i ($i = 2, \ldots, N+1$) identify explicitly the target pedestrian and the rest of the incoming crowd. For the sake of brevity, we used the notation $\{F_{vision,i}\}$ to indicate the set of pair-wise forces $\{F_{vision,i}, i = 2, \ldots, N+1\}$ between the target pedestrian and the N other individuals.

The highly complex dynamics, in combination with the relative shortness of our observation window, allows us to highlight some modeling challenges connected to finding and validating functional forms to the terms in Eqs. (11)–(16). We list these here and address them through additional hypotheses or simplifications on the dynamics model.

- *Bi-stable dynamics vs. contact avoidance forces.* Avoidance forces interplay with our bi-stable velocity dynamics (cf. Fig. 7). Effectively they increase the probability of hopping between the two stable velocity states and provide nonphysical trajectory inversions. Although it is reasonable to expect an higher trajectory inversion rate when a pedestrian faces a large crowd walking in opposite direction, such rate has to be probabilistically characterized. In modeling terms, we expect the height of the potential barrier $U(u_p) - U(0)$ between the stable velocity state, $u = \pm u_p$, and the zero walking velocity, $u = 0$, to be altered by the incoming crowd. In absence of validation data, here we simplify our model by considering a second-order Taylor expansion of the potential U around $u = +u_p$. In this way, $u = +u_p$ remains the only stable state of the dynamics and trajectory inversions are therefore impossible. While this is a strong simplification, it serves the present purpose of studying 1 vs. N scenarios.
- *Preferred path.* In presence of many consecutive avoidance maneuvers, as in a typical 1 vs. N case, the trajectory of the target pedestrian is continuously adjusted. These adjustments likely include modifications of the preferred path. Our monitoring area along the longitudinal walking direction is relatively short (about 3 m). As such, local avoidance maneuvers (operational level) remain mostly indistinguishable for re-adjustments of the preferred path (tactical level). Therefore, we opt to address path variations as avoidance maneuvers (i.e., operational-level movements). As we hypothesize that tactical-level movements are negligible, we opt to set the preferred path to the average longitudinal path measured. Longer recording sites would open the possibility of addressing statistically the dynamics of preferred paths in presence of many successive interactions.
- *Preferred velocity.* The diluted motion comes with a measurable notion of preferred walking velocity (or velocities in case of multiple walking modes). In Fig. 3a we report the pdf of the longitudinal component of the velocity for undisturbed pedestrians, u, displaying the superposition of two dominant behaviors, pedestrians walking and running with averages velocity $u_{p,w} = 1.29$ m/s, $u_{p,r} = 2.70$ m/s, respectively. In the generic 1 vs. N case, we expect an "adjusted" preferred velocity depending on the surrounding traffic. In other words, although a pedestrian would keep his/her desired velocity constant at all times, the constraints given by the presence of other pedestrians require its temporary reduction. The velocity reduction is generally reported in average

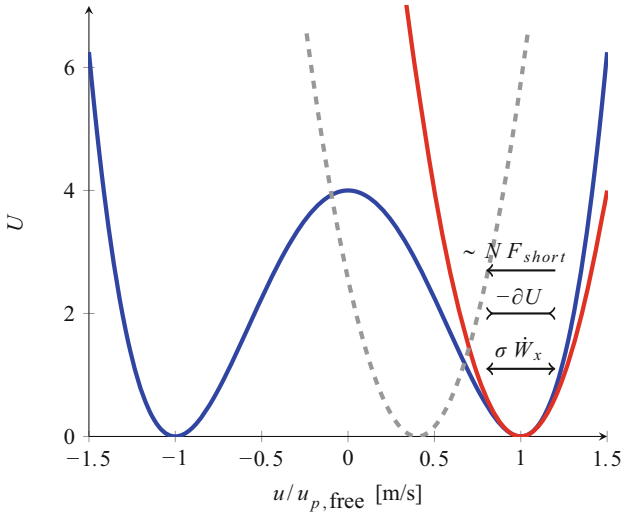

Fig. 7 The longitudinal walking dynamics of a pedestrian in diluted conditions, according to Eqs. (2)–(4), is defined by the interplay of a velocity gradient force, $-\partial U$, that brings the system toward a stable state (in this case, say $u = +u_p$; a sketch of the potential U is reported in blue), a random forcing, σW_x, that brings the system away from the stable state (and possibly yields transitions between the stable states), and the longitudinal component of the short-range, contact avoidance, force, F_{short}. As these forces linearly accumulate when N increases, the system gets more and more "unbalanced" toward the unstable state $u = 0$ or the negative velocities. In other words excessive forcing increases the hopping probability towards negative velocities and effectively reduces the potential barrier that separates the stable states. Although it is reasonable to expect that the probability of trajectory inversion increases in presence of a large incoming crowd, the phenomenon has to be probabilistically characterized. Here we bring this probability (unrealistically high for the original double well potential, as in [5, 6]) to zero, by considering a Taylor approximation of the potential around the positive velocity stable state, i.e. $U(u) \approx C(u-u_p)^p$, where C is a positive constant. Finally, in presence of a large incoming crowd, the desired walking velocity (that one would keep in diluted flow) most likely cannot be employed due to "resistance" of the surrounding crowd. Hence, the effective walking velocity is reduced (cf. fundamental diagram in [4]). In presence of enough data the statistics of such reduction can be quantified. Here, focusing on the path fluctuations, we set the locally preferred velocity to the average longitudinal walking velocity of the target pedestrian. This translates the velocity potential towards velocities lower in absolute value (gray dashed line)

terms through fundamental diagrams (i.e., density–velocity relations [22]) that for our setup we quantified in [4]. At the microscopic level, we expect a number of elements influencing the adjusted preferred speed, e.g. surrounding crowd density, geometry of and position in the domain, presence of a visible walkable free space within the incoming crowd, etc. These aspects are also likely statistically quantifiable in presence of a large enough observation window, that enables to disentangle tactical- and operational-level aspects of the dynamics. Similarly to the preferred path, here we set the preferred velocity to the average walking velocity of the target pedestrian.

- *Superposition rule for vision-based interactions.* Vision-based interactions are long-range, and relatively narrow angled (cf. Sect. 3 and [6]). This makes them mostly irrelevant in a 1 vs. N condition as in Fig. 1, where there is limited frontal interaction as compared to interactions with other neighboring neighbors. As such, we opt to simplify the superposition rule for this forces to a linear summation, that is $\mathcal{N}_{vision}(\{f_i\}) = \sum_{i=2}^{N+1} f_i$.

Given these simplifications, we consider four superposition rules for the short-range contact avoidance forces:

(C1) $\mathcal{N}_{short}(\{f_i\}) = \sum_{i=2}^{N+1} f_i$—this is a linear extension to Eqs. (4)–(5) and serves as a baseline reference;
(C2) $\mathcal{N}_{short}(\{f_i\}) = \frac{1}{10} \sum_{i=2}^{N+1} f_i$—this case is analogous (C1), but a scaling of the interaction by a factor 10;
(C3) $\mathcal{N}_{short}(\{f_i\}) = \frac{1}{10} \sum_{i=2}^{N+1} f_i$ and $\alpha \to 10\alpha$—this case extends (C2) by steepening the velocity potential around the stable velocity state by a factor 10;
(C4) $\mathcal{N}_{short}(\{f_i\}) = \frac{1}{2} \max_i(f_i)$—this is a non-linear superposition of forces: because of the decreasing monotonicity of the short-range interactions, this is equivalent to consider interactions exclusively with the nearest-neighbor.

Considering the stochastic dynamics, we compare the simulations and data as follows. We sample 200 random occurrences in a 1 vs. N scenario from our measurement in which the target pedestrian enters in the bulk section of the domain; each scenario is similar to what depicted in Fig. 1. We specifically consider $N = 10^+$, that according to Fig. 6b, spans among the most challenging cases in terms of variability of the paths. For each occurrence, we opt to simulate through Eqs. (11)–(16) exclusively the target pedestrian dynamics, while we update the position of the other N individuals according to the data (our simulation step, Δt, is equal to the sampling period of the sensor, i.e. $(15\,\text{Hz})^{-1} = 66\,\text{ms}$). Employing the measured initial position of the target pedestrian and initial velocity sampled from the target measured walking velocities, we simulate his or her dynamics, from the entrance in our observation window to the exit, for $M = 50$ independent realizations. We report in Fig. 8 examples of such simulations (green lines) overlaying real measured trajectories of the target pedestrian and of the rest of the crowd (respectively, in red and blue). Employing the simulated trajectories, we can compute an ensemble-averaged path, $\bar{z}_1^r(t) = (\bar{x}_1^s(t), \bar{y}_1^s(t), \bar{y}_{p,1}^s(t))$ (i.e., with some abuse of terminology from the quantum path integral language [7], this would correspond to the "classical path") as

$$\bar{z}_1^s(t) = \frac{1}{M} \sum_{k=1}^{M} z_{1,j}^s(t), \tag{17}$$

where j indexes the realizations, the average is performed on the position vectors $z_{1,j}^s(t) = (x_{1,j}^s(t), y_{1,j}^s(t), y_{p,1,j}^s(t))$ and the superscript s indicates that the

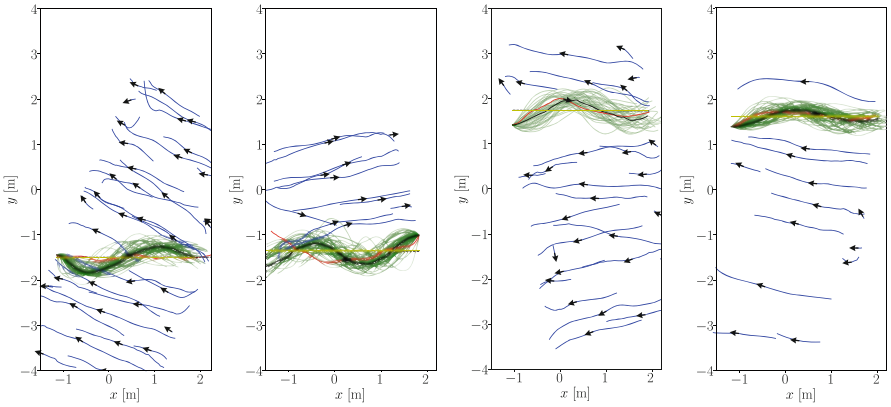

Fig. 8 Comparison of measurements and simulations performed via Eqs. (11)–(16) and non-linear force superposition model (C4) in four 1 vs. N scenarios **(a,b,c,d)**. We consider the coordinates, (x, y), aligned with the preferred path of the target pedestrian (i.e., the whole domain has been rotated accordingly). The measured trajectory of the target pedestrian is reported in red, in blue are the measured trajectories of the incoming crowd. We display in green different target pedestrian trajectory realizations as generated by our model, and in black the classical path or the (time-)averaged simulated trajectory (cf. Eq. (17))

quantities involved are from simulated data. Hence, we can compute the pdf of the instantaneous fluctuation, $d_B(\bar{z}_1^s, z_1)(t)$, with respect to the classical path

$$d_B(\bar{z}_1^s, z_1)(t) = ||(\bar{x}_1^s(t), \bar{y}_1^s(t)) - (x_1(t), y_1(t))||_2, \tag{18}$$

where the position z_1 can be either from the simulated data themselves or from the measurements. The underlying idea is to probe how likely it is that a measured trajectory is prompted by the model, for which, a necessary condition is a similar d_B probability distribution. Note that in the case of simulated trajectories, the distribution of d_B gives a measure for the size of the trajectory bundle (cf. bundle of green simulated trajectories in Fig. 8).

In Fig. 9, we report the probability distribution of the distance d_B for the four force superposition rules (C1)–(C4). We observe that a first-neighbor only reaction (C4) yields a distance distribution, in case of measured and simulated trajectories, that is mutually closest while incorporating the least parameter variations with respect to the validated 1 vs. 1 case. In this case, we exclusively halved the intensity of the short-range interaction force. Such reduction might be further justified by the fact that only the target pedestrian has been simulated, which included no reaction of the other pedestrians that were passively moved according to the measurements. We stress that possibly many other superposition rules may exist: in case (C3) in fact, we achieved a good agreement between the distance distribution. Nevertheless, this involved not only a reduction of the interaction forces by a factor 10, which

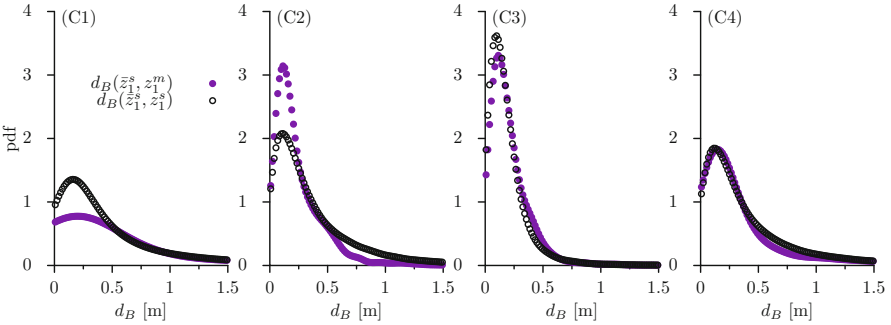

Fig. 9 Probability distribution functions of the distance d_B between the simulated classical path (i.e., the average simulated trajectory, cf. Eq. (18)) and the measured or the simulated trajectories, respectively, $d_B(\bar{z}_1^s, z_1^m)$ and $d_B(\bar{z}_1^s, z_1^s)$, for short-range force superposition rules (C1)–(C4). The non-linear force superposition, considering interactions with the first-neighbor only, allows highest similarities in the distance distributions, with minimum variation of parameters with respect to the 1 vs.1 case

may agree with a mean-field like interaction scaling (here $N \approx 10$ holds), but we needed to heavily steepen the velocity potential around the stable state, with respect to the validated value in the 1 vs. 0 case, i.e. we increased α and so the likelihood of a pedestrian to keep their desired velocity.

6 Discussion

In this chapter we addressed complex avoidance scenarios involving one pedestrian walking in a corridor, while avoiding a crowd of N other individuals walking in the opposite direction, that we conveniently named 1 vs. N. This work aimed at a first step towards general crowd models, quantitative in probabilistic sense, where the dynamics is in agreement with large ensembles of measurements and statistics evaluated thereof. Our analysis has been based on real-life data collected in an unprecedented experimental campaign held over about a six months time-span, held in the train station of Eindhoven, The Netherlands, in which millions of individual trajectories have been recorded with high space- and time-resolution. We considered this scenario a first step to tackle avoidance in non-diluted conditions; we based our analysis and modeling on our previous works on diluted 1 vs. 0 and 1 vs.1 conditions that we briefly reviewed in the first part of the chapter.

Our contribution has been twofold. First we evidenced, on the basis of the experimental data, complex aspects of the dynamics arising in comparison to a diluted flow: namely the increased randomness in the motion, both in terms of small-scale fluctuations and of avoidance maneuvers (operational-level dynamics), and the increased relevance of geometric aspects. These elements also show how

our current trajectory database enables to explore just a small portion of the overall 1 vs. N dynamics, that we could mainly address in its operational aspects, while we had to make assumptions on the tactical part.

On this basis, we considered a generalization of our previous model for the diluted dynamics. Assuming the preferred path and speed known, we could show that a non-linear superposition of short-ranged contact avoidance forces, focusing on the first-neighbor only, could produce a position-wise fluctuation distribution with respect to the classical path that was in better agreement with the measurements. In other words, the trajectories measured in real-life had higher chance to be generated by our stochastic model. It is important to stress that this is possibly one among many fitting forces superposition schemes. In fact, we could produce fluctuations distributions with good agreement between simulations and data also with a linear superposition of forces; this however required multiple parameter changes with respect to the validated baseline 1 vs. 0 and 1 vs.1 models.

While extending the model to the 1 vs. N case we could also point out a limitation in our 1 vs. 0 modeling approach. We cast both types of identified longitudinal velocity fluctuations, i.e. the frequent and small oscillations and the rare and large path deviations (trajectory inversions), in a unified perspective through a double well potential in velocity. In presence of interaction forces among pedestrians, these interplay with the gradient force due to the potential altering, among others, the probability of inversion. Although the trajectory inversion probability is likely to be affected by pedestrians coming in the opposite direction, the exact extent to which this happens has to be measured. From the modeling perspective, this modification can be rendered in terms of a dynamic modification of the potential barrier $(U(u_p) - U(0))$ in dependence of the surrounding crowd. This dynamics can also be extended to other parameters of the potential, like the preferred velocity u_p that has now been inferred from the data rather than modeled.

In general, we evidenced the increase of complexity when analyzing and modeling dense 1 vs. N avoidance scenarios vs. diluted (1 vs. 0 and 1 vs.1), with higher relevance of geometric aspects, mainly the position in the domain. Moreover, in order to resolve and model tactical level dynamics, one would require even longer measurement campaigns, to extensively sample complex and dense pedestrian configurations, as well as longer observation windows, to disentangle tactical and operational-level dynamics. Finally, from the modeling perspective, we reckon that employing Langevin-like equations can get prohibitively complex as one considers scenarios that are crowded and/or geometrically complicated: the involved potentials, in fact, can get excessively complex to identify and model. On the opposite, more trajectory-centric approaches, e.g. based on tools well established in modern physics such as path integrals [7], can provide more natural modeling environments.

Acknowledgments We acknowledge the Brilliant Streets research program of the Intelligent Lighting Institute at the Eindhoven University of Technology, Nederlandse Spoorwegen, and the technical support of C. Lee, A. Muntean, T. Kanters, A. Holten, G. Oerlemans and M. Speldenbrink. This work is part of the JSTP research programme "Vision driven visitor behaviour analysis and crowd management" with project number 341-10-001, which is financed by the Netherlands Organisation for Scientific Research (NWO). A.C. acknowledges the support of the Talent Scheme (Veni) research programme, through project number 16771, which is financed by the Netherlands Organization for Scientific Research (NWO).

References

1. N. Bellomo, B. Piccoli, A. Tosin, Modeling crowd dynamics from a complex system viewpoint. Math. Models Methods Appl. Sci. **22**, 1230004 (2012)
2. D. Brščić, T. Kanda, T. Ikeda, T. Miyashita, Person tracking in large public spaces using 3-d range sensors. IEEE Trans. Human-Mach. Syst. **43**(6), 522–534 (2013). https://doi.org/10.1109/THMS.2013.2283945
3. A. Corbetta, L. Bruno, A. Muntean, F. Toschi, High statistics measurements of pedestrian dynamics. Transp. Res. Proc. **2**, 96–104 (2014). https://doi.org/10.1016/j.trpro.2014.09.013
4. A. Corbetta, J. Meeusen, C. Lee, F. Toschi, Continuous measurements of real-life bidirectional pedestrian flows on a wide walkway, in *Pedestrian and Evacuation Dynamics 2016* (University of Science and Technology of China Press, Hefei, 2016), pp. 18–24
5. A. Corbetta, C. Lee, R. Benzi, A. Muntean, F. Toschi, Fluctuations around mean walking behaviours in diluted pedestrian flows. Phys. Rev. E **95**, 032316 (2017)
6. A. Corbetta, J.A. Meeusen, C.M. Lee, R. Benzi, F. Toschi, Physics-based modeling and data representation of pairwise interactions among pedestrians. Phys. Rev. E **98**(6), 062310 (2018)
7. A. Corbetta, F. Toschi, Path-integral representation of diluted pedestrian dynamics, in *Complexity Science: An Introduction* (World Scientific, Singapore, 2019)
8. E. Cristiani, B. Piccoli, A. Tosin, Multiscale modeling of pedestrian dynamics, in *Modeling, Simulation and Applications*, vol. 12 (Springer, Singapore, 2014)
9. J.J. Fruin, *Pedestrian Planning and Design* (Elevator World Inc., Mobile, 1987)
10. D. Helbing, Traffic and related self-driven many-particle systems. Rev. Mod. Phys. **73**(4), 1067 (2001)
11. D. Helbing, P. Molnár, Social force model for pedestrian dynamics. Phys. Rev. E **51**(5), 4282–4286 (1995)
12. S.P. Hoogendoorn, P.H. Bovy, Normative pedestrian behaviour theory and modelling, in *Transportation and Traffic Theory in the 21st Century: Proceedings of the 15th International Symposium on Transportation and Traffic Theory*, Adelaide, 16–18 July 2002 (Emerald Group Publishing Limited, Bingley, 2002), pp. 219–245
13. R.L. Hughes, The flow of human crowds. Ann. Rev. Fluid Mech. **35**(1), 169–182 (2003)
14. W. Kroneman, A. Corbetta, F. Toschi, Accurate pedestrian localization in overhead depth images via height-augmented hog. Pedestr. Evac. Dynam. (2018, to appear). arXiv:1805.12510
15. M.C. Marchetti, J.F. Joanny, S. Ramaswamy, T.B. Liverpool, J. Prost, M. Rao, R.A. Simha, Hydrodynamics of soft active matter. Rev. Mod. Phys. **85**, 1143–1189 (2013)
16. Microsoft Corp., *Kinect for Xbox 360* (Microsoft, Redmond, WA, 2012)
17. M. Moussaïd, S. Garnier, G. Theraulaz, D. Helbing, Collective information processing and pattern formation in swarms, flocks, and crowds. Top. Cogn. Sci. **1**(3), 469–497 (2009)
18. M. Moussaïd, D. Helbing, S. Garnier, A. Johansson, M. Combe, G. Theraulaz, Experimental study of the behavioural mechanisms underlying self-organization in human crowds. Proc. R. Soc. Lond., B Biol. Sci. (2009). https://doi.org/10.1098/rspb.2009.0405
19. M. Moussaïd, D. Helbing, G. Theraulaz, How simple rules determine pedestrian behavior and crowd disasters. Proc. Natl. Acad. Sci. **108**(17), 6884–6888 (2011)

20. P. Romanczuk, M. Bär, W. Ebeling, B. Lindner, L. Schimansky-Geier, Active Brownian particles. Eur. Phys. J. Spec. Top. **202**(1), 1–162 (2012)
21. S. Seer, N. Brändle, C. Ratti, Kinects and human kinetics: a new approach for studying pedestrian behavior. Transp. Res. C-Emer. **48**, 212–228 (2014)
22. A. Seyfried, B. Steffen, W. Klingsch, M. Boltes, The fundamental diagram of pedestrian movement revisited. J. Stat. Mech. Theory Exp. **2005**(10), P10002 (2005)
23. A. Seyfried, O. Passon, B. Steffen, M. Boltes, T. Rupprecht, W. Klingsch, New insights into pedestrian flow through bottlenecks. Transp. Sci. **43**(3), 395–406 (2009)

Modeling Collective Behaviour: Insights and Applications from Crowd Psychology

Anne Templeton and Fergus Neville

Abstract Research from crowd psychology and pedestrian dynamics can inform one another to improve understandings and predictions of collective behaviour. In this chapter, we provide an overview of theoretical insights from crowd psychology on intragroup and intergroup behaviour and discuss possible avenues for implementing principles of the social identity approach into pedestrian models. Specifically, we debate the use of outdated assumptions of crowd behaviour, discuss how the core tenets of social identity theory and self-categorisation theory are central to understanding collective behaviour, showcase how perceptions and experiences of crowd members can be dynamic and influence their perceived safety and behaviour, and then point to recent trends in using crowd psychology to inform models of pedestrian movement and behaviour in emergencies. Finally, we examine barriers to incorporating social psychological theory into models, and look ahead to potential collaborative projects to improve crowd safety and experiences.

1 Introduction

Picture a crowd scene. It could be worshipers walking together during a religious pilgrimage, supporters of sports teams chanting songs at rival fans across a stadium, or passengers on a train helping one another in a sudden emergency. What unites these diverse behaviours and contexts is not only the physical co-presence of many people, but their feeling of being together as a group. An important part to making sense of their behaviour is understanding the *social identities* involved. That is, their identification as a member of the social group. In these examples the crowd members see themselves as being in the same social group and act in line with beliefs that the

A. Templeton (✉)
Department of Psychology, University of Edinburgh, Edinburgh, UK
e-mail: a.templeton@ed.ac.uk

F. Neville
School of Management, University of St Andrews, St Andrews, UK
e-mail: fgn@st-andrews.ac.uk

L. Gibelli (ed.), *Crowd Dynamics, Volume 2*, Modeling and Simulation in Science, Engineering and Technology, https://doi.org/10.1007/978-3-030-50450-2_4

group holds, known in psychology as the social norms of the group [1]. The social identities and norms are somewhat pre-established for the pilgrimage and sports crowds, but emergent for the train passengers responding to the attack as they come to recognise each other as sharing a common threat.

These are all examples of what social psychologists call *psychological crowds* as opposed to *physical crowds* [2, 3]. The latter are large groups of co-present people who think and act as individuals or small subgroups of friends and families. Suitable examples might include shoppers on a high street or commuters on public transport. Unlike in psychological crowds, members of physical crowds do not perceive themselves to be in the same social group with other crowd members other than their subgroup of families or friends.

However, crowds are dynamic environments. Physical crowds can transition to psychological crowds when something in the context changes to unite people within a shared social identity. To use the example of a physical crowd of commuters on public transport, if their train were to break down and they were badly treated by the train company then the individual crowd members may become a psychological crowd. People cease being 'other' and become fellow group members who share the same fate and social identity. This shared identity can then lead to a positive shift in social relations such that people support rather than ignore or compete with one another [4]. A physical crowd can also consist of one or more psychological crowds, such as two psychological crowds of opposing football fans within a stadium, or a psychological crowd of concert attendees travelling through a physical crowd of others at a transport hub.

Despite the importance of social identity processes for understanding crowd behaviour, they remain largely neglected in pedestrian models of crowds. A systematic review of contemporary models of crowd behaviour noted that the models continued to rely on mistaken or outdated assumptions of collective behaviour rather than on the findings of empirical research [5]. The review concluded that existing pedestrian models simulated crowds in one of three ways. Crowds were either treated as (1) homogenous masses where all members acted in the same way, (2) independently acting individuals without any sense of collectivity (often with the underlying assumptions of panic or selfish behaviour), or (3) a series of subgroups with various levels of cognitive connections to others in the model (e.g. leader-follower models).

The review indicated an upsurge in the publication of crowd modeling articles, with the homogenous mass approach becoming the most prevalent. While these models have made important gains in simulating collective behaviour, existing approaches do not integrate the social identity processes which underpin crowd behaviour. Instead, the models are often based on outdated assumptions from transformation and dispositional theories which hark back to discredited 'classical' crowd psychology. Basing models on these invalidated theories can have significant consequences for crowd safety since an incorrect premise in a model will result in an incorrect outcome. We argue that if modellers want to accurately predict and monitor crowd behaviour to increase safety, then we need to look to contemporary research in crowd psychology to incorporate accurate assumptions and behavioural

outcomes into models. Specifically, models should look to recent research from a social identity perspective to explain how and when crowd members perceive themselves and others to be fellow group members, and what forms of collective behaviour can emerge from this process.

In this chapter we will set out some of the core considerations that modellers can take from contemporary crowd psychology. First, in Sect. 2 we provide a summary of classical theories in crowd psychology, highlighting their strengths and weakness, and implications for crowd modeling. In Sect. 3, we present the core theoretical tenants of the social identity approach [6] to both demonstrate its importance in modeling the root of collective behaviour, and to lay out the foundations of group processes that are needed to implement collective behaviour in psychological crowds. Following this, in Sect. 4 we provide more nuanced and dynamic aspects of the social identity approach to show why crowd members' cognitive appraisals of others, relations, and emotions can transform over time. In the fifth section, we give applied examples from previous research to show how these transformations can influence phenomena such as feelings of safety, perception of crowdedness, intimacy with others, and enjoyment of events.

In Sect. 6, we summarise how social identification influences pedestrian proximity and pedestrian flow in psychological crowds. Here, we focus on how experimental methods from crowd psychology and pedestrian movement can be combined by researchers who aim to explore group processes in crowd movement. We then turn our attention in Sect. 7 to understanding collective behaviour in emergencies. We discuss research on emergency behaviour (e.g. motivation for helping behaviour), and initial attempts to implement theoretical principles from the social identity approach into a pedestrian model. Finally, in Sect. 8 we look ahead to potential research avenues. We discuss current challenges such as barriers to combining complex psychological theory with concise models, possible solutions to pressing questions using methods from psychology and pedestrian dynamics, offer suggestions for integrating contemporary crowd psychology into models, and pose future theoretical and applied directions to improve our understanding and modeling of crowd behaviour.

2 Classical Theories of Crowd Behaviour

Classical crowd psychology refers to early theories of crowd behaviour which became popular at the end of the nineteenth century. These approaches broadly fall into two categories: transformational theories and dispositional theories. There are several detailed and entertaining reviews of the historical origins, authors, and theories of classical crowd psychology which explain how this work emerged as a conservative reaction to popular struggle and democratic politics (e.g. [7–14]). We provide a brief summary of the classical theories of crowd behaviour in Table 1.

Transformation or 'group mind' theories argue that crowds fundamentally alter the character of their members through a loss of identity [15–17]. Identity here

Table 1 Classical theories of crowd behaviour

Theory-type	Characterisations	Neglects
Transformative	• Loss of individual identity and self-control • Submergence to the crowd • Contagion of emotions and behaviours	• Normative influences • Collective pro-social behaviour in absence of leaders • Social influence is constrained by group membership
Dispositional	• The collective is a nominal fallacy • Collective behaviour due to common traits and characteristics of individuals • Social facilitation through convergence	• Social context such as emergent and pre-established social norms, intergroup dynamics in unfolding events (e.g. collective action)
Deindividuation	• Loss of individual identity, awareness, and restraint • Anonymity leads to anti-social behaviour	• Reasons for crowd assembly • Intergroup dynamics in conflict in behaviour

is conceived of as a unitary and individual entity which is 'submerged' when people enter crowds. A loss of identity leads to a loss of behavioural constraint and thus any emotions or behaviour can pass 'contagiously' through crowds leading them to behave in 'primitive', 'irrational', and unpredictable ways. The apparently 'contagious' nature of crowd behaviour and emotion has been integrated into some computer simulations of crowds (e.g. [18, 19]). However, there are three primary dangers of modeling crowd behaviour upon transformation theories.

First, the transformation approach fails to account for normative influences on behaviour such as how group members will self-police negative behaviour within crowds if people act outside the norm (see [20, 21]). Second, their inherently negative views of crowds and ideas of hypnotic suggestibility to leaders fail to account for instances in which crowds act pro-socially and work collectively in the absence of leaders, including maintaining everyday norms such as queuing rather than losing their ordinary civility (e.g. [22]). Third, they neglect how emotion transference is constrained by group membership, whereby we are more influenced by the emotions/actions of people within our group (ingroup members) than those not in our group (outgroup members) [23–26].

Transformation theories and the concept of identity 'submergence' was the inspiration for the deindividuation literature which continued to argue that (individual) identity is lost in crowds, thereby causing people in them to act pathologically [27]. For example, Festinger and colleagues [28] claimed that individual anonymity within groups led to anti-social behaviour; Diener [29] and Duval and Wicklund [30] suggested that deindividuation caused a loss of objective (individual) self-awareness preventing reliance upon individual standards, while Zimbardo [31] proposed that deindividuation led to a 'lower threshold of normally restrained behaviour' (p251) (for reviews see [32, 33]).

A key reason why crowds were pathologised in classical theories was their decontextualisation at both distal and proximal levels. In other words, no attention was given either to the motivating forces that led crowds to assemble, or to the role in which other groups (namely the security forces) played in intergroup collective conflict [12]. Violent interactions between groups were consequently seen as having their origins solely within the crowd, and changes in collective behaviour and emotion seemed random and unpredictable when considered in isolation. This decontextualisation engendered a reification of crowd behaviour such that the brutality and emotionality of specific crowds in particular settings were used to condemn collective behaviour in general [10, 12, 34].

Dispositional theories of the crowd evolved in direct opposition to the transformation literature. These theories argued that groups were made up of individuals who shared common traits and characteristics which were amplified through social facilitation as similar individuals converged together [35, 36]. This work was reflected in subsequent individualistic accounts of crowd behaviour that explained the behaviour of crowds as a consequence of individual (Freudian) personality conflicts (see [37, 38]). For example, Kornhauser [39] suggested that crowd members were alienated individuals, while Lasswell [40], Hoffer [41], and Klapp [42] characterised political 'types' who engaged in collective behaviour to fulfil inner needs.

Empirically, the dispositional approach finds little support. Numerous studies have failed to find common traits that predict participation in collective behaviour (e.g. [9, 43]; Stott and Adang [114]; [14]). Despite being a response to transformation theories, the dispositional account shares many of its criticisms [44]. Both traditions rely upon a unitary notion of identity such that the isolated individual is considered the only locus of self and reason (see [9, 12]). Moreover, by detaching collective action from its social context, crowd behaviour appears meaningless and is explicable only by invoking some hidden factor. The difference between transformation and disposition theories is merely whether this factor is a metaphysical group mind or the predisposition of individual crowd members. Decontextualised, the pathologised behaviour of particular crowds are reified and generalised to all collective contexts such that participation in crowd action becomes in itself a sign of individual pathology [12].

Although strong in their convictions, classic crowd psychologists rarely provided detailed descriptions of the collective events upon which they based their conclusions. When one does systematically examine crowd action, including the violent incidences of collective behaviour that dominated the classic theories, one finds order in place of chaos. Rather than exemplifying collective irrationality, crowd behaviour instead appears grounded in shared systems of belief and identification, and to operate in relation to social context [14, 44–46].

Emergent Norm Theory (ENT; [47]; for summaries see [12, pp. 192–4], [48, pp. 424–6]) rejected psychology's depiction of crowds as irrational and pathological. Instead of reducing collective action to the 'rational' actions of individuals, ENT contended that emergent norms shaped crowd behaviour. ENT fused symbolic interactionism (the process whereby meanings materialise from micro-social relations)

with social psychological research into group norm formation ([49, 50]; see [12]). It was argued that collective action was preceded by an episode of 'milling' during which time group members exchanged views and discussed advisable courses of action through interpersonal interaction. Some individuals—'keynoters'—had particular influence during this period through their forceful delivery and resolve of opinion. Gradually there emerged an 'illusion of unanimity' as keynoters' positions were adopted by crowd members.

ENT made an important move away from the irrationalist crowd models and restored the relationship between the self-understandings of crowd members and their collective behaviour [12]. However, ENT is vulnerable to several criticisms that showcase substantial shortcomings for a modeller attempting to simulate crowd behaviour. Firstly, while collective action does often follow a period of mingling and discussion, this process is unable to account for the coherence of crowd action throughout rapid changes in social context [9, 12, 51, 52]. Also, by focussing upon interindividual interactions without grounding norm formation in wider issues of group and societal identification, ENT cannot explain how the emerging norms of collective behaviour come to echo shared understandings or predict who or what becomes influential. One prominent theoretical framework that addresses these shortcomings is the social identity approach.

3 The Social Identity Approach

Reicher's [44, 51–53] social identity model (SIM) of crowd behaviour critiqued decontextualised accounts that examined either the individual or the crowd in isolation, and instead argued that to understand collective co-action one needs 'a social psychology that places the individual in society, and relates conduct to context' (ibid, 1987, p171). The model claimed that the social identity approach to group behaviour provides such a social psychology. By the 'social identity approach' (see Reicher et al. [6] for a review) we refer to social identity theory (SIT; [54, 55]), self-categorisation theory (SCT; [56, 57]), and the Elaborated Social Identity Model (ESIM; [12, 51, 52, 58, 59]). A brief glossary of key terms within the social identity approach are presented in Table 2.

The social identity approach sets out a strong theoretical and practical base to be adapted into computer models of crowd behaviour. Instead of a loss of identity in groups, the social identity approach argues that as one's membership with a relevant social category becomes salient, there is a shift from personal to social level identification. Personal identity refers to 'I', or how one's characteristics and qualities are distinct to other individuals, while social identity refers to 'we', or how group members understand their membership in a social category such that they are unique in comparison to members of other social groups [6, 54, 60]. In this sense, when one's group identity becomes salient, the 'social collectivity becomes self' ([61, p. 12]). The dependence of collective action on group norms and social context gives crowds the capability to act coherently in rapidly changing non-routinised situations without the 'milling' process required by ENT [12].

Table 2 A glossary of key terms within the social identity approach

Term	Brief definition
Social identity theory	We have a personal identity (referring to our idiosyncratic self) and social identities (our membership of social groups) and operate on a continuum between these. People are members of multiple social groups and each group has social norms, values, and beliefs that guide our meaning-making and behaviour. People within our group are referred to as ingroup members, and people in another group are referred to as outgroup members
Social norms	Shared rules regarding how to think, feel, and act within a social group. These can be descriptive (what group members do) and injunctive (what group members ought to do)"
Salience	The extent to which a social identity is cognitively present at a particular time
Social identification	Refers to how much one identifies as a member of a particular social group
Shared social identification	The extent to which people believe that they and others feel part of the same social group
Self-categorisation theory	Described the process in which people are cognitively categorised into social groups. Categorisation involves a process of self-stereotyping, depersonalisation, comparative fit, and normative fit
Self-stereotyping	The process whereby individuals define their self in terms of their social identity and act in line with the group's social norms
Depersonalisation	A shift from personal identity to social identity.
Meta-contrast principle	When differences between people in the ingroup are perceived as smaller than the differences with the outgroup
Comparative fit	Based on the meta-contrast principle, the level of context-specific comparative (dis)similarity that the self and others have to group members. A group of people can be categorised as being in the same group as one another if the differences between themselves are less than their differences with another group. This is part of the meta-contrast principle
Normative fit	The extent to which stimuli align with the perceived norms of the group. For example, if someone acts in line with a group's social norms, then they are likely to be categorised as a member of that group

Of particular interest for crowd modellers simulating how crowd behaviour develops over time, Reicher [44] explains how behaviour emerges and develops within crowded contexts. For example, in his study of the St Paul's riot in Bristol, Reicher [44] noted how crowd members' identification with the local St Paul's community determined the limits of their behaviour. Rather than having rigid unyielding accounts of normative and anti-normative behaviour, Reicher shows how norms are dynamic and can change within the intergroup context. Conflict with the police—who were perceived as an illegitimate presence within the community space—was deemed appropriate such that throwing stones at police cars became normative behaviour. However, when a crowd member threw a stone at a passing bus

the behaviour was not repeated. Instead, the fellow crowd members actively stopped the behaviour due to the illegitimacy of the target in relation to the community identity. The community identity had very clear boundaries of who and what was associated with the ingroup, and the normative behaviour operated within this understanding.

SCT contends that the categorisation of others into groups depends upon both perceiver readiness (the extent to which particular social categories are available to us and how familiar we are in applying them), and the comparative and normative components of category fit [56]. *Comparative fit* is a function of the meta-contrast ratio (the ratio of intragroup to intergroup differences), such that an aggregate of people will be categorised as a group when the differences between them are less than the differences with a comparator aggregate. In this way the categorisation of self and others is inherently contextual because comparative fit will always depend upon one's relative frame of reference [57]. *Normative fit* refers to the congruence between perceived social stimuli and normative expectations about different social groups, such that one is more likely to be classed as a member of a group when one's behaviour matches that group's norms [56].

The social identity approach argues that one is in possession of multiple social identities, the salience of which changes as a function of social context. As different identities become relevant, behaviour is shaped by the norms associated with that identity. In a pedestrian model, it could be possible for each pedestrian to have multiple available social identities and have one identity that is salient (prominent in governing behaviour) at any one time. For instance, our identities as academics might be most prominent while attending a conference, compared to our identities as climate activists when attending a protest. As one defines or 'self-categorises' oneself in terms of these different group memberships, one self-stereotypes and adopts the norms and behaviours associated with that relevant identity. While these identities are of real importance to me as an individual, they cannot be reduced to an individual level because they are collective constructs. In this way, Reicher [62] describes social identity as the pivot between the individual and the social.

Self-categorisation therefore becomes the psychological basis for crowd behaviour, such that group members are able to act collectively towards common goals because they possess a shared social identity [22, 53, 56, 60, 63]. This point is worth emphasising; *identity is not lost in groups but is the very foundation of collectivity*. When group objectives are achieved—a process named collective self-realisation (CSR)—participants can feel empowered and efficacious [64–66], leading to positive affect and a willingness to participate in future group action. The power of crowds is not therefore due to a loss of identity (as argued by Le Bon 1895/[15]), but is rather a consequence of shared identification and co-action. More support for this can be found in a meta-analysis of 60 independent studies examining the issue by Postmes and Spears [32]. Here, Postmes and Spears found evidence in favour of the social identity approach and not the deindividuation account. That is, participants who had their anonymity, self-awareness, and group size manipulated did not act pathologically, but rather conformed to situation specific social norms.

The core theoretical principles for the social identity approach have several implications for crowd and pedestrian modellers. First, it demonstrates how people act as collectives, share beliefs, and have positive or negative relations with others. The literature on depersonalisation provides the framework for modeling how people transition from their personal to social identities, i.e. how they change from acting as an individual to acting collectively with other ingroup members. Moreover, it poses that we have multiple social identities with different norms and values, and shows how a social identity can become salient and influence our perceptions and behaviour. It illustrates how agents in a model may decipher group membership: through their relative similarity or difference to us compared to others (comparative fit) and their behaviour (normative fit).

Crucially for crowded contexts, the social identity approach sets out how norms are dynamic and how crowd behaviour is limited within these norms. It shows how clear and important boundaries on behaviour are governed by group norms, and how crowd members may collectively work together to regulate behaviour to ensure it operates within their understanding of the group. This, however, is far from all that the social identity approach can offer to modellers. In order to properly dig into how crowds can be behaviourally and emotionally dynamic, we now turn to the cognitive, relational, and emotional transformations that social identity processes entail.

4 Transformations in Psychological Crowds

As noted in the previous sections, crowd members and the relationships between them can be transformed in various ways which are of relevance to those seeking to model crowd behaviour. To be more concrete, recent work from the social identity approach has noted three potential transformations when people perceive themselves as being members of a psychological group (i.e. sharing a social identity with co-present other): cognitive, relational and emotional transformations [3, 67]. Please see Table 3 for a brief glossary of the transformations.

Table 3 Glossary of transformations in the social identity approach

Transformation	Brief definition
Cognitive	A shift in identification. This can involve a shift from a personal identity to a social identity, or from one social identity to another social identity
Relational	Shared identity leads to a shift in social and sensual relations as crowd members cease to be 'other' and become 'one of us'. Incurs increased feelings of closeness, higher trust, support, respect, and cooperation
Emotional	The emotional consequences of being in a group. This includes feelings of collective empowerment, joy, pride, and anger on the basis of group membership

First, based upon the process of self-categorisation, crowd members can undergo a *cognitive transformation* such that they come to think and behave in terms of the goals and norms of their salient social identity rather than their individual identities. For example, if crowd members come to define themselves as climate justice activists, then they might chant anti-fracking songs, carry pro-environmental banners, and march towards sites of particular interest to their identity, such as centres of political power or offices of fossil fuel companies. How the crowd will act at those sites (such as a sit-down protest, handing out flowers, throwing rocks, etc.) will depend upon the social norms associated with that group, and interactions with other groups (including the police). Moreover, how group members experience the world around them will also be perceived through the prism of their social identity. For example, noise regarded as meaningful to one's group will be rated as more positive than irrelevant noise [68, 69].

Furthermore, as members of the crowd come to see each other as sharing the same social identity—such that they are part of the socially extended self rather than 'other'—this can lead to *relational transformations.* Multiple laboratory studies have used the social identity framework to explore the role that shared identity plays in transforming intragroup social relations (alternatively termed 'relatedness') (for reviews see [70–72]). For example, Haslam et al. [73] reported that ingroup members expected to agree with one another during conversations, and in so doing picked up upon common points of agreement that led to consensualisation. In a quasi-experimental field study (BBC Prison Experiment; [74]), shared identity could encourage intragroup trust, respect, cooperation, and a decrease in stress. Novelli et al. [75] built upon these findings to demonstrate that ingroup members were more comfortable in close physical proximity to one another than they were to outgroup members or people whose group membership they did not know. As noted in the introduction, laboratory studies in which participants imagine their train breaking down can lead to a perception of shared identity with fellow passengers and subsequent comfort in social and sensual interactions [4].

Outside of the laboratory, a number of fieldwork studies have likewise found evidence for a positive relational transformation of social relations in groups of common identity (e.g. [76–79]). As a heterogeneous crowd unites to form a homogeneous group (perhaps in response to a shared outgroup), interpersonal relationships with strangers often become characterised by trust and support, rather than threat and misunderstanding. Importantly, these transformed social relations can have behavioural manifestations, exemplified in the positive impact that shared identity has upon resilience and willingness to help strangers in both emergency and mundane situations ([22, 24, 80–83]).

Finally, the cognitive and relational transformations can lead to *emotional transformations* within crowds. Collective gatherings can clearly be sites of intense passion [37, 38, 84]. While classical crowd psychology theories explained the emotionality of crowds as a consequence (personal) identity loss, recent research within the social identity literature has begun to show the various ways in which crowd emotion is linked to social identification.

First, to the extent that one identifies with a social group, then group relevant events are appraised and experienced emotionally as a function of group membership (Intergroup Emotions Theory; [85]). For example, when a football team scores a goal then its supporters will experience this with joy and pride while fans of the conceding team will experience the event negatively [79, 86]. This can also lead to negative emotions, such as when police action to block a march is perceived as illegitimate by the crowd and leads to collective anger [51, 52]. Second, when crowds achieve their collective objectives (collective self-realisation) this can be experienced with a sense of empowerment such as being able to shape the world rather than being shaped by it, and joy [65, 66]. Such feelings of empowerment can then act as a predictor of participation in future collective action [65, 66, 87, 88]. Finally, when social relations between crowd members are positively transformed through shared identity, solidarity and recognition from fellow group members can be experienced positively, and emotions related to the group experience can be validated and amplified (e.g. [78, 79, 89]).

5 The Effects of Social Identities on Perceptions of Crowds and Crowd Events

Social identities affect perceptions and experiences of crowd events. Social identification as a member of a crowd can influence feelings of relatedness with others and, in turn, positive appraisal of events, experiences of crowding, feelings of safety, and comfort levels in close proximity to others. An illustrative example of the relationship between social identification and crowd experiences can be seen in Neville and Reicher's [79] research on attendees of the Rock Ness festival in Scotland. Neville and Reicher [79] surveyed attendees of the Rock Ness festival in Scotland to further explore how social identities affect people's experiences of crowd events. They asked respondents to rate their shared social identity with others in the crowd (i.e. the extent to which others in the crowd shared a social identity), their sense of relatedness with others in the crowd, and the extent to which their experience of the crowd was positive. They found that having a shared social identity was not enough to create a positive evaluation of the crowd, but that a sense of relatedness with others was needed to explain how a sense of shared identity created a positive experience. That is, respondents who had a stronger sense of shared social identification with the other crowd members felt more related to them and therefore had higher positive evaluations of the crowd experience.

In similarly themed research with pilgrims of the Magh Mela, Hopkins et al. [89] found that shared social identity among crowd members predicted a positive experience of the pilgrimage when accounting for the sense of intimacy felt with other crowd members. Here, as pilgrims felt a stronger shared social identity, they had an increased sense of intimacy with the other crowd members and this led to higher positive judgements of the pilgrimage experience itself.

Comparable results were found with pilgrims at the Hajj by Alnabulsi et al. [90]. The Hajj is comprised of pilgrims for across the world with different languages, religious denominations, and cultures. Despite these differences, the more strongly pilgrims perceived the crowd to be united, the more they identified with the crowd (i.e. felt a sense of togetherness with other people on the Hajj), and the more they identified as being Muslim. Moreover, they found that as positive experiences of the crowd increased, so too did identification with the crowd, and in turn the more important their Muslim identity was to them compared to before the Hajj. Taken together, this research indicates that inter-related components of social identification and relatedness are pivotal to understanding crowd experiences.

Another important component of crowd experience is the extent to which the crowd members are able to act in group normative ways that align with their group values. For example, in the Magh Mela pilgrimage, the more the pilgrims felt that all kalpwasis (pilgrims who stayed at the Magh Mela for the entire month of the pilgrimage) thought of themselves as part of a single group, the more they felt they were able to live a simple life in accordance with the religious teachings, and therefore the more fulfilled they felt. Here, being able to act in line with group values through following religious teachings of a simple life was central to the pilgrims' emotional experience of the event.

Moreover, group relations influence how close crowd members are willing to be to others, even smelly people. A common assumption within crowd modeling is that humans have a maximum threshold level of tolerated density or proximity with others in a crowd before trying to move away (e.g. [91, 92]). This is important for considering ingress, egress, how people will distribute within spaces, and how people's emotional experiences will be influenced by the density. A pedestrian modeller may understandably assume that participants at a crowd event will try to avoid those who are smelly and disgusting, yet this too is influenced by group processes. As shown by Reicher et al. [93], we are less disgusted by smelly stimuli that we believe belongs to an ingroup member.

Over two studies on perceived disgust, Reicher et al. [93] explored the extent to which participants were disgusted by a t-shirt supposedly belonging to an ingroup member, an outgroup member, or a plain t-shirt that acted as a control. Results from study 1 suggested that participants were less disgusted by smelly ingroup t-shirts because the t-shirt owner was perceived as more similar to them than in the outgroup or control conditions. Moreover, the more people perceived the owner of the t-shirt to be ingroup, the less disgusted they were by them, and therefore the higher willingness they felt to socially interact with them. In study 2, the results showed that participants who perceived the owner of the t-shirt to be ingroup spent less time walking to hand sanitiser that was placed across the room, and indeed used fewer pumps of it when they got there.

Taken together, the research suggests that having a shared social identity influences how close we feel to others, how much we are able to enact our group's desired behaviour, and therefore our evaluations of crowds and crowd events. The implications of this research are important from a crowd planning perspective: hindering a psychological crowd from enacting group-specific behaviours that are

expected by those with a shared group identity could lead to less positive evaluations of the event. Although the studies by Reicher et al. [93] were based on smelly t-shirts, the implications for crowd management and modeling are substantial. They indicate that disgust perceptions are influenced by group relationships. The studies provide initial evidence that modellers' underlying assumptions of proximity and repulsion need to be re-evaluated to include group processes.

In contrast to assumptions that people will avoid highly dense areas, Novelli et al. [94] found that social identification influences people's perceptions of how crowded they are, and that people who identify with the crowd actually experience more positive emotions in denser areas. Novelli et al. surveyed attendees of the Fatboy Slim Big Beach Boutique 2 in the UK. Attendees were standing on an uneven beach, wedged between an incoming tide of water and the city, in a crowd so dense that security personnel struggled to enter without causing danger. Despite this, Novelli et al. found that attendees felt less crowded the more they identified with the crowd, and in turn experienced a greater intensity of positive emotions during the event. In contrast, those who had low identification with the crowd reported more negative emotions the more crowded they felt. Remarkably, the attendees who highly identified with the crowd wanted to be in the centre of the crowd because they associated that area with a more positive experience. In short, the more attendees identified with the crowd, the less crowded they felt, the more central in the crowd they wanted to be, and the more positive experience they then had during the event.

One possible explanation for why people who highly identify with the crowd are happy when surrounded by group members is that they feel safer when they are with members of their group. Alnabulsi and Drury [95] found compelling evidence for this when surveying pilgrims attending Hajj. Pilgrims who reported low identification with the other pilgrims in the crowd felt less safe in denser areas of the crowd. In contrast, pilgrims who highly identified with the crowd felt *safer* in *denser* areas. Evidence suggests that feeling safe may due to an expectation that people in our group will support us. Further analysis by Alnabulsi et al. [90] found that Hajj pilgrims in the plaza (outside the Grand Mosque) who perceived other pilgrims to be supportive of others were more likely to give social support to others themselves if they perceived others in the crowd be to ingroup members and highly identified with the crowd. Importantly, this occurred if they perceived others in the crowd to be ingroup members and had a high social identification with the crowd. Thus, identifying with other members of the crowd is related to feeling safer in dense areas (compared to those who do not identify with the crowd) and giving support to others if they see the others as good ingroup members.

The effect of social identities on experiences of crowd events has a number of implications for pedestrian modeling and collective dynamics. Our positive experiences of events are affected by how related we feel to others, even attenuating our level of disgust to ingroup members in smelly situations. Crucially, social identification with others in the crowd influences our perceptions of crowding, safety, and expected support. A positive side to these findings is that people may feel safer than commonly assumed. There are, however, potentially negative consequences which need considered in pedestrian modeling and planning for

crowd events. Specifically, crowd members may seek out more crowded areas because they perceive them to be safe and believe they will have a more positive experience there, which could potentially lead to dangerously high densities. This should be a key consideration in risk anticipation: people may not avoid dense areas or spread out in uniform distributions. Instead, models should consider the effects of social identification on desired proximity of crowd members, and the impact of this on use of space and pedestrian flow.

6 Modeling Social Identification in Pedestrian Movement

Within the modeling literature, the influence of pedestrian relations on behaviour has primarily focussed on the effects of interpersonal and intergroup effects on route choice, way-finding, and collision avoidance. The research into pedestrian movement in crowds can be divided into four overarching areas.

The first area of research explores the effects of group behaviour on crowd flow, such as how the sizes, numbers, and formations of groups influence movement. This affiliative approach—where people stay with whom they have pre-existing bonds—is also common in evacuation and egress models (e.g. [98]) and the walking formations of groups in crowds (e.g. [99, 100]). Crucially, however, these studies investigate pre-existing subgroups within a crowd rather than when an entire crowd acts as a group. They do not aim to analyse what makes a 'group' and how perceptions of group membership can change as a function of changing context (e.g. the cognitive transformations discussed earlier). A second method focuses on individualist approaches to crowd behaviour, exploring how unique traits or attributes of the members of the crowd affects way-finding. However, this approach ignores interactions between people and instead focuses on individual differences and traits based on risk estimates. Thus, it bypasses the fundamental effect that self-categorisation can have on collective behaviour, such as how social connections between pedestrians can influence evacuation behaviour by reducing competitive actions [81].

A third area explores navigation in crowds as a consequence of responses to social information in the environment, such as the perception of others' intended behaviour. For example, where other pedestrians look and walk (e.g. [18]), and how quickly other pedestrians respond at the beginning of an evacuation [101]. However, this approach examines fleeting interactions between individuals and is based solely on avoiding collision with others. It neglects how a crowd can self-organise behaviour for reasons other than collision avoidance based on their shared social identities, such as how large groups of people may try to stay together when walking, or how a crowd of pilgrims can coordinate movement for complex religious rituals in high crowd densities. A fourth approach looks at how social transference of information affects crowd movement and group structures (e.g. [102]). A benefit of these approaches is that they foreground the need for social influence in models. However, they either do not account for how human social interactions can be more

complex than in birds or fish, or they neglect the research suggesting that we are more influenced by ingroup than outgroup members.

Together, these approaches investigate either interactions between individuals or subgroups within a crowd. They do not address crowd members who act as a collective, or truly grapple with the psychological underpinnings of what a 'crowd' is and how group processes can influence movement. Research from crowd psychology suggests that collective self-organisation and proximity to group members are a function of (shared) social identification. Thus far we have discussed the psychological considerations of perceptions and feelings on overall crowd behaviour, but social identity influences behaviour at the core pedestrian level. Social identities influence how close people are willing to be to one another, the size of subgroups, walking speed, and distance.

Examples of willingness to be closer to ingroup members, or being more comfortable with ingroup members, can be seen in the previously discussed sweaty t-shirt study [93], pilgrims performing the Hajj feeling safer in high densities when they had high social identification as a member of the crowd [95], and attendees at a music festival feeling less crowded when they had a high shared social identification [94]. Novelli et al. [75] sought to explore the effects of social identities on physical proximity experimentally. Participants completed a task where they estimated the number of dots on a screen. They were subsequently told that people were either dot over-estimators or dot under-estimators, and that they fell into the dot under-estimator group. Finally, the participants had to set up chairs in a room for themselves and either an ingroup (dot under-estimator) or outgroup (dot over-estimator) member who was supposedly also a participant. They found that participants who thought they were setting up the chairs for an ingroup member placed the chair significantly closer to their own chair than if the participant thought they were setting up the chairs for an outgroup member. Moreover, participants who believed the other person was an outgroup member rated a higher perceived difference between themselves and the other person, compared to less perceived difference if the other person was believed to be an ingroup member.

The study was repeated but in Study 2 the participants were asked to place chairs around a chair that had supposedly already been set up by the other participant who was manipulated to be an ingroup or outgroup member. Again, participants who thought they would be sitting with an ingroup member placed the chairs closer together than if they thought they would be sitting with an outgroup member. Together, this suggests that personal space is affected by the context of group relations: participants move closer to an ingroup member than to an outgroup member. Sorting people into groups without strong significance to their ordinary lives was sufficient to achieve this intergroup discrimination and subsequent willingness for proximity. Specifically, it suggests that the categorisation of people as ingroup or outgroup members is important for modeling collective movement in crowds as ingroup members tend to move closer to one another than to outgroup members.

To explore the role of group processes on proximity, Templeton et al. [103] conducted a quasi-field experiment to investigate how intragroup dynamics effect

pedestrian movement in physical and psychological crowds. In the first part of the study, 121 pedestrians were filmed without manipulation while walking from an undergraduate Psychology statistics lecture. We did this to obtain a baseline of participants' proximity, speed, distance, and group size in a *physical* crowd which we would then compare to the behaviour of a *psychological* crowd when a shared social identity was made salient. Afterwards, we recruited the Psychology students at the end of their statistics lecture and primed them to have a shared social identity. Participants were told that they were being recruited because they were Psychology students at that university and were given baseball caps which had labels denoting their shared group membership as Psychology students. The baseball caps doubly served as a method to track which pedestrians were part of the experiment. Participants were then filmed as they walked the same route from their lecture as they had previously walked without manipulation.

We tracked the pedestrians' locations to obtain their coordinates every five frames (1/3rd of a step), and then transformed the footage to planar view. In the non-manipulation condition, there were 66 people walking from the lecture and 55 people walking in counterflow. In the manipulation condition, there were 112 participants primed to share a social identity, 34 other people walking in the same direction as the recruited participants, and 13 people walking in counterflow.

Our primary focus was to compare the speed, distance, proximity, and group size of the pedestrians who walked from their lecture during our observation stage (no manipulation), and when we had primed a shared social identity. We measured their speed based on distance divided by time, and their distance by summing the distance between their coordinates of each tracked step. The proximity between pedestrians was calculated using Sievers' [115] method for Voronoi decomposition in MATLAB with vertices constrained so that the maximum tessellation area radius was 1 m to avoid artificially inflating the space around individuals walking alone or on the periphery of the crowd. Group size was measured using cluster analysis on participants' coordinates.

The results indicated that the shared social identity among members of the psychological crowd motivated the collective self-organisation of speed and distance so that ingroup members could maintain close proximity. Specifically, participants walked more slowly and further when in the psychological crowd than when in the physical crowd. Crucially, when participants were in the psychological crowd, they maintained closer proximity with ingroup members regardless of how many other pedestrians were in the area. Contrary to what the modeling literature would suggest, the psychological crowd did not divide into small subgroups and instead maintained sizes of up to 11 people compared to a maximum of three people in the physical crowd.

Our study raised key issues for modeling crowds and broader safety planning. First, individual ingroup members within psychological crowds may try to stay in close proximity to other ingroup members even when there is space around, suggesting that close proximity is not merely caused by the number of people around. Second, psychological crowds may alter their speed and distance in order to stay together. This has particular implications for planning ingress and egress in

models. It suggests that pedestrians in psychological crowds will prioritise staying with fellow group members over walking quickly, and will walk further distance in order to stay together. Moreover, pedestrians in psychological crowds may not split into smaller groups to ease crowd flow and evacuate more quickly.

Our study was the first to explore the effect of social identities on pedestrian behaviour in a psychological crowd. However, there are often two or more psychological crowds within the same physical space. For example, fans of different sports teams entering a stadium, protestors and counter-protestors, fans at different music stages in a festival. In our next study we aimed to explore the effect that another psychological group had on pedestrian behaviour.

To explore the effects of another psychological group on crowd movement, we created two distinct psychological groups by randomly allocating participants to be in either group A or group B. The participants were given identity markers via baseball caps with either 'A' or 'B' on them to allow them to see if others were in the same or different group from them. We measured their level of social identification with members of their own group (e.g. 'I feel a bond with the people in this group', $a = 0.846$) and the other group to ensure they had higher identification with their own group compared to the outgroup. Each group had significantly higher identification with members of their own group compared to members of the other group. We then used the same methodology as the 2018 paper to measure the proximity, speed, and distance of pedestrians. First, we had members of group A walk alone to get their baseline speed, distance, and proximity to other group members. Second, we had the members of group A and group B walk in counterflow. This enabled us to compare the behaviour of group A when walking alone to when walking the presence of group B.

Overall, the results suggested that pedestrians in group A walked in closer proximity, slower, and less distance when walking in the presence of the other psychological group. Moreover, the group members did not split into single file to ease crowd flow but instead moved closer to ingroup members and stayed three of four people abreast. This suggests that when a shared social identity with others in the crowd is salient, members of the crowd may remain in larger groups to stay together rather than splitting up to ease movement. Speed, distance, and proximity are crucial factors to consider when planning how a crowd will behave during ingress, egress, or in non-emergency and emergency situations. Taken together, the two studies on crowd movement suggest that social identification is a core component that influences the microscopic level factors in pedestrian movement.

7 Collective Self-Organisation and Helping Behaviour in Emergencies

One area where aspects of SIT and SCT have been included in pedestrian models is in simulated responses to disasters. Previous research from social psychology has demonstrated that we are more likely to help those who we perceive as ingroup

members (e.g. [105]), and in emergencies crowds maintain everyday norms such as queuing and staying behind to help others (e.g. [22, 81, 106]). Rather than irrational panicking, crowd members in potentially risky situations share resources and collectively self-regulate anti-social behaviour to maintain a safety (e.g. [20]).

The psychological transformations and corresponding behaviour that occur in emergencies are detailed by Drury et al. [81] in their research into survivor experiences of the July 7th 2005 London bombings. During the terror attack, three bombs were detonated in London underground tube trains, leaving survivors in dark tunnels and emergency services hindered from reaching them. The researchers combined interviews with survivors of the event and contemporaneous accounts and found that shared social identification among the survivors was a key influence on their reactions to the incident. The survivors experienced a cognitive transformation from being a member of a *physical* group to a *psychological* one. In physical groups, people think, feel, and act as individuals, and co-present others are regarded as irrelevant or perhaps even competitors. However, when something happens to re-frame the group boundaries—in this extreme example bombs being detonated—fellow passengers ceased to be 'other' and instead became co-members of a group united by shared threat and fate. This shift from seeing people as 'ingroup' rather than irrelevant or 'outgroup' transforms social relationships and behaviours.

The participants reported sharing emotional (e.g. reassurance) and practical (e.g. first aid) help on the basis that they were fellow group members. The people who had previously been individualised came together collectively to help one another, often at risk to their personal safety (e.g. delaying their own evacuation). Instead of competing to evacuate, the survivors queued in an orderly fashion, let others go first, and helped one another to escape. The lack of competition among group members was also found by Drury et al. [107] in a laboratory simulation of an emergency. Here, when participants perceived others in the evacuation as ingroup members, they exhibited less competitive behaviour such as pushing and shoving. Conversely, where crowd members did not perceive co-present others as sharing their social identity, it could lead to a lack of solidarity behaviours or even the presence of selfish behaviours [22, 81, 107]. Crowd managers or those in authority should therefore seek to facilitate shared identification within crowds, particularly within emergency contexts.

The cognitive transformation from being a physical to psychological crowd, combined with evidence of cooperative behaviour, provides prime ground to begin a model of evacuation behaviour that incorporates social identities. Von Sivers et al. [108] simulated survivor reactions to the bombings by implementing the cognitive transformations and subsequent helping behaviour based on shared group membership. In the agent-based model, each agent had the capacity to have either a personal or shared social identity salient, and to know the identities of other agents to allow for collective behaviour. The agents in each train carriage had a salient personal identity until the bomb was detonated. The detonation caused a cognitive transformation: now a set percentage of the total agents could have a shared social identity to replicate the perception of a common fate reported by the real-world survivors. In addition, we set a percentage of participants to be injured and others

to be healthy. We created a rule where healthy agents with the shared social identity would help injured agents with the same social identity to evacuate if they were within a certain radius. The model was dynamic; the number of agents with a shared social identity could be increased or decreased, as could the number of injured and healthy agents and radius dictating the locations within which people could be helped. Further work by von Sivers et al. [109] developed this model using uncertainty quantification to further explore the effects of different components of the model (e.g. number of pedestrians with a shared social identification), and provides an example of how the effects of social identification on behaviour can be explored in future models.

The simulations of the July 7th 2005 London bombings provide a starting point for considering how to implement the psychological transformations associated with social identities. However, there is much more work to be done. One avenue for future research would be to explore the extent to which people will go out of their way to provide support to ingroup members. Currently, our models (von Sivers et al. [108, 109]) result in small groups evacuating together and the agents do not go very far out of their way from their initial position to help others before evacuating. In contrast, the accounts by survivors suggest that people go to great lengths to support multiple people with first aid before evacuating and people would help others escape and then return to help more people.

Another limitation to the evacuation models is that we do not have quantitative behavioural data to calibrate the model against. Emergencies are difficult to simulate because we do not often have reliable footage or measures of the behaviour due to the natures of the emergencies. Although qualitative accounts cannot provide exact reaction times or specific information about route-taking, they do provide valuable insight into respondents' own experiences of the events and behaviour which is crucial to understanding people's perceptions and motivations. It demonstrates that the transformation from a physical to psychological crowd is an important component to understanding collective processes—and the type of behaviour—in the aftermath of emergencies.

8 Summary and Future Directions

Crowd models serve a myriad of benefits. They provide a method to formalise and test hypotheses about crowd behaviour and allow users to neatly simulate scenarios to predict behaviour for crowd safety planning. A modeller reading this chapter could justifiably ask 'crowd psychology sounds very interesting, but how am I supposed to put all this theory in a model?'. Herein lies the crux of the practical limitations to integrating crowd psychology into models. As Seitz et al. [110] indicate, models are usually focused on pedestrian movement rather than complex social cognition behind the movement. From a modeling perspective, models must be parsimonious as they can only have a limited number of parameters before the model becomes unfalsifiable. From a psychological theorist's perspective, there is

a dilemma in how to model the theory accurately without being reductionist. For both parties, there is the shared issue of how to boil down the components to what is most needed to accurately depict the behaviour, and can be generalisable to multiple crowd events rather than only representing one specific scenario.

Pedestrian modellers and crowd psychologists can learn from one another by collaboratively conducting further research on the effects of social identification on behaviour. Together, we can design experiments to isolate and explore behavioural phenomena and the psychological processes underpinning them. Working together has clear benefits to crowd psychologists, as models can allow crowd psychologists to test theories by simulating scenarios in controlled safe environments. A substantial step forward would be for pedestrian modellers and crowd psychologists to jointly map out some of the core theoretical considerations for collective behaviour in crowds. In this chapter, we have outlined some starting points that provide fruitful ground: the effects of social identities on emotional experiences of mass events, perceptions of crowdedness and safety, collective self-organisation in pedestrian movement, and helping behaviour in disasters.

Agent-based modeling provides a prime platform for integrating the social identity approach into pedestrian models. Agent-based models can represent varying levels of perceptual and cognitive processes and offer the unique ability to model multiple levels of behaviour, from the individual level to the collective level, that enables the simulation of social influence from individual actions. They can represent varying levels of perceptual and cognitive processes. Importantly, they are also dynamic, as the behaviour of the agents within the crowd, their individual characteristics, and the 'information' that the agents receive, together drive their actions and can be updated at each time step of the simulation (e.g., [91, 111, 112]). Crucially, agent-based models allow us to ask why and how behaviour emerges by exploring the underlying psychological mechanisms, and allow us to operationalise social connections between crowd members. In the next few paragraphs we set out some core foundations to model social identities and principles of self-categorisation.

First, each agent should be given the ability to have both a personal and social identity. That is, they should be able to act both as an individual and a group member, and be able to change from acting in line with their personal identity to their social identity (and vice versa) depending on which identity is salient in a particular context. This will enable modellers to simulate updates in events such as emergencies where the crowd changes from a physical crowd prior to the emergency to a psychological crowd once the emergency is underway (e.g. [108, 109]). The limited work that includes social identities in models could be refined and expanded. Thus far, the models have treated social identification as binary where agents either have a salient social identity or do not, and this is activated as soon as an emergency occurs. Strength of identification exists on a continuum, as exemplified by the scale measures for social identification used in much of the research we have discussed (e.g. [75, 95]). Further work is needed to explore the effects of the strength of social

identity (one's strength of feeling of being a member of their group) and the strength of shared social identity (one's strength of feeling that others also see themselves as being part of the same group) on behaviour.

Second, agents should be given social identities and the ability to know both their own social identity and the social identities of others. This will provide to basis for collective self-organisation as it will enable agents to discern whether other agents are ingroup or outgroup members. Discerning group membership is fundamental for modeling intra- and intergroup scenarios, such as pilgrims performing rituals together, or opposing fans of sports teams during ingress at a stadium.

Third, further research could focus on the changing perceptions of group membership and the implications this has for levels of help provided among crowd members. Identities are dynamic, and categories can be expanded or narrowed depending on what criteria are used to define group membership at the time. For example, if someone was at a meeting within their organisation dedicated to crowd modeling, then they might have a salient social identity as being a member of their particular crowd modeling organisation, and people outside of the organisation are perceived to be outgroup. However, in another context such as a conference for crowd modellers, you may perceive everyone as being a fellow ingroup member, including those who were previously considered to be outgroup. The dynamic nature of identities also has important implications for modeling safety planning at mass events, such as the role of social identity on helping behaviour (e.g. [105]) and providing social support (e.g. [113]). Agent-based modeling with event driven update schemes provides a prime platform to explore changes in perceived group membership and the corresponding effects on behaviour.

Fourth, we can begin to incorporate group processes based on empirical research. One starting point could be modeling the attraction to fellow group members while walking to mimic the collective self-organisation of the psychological crowd found in Templeton et al. [103]. Modellers can use behavioural data to calibrate, validate, and verify their models and test their behavioural outcomes. For example, in Templeton et al. [103], modellers could test their behavioural outcomes of speed, distance, proximity, and group size in a model against the behavioural results from the psychology study.

A fifth avenue for research is to explore the effects of multiple psychological groups in the same areas on crowd movement. The research by Templeton et al. [104] suggested that group members moved in closer proximity and walked slower, less distance, and in closer proximity when walking in counterflow to another psychological group compared to when walking alone. These findings suggest that when considering pedestrian counterflow in crowds, research should consider that groups with a shared social identity prioritise staying together even when it impedes their speed. Further research could explore the effects of multiple groups in different types on environments and when two or more psychological groups move in the same direction.

There are many more opportunities for joint research ventures beyond the five recommendations that we set out in this chapter. Collectively, our different disciplinary backgrounds from pedestrian modeling, event management, crowd psy-

chology, and broader research on collective behaviour has equipped us with a range of skills that could be combined to approach crowd behaviour in a more rigorous and prosperous way. By combining our methodologies and skills we can work together to ascertain a better understanding of crowd behaviour, improve confidence in our predictive models, advance event planning, and ultimately enhance safety and experiences of crowd events.

References

1. D.J. Terry, M.A. Hogg, Group norms and the attitude-behaviour relationship: a role for group identification. Personal. Soc. Psychol. Bull. **22**(8), 776–793 (1996). https://doi.org/10.1177/0146167296228002
2. F.G. Neville, S.D. Reicher, Crowds, social identities, and the shaping of everyday social relations, in *Political Psychology: A Social Psychological Approach*, (Wiley, Hoboken, 2018), pp. 231–252. https://doi.org/10.1002/9781118982365.ch12
3. S. Reicher, Mass action and mundane reality: An argument for putting crowd analysis at the centre of the social sciences. Contemp. Soc. Sci. **6**(3), 433–449 (2011). https://doi.org/10.1080/21582041.2011.61
4. F. Neville, D. Novelli, S. Reicher, J. Drury, Shared identity transforms social relations in imaginary crowds. Group Processes Intergroup Relations (under review).
5. A. Templeton, J. Drury, A. Philippides, From mindless masses to small groups: conceptualizing collective behavior in crowd modeling. Rev. Gen. Psychol. **19**(3), 215–229 (2015). https://doi.org/10.1037/gpr0000032
6. S. Reicher, R. Spears, A. Haslam, The social identity approach in social psychology, in *The SAGE Handbook of Identities*, ed. by M. Wetherall, C. T. Mohanty, (Sage, London, 2010), pp. 45–62
7. S. Barrows, The crowd in the late nineteenth century, in *Distorting Mirrors: Visions of the Crowd in Late Nineteenth-Century France*, ed. by S. Barrows, (The Alpine Press, Soughton, 1981), pp. 7–42
8. S. Jonsson, The invention of the masses: the crowd in French culture from the revolution to the commune, in *Crowds*, ed. by J. T. Schnapp, M. Tiews, (Stanford University Press, Stanford, 2006), pp. 47–75
9. C. McPhail, *The Myth of the Maddening Crowd* (Routledge, New York, 1991)
10. S. Moscovici, *The Age of the Crowd* (Cambridge University Press, Cambridge, 1981/1985)
11. R.A. Nye, *The Origins of Crowd Psychology: Gustave le Bon and the Crisis of Mass Democracy in the Third Republic* (Sage, Beverley Hills, 1976)
12. S. Reicher, The psychology of crowd dynamics, in *Blackwell Handbook of Social Psychology: Group Processes*, ed. by M. Hogg, S. Tindale, (Blackwell Publishers Inc., Malden, 2001), pp. 182–208
13. S. Reicher, Crowds, in *Encyclopaedia of Group Processes and Intergroup Relations*, ed. by J. M. Levine, M. A. Hogg, (Sage, London, 2010)
14. N. Rogers, *Crowds, Culture, and Politics in Georgian Britain* (Oxford University Press, New York, 1998)
15. G. Le Bon (2002), *The Crowd: A Study of the Popular Mind* (T. Fisher Unwin, Trans.) (Dover Publications Inc., Mineola, NY, 2002). (Reprinted from La psychologie des foules, by G. L. Bon, 1895, Paris, France: Les Presses universitairs de France)
16. H. Taine, *Les origines de la France contemporaine* (R. Laffont, Paris, 1878). Bouqins
17. G. Tarde, *Les crimes des foules* (Masson, Paris, 1892)
18. A. Gallup, A. Chong, I. Couzin, The directional flow of visual information transfer between pedestrians. Biol. Lett. **8**(4), 520–522 (2012). https://doi.org/10.1098/rsbl.2012.0160

19. R.P. Mann, J. Faria, D.J. Sumpter, J. Krause, The dynamics of audience applause. J. R. Soc. Interface **10**(85), 20130466 (2013). https://doi.org/10.1098/rsif.2013.0466
20. J. Drury, D. Novelli, C. Stott, Managing to avert disaster: explaining collective resilience at an outdoor music event. Eur. J. Soc. Psychol. **45**(4), 533–547 (2015). https://doi.org/10.1002/ejsp.2108
21. C. Stott, P. Hutchison, J. Drury, 'Hooligans' abroad? Intergroup dynamics, social identity and participation in collective 'disorder' at the 1998 world cup finals. Br. J. Soc. Psychol. **40**(3), 359–384 (2001). https://doi.org/10.1348/014466601164876
22. J. Drury, C. Cocking, S.D. Reicher, The nature of collective resilience: survivor reactions to the 2005 London bombings. Int. J. Mass Emerg. Disasters **27**(1), 66–95 (2009). Retrieved from http://www.ijmed.org/articles/113/download/
23. R. Ball, C. Stott, J. Drury, F. Neville, S. Reicher, S. Choudhury, Who controls the city? A micro-historical case study of the spread of rioting across North London in August 2011. City **23**(4–5), 483–504 (2019). https://doi.org/10.1080/13604813.2019.1685283
24. J. Drury, H. Carter, C. Cocking, E. Ntontis, S. Guven, R. Amlôt, Facilitating collective psychosocial resilience in the public in emergencies: twelve recommendations based on the social identity approach. Front. Public Health **7** (2019). https://doi.org/10.3389/fpubh.2019.00141
25. J. Drury, C. Stott, R. Ball, S. Reicher, F. Neville, L. Bell, M. Biddlestone, S. Choudhury, M. Lovell, C. Ryan, A social identity model of riot diffusion: from injustice to empowerment in the 2011 London riots. Eur. J. Soc. Psychol. **50**(3), 646–661 (2019). https://doi.org/10.1002/ejsp.2650
26. C. Stott, R. Ball, J. Drury, F. Neville, S. Reicher, A. Boardman, S. Choudhury, The evolving normative dimensions of 'riot': towards an elaborated social identity explanation. Eur. J. Soc. Psychol. **48**(6), 834–849 (2018). https://doi.org/10.1002/ejsp.2376
27. F. Cannavale, H. Scarr, A. Pepitone, De-individuation in the small group: further evidence. J. Pers. Soc. Psychol. **16**, 141–147 (1970). https://doi.org/10.1037/h0029837
28. L. Festinger, A. Pepitone, T. Newcombe, Some consequences of deindividuation in a group. J. Abnorm. Soc. Psychol. **47**, 382–389 (1952). https://doi.org/10.1037/h0057906
29. E. Diener, Deindividuation: the absence of self-awareness and self-regulation in group members, in *The Psychology of Group Influence*, ed. by P. Paulus, (Erlbaum, Hillsdale, 1980), pp. 209–242
30. S. Duval, R.A. Wicklund, *A Theory of Objective Self Awareness* (Academic Press, Oxford, 1972)
31. P.G. Zimbardo, The human choice: Individuation, reason, and order versus deindividuation, impulse and chaos, in *Nebraska Symposium on Motivation*, ed. by W. J. Arnold, D. Levine, (University of Nebraska Press, Lincoln, NE, 1969), pp. 237–307
32. T. Postmes, R. Spears, Deindividuation and antinormative behavior: a meta-analysis. Psychol. Bull. **123**(3), 238–259 (1998). https://doi.org/10.1037/0033-2909.123.3.238
33. S.D. Reicher, R. Spears, T. Postmes, A social identity model of deindividuation phenomena. Eur. Rev. Soc. Psychol. **6**, 161–198 (1995). https://doi.org/10.1080/14792779443000049
34. J. Carey, *The Intellectuals and the Masses: Pride and Prejudice among the Literary Intelligentsia, 1880–1939* (Faber & Faber, London, 1992)
35. F.H. Allport, The group fallacy in relation to social science. Am. J. Sociol. **29**(6), 668–706 (1924). https://doi.org/10.1086/213647
36. S. Sighele, *La folla delinquente* (Bocca, Turin, 1891)
37. J. Goodwin, J.M. Jasper, F. Polletta, Introduction: why emotions matter, in *In Passionate Politics: Emotions and Social Movements*, ed. by J. Goodwin, J. Jasper, F. Polletta, (University of Chicago Press, Chicago, 2001), pp. 1–24
38. J. Goodwin, J. M. Jasper, F. Polletta (eds.), *Passionate Politics: Emotions and Social Movements* (University of Chicago Press, London, 2001)
39. W. Kornhauser, *The Politics of Mass Society* (The Free Press, Glencoe, 1959)
40. H.D. Lasswell, *Psychopathology and Politics* (University of Chicago Press, Chicago, 1930)
41. E. Hoffer, *The True Believer: Thoughts on the Nature of Mass Movements* (Harper and Row, New York, 1951)

42. O. Klapp, *Collective Search for Identity* (Holt, Rinehart, New York, 1969)
43. G. Rudé, *The Crowd in the French Revolution* (Oxford University Press, London, 1959)
44. S.D. Reicher, The St. Pauls' riot: an explanation of the limits of crowd action in terms of a social identity model. Eur. J. Soc. Psychol. **14**, 1–21 (1984). https://doi.org/10.1002/ejsp.2420140102
45. N.Z. Davis, The rites of violence: religious riot in sixteenth-century France. Past Present **59**, 51–91 (1973)
46. E.P. Thompson, The moral economy of the English crowd in the eighteenth century. Past Present **50**, 76–136 (1971)
47. R.H. Turner, L. Killian, *Collective Behaviour* (Prentice Hall, Engelwood Cliffs, 1957)
48. M.A. Hogg, G.M. Vaughan, *Social Psychology*, 5th edn. (Essex, Pearson Education Ltd, 2008)
49. S.E. Asch, Group forces in the modification and distortion of judgments, in *Social Psychology*, ed. by S. E. Asch, (Prentice-Hall, Inc., Englewood Cliffs, 1952), pp. 450–501
50. M. Sherif, An experimental approach to the study of attitudes. Sociometry **1**(1/2), 90–98 (1937). https://doi.org/10.2307/2785261
51. S.D. Reicher, 'The Battle of Westminster': developing the social identity model of crowd behaviour in order to explain the initiation and development of collective conflict. Eur. J. Soc. Psychol. **26**, 115–134 (1996). https://doi.org/10.1002/(SICI)1099-0992(199601)26:1<115::AID-EJSP740>3.0.CO;2-Z
52. S.D. Reicher, The Battle of Westminster: developing the social identity model of crowd behaviour in order to deal with the initiation and development of collective conflict. Eur. J. Soc. Psychol. **26**, 115–134 (1996). https://doi.org/10.1002/(SICI)1099-0992(199601)26:1<115::AID-EJSP740>3.0.CO;2-Z
53. S.D. Reicher, Crowd behaviour as social action, in *Rediscovering the Social Group: A Self-Categorization Theory*, ed. by J. Turner, M. Hogg, P. Oakes, S. D. Reicher, M. Wetherell, (Blackwell, Oxford, 1987), pp. 171–202
54. H. Tajfel, *Differentiation Between Social Groups* (Academic Press, London, 1978)
55. H. Tajfel, J.C. Turner, An integrative theory of intergroup conflict, in *The Social Psychology of Intergroup Relations*, ed. by W. G. Austin, S. Worchel, (Brooks/Cole, Monterey, 1979), pp. 33–47
56. J.C. Turner, M.A. Hogg, P.J. Oakes, S.D. Reicher, M.S. Wetherell, *Rediscovering the Social Group: A Self-Categorization Theory* (Basil Blackwell, Oxford, 1987)
57. J.C. Turner, P.J. Oakes, S.A. Haslam, C. McGarty, Self and collective: cognition and social context. Personal. Soc. Psychol. Bull. **20**, 454–463 (1994). https://doi.org/10.1177/0146167294205002
58. J. Drury, S. Reicher, Collective action and psychological change: the emergence of new social identities. Br. J. Soc. Psychol. **39**, 579–604 (2000). https://doi.org/10.1348/014466600164642
59. C.J. Stott, S.D. Reicher, How conflict escalates: the inter-group dynamics of collective football crowd 'violence'. Sociology **32**, 353–377 (1998). https://doi.org/10.1177/0038038598032002007
60. J.C. Turner, Towards a cognitive redefinition of the social group, in *Social Identity and Intergroup Relations*, ed. by H. Tajfel, (Cambridge University Press, Cambridge, 1982), pp. 15–40
61. J.C. Turner, Some current issues in research on social identity and self-categorization theories, in *Social Identity Context, Commitment, Content*, ed. by N. Ellemers, R. Spears, B. Doosje, (Blackwell Publishers, Oxford, 1999), pp. 6–34
62. S.D. Reicher, The context of social identity: domination, resistance, and change. Polit. Psychol. **25**, 921–945 (2004). https://doi.org/10.1111/j.1467-9221.2004.00403.x
63. S. Reicher, The determination of collective behaviour, in *Social Identity and Intergroup Relations*, ed. by H. Tajfel, (Cambridge University Press, Cambridge, 1982), pp. 41–83

64. J. Drury, S. Reicher, The intergroup dynamics of collective empowerment: substantiating the social identity model of crowd behaviour. Group Process. Intergroup Relat. **2**(4), 381–402 (1999). https://doi.org/10.1177/1368430299024005
65. J. Drury, S. Reicher, Explaining enduring empowerment: a comparative study of collective action and psychological outcomes. Eur. J. Soc. Psychol. **35**, 35–58 (2005). https://doi.org/10.1002/ejsp.231
66. J. Drury, S. Reicher, Collective psychological empowerment as a model of social change: researching crowds and power. J. Soc. Issues **65**, 707–772 (2009). https://doi.org/10.1111/j.1540-4560.2009.01622.x
67. S. Reicher, "La beauté Est dans la rue": four reasons (or perhaps five) to study crowds. Group Process. Intergroup Relat. **20**(5), 593–605 (2017). https://doi.org/10.1177/1368430217712835
68. S. Shankar, C. Stevenson, K. Pandey, S. Tewari, N.P. Hopkins, S.D. Reicher, A calming cacophony: social identity can shape experience of loud noise. J. Environ. Psychol. **36**, 87–95 (2013). https://doi.org/10.1016/j.jenvp.2013.07.004
69. N. Srinivasan, N. Hopkins, S.D. Reicher, S.S. Khan, T. Singh, M. Levine, Social meaning of ambiguous sounds influences retrospective duration judgments. Psychol. Sci. **24**(6), 1060–1062 (2013). https://doi.org/10.1177/0956797612465293
70. N. Ellemers, R. Spears, B. Doosje (eds.), *Social Identity: Context, Commitment, Content* (Blackwell, Oxford, 1999)
71. S.A. Haslam, *Psychology in Organizations: The Social Identity Approach* (Sage, Thousand Oaks, CA, 2001)
72. T. Tyler, S.L. Blader, *Cooperation in Groups: Procedural Justice, Social Identity, and Behavioral Engagement* (Psychology Press, Sussex, 2000)
73. S.A. Haslam, J.C. Turner, P.J. Oakes, C. McGarty, K.J. Reynolds, The group as a basis for emergent stereotype consensus. Eur. Rev. Soc. Psychol. **8**, 203–239 (1998). https://doi.org/10.1080/14792779643000128
74. S.A. Haslam, S.D. Reicher, Stressing the group: social identity and the unfolding dynamics of responses to stress. J. Appl. Psychol. **91**, 1037–1052 (2006). https://doi.org/10.1037/0021-9010.91.5.1037
75. D. Novelli, J. Drury, S. Reicher, Come together: two studies concerning the impact of group relations on personal space. Br. J. Soc. Psychol. **49**(2), 223–236 (2010). https://doi.org/10.1348/014466609X449377
76. D. Barr, J. Drury, Activist identity as a motivational resource: dynamics of (dis)empowerment at the G8 direct actions, Gleneagles, 2005. Soc. Mov. Stud. **8**, 243–260 (2009). https://doi.org/10.1080/14742830903024333
77. J. Drury, S. Reicher, C. Stott, Transforming the boundaries of collective identity: from the "local" anti-road campaign to "global" resistance? Soc. Mov. Stud. **2**, 191–212 (2003). https://doi.org/10.1080/1474283032000139779
78. N. Hopkins, S. Reicher, C. Stevenson, K. Pandey, S. Shankar, S. Tewari, Social relations in crowds: recognition, validation and solidarity. Eur. J. Soc. Psychol. **49**, 1283 (2019). https://doi.org/10.1002/ejsp.2586
79. F. Neville, S. Reicher, The experience of collective participation: shared identity, relatedness and emotionality. Contemp. Soc. Sci. **6**(3), 377–396 (2011). https://doi.org/10.1080/21582041.2012.627277
80. C. Cocking, J. Drury, S.D. Reicher, The psychology of crowd behaviour in emergency evacuations: results from two interview studies and implications for the Fire & Rescue Services. Ir. J. Psychol. **30**, 59–73 (2009). https://doi.org/10.1080/03033910.2009.10446298
81. J. Drury, C. Cocking, S.D. Reicher, Everyone for themselves? A comparative study of crowd solidarity among emergency survivors. Br. J. Soc. Psychol. **48**(3), 487–506 (2009). https://doi.org/10.1348/014466608X357893
82. E. Ntontis, J. Drury, R. Amlôt, G.J. Rubin, R. Williams, Emergent social identities in a flood: implications for community psychosocial resilience. J. Community Appl. Soc. Psychol. **28**(1), 3 (2017). https://doi.org/10.1002/casp.2329

83. E. Ntontis, J. Drury, R. Amlôt, G.J. Rubin, R. Williams, Community resilience and flooding in UK guidance: a critical review of concepts, definitions, and their implications. J Contingencies Crisis Manag **27**(1), 2–13 (2019). https://doi.org/10.1111/1468-5973.12223
84. J.M. Jasper, *The Emotions of Protest* (University of Chicago Press, Chicago, 2018)
85. E.R. Smith, C. Seger, D.M. Mackie, Can emotions be truly group level? Evidence regarding four conceptual criteria. J. Pers. Soc. Psychol. **93**, 431–446 (2007). https://doi.org/10.1037/0022-3514.93.3.431
86. G. B. Sullivan (ed.), *Understanding Collective Pride and Group Identity: New Directions in Emotion Theory, Research and Practice* (Routledge, London, 2014)
87. A. Poma, T. Gravante, Emotions and empowerment in collective action: the experience of a women's collective in Oaxaca, Mexico, 2006–2017. Emotions History, Culture, Society **1**(2), 59–79 (2017)
88. S. Vestergren, J. Drury, E.H. Chiriac, How collective action produces psychological change and how that change endures over time: a case study of an environmental campaign. Br. J. Soc. Psychol. **57**(4), 855–877 (2018). https://doi.org/10.1111/bjso.12270
89. N. Hopkins, S.D. Reicher, S.S. Khan, S. Tewari, N. Srinivasan, C. Stevenson, Explaining effervescence: investigating the relationship between shared social identity and positive experience in crowds. Cognit. Emot. **30**(1), 20–32 (2016). https://doi.org/10.1080/02699931.2015.1015969
90. H. Alnabulsi, J. Drury, V.L. Vignoles, S. Oognik, Understanding the impact of the Hajj: explaining experiences of self-change at a religious mass gathering. Eur. J. Soc. Psychol. **50**(2), 292–308 (2018). https://doi.org/10.1002/ejsp.2623
91. Z. Fang, S.M. Lo, J.A. Lu, On the relationship between crowd density and movement velocity. Fire Saf. J. **38**(3), 271–283 (2003). https://doi.org/10.1016/S0379-7112(02)00058-9
92. R.S.C. Lee, R.L. Hughes, Prediction of human crowd pressures. Acc. Anal. Prevent. **38**(4), 712–722 (2006). https://doi.org/10.1016/j.aap.2006.01.001
93. S.D. Reicher, A. Templeton, F. Neville, L. Ferrari, J. Drury, Core disgust is attenuated by ingroup relations. Proc. Natl. Acad. Sci. **133**(10), 2631–2635 (2016). https://doi.org/10.1073/pnas.1517027113
94. D. Novelli, J. Drury, S. Reicher, C. Stott, Crowdedness mediates the effect of social identification on positive emotion in a crowd: a survey of two crowd events. PLoS One **8**(11), e78983 (2013). https://doi.org/10.1371/journal.pone.0078983
95. H. Alnabulsi, J. Drury, Social identification moderates the effect of crowd density on safety at the Hajj. Proc Natl. Acad. Sci. **111**(25), 9091–9096 (2014). https://doi.org/10.1073/pnas.1404953111
96. K. Alfahdli, M. Guler, H. Cakal, J. Drury, The role of emergent shared identity in psychosocial support among refugees of conflict in developing countries. Int. Rev. Soc. Psychol. **32**(1), 1–16 (2019). https://doi.org/10.5334/irsp.176
97. J. Drury, R. Brown, R. Gonzalez, D. Miranda, Emergent social identity and observing social support predict social support provided by survivors in a disaster: solidarity in the 2010 Chile earthquake. Eur. J. Soc. Psychol. **46**(2), 209–233 (2015). https://doi.org/10.1002/ejsp.2146
98. L.Z. Yang, D.L. Zhao, J. Li, T.Y. Fang, Simulation of the kin behavior in building occupant evacuation based on cellular automaton. Build. Environ. **40**(3), 411–415 (2005). https://doi.org/10.1016/j.buildenv.2004.08.005
99. G. Köster, F. Treml, M. Seitz, W. Klein, Validation of crowd models including social groups, in *Pedestrian and Evacuation Dynamics*, ed. by U. Wedmann, U. Kirsch, M. Schreckenberg, (Springer, New York, 2014), pp. 1051–1063. https://doi.org/10.1007/978-3-319-02447-9_87
100. V. Reuter, B.S. Bergner, G. Köster, M. Seitz, F. Treml, D. Hartmann, On modelling groups in crowds: empirical evidence and simulation results including large groups, in *Pedestrian and Evacuation Dynamics*, ed. by U. Weidmann, U. Kirsch, M. Schreckenberg, (Springer, Berlin, 2012), pp. 835–845. https://doi.org/10.1007/978-3-319-02447-9_70
101. D. Nilsson, A. Johansson, Social influence during the initial phase of a fire evacuation-analysis of evacuation experiments in a cinema theatre. Fire Saf. J. **44**(1), 71–79 (2009). https://doi.org/10.1016/j.firesaf.2008.03.008

102. J.R. Dyer, A. Johansson, D. Helbing, I.D. Couzin, J. Krause, Leadership, consensus decision making and collective behaviour in humans. Philos. Trans. Royal Soc. London B Biol. Sci. **364**(1518), 781–789 (2009). https://doi.org/10.1098/rstb.2008.0233
103. A. Templeton, J. Drury, A. Philippides, Walking together: behavioural signatures of psychology crowds. R. Soc. Open Sci. **5**(7), 1–14 (2018). https://doi.org/10.1098/rsos.180172
104. A. Templeton, J. Drury, A. Philippides, Placing large group relations into pedestrian dynamics: psychological crowds in counterflow. Collective Dynamics **4**(A23) (2020). https://doi.org/10.17815/CD.2019.23
105. M. Levine, A. Prosser, D. Evans, S. Reicher, Identity and emergency intervention: how social group membership and inclusiveness of group boundaries shape helping behaviour. Personal. Soc. Psychol. Bull. **34**(4), 443–453 (2005). https://doi.org/10.1177/0146167204271651
106. J. Drury, Collective resilience in mass emergencies and disasters, in *The Social Cure: Identity, Health and Well-being*, ed. by J. Jetten, C. Haslam, A. S. Haslam, (Psychology Press, Hove, 2012), pp. 195–216
107. J. Drury, C. Cocking, S. Reicher, A. Burton, D. Schofield, A. Hardwick, D. Graham, P. Langston, Cooperation versus competition in a mass emergency evacuation: a new laboratory simulation and a new theoretical model. Behav. Res. Methods **41**(3), 957–970 (2009). https://doi.org/10.3758/BRM.41.3.957
108. I. von Sivers, A. Templeton, G. Köster, J. Drury, A. Philippides, Humans do not always act selfishly: social identity and helping in emergency evacuation simulation. Transport. Res. Proc. **2**, 585–593 (2014). https://doi.org/10.1016/j.trpro.2014.09.099
109. I. von Sivers, A. Templeton, F. Kunzner, G. Köster, J. Drury, A. Philippides, T. Neckel, H. Bungartz, Modelling social identification and helping in evacuation simulation. Saf. Sci. **89**, 288–300 (2016). https://doi.org/10.1016/j.ssci.2016.07.001
110. M.J. Seitz, A. Templeton, J. Drury, G. Köster, A. Philippides, Parsimony versus reductionism: how can crowd psychology be introduced into computer simulation? Rev. Gen. Psychol. **21**(1), 95–102 (2016). https://doi.org/10.1037/gpr0000092
111. Q. Ji, C. Gao, Simulating crowd evacuation with a leader-follower model. Int. J. Comp. Sci. Eng. Syst. **1**(4), 249–252 (2007)
112. G. Köster, M. Seitz, F. Treml, D. Hartmann, W. Klein, On modelling the influence of group formations in a crowd. Contemp. Soc. Sci. J. Acad. Soc. Sci. **6**(3), 387–414 (2011). https://doi.org/10.1080/21582041.2011.619867
113. H. Alnabulsi, J. Drury, A. Templeton, Predicting collective behaviour at the hajj: places, space and the process of cooperation. Philos. Transact. B **373**, 20170240 (2018). https://doi.org/10.1098/rstb.2017.0240
114. C.J.T. Stott, O. Adang, Disorderly conduct: social psychology and the control of football 'hooliganism' at Euro2004. The Psychologist **17**, 318–319 (2004)
115. J. Sievers, VoronoiLimit(varagin) [Software] (2012). Available from https://uk.mathworks.com/matlabcentral/fileexchange/34428-voronoilimit-varargin requestedDomain=www.mathworks.com

Crowd Dynamics Through Conservation Laws

Rinaldo M. Colombo, Magali Lecureux-Mercier, and Mauro Garavello

Abstract We consider several macroscopic models, based on systems of conservation laws, for the study of crowd dynamics. All the systems considered here contain nonlocal terms, usually obtained through convolutions with smooth functions, used to reproduce the visual horizon of each individual. We classify the various models according to the physical domain (the whole space $\mathbb{R}^N$ or a bounded subset), to the terms affected by the nonlocal operators, and to the number of different populations we aim to describe. For all these systems, we present the basic well posedness and stability results.

1 Introduction

From a macroscopic point of view, a crowd can be described through a density function ρ, i.e., a time and space dependent quantity measuring the fraction of space occupied by individuals. It is then natural to ground macroscopic crowd dynamics models on *Conservation Laws*, which are partial differential equations of the form

$$\partial_t \rho + \mathrm{div}_x(\rho\, v) = 0 \qquad \begin{array}{l} t \in \mathbb{R}^+ \text{ (time)}, \\ x \in \Omega \quad \text{(space coordinate)}, \end{array} \tag{1.1}$$

R. M. Colombo (✉)
University of Brescia, Brescia, Italy
e-mail: rinaldo.colombo@unibs.it

M. Lecureux-Mercier
Lycée Lakanal, 3 Avenue du Président Franklin Roosevelt, 92330, Sceaux

M. Garavello
Department of Mathematics and Its Applications, University of Milano-Bicocca, Milano, Italy
e-mail: mauro.garavello@unimib.it

L. Gibelli (ed.), *Crowd Dynamics, Volume 2*, Modeling and Simulation in Science, Engineering and Technology, https://doi.org/10.1007/978-3-030-50450-2_5

where Ω, typically a subset of $\mathbb{R}^2$, is the domain available to crowd's movements. A key role is played by the *speed law* v, a map assigning to each $(t, x) \in \Omega$ the velocity vector describing the movement of the individual at position x at time t.

Equation (1.1), also known as the *continuity equation*, is used in a variety of modeling frameworks, ranging from fluid dynamics to vehicular traffic. Specific features of crowd motion are its being not isotropic and the fact that each *"particle"* moves according to what he/she sees within his/her own visual horizon. These features are present in the speed law: in particular, in the models presented in the sequel, v depends on ρ or on its space gradient $\nabla_x \rho$ through spatial averages, usually obtained through convolutions $\rho * \eta$, or $\nabla_x(\rho * \eta)$, with an averaging kernel η, i.e., $\eta \in \mathbf{C}^1(\mathbb{R}^2; \mathbb{R}^+)$ and $\int_{\mathbb{R}^2} \eta = 1$. The geometry of the support of η, in particular its diameter, describes the visual horizon of the individuals in the crowd.

Moreover, again differently from fluid particles, individuals in a crowd may well have different destinations, behaviors or reactions. Within the framework provided by (1.1), this variety can be described through the introduction of different populations, replacing (1.1) with a system, say

$$\partial_t \rho_i + \mathrm{div}_x(\rho_i\, v_i) = 0 \qquad i = 1, \dots, n, \tag{1.2}$$

where members of the same populations, that is, counted within the same density ρ_i, have somewhat homogeneous behaviors, for instance, sharing the same destination. Otherwise, when a few single individuals play a leading role in directing the crowd motion, we use equations of the type (1.1) or (1.2) coupled with ordinary differential equations describing the leaders' movements.

A natural question arising from the results below is the relation between *nonlocal* and *local* models, the latter referring to situations where v depends on $\rho(x)$, i.e., on ρ evaluated at a single point x. Since, as is well known, $\rho * \eta \to \rho$ as $\eta \to \delta$, δ being Dirac's delta, one might expect similar convergence results ensuring the convergence of nonlocal models to local ones as the visual horizon vanishes, see [3]. This question motivated various results yielding negative answers [35–38] as well as positive results, see [18].

Crowd dynamics is currently described also through other analytic tools: from systems of partial differential equations motivated through fluid dynamics [59], to cellular automata [4], to measure valued partial differential equations [55, 56], to kinetic models [2, 6], to discrete or microscopic models [5, 24, 51]. Also the level of the related works is very diverse, ranging from purely analytic investigations [39], to numerically oriented results [14], to data analysis [54]. For more information on mixed systems and relations among the different descriptions, refer for instance to [7, 8, 43] and to the references therein.

It is worth mentioning also the modeling of crowd dynamics through conservation laws that mimic fluid dynamics, developed, for instance, in [41, 45].

On the other hand, nonlocal conservation laws are currently used also in the modeling of vehicular traffic [9, 21–23], in that of supply chains [40, 58], in predator prey dynamics [27], in the modeling of laser beams cutting steel [25, 53] as well as in the modeling of biological pest control [31]. Other strictly analytical investigations on nonlocal conservation or balance laws are, for instance, [42].

Hoping that this work might serve as a reference, all statements are placed in $\mathbb{R}^N$ wherever this generality does not require any extra effort.

Throughout, I is a fixed time interval, say $I = [0, T]$ for a positive T, or $I = \mathbb{R}^+$. The notation used for function spaces and differential operators is standard and collected in section "List of Symbols" in Appendix.

The next section is devoted to the analytic results that serve as a basis for the later sections. In Sect. 3 we describe models for one or more populations defined on all of $\mathbb{R}^N$, so that the geometric constraints to crowd movements are encoded in the speed law v. The case of Initial Boundary Value Problems (IBVP) is treated in Sect. 5 while mixed systems consisting of coupled ordinary and partial differential equations are deferred to Sect. 6.

2 Stability and Well Posedness in MultiD Conservation Laws

This section provides the basic well posedness and stability results on the Cauchy Problem for a scalar multiD balance law of the type

$$\begin{cases} \partial_t \rho + \operatorname{div}_x f(t, x, \rho) = F(t, x, \rho) \\ \rho(0, x) = \rho_o(x)\,. \end{cases} \tag{2.1}$$

The definitions and theorems in this section serve both as a tool and as a model for the subjects developed in later sections. Several monographs cover the basic theory of conservation, or balance, laws. We refer, for instance, to [16, 44, 47].

Definition 2.1 ([47, Chapter 1]) Fix an initial datum $\rho_o \in \mathbf{L}^\infty(\mathbb{R}^N; \mathbb{R})$. A function $\rho \in \mathbf{L}^\infty\big(I; \rho_o + \mathbf{L}^1(\mathbb{R}^N; \mathbb{R})\big)$ is a *weak solution* to (2.1) if $\lim_{t\to 0+} \rho(t) = \rho_o$ in $\mathbf{L}^1$ and for any test function $\varphi \in \mathbf{C}_c^\infty(\mathring{I} \times \mathbb{R}^N; \mathbb{R}^+)$

$$\int_I \int_{\mathbb{R}^N} \Big[\rho(t,x)\, \partial_t \varphi(t,x) + f\big(t, x, \rho(t,x)\big) \cdot \nabla_x \varphi(t,x) + F\big(t, x, \rho(t,x)\big)\, \varphi(t,x) \Big] \mathrm{d}x\, \mathrm{d}t = 0.$$

Even in the case of a (nonlinear) Riemann Problem [16, Chapter 5] in one space dimension, such as

$$\begin{cases} \partial_t \rho + \partial_x \left(\frac{1}{2}\, \rho^2 \right) = 0 \\ \rho(0, x) = \begin{cases} -1 & x < 0 \\ 1 & x \geq 0\,, \end{cases} \end{cases} \tag{2.2}$$

the above definition does not single out a unique solution, since both the maps

$$\rho(t,x) = \begin{cases} -1 & x < 0 \\ 1 & x \geq 0 \end{cases} \quad \text{and} \quad \rho(t,x) = \begin{cases} -1 & x \leq t \\ x/t & x \in]-t, t[\\ 1 & x \geq t \end{cases}$$

solve (2.2) in the sense of Definition 2.1.

It is the next, classical, definition that under suitable assumptions singles out a unique solution to (2.1) and is used throughout the next sections.

Definition 2.2 ([49, Definition 1], [47, § 2.1]) Fix an initial datum $\rho_o \in \mathbf{L}^\infty(\mathbb{R}^N;\mathbb{R})$. A function $\rho \in \mathbf{L}^\infty\big(I;\rho_o + \mathbf{L}^1(\mathbb{R}^N;\mathbb{R})\big)$ is a *Kružkov solution* to (2.1) if $\lim_{t\to 0+} \rho(t) = \rho_o$ in $\mathbf{L}^1$ and for any constant $k \in \mathbb{R}$ and for any test function $\varphi \in \mathbf{C}_c^\infty(\mathring{I} \times \mathbb{R}^N;\mathbb{R}^+)$

$$\int_I \int_{\mathbb{R}^N} \Big[\big(\rho(t,x) - k\big)\, \partial_t \varphi(t,x) + \big(f\big(t,x,\rho(t,x)\big) - f(t,x,k)\big) \cdot \nabla_x \varphi(t,x) + \big(F\big(t,x,\rho(t,x)\big) - \operatorname{div}_x f(t,x,k)\big)\, \varphi(t,x) \Big] \operatorname{sgn}\big(\rho(t,x) - k\big)\, \mathrm{d}x\, \mathrm{d}t \geq 0\,.$$

Both choices $k > \|\rho\|_{\mathbf{L}^\infty(I\times\mathbb{R}^N;\mathbb{R})}$ and $k < -\|\rho\|_{\mathbf{L}^\infty(I\times\mathbb{R}^N;\mathbb{R})}$ show that a Kružkov solution is also a weak solution.

The results collected below ensure that Definition 2.2 is the correct tool to establish a well posedness theory for the Cauchy Problem (2.1).

2.1 The Linear Case

We consider first the case where f in (2.1) is linear in ρ and F is affine in ρ, i.e.:

$$\partial_t \rho + \operatorname{div}_x (\rho\, v(t,x)) = \alpha(t,x)\, \rho + \beta(t,x)\,. \tag{2.3}$$

In the study of (2.3), the *characteristic equation* $\dot{x} = v(t,x)$ plays a key role. Therefore, with reference to (2.3), introduce the notation

$$t \to X(t;t_o,x_o) \quad \text{is the solution to} \quad \begin{cases} \dot{x} = v(t,x) \\ x(t_o) = x_o\,. \end{cases} \tag{2.4}$$

We collect here a few results about the map X above.

Lemma 2.3 *Assume that*

$$\begin{aligned} v &\in \mathbf{C}^0(I \times \mathbb{R}^N; \mathbb{R}^N)\,, \\ v(t) &\in \mathbf{C}^1(\mathbb{R}^N; \mathbb{R}^N) \qquad \textit{for all } t \in I\,, \\ \|v(t,x)\| &\leq A(t) + B\,\|x\| \qquad \textit{where } A \in \mathbf{L}^1(I; \mathbb{R}^+) \textit{ and } B \in \mathbb{R}^+\,. \end{aligned} \tag{2.5}$$

Then, the map X defined in (2.4) is well defined and, for a.e. $t, t_o \in I$, $x \in \mathbb{R}^N$ and $\delta_o \in \mathbb{R}^N$

$$\begin{aligned} \partial_t X(t; t_o, x_o) &= v\left(t, X(t; t_o, x_o)\right)\,, \\ \partial_{t_o} X(t; t_o, x_o) &= -v(t_o, x_o)\, \exp \textstyle\int_{t_o}^t \nabla_x v\left(\tau, X(\tau; t_o, x_o)\right) \mathrm{d}\tau\,, \\ D_{x_o} X(t; t_o, x_o)\, \delta_o &= \delta(t) \quad \textit{where} \quad \begin{cases} \dot\delta = \nabla_x v\left(t, X(t; t_o, x_o)\right)\, \delta \\ \delta(t_o) = \delta_o\,, \end{cases} \\ \det D_{x_o} X(t; t_o, x_o) &= \exp\left(\textstyle\int_{t_o}^t \mathrm{div_x}\, v\left(\tau, X(\tau; t_o, x_o)\right) \mathrm{d}\tau \right)\,. \end{aligned}$$

The proof relies on classical ordinary differential equations techniques; see for instance [17, § 2.3] and [33, § 5.1].

A careful mixing of [33, Lemma 5.1, Lemma 5.2] and [27, Proposition 2.8], see also [29], yields the following result.

Theorem 2.4 *Consider the Cauchy Problem*

$$\begin{cases} \partial_t \rho + \mathrm{div_x}\left(\rho\, v(t,x)\right) = \alpha(t,x)\, \rho + \beta(t,x) \\ \rho(0,x) = \rho_o(x), \end{cases} \tag{2.6}$$

where v satisfies (2.5) and

$$\begin{aligned} \alpha &\in \mathbf{L}^\infty\big(I; \mathbf{L}^1(\mathbb{R}^N; \mathbb{R})\big)\,, & \alpha(t) &\in \mathbf{C}^0(\mathbb{R}^N; \mathbb{R})\,, \\ \beta &\in \mathbf{L}^\infty(I \times \mathbb{R}^N; \mathbb{R})\,, & \beta(t) &\in \mathbf{C}^0(\mathbb{R}^N; \mathbb{R})\,. \end{aligned}$$

Then, for all $\rho_o \in (\mathbf{L}^1 \cap \mathbf{L}^\infty)(\mathbb{R}^N; \mathbb{R})$, the map

$$\begin{aligned} \rho(t,x) = \rho_o\big(X(t_o; t, x)\big)\, \exp\left(\int_{t_o}^t \big(\alpha\big(\tau, X(\tau; t, x)\big) - \mathrm{div_x}\, v\big(\tau, X(\tau; t, x)\big)\big)\, \mathrm{d}\tau \right) \\ + \int_{t_o}^t \beta\big(s, X(s; t, x)\big) \exp\left(\int_s^t \big(\alpha\big(\tau, X(\tau; t, x)\big) - \mathrm{div_x}\, v\left(\tau, X(\tau; t, x)\right)\big)\mathrm{d}\tau \right) \mathrm{d}s \end{aligned} \tag{2.7}$$

solves (2.6) in the sense of Definition 2.2 (Kružkov solution). Moreover, any solution to (2.6) in the sense of Definition 2.1 (weak solution) coincides with ρ as given by (2.7).

The explicit expression (2.7) allows to prove a variety of estimates, see [27, 29, 33].

2.2 The General Case

The classical work by Kružkov [49] ensures the existence of a solution to (2.1), its uniqueness and its continuous dependence on the initial datum with respect to the $\mathbf{L}^1$ norm.

The stability of solutions with respect to the flow f and source F is more recent. The case of a conservation law, i.e. $F = 0$, was initially addressed assuming that the flow depends only on the unknown variable, i.e. $f = f(\rho)$. A first result in this direction is in [52], inspired by numerics, and an improvement was then obtained in [15], while the case of systems in one space dimension was solved in [10].

An x dependent flow was then considered in [20] where the necessity of *a priori* bounds on the total variation in space of the solution is evident.

The stability of the solutions to the general balance law (2.1) with respect to variations in the time and space dependent flow and source was first addressed in [32], with further improvements being provided in [50].

Introduce the following assumptions on (2.1):

(H.1) $f \in \mathbf{C}^0(I \times \mathbb{R}^N \times \mathbb{R}; \mathbb{R}^N)$, the derivatives $\partial_\rho f, \partial_\rho \nabla_x f, \nabla_x^2 f$ exist and are continuous and for all $R > 0$, $\partial_\rho f \in \mathbf{L}^\infty(I \times \mathbb{R}^N \times [-R, R]; \mathbb{R}^N)$.
$F \in \mathbf{C}^0(I \times \mathbb{R}^N \times \mathbb{R}; \mathbb{R})$ and the derivatives $\partial_\rho F, \nabla_x F$ exist and are continuous.
For all $R > 0$, $(F - \mathrm{div}_{\mathrm{x}} f)$, $\partial_\rho (F - \mathrm{div}_{\mathrm{x}} f) \in \mathbf{L}^\infty(I \times \mathbb{R}^N \times [-R, R]; \mathbb{R})$.

(H.2) For all $R > 0$, $\partial_\rho \nabla_x f \in \mathbf{L}^\infty(I \times \mathbb{R}^N \times [-R, R]; \mathbb{R}^{N \times N})$, $\partial_\rho F \in \mathbf{L}^\infty(I \times \mathbb{R}^N \times [-R, R]; \mathbb{R})$ and $\int_I \int_{\mathbb{R}^N} \|\nabla_x (F - \mathrm{div}_{\mathrm{x}} f)(t, x, \cdot)\|_{\mathbf{L}^\infty([-R,R];\mathbb{R})} \mathrm{d}x \mathrm{d}t < +\infty$.

(H.3) For all $R > 0$, $\partial_\rho f \in \mathbf{L}^\infty(I \times \mathbb{R}^N \times [-R, R]; \mathbb{R}^{N \times N})$, $\partial_\rho F \in \mathbf{L}^\infty(I \times \mathbb{R}^N \times [-R, R]; \mathbb{R})$ and $\int_I \int_{\mathbb{R}^N} \|(F - \mathrm{div}_{\mathrm{x}} f)(t, x, \cdot)\|_{\mathbf{L}^\infty([-R,R];\mathbb{R})} \mathrm{d}x \mathrm{d}t < +\infty$.

First, we recall the key well posedness result by Kružkov.

Theorem 2.5 ([49, Theorem 1]) *Let f, F satisfy **(H.1)** and fix $\rho_o \in \mathbf{L}^\infty(\mathbb{R}^N; \mathbb{R})$. Then, the Cauchy Problem (2.1) admits a unique Kružkov solution ρ defined on all I and $\mathbf{L}^1$-continuous in time from the right.*

The following total variation estimate is a necessary step towards the stability estimate on the dependence of the solution to (2.1) on flow and source.

Theorem 2.6 ([50, Theorem 2.2]) *Let **(H.1)** and **(H.2)** hold. Fix an initial datum $\rho_o \in (\mathbf{L}^1 \cap \mathbf{L}^\infty \cap \mathbf{BV})(\mathbb{R}^N; \mathbb{R})$. Then, the Kružkov solution ρ to (2.1) satisfies $\rho(t) \in \mathbf{BV}(\mathbb{R}^N; \mathbb{R})$ for all $t \in I$.*

Define

$$\begin{array}{ll} \mathcal{R} = \|\rho\|_{\mathbf{L}^\infty([I \times \mathbb{R}^N; \mathbb{R})}\,, & \mathcal{S}_t = \bigcup_{\tau \in [0,t]} \mathrm{spt}\, \rho(\tau)\,, \\ R_t = \|\rho(t)\|_{\mathbf{L}^\infty(\mathbb{R}^N; \mathbb{R})}\,, & \Sigma_t = I \times \mathcal{S}_t \times [-\mathcal{R}, \mathcal{R}]\,, \\ \kappa = (2N+1)\|\partial_u \nabla_x f\|_{\mathbf{L}^\infty(\Sigma_\rho; \mathbb{R}^{N \times N})} + \|\partial_u F\|_{\mathbf{L}^\infty(\Sigma_\rho; \mathbb{R})}\,. & \end{array} \tag{2.8}$$

Then, for all $t \in I$, setting $W_N = \int_0^{\pi/2} (\cos\theta)^N \mathrm{d}\theta$,

$$\mathrm{TV}\left(\rho(t)\right) \leq \mathrm{TV}\left(\rho_o\right) \mathrm{e}^{\kappa t} + N W_N \int_0^t \mathrm{e}^{k(t-\tau)} \int_{\mathbb{R}^N} \|\nabla_x (F - \mathrm{div}_{\mathrm{x}}\, f)(\tau, x, \cdot)\|_{\mathbf{L}^\infty([-R_\tau, R_\tau];\mathbb{R}^N)} \mathrm{d}x \mathrm{d}\tau.$$

Remark that when (2.1) reduces to the usual case $\partial_t \rho + \mathrm{div}_{\mathrm{x}}\, f(\rho) = 0$, the above estimate reduces to the well known property that solutions to conservation law have a nonincreasing total variation in space.

Moreover, setting $f = 0$ and $F = F(t, \rho)$, (2.1) reduces to a Cauchy Problem for an ordinary differential equation and, coherently, the estimate provided by Theorem 2.6 reduces to the standard ODE estimate resulting from the application of Gronwall Lemma.

The continuous dependence of the solutions to (2.1) on time directly follows from Theorem 2.6.

Corollary 2.7 ([50, Corollary 2.4]) *Let (H.1)–(H.3) hold. Fix an initial datum $\rho_o \in (\mathbf{L}^1 \cap \mathbf{L}^\infty \cap \mathbf{BV})(\mathbb{R}^N; \mathbb{R})$. Then, the Kružkov solution ρ to (2.1) satisfies $\rho \in \mathbf{C}^0\big(I; \rho_o + \mathbf{L}^1(\mathbb{R}^N; \mathbb{R})\big)$ and moreover for any $t_1, t_2 \in I$, with the notation (2.8),*

$$\|\rho(t_1) - \rho(t_2)\|_{\mathbf{L}^1(\mathbb{R}^N;\mathbb{R})} \leq \left| \int_{t_1}^{t_2} \int_{\mathbb{R}^N} \|(F - \mathrm{div}_{\mathrm{x}}\, f)(\tau, x, \cdot)\|_{\mathbf{L}^\infty([-\mathcal{R}, \mathcal{R}];\mathbb{R})} \mathrm{d}x \mathrm{d}\tau \right| + \|\partial_u f\|_{\mathbf{L}^\infty(\Sigma_\rho;\mathbb{R})} \sup_{\tau \in [0,t]} \mathrm{TV}\left(\rho(\tau)\right) |t_1 - t_2|\,.$$

Moreover, under the stronger condition

$$\sup_{t \in I} \int_{\mathbb{R}^N} \|(F - \mathrm{div}_{\mathrm{x}}\, f)(\tau, x, \cdot)\|_{\mathbf{L}^\infty([-\mathcal{R}, \mathcal{R}];\mathbb{R})} \mathrm{d}x < +\infty\,,$$

we have $\rho \in \mathbf{C}^{0,1}\big(I; \rho_o + \mathbf{L}^1(\mathbb{R}^N; \mathbb{R})\big)$.

We are now ready to tackle the stability of the solutions to (2.1) with respect to variations in the flow f and in the source F. To this aim, we consider the two Cauchy Problems

$$\begin{cases} \partial_t \hat{\rho} + \mathrm{div}_{\mathrm{x}}\, \hat{f}(t, x, \hat{\rho}) = \hat{F}(t, x, \hat{\rho}) \\ \hat{\rho}(0, x) = \hat{\rho}_o(x) \end{cases} \text{ and } \begin{cases} \partial_t \check{\rho} + \mathrm{div}_{\mathrm{x}}\, \check{f}(t, x, \check{\rho}) = \check{F}(t, x, \check{\rho}) \\ \check{\rho}(0, x) = \check{\rho}_o(x)\,. \end{cases} \tag{2.9}$$

Theorem 2.8 ([50, Theorem 2.5]) *Let both pairs $(\hat{f}, \hat{F})$ and $(\check{f}, \check{F})$ satisfy (H.1), $(\hat{f}, \hat{F})$ satisfy (H.2) and $(\hat{f} - \check{f}, \hat{F} - \check{F})$ satisfy (H.3). Fix initial data $\hat{\rho}_o$, $\check{\rho}_o$ in $(\mathbf{L}^1 \cap \mathbf{L}^\infty \cap \mathbf{BV})(\mathbb{R}^N)$ and call $\hat{\rho}$, $\check{\rho}$ the corresponding solutions. Besides the quantities defined in (2.8), introduce also*

$$
\begin{aligned}
&\bar{\mathcal{S}}_t = \bigcup_{\tau\in[0,t]} \operatorname{spt}\hat{\rho}(\tau) \cup \operatorname{spt}\check{\rho}(\tau)\,, \qquad
\bar{\mathcal{R}} = \max\left\{\|\hat{\rho}\|_{\mathbf{L}^\infty(I\times\mathbb{R}^N;\mathbb{R})}, \|\check{\rho}\|_{\mathbf{L}^\infty(I\times\mathbb{R}^N;\mathbb{R})}\right\},\\
&\Sigma_t = [0,t]\times\mathcal{S}_t\times[-\bar{\mathcal{R}},\bar{\mathcal{R}}]\,, \qquad
\bar{R}_t = \sup_{x\in\mathbb{R}^N}\max\left\{\hat{\rho}(t,x),\check{\rho}(t,x)\right\},\\
&M = \left\|\partial\check{\rho}\right\|_{\mathbf{L}^\infty(I\times\mathbb{R}^N\times[-\check{R},\check{R}];\mathbb{R})}, \qquad
\kappa^* = \left\|\partial_\rho F\right\|_{\mathbf{L}^\infty(\Sigma_t;\mathbb{R})} + \left\|\partial_\rho \operatorname{div}_{\mathrm{x}}(\check{f}-\hat{f})\right\|_{\mathbf{L}^\infty(\Sigma_t;\mathbb{R})}.
\end{aligned}
$$

Then, for any positive r and for any x_o in $\mathbb{R}^N$, the solutions $\hat{\rho}$ and $\check{\rho}$ to (2.9) satisfy:

$$
\begin{aligned}
&\int_{\|x-x_o\|\le r} \left|\hat{\rho}(t,x)-\check{\rho}(t,x)\right|\mathrm{d}x\\
&\le \mathrm{e}^{\kappa^* t}\int_{\|x-x_o\|\le r+Mt}\left|\hat{\rho}_o(x)-\check{\rho}_o(x)\right|\mathrm{d}x\\
&+\frac{\mathrm{e}^{\kappa t}-\mathrm{e}^{\kappa^* t}}{\kappa-\kappa^*}\operatorname{TV}(\hat{\rho}_o)\left\|\partial_\rho(\hat{f}-\check{f})\right\|_{\mathbf{L}^\infty(\Sigma_t;\mathbb{R}^N)}\\
&+NW_N\int_0^t\frac{\mathrm{e}^{\kappa(t-\tau)}-\mathrm{e}^{\kappa^*(t-\tau)}}{\kappa-\kappa^*}\int_{\mathbb{R}^N}\left\|\nabla_x(\hat{F}-\operatorname{div}_{\mathrm{x}}\hat{f})(\tau,x,\cdot)\right\|_{\mathbf{L}^\infty([-R_\tau,R_\tau];\mathbb{R}^N)}\mathrm{d}x\mathrm{d}\tau\\
&\qquad\qquad\times\left\|\partial_\rho(\hat{f}-\check{f})\right\|_{\mathbf{L}^\infty(\Sigma_t;\mathbb{R})}\\
&+\int_0^t \mathrm{e}^{\kappa^*(t-\tau)}\int_{\|x-x_o\|\le r+M(t-\tau)}\left\|\left((\hat{F}-\check{F})-\operatorname{div}_{\mathrm{x}}(\hat{f}-\check{f})\right)(\tau,x,\cdot)\right\|_{\mathbf{L}^\infty([-\bar{R}_\tau,\bar{R}_\tau];\mathbb{R})}\mathrm{d}x\mathrm{d}\tau.
\end{aligned}
$$

The above estimate can be easily extended to bound the $\mathbf{L}^1$ distance between solutions over all of $\mathbb{R}^N$.

As a side remark, we observe that the recurrent appearance of the term $F-\operatorname{div}_{\mathrm{x}} f$ is to be expected, for it reflects the obvious nonuniqueness of the distinction between *flow* and *source*. Indeed, for instance, in the case $n=N=1$, the two flow–source pairs

$$
\begin{matrix}\check{f}(t,x,u)=u-x\\ \check{F}(t,x,u)=0\end{matrix}
\qquad\text{and}\qquad
\begin{matrix}\hat{f}(t,x,u)=u\\ \hat{F}(t,x,u)=1\end{matrix}
$$

define the same balance law and, clearly, $\check{F}-\operatorname{div}_{\mathrm{x}}\check{f}=\hat{F}-\operatorname{div}_{\mathrm{x}}\hat{f}$.

3 A Single Population in $\mathbb{R}^N$

While moving in a crowd, each individual is affected by what happens within his/her visual horizon. It is then natural to choose the speed law v in the general model (1.1) so that its value at time t and position x depends on the density ρ as a *function*, not only on the value $\rho(t,x)$ attained by ρ at (t,x). In other words, the term *nonlocal* means that the flux function may depend in a nonlocal way on the density. More

precisely, we consider the Cauchy Problem

$$\begin{cases} \partial_t \rho + \mathrm{div}_x \left(\rho\, V\big(t, x, \rho, \mathcal{I}(\rho)\big)\right) = 0 \\ \rho(0, x) = \rho_o(x), \end{cases} \tag{3.1}$$

where ρ is the crowd density, V is the velocity vector field, and $\mathcal{I}$ is a nonlocal operator. A typical choice for the operator $\mathcal{I}$ is a convolution operator, such as

$$\big(\mathcal{I}\big(\rho(t)\big)\big)(x) = \big(\rho(r) * \eta\big)(x) = \int_{\mathbb{R}^N} \rho(t, \xi)\ \eta(x - \xi)\, \mathrm{d}\xi\ .$$

As soon as η is sufficiently regular, nonnegative and with integral 1, the quantity $\big(\mathcal{I}\big(\rho(t)\big)\big)(x)$ above yields a weighted average of the values attained by ρ at time t around x.

Below, we addressed the basic well posedness and stability issues related to (3.1). In doing this, we distinguish two different nonlocalities in V^i, namely the one where the speed modulus is given by a nonlocal operator, and that where it is (also) the velocity direction which is a nonlocal operator.

A numerical procedure to integrate (3.1) is detailed in [3].

3.1 A NonLocal Speed Modulus

As a first example of (3.1) we assume that the pedestrians' trajectories are assigned, but their speed depends on the local average of the crowd density. Hence, we consider a speed law of the form

$$V\big(t, x, \rho, \mathcal{I}(\rho)\big) = v\left(\mathcal{I}\big(\rho(t)\big)\right)\ \mathbf{v}(x), \tag{3.2}$$

where $\mathcal{I}(\rho) = \rho * \eta$, the convolution kernel η being smooth, nonnegative and with $\int_{\mathbb{R}^N} \eta(x)\mathrm{d}x = 1$, so that $(\rho(t) * \eta)(x)$ results in the local average of the density $\rho(t)$ in $x + \mathrm{spt}\,\eta$. The scalar nonnegative function v is nonincreasing, meaning that at higher densities the speed is lower. The unit vector $\mathbf{v}(x)$ describes the direction typically followed by the individual at x.

Definition 3.1 ([33, Definition 2.1]) Fix $\rho_0 \in \mathbf{L}^\infty(\mathbb{R}^N; \mathbb{R})$. A *weak entropy solution to* (3.1)–(3.2) *on* I is a bounded measurable map $\rho \in \mathbf{C}^0\big(I; \mathbf{L}^1_{loc}(\mathbb{R}^N; \mathbb{R})\big)$ which is a Kružkov solution to

$$\begin{cases} \partial_t \rho + \mathrm{div}_x\, (\rho\, w(t, x)) = 0 \\ \rho(0, x) = \rho_0(x) \end{cases} \qquad \text{where} \qquad w(t, x) = \big(V(\rho(t))\big)(x)\,.$$

The basic well posedness and stability result for (3.1)–(3.2) is as follows.

Theorem 3.2 ([33, Theorem 2.2 and Proposition 4.1]) *Consider the conservation law (3.1) with speed law (3.2). Assume that*

$v \in \mathbf{C}^2(\mathbb{R};\mathbb{R})$
$\mathbf{v} \in (\mathbf{C}^2 \cap \mathbf{W}^{2,1})(\mathbb{R}^N;\mathbb{R}^N)$ *with* $\sup_{\mathbb{R}^N} \|\mathbf{v}(s)\| \le 1$,
$\eta \in \mathbf{C}^2_c(\mathbb{R}^N;\mathbb{R}^+)$ *is such that* $\operatorname{spt}\eta \subseteq \overline{B(0,1)}$ *and* $\|\eta\|_{\mathbf{L}^1(\mathbb{R}^N;\mathbb{R})} = 1$.

Then, for all $\alpha, \beta > 0$ with $\beta > \alpha$, there exists a time $T(\alpha,\beta) > 0$ such that for all $\rho_0 \in (\mathbf{L}^1 \cap \mathbf{BV})(\mathbb{R}^N;[0,\alpha])$, problem (3.1)–(3.2) admits a unique weak entropy solution $\rho \in \mathbf{C}^0\big([0,T(\alpha,\beta)];(\mathbf{L}^1 \cap \mathbf{BV})(\mathbb{R}^N;[0,\beta])\big)$ in the sense of Definition 3.1. Moreover,

1. $\|\rho(t)\|_{\mathbf{L}^\infty(\mathbb{R}^N;\mathbb{R})} \le \beta$ *for all* $t \in [0,T(\alpha,\beta)]$.
2. *There exists a function $L \in \mathbf{C}^0(\mathbb{R}^+;\mathbb{R}^+)$ such that for all $\rho_{0,1}, \rho_{0,2}$ in $(\mathbf{L}^1 \cap \mathbf{BV})(\mathbb{R}^N;[0,\alpha])$, the corresponding solutions satisfy, for all $t \in [0,T(\alpha,\beta)]$,*

$$\|\rho_1(t) - \rho_2(t)\|_{\mathbf{L}^1(\mathbb{R}^N;\mathbb{R})} \le L(t) \left\|\rho_{0,1} - \rho_{0,2}\right\|_{\mathbf{L}^1(\mathbb{R}^N;\mathbb{R})}.$$

3. *There exists a constant $\mathcal{L} = \mathcal{L}(\beta)$ such that for all $\rho_0 \in (\mathbf{L}^1 \cap \mathbf{BV})(\mathbb{R}^N;[0,\alpha])$, the corresponding solution satisfies for all $t \in [0,T(\alpha,\beta)]$*

$$\begin{aligned} \operatorname{TV}(\rho(t)) &\le \big(\operatorname{TV}(\rho_0) + \mathcal{L}\, t\, \|\rho_0\|_{\mathbf{L}^\infty(\mathbb{R}^N;\mathbb{R})}\big)\, \mathrm{e}^{\mathcal{L}t} \\ \|\rho(t)\|_{\mathbf{L}^\infty(\mathbb{R}^N;\mathbb{R})} &\le \|\rho_0\|_{\mathbf{L}^\infty(\mathbb{R}^N;\mathbb{R})}\, \mathrm{e}^{\mathcal{L}t}. \end{aligned}$$

The above result can be easily extended to ensure the existence of global in time solutions, see Sect. 4.1 below and [33].

On the basis of Theorem 3.2, a few control problems can be addressed, leading to the corresponding optimality conditions, see [33, § 2.2 and § 2.3].

3.2 A NonLocal Velocity Direction

Now, we consider a single nonlocal conservation law in all of $\mathbb{R}^N$, i.e. $n = 1$, where the unknown $\rho = \rho(t,x)$ is defined for $t \ge 0$ and $x \in \Omega = \mathbb{R}^N$. More precisely, we study the following Cauchy problem:

$$\begin{cases} \partial_t \rho + \operatorname{div}_{\mathrm{x}}\left(\rho\, v(\rho)\, (\sigma(x) + \mathcal{I}(\rho))\right) = 0 \\ \rho(0,x) = \rho_o(x). \end{cases} \tag{3.3}$$

Here the velocity function $V(t,x,\rho,\mathcal{I})$ in (4.1) is equal to $v(\rho)\,(\sigma(x) + \mathcal{I}(\rho))$, where the scalar function $\rho \mapsto v(\rho)$ describes the pedestrians' speed, independently of geometrical considerations, the vector $\sigma(x) \in \mathbb{R}^N$ is the preferred direction of the pedestrian at x, while the nonlocal term $\mathcal{I}(\rho)(x)$ describes how the pedestrian at x deviates from the preferred direction, due to the crowd distribution. Roughly

speaking, an individual at position $x \in \mathbb{R}^2$ moves at the speed $v\,(\rho(t,x))$ depending only on the density $\rho(t,x)$. Moreover the individual at position x and time t is assumed to move along the direction $\sigma(x) + \big(\mathcal{I}\big(\rho(t)\big)\big)\,(x)$.

On the functions defining (3.3), we introduce the following hypotheses:

(v) $v \in \mathbf{C}^2(\mathbb{R};\mathbb{R})$ is nonincreasing, $v(0) = V$ and $v(R) = 0$ for fixed $V, R > 0$.

($\boldsymbol{\sigma}$) $\sigma \in (\mathbf{C}^2 \cap \mathbf{W}^{1,\infty})(\mathbb{R}^N;\mathbb{R}^N)$ is such that $\mathrm{div}_{\mathrm{x}}\,\sigma \in (\mathbf{W}^{1,1} \cap \mathbf{W}^{1,\infty})(\mathbb{R}^N;\mathbb{R})$.

(I) $\mathcal{I} \in \mathbf{C}^0\big(\mathbf{L}^1(\mathbb{R}^N;[0,R]);\mathbf{C}^2(\mathbb{R}^N;\mathbb{R}^N)\big)$ satisfies the following estimates:

(I.1) There exists an increasing $C_I \in \mathbf{L}^\infty_{loc}(\mathbb{R}^+;\mathbb{R}^+)$ such that, for all $r \in \mathbf{L}^1(\mathbb{R}^N;[0,R])$,

$$\begin{aligned} \|\mathcal{I}(r)\|_{\mathbf{W}^{1,\infty}(\mathbb{R}^N;\mathbb{R}^N)} &\le C_I(\|r\|_{\mathbf{L}^1(\mathbb{R}^N;\mathbb{R})}) \quad \text{and} \\ \|\mathrm{div}_{\mathrm{x}}\,\mathcal{I}(r)\|_{\mathbf{L}^1(\mathbb{R}^N;\mathbb{R})} &\le C_I(\|r\|_{\mathbf{L}^1(\mathbb{R}^N;\mathbb{R})})\,. \end{aligned}$$

(I.2) There exists an increasing $C_I \in \mathbf{L}^\infty_{loc}(\mathbb{R}^+;\mathbb{R}^+)$ such that, for all $r \in \mathbf{L}^1(\mathbb{R}^N;[0,R])$,

$$\|\nabla_x\,\mathrm{div}_{\mathrm{x}}\,\mathcal{I}(r)\|_{\mathbf{L}^1(\mathbb{R}^N;\mathbb{R}^N)} \le C_I(\|r\|_{\mathbf{L}^1(\mathbb{R}^N;\mathbb{R})})\,.$$

(I.3) There exists a constant K_I such that for all $r_1, r_2 \in \mathbf{L}^1(\mathbb{R}^N;[0,R])$,

$$\begin{aligned} \|\mathcal{I}(r_1) - \mathcal{I}(r_2)\|_{\mathbf{L}^\infty(\mathbb{R}^N;\mathbb{R}^N)} &\le K_I \cdot \|r_1 - r_2\|_{\mathbf{L}^1(\mathbb{R}^N;\mathbb{R})} \\ \|\mathcal{I}(r_1) - \mathcal{I}(r_2)\|_{\mathbf{L}^1(\mathbb{R}^N;\mathbb{R}^N)} &\le K_I \cdot \|r_1 - r_2\|_{\mathbf{L}^1(\mathbb{R}^N;\mathbb{R})} \\ \big\|\mathrm{div}_{\mathrm{x}}\big(\mathcal{I}(r_1) - \mathcal{I}(r_2)\big)\big\|_{\mathbf{L}^1(\mathbb{R}^N;\mathbb{R})} &\le K_I \cdot \|r_1 - r_2\|_{\mathbf{L}^1(\mathbb{R}^N;\mathbb{R})}\,. \end{aligned}$$

Following Definition 2.2, we introduce the notion of solution for (3.3).

Definition 3.3 ([34, Definition 2.1]) Fix a positive T and an initial datum $\rho_o \in \mathbf{L}^1(\mathbb{R}^N;[0,R])$. A function $\rho \in \mathbf{C}^0\big(I;\mathbf{L}^1(\mathbb{R}^N;\mathbb{R})\big)$ is a *weak entropy solution to* (3.3) if it is a Kružkov solution (see Definition 2.2) to the Cauchy problem

$$\begin{cases} \partial_t \rho + \mathrm{div}_{\mathrm{x}}\,(\rho\, v(\rho)\, w(t,x)) = 0 \\ \rho(0,x) = \rho_o(x) \end{cases} \qquad \text{where} \qquad w(t,x) = \sigma(x) + \big(\mathcal{I}\big(\rho(t)\big)\big)\,(x)\,.$$

Note that Definitions 2.2 and 3.3 imply that for all $k \in \mathbb{R}$ and for all $\varphi \in \mathbf{C}^\infty_c(]-\infty,T[\times\mathbb{R}^N;\mathbb{R}^+)$,

$$\begin{aligned} &\int_0^T\!\!\int_{\mathbb{R}^N} \big[|\rho-k|\,\partial_t\varphi + (\rho\,v(\rho) - k\,v(k))\; w\cdot\nabla_x\varphi\,\mathrm{sgn}(\rho-k)\big]\,\mathrm{d}x\mathrm{d}t \\ &- \int_0^T\!\!\int_{\mathbb{R}^N} k\,v(k)\;\mathrm{div}_{\mathrm{x}}\,w\,\varphi\,\mathrm{sgn}(\rho-k)\mathrm{d}x\mathrm{d}t + \int_{\mathbb{R}^N} |\rho_o(x)-k|\,\varphi(0,x)\mathrm{d}x \ge 0\,, \end{aligned}$$

where $w(t,x) = \sigma(x) + \big(\mathcal{I}\big(\rho(t)\big)\big)(x)$.

The following existence and uniqueness result for (3.3) holds.

Theorem 3.4 ([34, Theorem 2.1]) *Let* **(v)**, **(σ)**, *and* **(I)** *hold. Fix* $\rho_o \in (\mathbf{L}^1 \cap \mathbf{BV})(\mathbb{R}^N; [0, R])$. *Then, there exists a unique weak entropy solution*

$$\rho \in \mathbf{C}^0\big(\mathbb{R}^+; \mathbf{L}^1(\mathbb{R}^N; [0, R])\big)$$

to (3.3) in the sense of Definition 3.3. Moreover, ρ *conserves the* $\mathbf{L}^1$ *norm, i.e. for a.e.* $t \in \mathbb{R}^+$,

$$\|\rho(t)\|_{\mathbf{L}^1(\mathbb{R}^N;\mathbb{R})} = \|\rho_o\|_{\mathbf{L}^1(\mathbb{R}^N;\mathbb{R})},$$

and, for a.e. $t \in \mathbb{R}^+$, *satisfies the total variation inequality*

$$\begin{aligned}\mathrm{TV}\big(\rho(t)\big) \leq\ & \mathrm{TV}\,(\rho_o)\,\mathrm{e}^{kt} \\ & + N\,W_N \|q\|_{\mathbf{L}^\infty([0,R];\mathbb{R})} \left(\|\nabla_x \operatorname{div}_{\mathrm{x}} \sigma\|_{\mathbf{L}^1(\mathbb{R}^N;\mathbb{R}^N)} + C_I\big(\|\rho_o\|_{\mathbf{L}^1(\mathbb{R}^N;\mathbb{R})}\big)\right) t\,\mathrm{e}^{kt},\end{aligned}$$

where

$$\begin{aligned} q(\rho) &= \rho\, v(\rho)\,, \\ k &= (2N+1)\left\|q'\right\|_{\mathbf{L}^\infty([0,R];\mathbb{R})} \left(\|\nabla_x \sigma\|_{\mathbf{L}^\infty(\mathbb{R}^N;\mathbb{R}^{N\times N})} + C_I\big(\|\rho_o\|_{\mathbf{L}^1(\mathbb{R}^N;\mathbb{R})}\big)\right), \\ W_N &= \int_0^{\pi/2} (\cos\vartheta)^N \,\mathrm{d}\vartheta\,. \end{aligned}$$

The proof relies on a careful application of Banach Fixed Point Theorem. Moreover the following theorem contains stability results for (3.3).

Theorem 3.5 ([34, Theorem 2.2]) *Let* **(v)**, **(σ)**, *and* **(I)** *be satisfied by both systems*

$$\begin{cases} \partial_t \rho + \operatorname{div}_{\mathrm{x}}\left[q_1(\rho)\ (\sigma_1(x) + \mathcal{I}_1(\rho))\right] = 0 \\ \rho(0,x) = \rho_{0,1}(x) \end{cases} \quad \begin{cases} \partial_t \rho + \operatorname{div}_{\mathrm{x}}\left[q_2(\rho)\ (\sigma_2(x) + \mathcal{I}_2(\rho))\right] = 0 \\ \rho(0,x) = \rho_{0,2}(x), \end{cases}$$

where $q_1(\rho) = \rho\, v_1(\rho)$ *and* $q_2(\rho) = \rho\, v_2(\rho)$ *and* $\rho_{0,1}, \rho_{0,2} \in (\mathbf{L}^1 \cap \mathbf{BV})(\mathbb{R}^N; [0, R])$. *Then, for a.e.* $t \in \mathbb{R}^+$, *the two solutions* ρ_1 *and* ρ_2 *satisfy*

$$\begin{aligned}\|\rho_1(t) - \rho_2(t)\|_{\mathbf{L}^1} \leq\ & (1 + C(t))\left\|\rho_{0,1} - \rho_{0,2}\right\|_{\mathbf{L}^1} \\ & + C(t)\left(\|\rho_1 v_1(\rho_1) - \rho_2 v_2(\rho_2)\|_{\mathbf{W}^{1,\infty}} + d\,(\mathcal{I}_1, \mathcal{I}_2)\right) \\ & + C(t)\left(\|\sigma_1 - \sigma_2\|_{\mathbf{L}^\infty} + \|\mathrm{div}_{\mathrm{x}}(\sigma_1 - \sigma_2)\|_{\mathbf{L}^1}\right),\end{aligned}$$

where

$$d(\mathcal{I}_1, \mathcal{I}_2)$$
$$= \sup \left\{ \|\mathcal{I}_1(\rho) - \mathcal{I}_2(\rho)\|_{\mathbf{L}^\infty} + \|\mathrm{div}_x\left(\mathcal{I}_1(\rho) - \mathcal{I}_2(\rho)\right)\|_{\mathbf{L}^1} \colon \rho \in \mathbf{L}^1(\mathbb{R}^N; [0, R]) \right\},$$

and the map $C \in \mathbf{C}^0(\mathbb{R}^+; \mathbb{R}^+)$ *vanishes at* $t = 0$ *and depends on* $\mathrm{TV}(\rho_{0,1})$, $\left\|\rho_{0,1}\right\|_{\mathbf{L}^1}$, $\|\sigma_1\|_{\mathbf{L}^\infty}$, $\|\mathrm{div}_x\, \sigma_1\|_{\mathbf{W}^{1,1}}$, $\|\rho_1 v_1\,(\rho_1)\|_{\mathbf{W}^{1,\infty}}$, $\|\rho_2 v_2\,(\rho_2)\|_{\mathbf{W}^{1,\infty}}$.

Theorems 3.4 and 3.5 allow to consider various realistic situations and control problems, among which we recall the important problem of evacuation of a room in minimum time; see [34, § 4] for more detailed discussions.

4 Several Populations in $\mathbb{R}^N$

In this part we consider a system of conservation laws, i.e. $n > 1$, in the whole domain $\mathbb{R}^N$, where the unknowns $\rho^i = \rho^1(t, x)$ are defined for $t \geq 0$ and $x \in \Omega = \mathbb{R}^N$.

More precisely, we consider the system

$$\partial_t \rho^i + \mathrm{div}_x \left(\rho^i \, V^i\left(t, x, \rho^i, \mathcal{I}^i(\rho)\right)\right) = 0 \qquad i = 1, \ldots, n, \tag{4.1}$$

where $\rho = (\rho^1, \cdots, \rho^n)$ is the vector of conserved quantities, $n \in \mathbb{N} \setminus \{0\}$ denotes the number of equations, $t > 0$ is time, $x \in \mathbb{R}^2$ is the space variable, $V = (V^1, \cdots, V^n)$ is the velocity vector field, and $\mathcal{I} = (\mathcal{I}^1, \cdots, \mathcal{I}^n)$ is a nonlocal operator, which depends on the whole vector ρ of the densities.

Remarkably, couplings among the different equations in (4.1) motivated by the description of moving crowds allow to prove the well posedness and stability of *systems* of nonlocal conservation laws in *several* space dimensions. As is well known, general results of this type for *local* conservation laws are currently unavailable.

For the description of a numerical procedure to tackle (4.1) we refer to [1].

4.1 A NonLocal Speed Modulus

In this part, we consider system (4.1) where the nonlocal operator acts only on the modulus of the speed, but not on the direction. More precisely, we study the following Cauchy problem:

$$\begin{cases} \partial_t \rho^1 + \mathrm{div}_{\mathrm{x}} \left(\rho^1 \, v^1\big(\mathcal{I}^1(\rho)\big) \, \sigma^1(x) \right) = 0 \\ \qquad \vdots \\ \partial_t \rho^n + \mathrm{div}_{\mathrm{x}} \left(\rho^n \, v^n\big(\mathcal{I}^n(\rho)\big) \, \sigma^n(x) \right) = 0 \\ \rho^1(0,x) = \rho^1_o(x) \\ \qquad \vdots \\ \rho^n(0,x) = \rho^n_o(x) \, . \end{cases} \tag{4.2}$$

Here the velocity functions $V^i(t, x, \rho^i, \mathcal{I}^i)$ in (4.1) are given by

$$V^i(t, x, \rho^i, \mathcal{I}^i) = v^i(\mathcal{I}^i) \; \sigma^i(x) \, , \tag{4.3}$$

where the functions $v^i(r)$ describe the pedestrians' speed of the i-th population, independently of geometrical considerations, the vectors $\sigma^i(x) \in \mathbb{R}^N$ represent the direction of the pedestrian of the i-th class at x, while $\mathcal{I}^i(\rho)$ are nonlocal functions of the overall total density. More precisely, we assume that $\mathcal{I}^i : \mathbf{L}^1(\mathbb{R}^d; \mathbb{R}^n) \to \mathbf{C}^0(\mathbb{R}^d; \mathbb{R}^n)$ are given by

$$\big(\mathcal{I}^i(\rho)\big)(x) = \sum_{j=1}^{n} \int_{\mathbb{R}^d} \rho^j(t, \xi) \; \eta^j(x - \xi) \, \mathrm{d}\xi \, ,$$

where η^j are suitable mollifiers functions.

Definition 4.1 ([26, Definition 2.1]) Fix a positive T and an initial datum $\rho_o \in \mathbf{L}^1(\mathbb{R}^N; \mathbb{R}^n)$. A function $\rho \in \mathbf{C}^0\big(I; \mathbf{L}^1(\mathbb{R}^N; \mathbb{R}^n)\big)$ is a *weak entropy solution to (4.2)* if, for every $i \in \{1, \cdots, n\}$, the i-th component ρ^i is a Kružkov solution (see Definition 2.2) to the Cauchy problem

$$\begin{cases} \partial_t \rho^i + \mathrm{div}_{\mathrm{x}} \left(\rho^i \, w(t,x) \right) = 0 \\ \rho^i(0,x) = \rho^i_o(x) \end{cases} \qquad \text{where} \qquad w(t,x) = v^i\big(\mathcal{I}^i(\rho)\big) \, \sigma^i(x) \, .$$

The following well posedness result holds.

Theorem 4.2 ([26, Theorem 2.2]) *Assume that for every $i \in \{1, \cdots, n\}$*

1. $v^i \in \big(\mathbf{C}^2 \cap \mathbf{W}^{2,\infty}\big)(\mathbb{R}; \mathbb{R})$;
2. $\sigma^i \in \big(\mathbf{C}^2 \cap \mathbf{W}^{2,1}\big)(\mathbb{R}^N; \mathbb{R}^N)$ *satisfies* $\big\|\sigma^i(x)\big\| \leq 1$ *for every* $x \in \mathbb{R}^N$;
3. $\eta^i \in (\mathbf{C}^2 \cap \mathbf{W}^{2,\infty})(\mathbb{R}^N; [0,1])$ *and* $\big\|\eta^i\big\|_{\mathbf{L}^1(\mathbb{R}^N;\mathbb{R})} = 1$.

Then, there exists a semigroup

$$S \colon \mathbb{R}^+ \times (\mathbf{L}^1 \cap \mathbf{L}^\infty \cap \mathbf{BV})(\mathbb{R}^N; \mathbb{R}^n) \to (\mathbf{L}^1 \cap \mathbf{L}^\infty \cap \mathbf{BV})(\mathbb{R}^N; \mathbb{R}^n)$$

such that the following conditions hold.

1. *For every initial datum* $\rho_o \in (\mathbf{L}^1 \cap \mathbf{L}^\infty \cap \mathbf{BV})(\mathbb{R}^N; \mathbb{R}^n)$*, for every* $t \geq 0$*, the orbit* $t \mapsto S_t \rho_o$ *is the unique solution to (4.2), in the sense of Definition 4.1. Furthermore, the map* $t \mapsto S_t \rho_o$ *belongs to* $\mathbf{C}^0\big(\mathbb{R}^+; \mathbf{L}^1(\mathbb{R}^N; \mathbb{R}^n)\big)$.
2. *For every* $\rho_o \in (\mathbf{L}^1 \cap \mathbf{L}^\infty \cap \mathbf{BV})(\mathbb{R}^N; (\mathbb{R}^+)^n)$*, we have that* $(S_t \rho_o)_i \geq 0$ *for all* $t > 0$ *and* $i \in \{1, \cdots, n\}$.
3. *There exists a constant* $\mathcal{L}$ *such that, for all* $\rho_o \in (\mathbf{L}^1 \cap \mathbf{L}^\infty \cap \mathbf{BV})(\mathbb{R}^N; \mathbb{R}^n)$ *and* $t \in \mathbb{R}^+$,

$$\mathrm{TV}\left(S_t(\rho_o)\right) \leq \left(\mathrm{TV}\left(\rho_o\right) + \mathcal{L}\, t\, \|\rho_o\|_{\mathbf{L}^\infty(\mathbb{R}^N;\mathbb{R}^n)}\right) \mathrm{e}^{\mathcal{L} t}$$

and

$$\|S_t(\rho)\|_{\mathbf{L}^\infty(\mathbb{R}^N;\mathbb{R}^n)} \leq \|\rho_o\|_{\mathbf{L}^\infty(\mathbb{R}^N;\mathbb{R}^n)}.$$

4. *There exists a function* $\mathcal{L} \in \mathbf{C}^0(\mathbb{R}^+; \mathbb{R}^+)$ *such that,*

$$\left\|S_t(\rho_o') - S_t(\rho_o'')\right\|_{\mathbf{L}^1(\mathbb{R}^N;\mathbb{R}^n)} \leq \big(1 + t\, \mathcal{L}(t)\big) \left\|\rho_o' - \rho_o''\right\|_{\mathbf{L}^1(\mathbb{R}^N;\mathbb{R}^n)}$$

for all ρ_o', $\rho_o'' \in (\mathbf{L}^1 \cap \mathbf{L}^\infty \cap \mathbf{BV})(\mathbb{R}^N; \mathbb{R}^n)$ *and* $t \in \mathbb{R}^+$.
5. *If* $\rho_o \in \mathbf{W}^{1,1}(\mathbb{R}^N; \mathbb{R}^n)$*, then* $S_t(\rho_o) \in \mathbf{W}^{1,1}(\mathbb{R}^N; \mathbb{R}^n)$ *for all* $t > 0$*. Moreover there exists a positive constant* C *such that, for* $t > 0$,

$$\|S_t(\rho)\|_{\mathbf{W}^{1,1}(\mathbb{R}^N;\mathbb{R}^n)} \leq (1 + C\, t)\, \mathrm{e}^{C t}\, \|\rho_o\|_{\mathbf{W}^{1,1}(\mathbb{R}^N;\mathbb{R}^n)}.$$

6. *If* $\rho_o \in \mathbf{W}^{1,\infty}(\mathbb{R}^N; \mathbb{R}^n)$*, then* $S_t(\rho_o) \in \mathbf{W}^{1,\infty}(\mathbb{R}^N; \mathbb{R}^n)$ *for all* $t > 0$*. Moreover, there exists a positive constant* C *such that, for* $t > 0$,

$$\|S_t(\rho)\|_{\mathbf{W}^{1,\infty}(\mathbb{R}^N;\mathbb{R}^n)} \leq (1 + C\, t)\, \mathrm{e}^{C t}\, \|\rho_o\|_{\mathbf{W}^{1,\infty}(\mathbb{R}^N;\mathbb{R}^n)}.$$

7. *If* $v \in \mathbf{C}^4(\mathbb{R}; \mathbb{R}^n)$*, then, for every initial datum* $\rho_o \in (\mathbf{W}^{2,\infty} \cap \mathbf{W}^{2,1})(\mathbb{R}^N; \mathbb{R}^n)$, $\sigma_o \in (\mathbf{W}^{1,1} \cap \mathbf{L}^\infty)(\mathbb{R}^N; \mathbb{R}^n)$ *and for all time* $t > 0$*, the semigroup* S *is strongly* $\mathbf{L}^1$ *Gâteaux differentiable in the direction* σ_o*. The derivative* $D\, S_t(\rho_o)(\sigma_o)$ *of* S_t *at the point* ρ_o *in the direction* σ_o *is* $\Sigma_t^{\rho_o}(\sigma_o)$*, where* Σ^{ρ_o} *is the linear semigroup whose orbits are the Kružkov solutions to*

$$\begin{cases} \partial_t \sigma^i + \mathrm{div}_{\mathrm{x}} \left(\sigma^i\, V^i\big(S_t(\rho_o)\big) + \big(S_t(\rho_o)\big)^i\, DV^i\big(S_t(\rho_o)\big)(\sigma)\right) = 0 \\ \sigma^i(0, x) = \sigma_o^i(x)\,, \end{cases}$$

where V^i *is defined in (4.3).*

The Cauchy problem (4.2) is also stable with respect to variations of the functions η^i, v^i, and σ^i. More precisely, consider the Cauchy problems

$$
\begin{cases}
\partial_t \rho^1 + \mathrm{div}_x\Big(\rho^1\, \hat{v}^1\big(\hat{\mathcal{I}}^1(\rho)\big)\, \hat{\sigma}^1(x)\Big) = 0 \\
\qquad\vdots \\
\partial_t \rho^n + \mathrm{div}_x\Big(\rho^n\, \hat{v}^n\big(\hat{\mathcal{I}}^n(\rho)\big)\, \hat{\sigma}^n(x)\Big) = 0 \\
\rho^1(0,x) = \hat{\rho}_o^1(x) \\
\qquad\vdots \\
\rho^n(0,x) = \hat{\rho}_o^n(x)
\end{cases}
\qquad
\begin{cases}
\partial_t \rho^1 + \mathrm{div}_x\Big(\rho^1\, \check{v}^1\big(\check{\mathcal{I}}^1(\rho)\big)\, \check{\sigma}^1(x)\Big) = 0 \\
\qquad\vdots \\
\partial_t \rho^n + \mathrm{div}_x\Big(\rho^n\, \check{v}^n\big(\check{\mathcal{I}}^n(\rho)\big)\, \check{\sigma}^n(x)\Big) = 0 \\
\rho^1(0,x) = \check{\rho}_o^1(x) \\
\qquad\vdots \\
\rho^n(0,x) = \check{\rho}_o^n(x)\,,
\end{cases}
$$

where

$$
\hat{\mathcal{I}}^i(\rho)(x) = \sum_{j=1}^{n} \int_{\mathbb{R}^N} \rho^j(t,\xi)\, \hat{\eta}^j(x-\xi)\, \mathrm{d}\xi\,, \quad \check{\mathcal{I}}^i(\rho)(x) = \sum_{j=1}^{n} \int_{\mathbb{R}^N} \rho^j(t,\xi)\, \check{\eta}^j(x-\xi)\, \mathrm{d}\xi\,.
$$

Denote by $\hat{\rho}$ and $\check{\rho}$ the respective solutions.

Theorem 4.3 ([26, Theorem 2.2]) *Fix a positive constant M. Then, there exists a function $\mathcal{L} \in \mathbf{C}^0(\mathbb{R}^+;\mathbb{R}^+)$ such that*

$$
\begin{aligned}
\big\|\hat{\rho}(t) - \check{\rho}(t)\big\|_{\mathbf{L}^1(\mathbb{R}^N;\mathbb{R}^n)} \leq{}& \big(1 + t\,\mathcal{L}(t)\big)\, \big\|\hat{\rho}_o - \check{\rho}_o\big\|_{\mathbf{L}^1(\mathbb{R}^N;\mathbb{R}^n)} \\
&+ t\,\mathcal{L}(t)\, \big\|\hat{\eta} - \check{\eta}\big\|_{\mathbf{W}^{1,\infty}(\mathbb{R}^N;\mathbb{R}^n)} \\
&+ t\,\mathcal{L}(t)\, \big\|\hat{v} - \check{v}\big\|_{\mathbf{W}^{1,\infty}(\mathbb{R};\mathbb{R}^n)} \\
&+ t\,\mathcal{L}(t)\, \Big(\big\|\hat{\sigma} - \check{\sigma}\big\|_{\mathbf{L}^\infty(\mathbb{R}^N;\mathbb{R}^{nd})} + \big\|\hat{\sigma} - \check{\sigma}\big\|_{\mathbf{W}^{1,1}(\mathbb{R}^N;\mathbb{R}^{nd})}\Big)
\end{aligned}
$$

for every initial data $\hat{\rho}_o, \check{\rho}_o \in \mathbf{L}^1(\mathbb{R}^N;\mathbb{R}^n)$, for every velocity functions $\hat{v}, \check{v} \in (\mathbf{C}^2 \cap \mathbf{W}^{2,\infty})(\mathbb{R};\mathbb{R}^n)$, for every directions $\hat{\sigma}, \check{\sigma} \in (\mathbf{C}^2 \cap \mathbf{W}^{2,1})\big(\mathbb{R}^N;\mathbb{R}^{Nn}\big)$, and for every mollifier $\hat{\eta}, \check{\eta} \in (\mathbf{C}^2 \cap \mathbf{W}^{2,\infty})(\mathbb{R}^N;[0,1]^n)$ with $\big\|\hat{\eta}^i\big\|_{\mathbf{L}^1(\mathbb{R}^N;\mathbb{R})} = \big\|\check{\eta}^i\big\|_{\mathbf{L}^1(\mathbb{R}^N;\mathbb{R})} = 1$ for $i \in \{1,\cdots,n\}$.

4.2 A NonLocal Velocity Direction

In this part, we consider system (4.1) where the nonlocal operator influences the geometric direction of the velocity. More precisely, we study the following Cauchy problem:

$$\begin{cases} \partial_t \rho^1 + \mathrm{div}_{\mathrm{x}} \left(\rho^1 \, v^1(\rho^1) \, \left(\mathbf{v}^1(x) + \mathcal{I}^1(\rho^1, \dots, \rho^n) \right) \right) = 0 \\ \qquad \vdots \\ \partial_t \rho^n + \mathrm{div}_{\mathrm{x}} \left(\rho^n \, v^n(\rho^n) \, \left(\mathbf{v}^n(x) + \mathcal{I}^n(\rho^1, \dots, \rho^n) \right) \right) = 0 \\ \rho^1(0, x) = \rho^1_o(x) \\ \qquad \vdots \\ \rho^n(0, x) = \rho^n_o(x) \, . \end{cases} \tag{4.4}$$

Here the velocity functions $V^i(t, x, \rho^i, \mathcal{I}^i)$ in (4.1), for $i \in \{1, \cdots, n\}$, are given by

$$V^i(t, x, \rho^i, \mathcal{I}^i) = v^i(\rho^i) \, \left(\mathbf{v}^i(x) + \mathcal{I}^i(\rho^1, \dots, \rho^n) \right) .$$

More precisely, the velocity V^i of the i-th population is the product of a scalar *crowding factor* $v^i(\rho^i)$ with a vector $\mathbf{v}^i(x) + \mathcal{I}^i(\rho^1, \dots, \rho^n)$, which is the sum of a *preferred direction* $\mathbf{v}^i(x)$ and a *deviation* $\mathcal{I}^i(\rho^1, \dots, \rho^n)$. The scalar $v^i(\rho^i)$ approximately gives the modulus of the speed. A possible choice for the preferred direction $\mathbf{v}^i$ is, for instance, the tangent vector at x to the geodesic that the individuals in the i-th population follow to reach their destination, if unaffected by any other individual. Instead, the term $\mathcal{I}^i(\rho^1, \dots, \rho^n)$ describes how the i-th population deviates from its preferred trajectory due to the interaction among individuals, both of the same and of different populations. It is a nonlocal functional, since its value at any position x depends on the population densities averaged over a neighborhood of x.

Definition 4.4 ([26, Definition 3.1]) Fix a positive T and, for every $i \in \{1, \cdots, n\}$, the initial datum $\rho^i_o \in (\mathbf{L}^1 \cap \mathbf{L}^\infty)(\mathbb{R}^N; \mathbb{R}^n)$. A map $\rho \in \mathbf{C}^0 \left([0, T]; \mathbf{L}^1(\mathbb{R}^N; \mathbb{R}^n) \right)$ is a *weak entropy solution to (4.4)* if, for $i = 1, \cdots, n$, ρ^i is a Kružkov solution to the Cauchy problem

$$\begin{cases} \partial_t \rho^i + \mathrm{div}_{\mathrm{x}} \left(\rho^i \, v^i(\rho^i) \, V^i(t, x) \right) = 0 \\ \rho^i(0, x) = \rho^i_o(x) \, , \end{cases}$$

where $V^i(t, x) = \mathbf{v}^i(x) + \mathcal{I}^i \left(\rho_1(t), \cdots, \rho_n(t) \right)(x)$.

The following well posedness result holds.

Theorem 4.5 ([26, Theorem 3.2]) *Assume that for every $i \in \{1, \cdots, n\}$,*

1. *$v^i \in \mathbf{C}^2(\mathbb{R}; \mathbb{R}^+)$ satisfies $v^i(R) = 0$ for a suitable $R > 0$;*
2. *$\mathbf{v}^i \in (\mathbf{C}^2 \cap \mathbf{W}^{1,\infty})(\mathbb{R}^N; \mathbb{R}^N)$ and $\mathrm{div}_{\mathrm{x}} \mathbf{v}^i \in \mathbf{W}^{1,1}(\mathbb{R}^N; \mathbb{R}^{N \times N})$;*
3. *there exists a constant $C_I > 0$ such that $\mathcal{I}^i : \mathbf{L}^1(\mathbb{R}^N; \mathbb{R}^n) \to \mathbf{C}^2(\mathbb{R}^N; \mathbb{R}^N)$ satisfies, for every $\rho, \rho' \in \mathbf{L}^1(\mathbb{R}^N; [0, R]^n)$,*

$$\begin{aligned}
\left\| \nabla_x \mathcal{I}^i(\rho) \right\|_{\mathbf{L}^\infty(\mathbb{R}^N;\mathbb{R}^N)} &\leq C_I \, \|\rho\|_{\mathbf{L}^1(\mathbb{R}^N;\mathbb{R}^n)},\\
\left\| \nabla_x \operatorname{div}_{\mathrm{x}} \left(\mathcal{I}^i(\rho) \right) \right\|_{\mathbf{L}^1(\mathbb{R}^N;\mathbb{R}^{N\times N})} &\leq C_I \, \|\rho\|_{\mathbf{L}^1(\mathbb{R}^N;\mathbb{R}^n)},\\
\left\| \mathcal{I}^i(\rho) - \mathcal{I}^i(\rho') \right\|_{\mathbf{L}^\infty(\mathbb{R}^N;\mathbb{R}^N)} &\leq C_I \, \left\|\rho - \rho'\right\|_{\mathbf{L}^1(\mathbb{R}^N;\mathbb{R}^n)},\\
\left\| \operatorname{div}_{\mathrm{x}} \left(\mathcal{I}^i(\rho) - \mathcal{I}^i(\rho') \right) \right\|_{\mathbf{L}^1(\mathbb{R}^N;\mathbb{R})} &\leq C_I \, \left\|\rho - \rho'\right\|_{\mathbf{L}^1(\mathbb{R}^N;\mathbb{R}^n)}.
\end{aligned}$$

Then, there exists a semigroup

$$S \colon \mathbb{R}^+ \times (\mathbf{L}^1 \cap \mathbf{BV})(\mathbb{R}^N; [0, R]^n) \to (\mathbf{L}^1 \cap \mathbf{BV})(\mathbb{R}^N; [0, R]^n)$$

such that the following conditions hold.

1. *For all $\rho_o \in (\mathbf{L}^1 \cap \mathbf{BV})(\mathbb{R}^N; [0, R]^n)$, the orbit $t \mapsto S_t \rho_o$ is the unique solution to (4.4) in the sense of Definition 4.4.*
2. *For all $\rho_o \in (\mathbf{L}^1 \cap \mathbf{BV})(\mathbb{R}^N; [0, R]^n)$ and $t > 0$*

$$\operatorname{TV}(S_t \rho_o) \leq \operatorname{TV}(\rho_o) \, \mathrm{e}^{\kappa_o t} + N \, K \, W_N \, \mathrm{e}^{\kappa_o t} \left(C_I + \|\operatorname{div}_{\mathrm{x}} \mathbf{v}\|_{\mathbf{L}^\infty(\mathbb{R}^N;\mathbb{R})} \right) t \,,$$

   where $W_N = \int_0^{\pi/2} \cos^N(\theta) \mathrm{d}\theta$, $K > 0$, and $\kappa_o > 0$.
3. *For $M > 0$, there exist $b \in \mathbf{C}^0(\mathbb{R}^+; \mathbb{R}^+)$ such that for all $\rho_{o,1}, \rho_{o,2} \in \mathbf{L}^1(\mathbb{R}^N; [0, R]^n)$ with $\operatorname{TV}(\rho_{o,i}) \leq M$ and for all $t \in \mathbb{R}^+$*

$$\left\| S_t \rho_{o,1} - S_t \rho_{o,2} \right\|_{\mathbf{L}^1(\mathbb{R}^N;\mathbb{R}^n)} \leq \left(1 + t \, \mathrm{e}^{t \, b(t)} \right) \left\| \rho_{o,1} - \rho_{o,2} \right\|_{\mathbf{L}^1(\mathbb{R}^N;\mathbb{R}^n)}.$$

The Cauchy problem (4.4) is also stable with respect to variations of the functions v^i and $\mathbf{v}^{\mathbf{i}}$.

Theorem 4.6 ([26, Theorem 3.2]) *There exists a function $\mathcal{L} \in \mathbf{C}^0(\mathbb{R}^+; \mathbb{R}^+)$ such that*

$$\begin{aligned}
\left\| \hat\rho(t) - \check\rho(t) \right\|_{\mathbf{L}^1(\mathbb{R}^N;\mathbb{R}^n)} \leq{}& \left(1 + t \, \mathcal{L}(t) \right) \left\| \hat\rho_o - \check\rho_o \right\|_{\mathbf{L}^1(\mathbb{R}^N;\mathbb{R}^n)}\\
&+ t \, \mathcal{L}(t) \left\| \hat v - \check v \right\|_{\mathbf{W}^{1,\infty}(\mathbb{R}^N;\mathbb{R}^n)}\\
&+ t \, \mathcal{L}(t) \left\| \hat{\mathbf{v}} - \check{\mathbf{v}} \right\|_{\mathbf{L}^\infty(\mathbb{R}^N;\mathbb{R}^{Nn})}\\
&+ t \, \mathcal{L}(t) \left\| \operatorname{div}_{\mathrm{x}} \left(\hat{\mathbf{v}} - \check{\mathbf{v}} \right) \right\|_{\mathbf{L}^1(\mathbb{R}^N;\mathbb{R}^n)}
\end{aligned}$$

for every initial data $\hat\rho_o, \check\rho_o \in \mathbf{L}^1(\mathbb{R}^N; \mathbb{R}^n)$, for every velocity functions $\hat v, \check v \in (\mathbf{C}^2 \cap \mathbf{W}^{2,\infty})(\mathbb{R}^N; \mathbb{R}^n)$, for every directions $\hat{\mathbf{v}}, \check{\mathbf{v}} \in (\mathbf{C}^2 \cap \mathbf{W}^{2,1})\left(\mathbb{R}^N; \mathbb{R}^{Nn}\right)$, where $\hat\rho$ (resp. $\check\rho$) denotes the solutions for $\hat\rho_o$, $\hat v$, and $\hat{\mathbf{v}}$ (resp. for $\check\rho_o$, $\check v$, and $\check{\mathbf{v}}$).

5 NonLocal Conservation Laws in Bounded Domains

In this part we consider a system of conservation laws, i.e. $n > 1$, in an open, connected, and bounded domain Ω of $\mathbb{R}^N$ with boundary of class $\mathbf{C}^2$. More precisely, we study the initial boundary value problem for system (4.1), i.e. the problem

$$\begin{cases} \partial_t \rho^i + \mathrm{div}_{\mathrm{x}} \left(\rho^i \, V^i\big(t, x, \mathcal{I}^i(\rho)\big)\right) = 0 & t > 0, \, x \in \Omega \, , \, i \in \{1, \cdots, n\} \\ \rho(0, x) = \rho_o(x) & x \in \Omega \\ \rho(t, x) = 0 & t > 0, x \in \partial\Omega \, , \end{cases} \tag{5.1}$$

where ρ denotes the vector $(\rho^1, \cdots, \rho^n)$. For numerical examples; see [30].

The presence of a boundary has two different effects. First, boundary conditions need to be carefully considered. Indeed, as is well known, the data imposed by boundary conditions need not be strictly assumed, see [57] and the references therein. Second, nonlocal terms have to be evaluated exclusively inside the domain of reference. Indeed, the presence, or absence, of people behind a wall cannot influence the pedestrians' speed choices, see the discussion in [30].

Definition 5.1 ([30, Definition 4.1]) Fix a positive T and an initial datum $\rho_o \in \mathbf{L}^1(\Omega; \mathbb{R}^n)$. A function $\rho \in \mathbf{C}^0\big(I; \mathbf{L}^1(\Omega; \mathbb{R}^n)\big)$ is a *solution to (5.1)* if, for every $i \in \{1, \cdots, n\}$, the i-th component ρ^i is a regular entropy solution, in the sense of Definition A.2, to

$$\begin{cases} \partial_t \rho^i + \mathrm{div}_{\mathrm{x}} \left(\rho^i \, w(t, x)\right) = 0 & t \in \mathring{I} \, , \, x \in \Omega \\ \rho^i(0, x) = \rho^i_o(x) & x \in \Omega \quad \text{where } w(t, x) = V^i\big(t, x, \mathcal{I}^i\big(\rho(t)\big)(x)\big). \\ \rho^i(t, x) = 0 & t \in \mathring{I} \, , \, x \in \partial\Omega \end{cases}$$

In the following well posedness result, the key assumptions require relations (bounds) on the nonlocal operator. Remark that these bounds all depend exclusively on values of the various functions *inside* the domain Ω. In other words, we substitute the usual convolution

$$(\rho * \eta)(x) = \int_{\mathbb{R}^N} \rho(x) \, \eta(x-\xi) \, \mathrm{d}\xi \qquad \text{with} \qquad (\rho *_\Omega \eta)(x) = \frac{\int_{\mathbb{R}^N} \bar\rho(x) \, \eta(x-\xi) \, \mathrm{d}\xi}{\int_\Omega \eta(x-\xi) \, \mathrm{d}\xi},$$

where $\bar\rho$ is the null extension of ρ from Ω to all of $\mathbb{R}^N$:

$$\bar\rho(x) = \begin{cases} \rho(x) & x \in \Omega \\ 0 & x \in \mathbb{R}^N \setminus \Omega \, . \end{cases}$$

This choice is coherent with the above remark about letting each individual react exclusively to what is within his/her horizon and *inside* Ω.

Theorem 5.2 ([28, Theorem 2.2]) *Assume the following hypotheses hold.*

1. *For every* $i \in \{1, \cdots, n\}$, $V^i \in (\mathbf{C}^0 \cap \mathbf{L}^\infty)\big(\mathring{I} \times \Omega \times \mathbb{R}^m; \mathbb{R}^N\big)$.
2. *There exists* $M > 0$ *such that for every* $i \in \{1, \cdots, n\}$ *and* $t \in \mathring{I}$, $V^i(t) \in \mathbf{C}^2(\Omega \times \mathbb{R}^m; \mathbb{R}^N)$ *and* $\left\|V^i(t)\right\|_{\mathbf{C}^2(\Omega \times \mathbb{R}^m; \mathbb{R}^N)} \leq M$.
3. *For every* $i \in \{1, \cdots, n\}$, $\mathcal{I}^i : \mathbf{L}^1(\Omega; \mathbb{R}^n) \to \mathbf{C}^2(\Omega; \mathbb{R}^m)$ *is such that there exists a positive* K *and a nondecreasing map* $\mathcal{K} \in \mathbf{L}^\infty_{loc}(\mathbb{R}^+; \mathbb{R}^+)$ *such that:*

   a. for all $r \in \mathbf{L}^1(\Omega; \mathbb{R}^n)$,

$$\begin{aligned}
\left\|\mathcal{I}^i(r)\right\|_{\mathbf{L}^\infty(\Omega; \mathbb{R}^m)} &\leq K \, \|r\|_{\mathbf{L}^1(\Omega; \mathbb{R}^n)} \,, \\
\left\|\nabla_x \mathcal{I}^i(r)\right\|_{\mathbf{L}^\infty(\Omega; \mathbb{R}^{m \times N})} &\leq K \, \|r\|_{\mathbf{L}^1(\Omega; \mathbb{R}^n)} \,, \\
\left\|\nabla_x^2 \mathcal{I}^i(r)\right\|_{\mathbf{L}^\infty(\Omega; \mathbb{R}^{m \times N \times N})} &\leq \mathcal{K}\big(\|r\|_{\mathbf{L}^1(\Omega; \mathbb{R}^n)}\big) \, \|r\|_{\mathbf{L}^1(\Omega; \mathbb{R}^n)} \,;
\end{aligned}$$

   b. for all $r_1, \, r_2 \in \mathbf{L}^1(\Omega; \mathbb{R}^n)$

$$\begin{aligned}
\left\|\mathcal{I}^i(r_1) - \mathcal{I}^i(r_2)\right\|_{\mathbf{L}^\infty(\Omega; \mathbb{R}^m)} &\leq K \, \|r_1 - r_2\|_{\mathbf{L}^1(\Omega; \mathbb{R}^n)} \,, \\
\left\|\nabla_x\big(\mathcal{I}^i(r_1) - \mathcal{I}^i(r_2)\big)\right\|_{\mathbf{L}^\infty(\Omega; \mathbb{R}^{m \times N})} &\leq \mathcal{K}\big(\|r_1\|_{\mathbf{L}^1(\Omega; \mathbb{R}^n)}\big) \, \|r_1 - r_2\|_{\mathbf{L}^1(\Omega; \mathbb{R}^n)} \,.
\end{aligned}$$

Then:

1. *For every* $\rho_o \in (\mathbf{L}^\infty \cap \mathbf{BV})(\Omega; \mathbb{R}^n)$, *there exists a unique* $\rho \in \mathbf{L}^\infty(\mathring{I} \times \Omega; \mathbb{R}^n)$ *solving (5.1) in the sense of Definition 5.1.*
2. *For every* $\rho_o \in (\mathbf{L}^\infty \cap \mathbf{BV})(\Omega; \mathbb{R}^n)$ *and for every* $t \in \mathring{I}$,

$$\begin{aligned}
\|\rho(t)\|_{\mathbf{L}^1(\Omega; \mathbb{R}^n)} &\leq \|\rho_o\|_{\mathbf{L}^1(\Omega; \mathbb{R}^n)} \,, \\
\|\rho(t)\|_{\mathbf{L}^\infty(\Omega; \mathbb{R}^n)} &\leq \|\rho_o\|_{\mathbf{L}^\infty(\Omega; \mathbb{R}^n)} \exp\left(t \, M(1 + K \, \|\rho_o\|_{\mathbf{L}^1(\Omega; \mathbb{R}^n)})\right) \,, \\
\mathrm{TV}\left(\rho(t)\right) &\leq \exp\left(t \, M(1 + K \, \|\rho_o\|_{\mathbf{L}^1(\Omega; \mathbb{R}^n)})\right) \\
&\quad \times \Bigg[O(1) \, n \, \|\rho_o\|_{\mathbf{L}^\infty(\Omega; \mathbb{R}^n)} + \mathrm{TV}\left(\rho_o\right) + n \, t \, \|\rho_o\|_{\mathbf{L}^1(\Omega; \mathbb{R}^n)} \, M \\
&\quad \times \Big(1 + \|\rho_o\|_{\mathbf{L}^1(\Omega; \mathbb{R}^n)} \Big(K + K^2 \|\rho_o\|_{\mathbf{L}^1(\Omega; \mathbb{R}^n)} + \mathcal{K}\big(\|\rho_o\|_{\mathbf{L}^1(\Omega; \mathbb{R}^n)}\big)\Big)\Big)\Bigg].
\end{aligned}$$

3. *For every* $\rho_o \in (\mathbf{L}^\infty \cap \mathbf{BV})(\Omega; \mathbb{R}^n)$ *and for any* $t, s \in \mathring{I}$,

$$\|\rho(t) - \rho(s)\|_{\mathbf{L}^1(\Omega; \mathbb{R}^n)} \leq \mathrm{TV}\left(\rho(\max\{t, s\})\right) \, |t - s| .$$

4. *For every initial data* $\rho_o, \tilde{\rho}_o \in (\mathbf{L}^\infty \cap \mathbf{BV})(\Omega; \mathbb{R}^n)$ *and for any* $t \in \mathring{I}$, *calling* ρ *and* $\tilde{\rho}$ *the corresponding solutions to (5.1),*

$$\|\rho(t) - \tilde{\rho}(t)\|_{\mathbf{L}^1(\Omega;\mathbb{R}^n)} \leq \mathrm{e}^{\mathcal{L}(t)} \, \|\rho_o - \tilde{\rho}_o\|_{\mathbf{L}^1(\Omega;\mathbb{R}^n)},$$

where $\mathcal{L}(t) > 0$ *depends on* Ω, V^i, $\mathcal{I}^i$, $\|\rho_o\|_{\mathbf{L}^1(\Omega;\mathbb{R}^n)}$, $\|\tilde{\rho}_o\|_{\mathbf{L}^1(\Omega;\mathbb{R}^n)}$, $\|\rho_o\|_{\mathbf{L}^\infty(\Omega;\mathbb{R}^n)}$, $\|\tilde{\rho}_o\|_{\mathbf{L}^\infty(\Omega;\mathbb{R}^n)}$, $\mathrm{TV}\,(\rho_o)$, *and on* $\mathrm{TV}\,(\tilde{\rho}_o)$.

5. *Fix* $\rho_o \in (\mathbf{L}^\infty \cap \mathbf{BV})(\Omega; \mathbb{R}^n)$. *Let* $\tilde{V}^i$ *satisfies the same assumptions of* V^i. *Call* ρ *and* $\tilde{\rho}$ *the solutions to problem (5.1) corresponding, respectively, to the choices* V *and* $\tilde{V}$. *Then, for every* $t \in \mathring{I}$,

$$\|\rho(t) - \tilde{\rho}(t)\|_{\mathbf{L}^1(\Omega;\mathbb{R}^n)} \leq C(t) \int_0^t \left\| V(s) - \tilde{V}(s) \right\|_{\mathbf{C}^1(\Omega \times \mathbb{R}^m; \mathbb{R}^{nN})} \mathrm{d}s,$$

where C *depends on* Ω, V^i, $\tilde{V}^i$, $\mathcal{I}^i$, *and on the initial datum.*

6. *For* $i \in \{1, \cdots, n\}$, *if* $\rho_o^i \geq 0$ *a.e. in* Ω, *then* $\rho^i(t) \geq 0$ *a.e. in* Ω *for all* $t \in \mathring{I}$.

We conclude this section noting that the extension of Theorem 5.2 to the case of several interacting populations in a bounded domain is, at present, apparently still to be considered.

6 Mixed Micro–Macro Models in $\mathbb{R}^N$

Here we consider the case of a system similar to (4.1) coupled with ordinary differential equations. In typical situations, the system of conservation laws is used to describe the evolution of several populations through their macroscopic densities, while the ordinary differential equations model the microscopic dynamics of few agents.

For $i \in \{1, \cdots, n\}$, we consider the system

$$\begin{cases} \partial_t \rho^i + \mathrm{div}_x \left[q^i(\rho^i) \; V^i\big(t, x, \mathcal{I}^i(\rho), p\big) \right] = 0 \\ \dot{p} = F\left(t, p, \mathcal{J}\big(\rho(t)\big)(p)\right), \end{cases} \tag{6.1}$$

where $q(\rho) = \rho \, v(\rho)$, $t > 0$, $x \in \Omega = \mathbb{R}^N$, $\rho = (\rho^1, \cdots, \rho^n)$ is the vector of the macroscopic densities, $p \in \mathbb{R}^m$ describes the positions and possibly the velocity of $d \in \mathbb{N}$ agents, so that $m = Nd$ or $m = 2Nd$. Moreover $\mathcal{I}^i$ and $\mathcal{J}$ are nonlocal operators, reflecting the fact that the behavior of the members of the population as well as of the agents depends on suitable spatial averages. System (6.1) is supplemented with the initial conditions

$$\rho(0, x) = \rho_o(x) \qquad \text{and} \qquad p(0) = p_o, \tag{6.2}$$

with $\rho_o \in \mathbf{L}^1(\mathbb{R}^N; \mathbb{R}^n)$ and $p_o \in \mathbb{R}^m$.

Definition 6.1 ([13, Definition 2.6]) Fix $\rho_o \in (\mathbf{L}^1 \cap \mathbf{BV})(\mathbb{R}^N; \mathbb{R}^n)$ and $p_o \in \mathbb{R}^m$. A couple (ρ, p) with

$$\rho \in \mathbf{C}^0\big(\mathbb{R}^+; \mathbf{L}^1(\mathbb{R}^N; \mathbb{R}^n)\big) \qquad \text{and} \qquad p \in \mathbf{W}^{1,1}(\mathbb{R}^+; \mathbb{R}^m)$$

is a *solution to (6.1)–(6.2)* if the following conditions are satisfied:

1. For every $i \in \{1, \cdots, n\}$, the map ρ^i is a Kružkov solution, in the sense of Definition 2.2, to the scalar conservation law

$$\partial_t \rho^i + \mathrm{div}_x \left[q^i(\rho^i)\, V(t,x)\right] = 0\,,$$

   where $V(t,x) = V^i\big(t, x, \mathcal{I}^i(\rho(t))(x), p(t)\big)$.
2. The map p is a Carathéodory solution to the ordinary differential equation

$$\dot p = \mathcal{F}(t,p) \quad \text{where} \quad \mathcal{F}(t,p) = F\big(t, p, \mathcal{J}\big(\rho(t)\big)(p)\big)\,.$$

3. $\rho(0,x) = \rho_o(x)$ for a.e. $x \in \mathbb{R}^N$.
4. $p(0) = p_o$.

The following well posedness and stability result holds; for a proof see [13, Theorem 2.2 and Section 4.1].

Theorem 6.2 ([13, Theorem 2.2]) *Assume the following hypotheses.*

1. *For every $i \in \{1, \cdots, n\}$, $q^i \in \mathbf{C}^2(\mathbb{R}^+; \mathbb{R}^+)$ satisfies $q^i(0) = 0$ and $q^i(R) = 0$, for some $R > 0$.*
2. *For every $i \in \{1, \cdots, n\}$, $V^i \in (\mathbf{C}^2 \cap \mathbf{L}^\infty)(\mathbb{R}^+ \times \mathbb{R}^N \times \mathbb{R}^N \times \mathbb{R}^m; \mathbb{R}^N)$.*
3. *The map $F \in \mathbf{C}^0(\mathbb{R}^+ \times \mathbb{R}^m \times \mathbb{R}^\ell; \mathbb{R}^m)$ is such that*
   a. *For all compact subset K of $\mathbb{R}^m$, there exists a constant $L_F > 0$ such that, for every $t \in \mathbb{R}^+$, $p_1, p_2 \in K$ and $b_1, b_2 \in \mathbb{R}^\ell$,*

$$\|F(t,p_1,b_1) - F(t,p_2,b_2)\|_{\mathbb{R}^m} \le L_F \left(\|p_1 - p_2\|_{\mathbb{R}^m} + \|b_1 - b_2\|_{\mathbb{R}^\ell}\right).$$

   b. *There exists a map $C_F \in \mathbf{L}^1_{loc}(\mathbb{R}^+; \mathbb{R}^+)$ such that for all $t > 0$, $b \in \mathbb{R}^\ell$, and $p \in \mathbb{R}^m$*

$$\|F(t,p,b)\|_{\mathbb{R}^m} \le C_F(t) \left(1 + \|p\|_{\mathbb{R}^m} + \|b\|_{\mathbb{R}^\ell}\right).$$

4. *For every $i \in \{1, \cdots, n\}$, the maps $\mathcal{I}^i : \mathbf{L}^1(\mathbb{R}^N; \mathbb{R}^n) \to (\mathbf{C}^2 \cap \mathbf{W}^{2,1})(\mathbb{R}^N; \mathbb{R}^N)$ are Lipschitz continuous and satisfy $\mathcal{I}^i(0) = 0$. In particular there exists a positive constant $L_{\mathcal{I}} > 0$ such that, for every $\rho_1, \rho_2 \in \mathbf{L}^1(\mathbb{R}^N; [0,R]^n)$,*

$$\left\|\mathcal{I}^i(\rho_1) - \mathcal{I}^i(\rho_2)\right\|_{\mathbf{W}^{2,1}(\mathbb{R}^N;\mathbb{R}^N)} + \left\|\mathcal{I}^i(\rho_1) - \mathcal{I}^i(\rho_2)\right\|_{\mathbf{C}^2(\mathbb{R}^N;\mathbb{R}^N)}$$

$$\leq L_{\mathcal{I}} \, \|\rho_1 - \rho_2\|_{\mathbf{L}^1(\mathbb{R}^N;\mathbb{R}^n)}.$$

5. *The map* $\mathcal{J}\colon \mathbf{L}^1(\mathbb{R}^N;\mathbb{R}^n) \to \mathbf{W}^{1,\infty}(\mathbb{R}^m;\mathbb{R}^\ell)$ *is Lipschitz continuous and satisfies* $\mathcal{J}(0) = 0$. *In particular, there exists a positive constant* $L_{\mathcal{J}} > 0$ *such that, for every* $\rho_1, \rho_2 \in \mathbf{L}^1(\mathbb{R}^N;[0,R]^n)$,

$$\|\mathcal{J}(\rho_1) - \mathcal{J}(\rho_2)\|_{\mathbf{W}^{1,\infty}(\mathbb{R}^m;\mathbb{R}^\ell)} \leq L_{\mathcal{J}} \, \|\rho_1 - \rho_2\|_{\mathbf{L}^1(\mathbb{R}^N;\mathbb{R}^n)}.$$

Then, given the sets

$$\mathcal{R} = \left\{ \rho \in (\mathbf{L}^1 \cap \mathbf{BV})(\mathbb{R}^N;[0,R]^n) \colon \operatorname{spt}\rho \text{ is compact} \right\},$$

$$\mathcal{T} = \{(t_1,t_2) \colon t_2 \geq t_1 \geq 0\},$$

there exists a process $\mathcal{P} \colon \mathcal{T} \times \mathcal{R} \times \mathbb{R}^m \to \mathcal{R} \times \mathbb{R}^m$ *such that:*

1. *for every* $t \in \mathbb{R}^+$, $\mathcal{P}_{t,t}$ *is the identity map;*
2. *for all* $t_1, t_2, t_3 \in \mathbb{R}^+$ *with* $t_3 \geq t_2 \geq t_1$, $\mathcal{P}_{t_2,t_3} \circ \mathcal{P}_{t_1,t_2} = \mathcal{P}_{t_1,t_3}$;
3. *for all* $(\rho_o, p_o) \in \mathcal{R} \times \mathbb{R}^m$ *and* $t_o \in \mathbb{R}^+$, *the map* $t \mapsto \mathcal{P}_{t_o,t}(\rho_o, p_o)$ *is continuous, defined for* $t \geq t_o$, *and the unique solution to (6.1) in the sense of Definition 6.1 with initial datum* (ρ_o, p_o) *assigned at time* t_o;
4. *for every* $(\rho_o^1, p_o^1), (\rho_o^2, p_o^2) \in \mathcal{R} \times \mathbb{R}^m$, *there exists a function* $\mathcal{L} \in \mathbf{C}^0(\mathbb{R}^+;\mathbb{R}^+)$ *such that* $\mathcal{L}(0) = 0$ *and, setting* $(\rho_i, p_i)(t) = \mathcal{P}_{0,t}(\rho_o^i, p_o^i)$,

$$\|\rho_1(t) - \rho_2(t)\|_{\mathbf{L}^1(\mathbb{R}^N;\mathbb{R}^n)} \leq \big(1+\mathcal{L}(t)\big) \left\|\rho_o^1 - \rho_o^2\right\|_{\mathbf{L}^1(\mathbb{R}^N;\mathbb{R}^n)} + \mathcal{L}(t) \left\|p_o^1 - p_o^2\right\|_{\mathbb{R}^m},$$

$$\|p_1(t) - p_2(t)\|_{\mathbb{R}^m} \leq \mathcal{L}(t) \left\|\rho_o^1 - \rho_o^2\right\|_{\mathbf{L}^1(\mathbb{R}^N;\mathbb{R}^n)} + \big(1+\mathcal{L}(t)\big) \left\|p_o^1 - p_o^2\right\|_{\mathbb{R}^m};$$

5. *for all* $(\rho_o, p_o) \in \mathcal{R} \times \mathbb{R}^m$, *if* q_1, q_2, V_1, V_2, *and* F_1, F_2 *satisfy the same assumptions as* q, V, *and* F, *then there exists a function* $\mathcal{K} \in \mathbf{C}^0(\mathbb{R}^+;\mathbb{R}^+)$ *such that* $\mathcal{K}(0) = 0$ *and, calling* (ρ_i, p_i) *the corresponding solutions, for* $t > 0$,

$$\begin{aligned}
&\|\rho_1(t) - \rho_2(t)\|_{\mathbf{L}^1(\mathbb{R}^N;\mathbb{R}^n)} + \|p_1(t) - p_2(t)\|_{\mathbb{R}^m} \\
&\leq \mathcal{K}(t) \left(\|q_1 - q_2\|_{\mathbf{W}^{1,\infty}(\mathbb{R}^+;\mathbb{R}^+)} + \|V_1 - V_2\|_{\mathbf{W}^{1,\infty}(\mathbb{R}^+ \times \mathbb{R}^N \times \mathbb{R}^N \times \mathbb{R}^m;\mathbb{R}^N)} \right) \\
&\quad + \mathcal{K}(t) \, \|F_1 - F_2\|_{\mathbf{L}^\infty(\mathbb{R}^+ \times \mathbb{R}^m \times \mathbb{R}^\ell;\mathbb{R}^m)}.
\end{aligned}$$

For further models based on the coupling of conservation laws with ordinary differential equations, see [11, 12].

7 Conclusions

Above, we collected various results that, together, allow a rigorous study of several macroscopic crowd dynamics models based on conservation laws. On these bases, several research directions naturally open.

From a strictly analytic point of view, a natural question is the relation between the models above and the so-called microscopic ones. It is apparently still unknown if a nonlocal conservation law model can be rigorously proved to be the limit as $n \to +\infty$ of a microscopic model for n individuals, typically based on ordinary differential equations. A few results in this direction, currently limited to a single space dimension, are, for instance, in [46, 48].

From a control theoretic point of view, the modeling frameworks introduced above allow to state many optimization problems. In particular, we stress the relevance of shape optimization problems: is there an optimal shape for an exit, so that emergency evacuations are as quick as possible? Preliminary results in this direction are, for instance, in [34]. Note that, in this connection, both necessary and sufficient conditions for optimality are nowadays apparently unknown.

From a numerical point of view, the introduction of efficient algorithms would definitely foster the development and the spread of these models. Indeed, nonlocal terms impose the computation of (possibly several) convolution integrals at each time step. A detailed numerical study aimed at optimizing the choices of the meshes used in the PDE integration and in the convolution integrals might have dramatic effects on the integration times. Preliminary numerical studies in this direction are, for instance, in [1, 3, 19].

Appendices

Regular Entropy Solutions for IBVP Problems

In this appendix we briefly recall the concept of regular entropy solutions for an initial boundary value problem. To this aim, fix $T > 0$, an open and bounded subset Ω of $\mathbb{R}^N$, and let us consider the system

$$\begin{cases} \partial_t \rho + \operatorname{div}_x (\rho u(t,x)) = 0 & t \in \mathring{I},\ x \in \Omega \\ \rho(t,x) = 0 & t \in \mathring{I},\ x \in \partial\Omega \\ \rho(0,x) = \rho_o(x) & x \in \partial\Omega\,, \end{cases} \tag{7.1}$$

where $u \in (\mathbf{C}^\infty \cap \mathbf{L}^\infty)(\mathring{I} \times \Omega; \mathbb{R}^N)$ satisfies, for every $t \in \mathring{I}$, $u(t) \in \mathbf{C}^2(\Omega; \mathbb{R}^N)$ and $\|u(t)\|_{\mathbf{C}^2(\Omega;\mathbb{R}^N)} \leq M$ for a suitable positive constant M. The definition of a boundary entropy–entropy flux pair is as follows.

Definition A.1 ([28, Definition 4.1], [60, Definition 2]) The pair of functions $(H, Q) \in \mathbf{C}^2\left(\mathbb{R}^2; \mathbb{R}\right) \times \mathbf{C}^2\left(\mathring{I} \times \overline{\Omega} \times \mathbb{R}^2; \mathbb{R}^N\right)$ is said a *boundary entropy–entropy flux pair for (7.1)* if:

1. the function $z \mapsto H(z, w)$ is convex for every $w \in \mathbb{R}$;
2. the equality $\partial_z Q(t, x, z, w) = (\partial_z H(z, w))\, u(t, x)$ holds for every $t \in \mathring{I}$, $x \in \overline{\Omega}$, and $z, w \in \mathbb{R}$;
3. the equalities $H(w, w) = 0$, $Q(t, x, w, w) = 0$, and $\partial_z H(w, w) = 0$ hold for every $t \in \mathring{I}$, $x \in \overline{\Omega}$, and $w \in \mathbb{R}$.

It is now possible to state the definition of regular entropy solution.

Definition A.2 ([57, Definition 3.3]) A *regular entropy solution to (7.1)* is a function $\rho \in \mathbf{L}^\infty(\mathring{I} \times \Omega; \mathbb{R})$ such that, for every boundary entropy–entropy flux pair (H, Q), in the sense of Definition A.1, for every $k \in \mathbb{R}$ and for every $\varphi \in \mathbf{C}^1_c(\mathbb{R} \times \mathbb{R}^N; \mathbb{R}^+)$, it holds

$$
\begin{aligned}
&\int_0^T \int_\Omega \left[H\left(\rho(t,x), k\right) \partial_t \varphi(t,x) + Q\left(t, x, \rho(t,x), k\right) \cdot \nabla_x \varphi(t,x)\right] \mathrm{d}x\mathrm{d}t \\
&- \int_0^T \int_\Omega \partial_z H\left(\rho(t,x), k\right) \rho(t,x)\, \mathrm{div}_{\mathrm{x}}\left(u(t,x)\right) \varphi(t,x) \mathrm{d}x\mathrm{d}t \\
&+ \int_0^T \int_\Omega \mathrm{div}_{\mathrm{x}}\, Q\left(t, x, \rho(t,x), k\right)\, \varphi(t,x) \mathrm{d}x\mathrm{d}t \\
&+ \int_\Omega H\left(\rho_o(x), k\right) \varphi(0,x) \mathrm{d}x \\
&+ \|u\|_{\mathbf{L}^\infty(\mathring{I} \times \Omega; \mathbb{R}^N)} \int_0^T \int_{\partial\Omega} H\left(0, k\right) \varphi(t,x) \mathrm{d}\mathcal{H}^{N-1}(x) \mathrm{d}t \geq 0,
\end{aligned}
$$

where $\mathcal{H}^{N-1}$ denotes the Hausdorff measure of dimension $N - 1$.

List of Symbols

$\mathbf{C}^{0,1}(A; B)$	with A and B subsets of normed vector spaces, is the set of functions defined on A, with values in B, that are Lipschitz continuous on A.
$\mathbf{C}^k(A; B)$	with A and B subsets of normed vector spaces, is the set of functions defined on A, with values in B, whose k-derivatives are continuous on A.
$\mathbf{C}^k_c(A; B)$	with A and B subsets of normed vector spaces, is the set of compactly supported functions defined on A, with values in B whose k-derivatives are continuous on A.
$\overline{I}$	is the closure of the set I.

$\mathring{I}$	is the interior of the set I.
$\mathbf{L}^p(A;B)$	with $p \geq 1$, $A \subseteq \mathbb{R}^n$ and $B \subseteq \mathbb{R}^m$, is the set of measurable functions f defined on A, with values in B, such that $\lvert f\rvert^p$ is Lebesgue integrable on A.
$\mathbf{L}^\infty(A;B)$	with $A \subseteq \mathbb{R}^n$ and $B \subseteq \mathbb{R}^m$, is the set of measurable functions f defined on A, with values in B, essentially bounded.
$\mathbb{R}^+$	is the set $[0, +\infty[$ of 0 and all positive real numbers.
$\mathring{\mathbb{R}}^+$	is the set $]0, +\infty[$ of all strictly positive real numbers.
$\mathbb{S}^{N-1}$	is the unit sphere in $\mathbb{R}^N$.
spt ρ	is the support of the function ρ.
$\mathbf{W}^{1,p}(A;B)$	with $1 \leq p \leq \infty$, $A \subseteq \mathbb{R}^n$ and $B \subseteq \mathbb{R}^m$, is the Sobolev space of functions defined in A with values in B whose first weak derivative is in $\mathbf{L}^p$.

References

1. A. Aggarwal, R.M. Colombo, P. Goatin, Nonlocal systems of conservation laws in several space dimensions. SIAM J. Numer. Anal. **53**(2), 963–983 (2015)
2. J.P. Agnelli, F. Colasuonno, D. Knopoff, A kinetic theory approach to the dynamics of crowd evacuation from bounded domains. Math. Models Methods Appl. Sci. **25**(1), 109–129 (2015)
3. P. Amorim, R.M. Colombo, A. Teixeira, On the numerical integration of scalar nonlocal conservation laws. ESAIM Math. Model. Numer. Anal. **49**(1), 19–37 (2015)
4. F. Bagarello, F. Gargano, F. Oliveri, A phenomenological operator description of dynamics of crowds: escape strategies. Appl. Math. Model. **39**(8), 2276–2294 (2015)
5. R. Bailo, J.A. Carrillo, P. Degond, Pedestrian models based on rational behaviour, in *Modeling and Simulation in Science, Engineering and Technology* (Birkhäuser, New York, 2018), pp. 259–292
6. N. Bellomo, A. Bellouquid, On multiscale models of pedestrian crowds from mesoscopic to macroscopic. Commun. Math. Sci. **13**(7), 1649–1664 (2015)
7. N. Bellomo, S. Berrone, L. Gibelli, A.B. Pieri, Macroscopic first order models of multicomponent human crowds with behavioral dynamics, in *Advances in Computational Fluid-Structure Interaction and Flow Simulation*. Modeling and Simulation in Science, Engineering and Technology (Birkhäuser/Springer, Cham, 2016), pp. 295–306
8. N. Bellomo, L. Gibelli, N. Outada, On the interplay between behavioral dynamics and social interactions in human crowds. Kinet. Relat. Models **12**(2), 397–409 (2019)
9. F. Berthelin, P. Goatin, Regularity results for the solutions of a non-local model of traffic flow. Discrete Contin. Dyn. Syst. **39**(6), 3197–3213 (2019)
10. S. Bianchini, R.M. Colombo, On the stability of the standard Riemann semigroup. Proc. Am. Math. Soc. **130**(7), 1961–1973 (2002)
11. R. Borsche, R.M. Colombo, M. Garavello, On the coupling of systems of hyperbolic conservation laws with ordinary differential equations. Nonlinearity **23**(11), 2749–2770 (2010)
12. R. Borsche, R.M. Colombo, M. Garavello, Mixed systems: ODEs - balance laws. J. Differ. Equ. **252**(3), 2311–2338 (2012)
13. R. Borsche, R.M. Colombo, M. Garavello, A. Meurer, Differential equations modeling crowd interactions. J. Nonlinear Sci. **25**(4), 827–859 (2015)
14. R. Borsche, A. Klar, F. Schneider, Numerical methods for mean-field and moment models for pedestrian flow, in *Crowd Dynamics. Vol. 1*. Modeling and Simulation in Science, Engineering and Technology (Birkhäuser/Springer, Cham, 2018), pp. 167–209

15. F. Bouchut, B. Perthame, Kružkov's estimates for scalar conservation laws revisited. Trans. Am. Math. Soc. **350**(7), 2847–2870 (1998)
16. A. Bressan, *Hyperbolic Systems of Conservation Laws*. Oxford Lecture Series in Mathematics and Its Applications, vol. 20 (Oxford University Press, Oxford, 2000). The one-dimensional Cauchy problem
17. A. Bressan, B. Piccoli, *Introduction to the Mathematical Theory of Control*. AIMS Series on Applied Mathematics, vol. 2 (American Institute of Mathematical Sciences, Springfield, 2007)
18. A. Bressan, W. Shen, On traffic flow with nonlocal flux: a relaxation representation (2019). arXiv: 1911.03636
19. C. Chalons, P. Goatin, L.M. Villada, High-order numerical schemes for one-dimensional nonlocal conservation laws. SIAM J. Sci. Comput. **40**(1), A288–A305 (2018)
20. G.-Q. Chen, K.H. Karlsen, Quasilinear anisotropic degenerate parabolic equations with time-space dependent diffusion coefficients. Commun. Pure Appl. Anal. **4**(2), 241–266 (2005)
21. F.A. Chiarello, P. Goatin, Global entropy weak solutions for general non-local traffic flow models with anisotropic kernel. ESAIM Math. Model. Numer. Anal. **52**(1), 163–180 (2018)
22. F.A. Chiarello, P. Goatin, Non-local multi-class traffic flow models. Netw. Heterog. Media **14**(2), 371–387 (2019)
23. F.A. Chiarello, P. Goatin, E. Rossi, Stability estimates for non-local scalar conservation laws. Nonlinear Anal. Real World Appl. **45**, 668–687 (2019)
24. A. Colombi, M. Scianna, A. Alaia, A discrete mathematical model for the dynamics of a crowd of gazing pedestrians with and without an evolving environmental awareness. Comput. Appl. Math. **36**(2), 1113–1141 (2017)
25. R.M. Colombo, F. Marcellini, Nonlocal systems of balance laws in several space dimensions with applications to laser technology. J. Differ. Equ. **259**(11), 6749–6773 (2015)
26. R.M. Colombo, L.-M. Mercier, Nonlocal crowd dynamics models for several populations. Acta Math. Sci. **32**(1), 177–196 (2012)
27. R.M. Colombo, E. Rossi, Hyperbolic predators vs. parabolic prey. Commun. Math. Sci. **13**(2), 369–400 (2015)
28. R.M. Colombo, E. Rossi, Nonlocal conservation laws in bounded domains. SIAM J. Math. Anal. **50**(4), 4041–4065 (2018)
29. R.M. Colombo, E. Rossi, Control in a mixed hyperbolic-parabolic predator prey model (2019, in preparation)
30. R.M. Colombo, E. Rossi, Modelling crowd movements in domains with boundaries. IMA J. Appl. Math. **84**(5), 833–853 (2019)
31. R.M. Colombo, E. Rossi, A modeling framework for biological pest control. Math. Biosci. Eng. **17**(mbe-17-02-072), 1413 (2020)
32. R.M. Colombo, M. Mercier, M.D. Rosini, Stability and total variation estimates on general scalar balance laws. Commun. Math. Sci. **7**(1), 37–65 (2009)
33. R.M. Colombo, M. Herty, M. Mercier, Control of the continuity equation with a non local flow. ESAIM Control Optim. Calc. Var. **17**(2), 353–379 (2011)
34. R.M. Colombo, M. Garavello, M. Lécureux-Mercier, A class of nonlocal models for pedestrian traffic. Math. Models Methods Appl. Sci. **22**(4), 1150023, 34 (2012)
35. M. Colombo, G. Crippa, L.V. Spinolo. Blow-up of the total variation in the local limit of a nonlocal traffic model (2018)
36. M. Colombo, G. Crippa, M. Graff, L.V. Spinolo. On the role of numerical viscosity in the study of the local limit of nonlocal conservation laws (2019)
37. M. Colombo, G. Crippa, M. Graff, L.V. Spinolo. Recent results on the singular local limit for nonlocal conservation laws (2019)
38. M. Colombo, G. Crippa, L.V. Spinolo, On the singular local limit for conservation laws with nonlocal fluxes. Arch. Ration. Mech. Anal. **233**(3), 1131–1167 (2019)
39. A. Corli, L. Malaguti, Viscous profiles in models of collective movement with negative diffusivity. Z. Angew. Math. Phys. **70**(2), Art. 47, 22 (2019)
40. J.-M. Coron, M. Kawski, Z. Wang, Analysis of a conservation law modeling a highly re-entrant manufacturing system. Discrete Contin. Dyn. Syst. Ser. B **14**(4), 1337–1359 (2010)

41. V. Coscia, C. Canavesio, First-order macroscopic modelling of human crowd dynamics. Math. Models Methods Appl. Sci. **18**(Suppl.), 1217–1247 (2008)
42. G. Crippa, M. Lécureux-Mercier, Existence and uniqueness of measure solutions for a system of continuity equations with non-local flow. Nonlinear Differ. Equ. Appl. **20**(3), 523–537 (2013)
43. E. Cristiani, B. Piccoli, A. Tosin, *Multiscale Modeling of Pedestrian Dynamics*. MS&A. Modeling, Simulation and Applications, vol. 12 (Springer, Cham, 2014)
44. C.M. Dafermos, *Hyperbolic Conservation Laws in Continuum Physics*. Grundlehren der Mathematischen Wissenschaften [Fundamental Principles of Mathematical Sciences], vol. 325, 4th edn. (Springer, Berlin, 2016)
45. E. De Angelis, Nonlinear hydrodynamic models of traffic flow modelling and mathematical problems. Math. Comput. Model. **29**(7), 83–95 (1999)
46. M. Di Francesco, M.D. Rosini, Rigorous derivation of nonlinear scalar conservation laws from follow-the-leader type models via many particle limit. Arch. Ration. Mech. Anal. **217**(3), 831–871 (2015)
47. H. Holden, N.H. Risebro, *Front Tracking for Hyperbolic Conservation Laws*. Applied Mathematical Sciences, vol. 152, 2nd edn. (Springer, Heidelberg, 2015)
48. H. Holden, N.H. Risebro, The continuum limit of Follow-the-Leader models—a short proof. Discrete Contin. Dyn. Syst. **38**(2), 715–722 (2018)
49. S.N. Kružhkov, First order quasilinear equations with several independent variables. Mat. Sb. (N.S.) **81**(123), 228–255 (1970)
50. M. Lécureux-Mercier, Improved stability estimates for general scalar conservation laws. J. Hyperbolic Differ. Equ. **8**(4), 727–757 (2011). See also the revised version at http://math.univ-lyon1.fr/~mercier
51. R. Loehner, On the modeling of pedestrian motion. Appl. Math. Model. **34**(2), 366–382 (2010)
52. B.J. Lucier, A moving mesh numerical method for hyperbolic conservation laws. Math. Comput. **46**(173), 59–69 (1986)
53. F. Marcellini, On the stability of a model for the cutting of metal plates by means of laser beams. Appl. Math. Lett. **68**, 143–149 (2017)
54. S. Motsch, M. Moussaïd, E.G. Guillot, M. Moreau, J. Pettré, G. Theraulaz, C. Appert-Rolland, P. Degond, Modeling crowd dynamics through coarse-grained data analysis. Math. Biosci. Eng. **15**(6), 1271–1290 (2018)
55. B. Piccoli, F. Rossi, Measure-theoretic models for crowd dynamics, in *Crowd Dynamics. Vol. 1*. Modeling and Simulation in Science, Engineering and Technology (Birkhäuser/Springer, Cham, 2018), pp. 137–165
56. B. Piccoli, A. Tosin, Time-evolving measures and macroscopic modeling of pedestrian flow. Arch. Ration. Mech. Anal. **199**(3), 707–738 (2011)
57. E. Rossi, Definitions of solutions to the IBVP for multi-dimensional scalar balance laws. J. Hyperbolic Differ. Equ. **15**(2), 349–374 (2018)
58. E. Rossi, V. Schleper, Convergence of numerical scheme for a mixed hyperbolic-parabolic system in two space dimensions. ESAIM Math. Model. Numer. Anal. **50**(2), 475–497 (2016)
59. M. Twarogowska, P. Goatin, R. Duvigneau, Macroscopic modeling and simulations of room evacuation. Appl. Math. Model. **38**(24), 5781–5795 (2014)
60. J. Vovelle, Convergence of finite volume monotone schemes for scalar conservation laws on bounded domains. Numer. Math. **90**(3), 563–596 (2002)

The Fokker–Planck Framework in the Modeling of Pedestrians' Motion

Alfio Borzì

Abstract Stochastic drift-diffusion processes and the related Fokker–Planck equations appear to be adequate for modeling the motion of pedestrians in different circumstances, and for the design of control strategies for different purposes. In this paper, some mathematical contribution in this field are reviewed that include different modeling issues concerning the control of a single pedestrian subject to perturbation and the development of a framework for pedestrian's avoidance dynamics based on the formulation of a Fokker–Planck Nash game. This review also includes a discussion on the mean-field approach to crowd motion and provides pointers to related models.

1 Introduction

The study of motion of animal/human crowds is a long-standing topic of research, probably starting with the empirical studies in [52]. However, crowd (collective) motion is ubiquitous in living systems: it has been observed in migration of cells [83], colonies of bacteria, herds of animals [84], swarms of birds and fishes [92]; see, e.g., [39] for a review on collective motion in biological systems.

On the other hand, there is a rich literature dedicated to the mathematical modeling of crowd motion, starting from the studies in [55, 67] and the paper [53] where pedestrians are modeled as interacting particles with mechanical attractive-repulsive forces. Further developments have resulted in many different modeling approaches including discrete and cellular automata, continuum fluid dynamics equations, conservation laws, and mesoscopic models; see, e.g., [3, 32, 34, 36, 49, 62, 72, 75, 86]. In this framework, pedestrian motion as a social process in crowds has been investigated in, e.g., [16, 89] for problems in one space dimension, and in [12] for multidimensional problems, including propagation in space of emotional

A. Borzì (✉)
Institut für Mathematik, Universität Würzburg, Würzburg, Germany
e-mail: alfio.borzi@mathematik.uni-wuerzburg.de

L. Gibelli (ed.), *Crowd Dynamics, Volume 2*, Modeling and Simulation in Science, Engineering and Technology, https://doi.org/10.1007/978-3-030-50450-2_6

patterns. Further, we remark that the investigation of pedestrian crowd motion has been strongly motivated by applications as, e.g., emergency evacuation procedures [11, 61, 74], efficient planning and designing of urban structures [26, 45], including the study of pattern formation, e.g., groups and lanes, and non-rational dynamics as in panic situation.

Notice that we have mentioned only few representative works concerning the vast research field of crowd and swarm systems; for a recent and comprehensive review of this field of applied mathematics we refer to [3].

We remark that the successful application of differential models has motivated further studies that suggest to include stochastic terms in the crowd dynamics [46, 92], and this new insight has motivated the development of new differential models [37, 70, 83, 92], where the underlying idea is that individual random dispersal results from, e.g., collision that can be described by Brownian motion.

With these assumptions, the simplest model of pedestrian motion is given by the following stochastic differential equation (SDE):

$$\begin{aligned} dX(t) &= u(X(t), t)\, dt + \sigma(X(t), t)\, dW(t), \\ X(0) &= X_0, \end{aligned} \tag{1}$$

where the position variable $X(t)$ is subject to deterministic infinitesimal increments driven by the vector-valued drift function $u = (u_1, \ldots, u_d)$, and to random infinitesimal increments proportional to a multidimensional Wiener process $dW(t) \in \mathbb{R}^d$, with stochastically independent components. However, we shall adopt a specific picture where X denotes the position of a pedestrian in a room $\Omega \subset \mathbb{R}^2$, and $u = (u_1, u_2)$ denotes the velocity field of motion of the pedestrian. For simplicity, we assume that the dispersion matrix $\sigma(X(t), t)$ is a diagonal matrix with both entries equal to the constant $\sigma > 0$ (we use the same symbol).

The model (1) has many advantages compared to the deterministic model $\dot{X}(t) = u(X(t), t)$. First of all, it models all possible realization of motion of a pedestrian with a given velocity field and subject to perturbations. Further, it allows to have the initial state X_0 prescribed by a probability density function (PDF) that accommodates uncertainties in our knowledge of initial conditions. Moreover, in our SDE model we can assume that the position of the pedestrian is considered in a bounded domain $X(t) \in \Omega$, and we can prescribe specific barriers that delimit the motion in this domain. Specifically, we can have absorbing barriers where the pedestrian 'disappears' or reflecting barriers, like rigid walls, that cannot be traversed by the pedestrian; see [82] for a formulation of barriers for stochastic processes. Notice that the model (1) remains equally valid in the case of many non-interacting pedestrians driven by the same drift function.

We see that a stochastic framework could very well address the fundamental aim to model pedestrian motion by differential equations that allow simulation and analysis in many application systems. Thus, the next step in our modeling effort becomes the design of control mechanisms in our kinetics model for purposes like evacuation procedures [62]. For this task, stochastic optimal control schemes are a

possible choice. However, in stochastic models the state evolution $X(t)$ is random and represents an outcome of a probability space, therefore a direct insertion of $X(t)$ into a functional objective J results into a random variable. For this reason, in stochastic optimal control theory, the following expected value of a cost functional is considered [44]:

$$J(X,u) = \mathbb{E}[\int_0^T L(t, X(t), u(X(t),t))\, dt + \Psi[X(T)]], \tag{2}$$

where L and Ψ are continuous functions which satisfy a polynomial growth condition, and T defines the time horizon where the motion is considered. The function L usually represents a pay-off along a trajectory that includes the cost of the control, whereas Ψ is related to the terminal state. In the context of pedestrian motion, these functions can be used to model the purpose of the motion, that is, to follow a desired path and to reach a final destination, and to model the cost of this motion.

It appears that a stochastic control problem leads to assume a statistical point of view, with the perspective of capturing the collective behaviour of motion in crowds, and for this purpose we notice that the state of the stochastic motion modeled by (1) can be completely characterized by its probability density function, whose evolution is governed by the following Fokker–Planck (FP) equation:

$$\begin{aligned} \partial_t f(x,t) + \nabla \cdot (u(x,t)\, f(x,t)) - \frac{\sigma^2}{2}\, \Delta f(x,t) = 0, \\ f(x,0) = f_0(x), \end{aligned} \tag{3}$$

where $f = f(x,t)$ is the probability density of the pedestrian to be in x at time t, where $(x,t) \in Q := \Omega \times (0,T)$, the space-time cylinder where our problem is formulated. With '$\nabla\cdot$' we denote the divergence operator.

The initial PDF distribution for X_0 is denoted with f_0, and it satisfies the following properties:

$$f_0 \geq 0, \qquad \int_\Omega f_0(x)\, dx = 1. \tag{4}$$

We remark that the PDF associated with (1) can be equally well be interpreted as a normalized material density of all pedestrians involved.

Now, to complete the formulation of our FP problem, we notice that (3) can be written in flux form as follows:

$$\partial_t f(x,t) = \nabla \cdot F(f)(x,t), \qquad f(x,0) = f_0(x), \tag{5}$$

where the flux F is given component-wise by

$$F_j(f)(x,t) = \frac{\sigma^2}{2}\partial_{x_j} f - u_j(x,t)\, f, \qquad j = 1, 2.$$

With this setting, we can formulate two types of barriers for the stochastic motion and consequently two types of boundary conditions for the FP equation. If absorbing barriers are prescribed, then we have homogeneous Dirichlet boundary conditions for the PDF, i.e., $f = 0$ on $\partial\Omega$. On the other hand, reflecting barriers correspond to the following flux-zero boundary conditions:

$$F \cdot n = 0, \qquad \text{on } \partial\Omega \times (0,T), \tag{6}$$

where n is the unit outward normal to $\partial\Omega$.

Notice that, with both choices of boundary conditions and the initial condition satisfying (4), the resulting FP problem has a unique non-negative solution $f \in L^2(0,T;H^1(\Omega)) \cap C([0,T];L^2(\Omega))$. Furthermore, in the case of flux-zero boundary conditions, we have conservation of the total probability, that is, $\int_\Omega f(x,t)\,dx = 1$ for all $t \geq 0$.

We see that the coefficients of the FP equation are directly determined by the coefficients of the SDE modeling the motion of the pedestrian. In particular, we can identify the velocity field u as our control function. Moreover, the solution of the FP problem gives us the PDF that allows to write the functional (2) in the following form:

$$J(f,u) := \int_0^T \int_\Omega L(s,x,u(x,s))\, f(x,s)\, ds\, dx + \int_\Omega \Psi(x)\, f(x,T)\, dx. \tag{7}$$

Therefore one can formulate a FP control framework where the problem is to find u that drives the solution to (3) in such a way to minimize (7) in the given time horizon.

It is the purpose of this paper to illustrate some interesting aspects of this approach to pedestrian motion and review a few contributions in this field. However, let us remark that, for the purpose of control design, the approach outlined above of lifting the stochastic dynamics modeled by a SDE to the corresponding continuity equation given by the FP model was initially proposed in [4, 5] and independently in [21, 22]. In fact, this is a general strategy that applies to many different classes of dynamical systems having a corresponding continuity equation; see [7, 9] for additional discussion and details.

2 The Motion of One Pedestrian

In this section, we focus on the modeling of motion of one pedestrian in the framework given above and discuss the formulation of a FP optimal control problem

that aims at determining an optimal velocity field u of the pedestrian for the purpose of performing some given tasks.

Clearly, in this modeling step we have to decide the functional space to which the vector function u belongs, and consequently formulate our FP optimization problem in such a way that a solution u in this space exists. In taking this decision, we notice that there is a striking difference between choosing a velocity field u that depends only on the time variable, $u = u(t)$, or only on the space variable $u = u(x)$, or on both variables. Roughly speaking, in the former case, we have an open-loop control, and in the latter cases we have a closed-loop control function, in the sense that a sudden change of the position of the pedestrian $X(t)$ provides instantaneously (feedback) the optimal control for the new state configuration. For a discussion on the significance of these two settings, we refer to [21, 22] and the discussion that follows.

In our framework, the case $u = u(t)$ has been discussed in detail in, e.g., [4, 5] and [9] in a general setting and is discussed later in this paper in correspondence to the avoidance problem. For this reason, we now focus on the case $u = u(x, t)$ as discussed in [78, 80].

In this case, we may suppose that the control field u is sought in the following admissible set:

$$U_{ad} = \{u \in U |\, u_a \leq u_i(x,t) \leq u_b,\ i = 1,2,\ \text{ a.e. in } \Omega,\ u_a, u_b \in \mathbb{R}, u_a < u_b\}. \tag{8}$$

Thus, U_{ad} is a convex, closed, and bounded set of our control space U.

In [78, 80], the space U is chosen to be the space $L^2(0, T; H^1(\Omega) \times H^1(\Omega))$; see these references for all details. However, for the purpose of this review to illustrate the main ideas and possible advantages of the FP control framework in modeling pedestrian motion, we make the simpler choice $U = L^q(Q) \times L^q(Q)$, $q > 2$; however, notice that $u \in U_{ad} \subset L^\infty(Q)$; see, e.g., [43] for a similar setting.

In this case, appropriate penalisation terms in the cost functional guaranteeing that $u \in U$ are given by

$$A(u(x,t)) = |u(x,t)|^2, \tag{9}$$

$$A(u(x,t)) = |u(x,t)|^2 f(x,t), \tag{10}$$

where $|\cdot|$ represents the standard Euclidean norm in $\mathbb{R}^2$, ∇u is the Jacobian matrix whose entries are defined by $(\nabla u)_{ij} = \dfrac{\partial u_i}{\partial x_j}$, and $|\nabla u|$ represents the Frobenius norm of ∇u. Notice that A can be considered the part of the pay-off function L that embodies the control.

On the other hand, we would like to formulate the purpose of motion of the pedestrian, that is, the purpose of the control u. A standard choice is to determine an optimal velocity field with which the pedestrian follows a desired path, and comes as close as possible to a final position at time T. This means that our objective functional should have a tracking-trajectory term and a terminal position

term that are consistent with the structure given in (7). This requirement is satisfied by introducing the concept of a 'valley' potential V, such that the minimization of the objective functional corresponds to concentrating the PDF along the bottom of the valley. This configuration corresponds to having the ensemble of all stochastic trajectories being close to the one defining the bottom of the valley. Specifically, let $x_t = (x^1(t), x^2(t))$ represents a desired trajectory in Ω, $t \in [0, T]$. Then a possible choice for V is a quadratic function, and in our objective functional we have

$$\int_0^T \int_\Omega V(x - x_t)\, f(x,t)\, dxdt.$$

A similar structure can be implemented for a desired final configuration x_T. Summarizing, we arrive at the following objective functional:

$$J(f,u) = \alpha \int_0^T \int_\Omega V(x - x_t)\, f(x,t)\, dxdt + \beta \int_\Omega V(x - x_T)\, f(x,T)\, dx + \frac{\nu}{2} \int_0^T \int_\Omega A(u(x,t))\, dxdt, \tag{11}$$

where $\alpha, \beta \geq 0$ are optimization weights for tuning the relative importance of the tracking and terminal tasks, whereas $\nu > 0$ is the weight of the cost of the control.

Notice that (11) has the structure (7) when choosing the cost of the control given by (10). On the other hand, choosing (9) results in a cost functional that has not the structure of an average functional. The former strategy is discussed in [80], while the latter is considered in [21, 22, 78].

In both cases, the problem formulation is to find $u \in U_{ad}$ that minimizes the objective functional J, given by (11), subject to the FP differential constraint (3), (4), (6), as follows:

$$\min_{u \in U_{ad}} J(f,u) \qquad \text{subject to (s.t.)} \quad (3)\text{–}(4)\text{–}(6). \tag{12}$$

This is a deterministic optimal control problem governed by a parabolic partial-differential equation (PDE) for which we can apply many theoretical and numerical techniques; see, e.g., [17, 66, 87].

However, the FP optimal control problem (12) has some distinct features that deserve further discussion. For this purpose, we recall that, subject to appropriate differentiability properties [66, 87], the solution to (12) must satisfy the first-order necessary optimality conditions that result in an optimality system that includes the FP equation with the given initial- and boundary conditions, an adjoint FP equation with terminal- and boundary conditions, and an optimality condition inequality.

For the case (9), the adjoint FP equation and the optimality condition are given by

$$\begin{aligned} -\partial_t p(x,t) - \frac{\sigma^2}{2}\Delta p(x,t) - u(x,t)\cdot\nabla p(x,t) + \alpha V(x-x_t) = 0 \\ p(x,T) = -\beta V(x-x_T) \qquad \text{in } \Omega, \qquad \frac{\partial p}{\partial n} = 0 \quad \text{on } \partial\Omega\times(0,T), \end{aligned} \tag{13}$$

and

$$(\nu u_i - \partial_{x_i} p\, f,\ v - u_k) \geq 0 \qquad \forall v \in U_{ad},\ i = 1,2. \tag{14}$$

For the case (10), we have

$$\begin{aligned} \partial_t p(x,t) - \frac{\sigma^2}{2}\Delta p(x,t) - u(x,t)\cdot\nabla p(x,t) + \alpha V(x-x_t) + \frac{\nu}{2}|u(x,t)|^2 = 0 \\ p(x,T) = -\beta V(x-x_T) \qquad \text{in } \Omega, \qquad \frac{\partial p}{\partial n} = 0 \quad \text{on } \partial\Omega\times(0,T), \end{aligned} \tag{15}$$

and

$$\left((\nu u_i - \partial_{x_i} p\right) f,\ v - u_k) \geq 0 \qquad \forall v \in U_{ad},\ i = 1,2, \tag{16}$$

where $(\cdot\,,\cdot)$ denotes the $L^2(Q)$ scalar product.

Now, for clarity, let us assume $U_{ad} = U$ (thus no pointwise constraints on the value of u). In this case, the optimality condition (14) becomes $\nu u_i - \partial_{x_i} p\, f = 0$, whereas (16) becomes $\left(\nu u_i - \partial_{x_i} p\right) f = 0$. This fact shows that the velocity field obtained with the setting (9) depends on both p and f, and because of the latter it depends on the distribution of the initial condition. Therefore it cannot be a feedback control although it may represent a good approximation of it. On the other hand, in the case of the setting (10), we notice that, since our FP equation is uniformly parabolic, the resulting PDF is almost everywhere non-negative for any $t > 0$ independently of the shape of f_0. Hence, the optimality condition becomes $\nu u_i - \partial_{x_i} p = 0$, that is, $u(x,t) = \nabla p(x,t)/\nu$, which means that u is uniquely determined by the adjoint equation that becomes

$$\begin{aligned} \partial_t p(x,t) + \frac{\sigma^2}{2}\Delta p(x,t) + \frac{1}{2\nu}|\nabla p(x,t)|^2 - \alpha V(x-x_t) = 0 \\ p(x,T) = -\beta V(x-x_T) \qquad \text{in } \Omega, \qquad \frac{\partial p}{\partial n} = 0 \quad \text{on } \partial\Omega\times(0,T). \end{aligned} \tag{17}$$

This is the Hamilton–Jacobi–Bellman equation for the stochastic pedestrian motion and the given expectation functional, whose solution gives the feedback law that optimally drives the pedestrian along x_t, and towards the final destination x_T. For further discussion on the connection between the HJB and the FP control frameworks see, e.g., [7, 8]. However, there is another way to construct feedback solutions also using the (9) setting that is based on the so-called model predictive

control (MPC) scheme [51]. For a discussion on the implementation of this scheme with FP models see, e.g., [5, 42]

We see that the FP framework provides a full scale of modeling features. For example, we can add another term in our functional with a concave potential that could be used to model a 'soft' obstacle. This situation has been considered in [78], see Fig. 1.

Further, one could reformulate the problem of designing the 'optimal' room (based on some criteria) as FP-based shape/topology optimization problems, and in general problems of structural design; see, e.g., [23].

We would like to remark that the FP framework is not limited to the case of motion modeled by the drift-diffusion model (1). In fact, it appears very natural to consider this model augmented with a jump process, which leads to a FP equation of integro-partial differential type that can be used to design a FP control strategy of the drift-diffusion-jump motion of the pedestrian; see, e.g., [47, 48]. Similarly, one could consider this motion modeled by a piecewise-deterministic process and consider the related (hyperbolic) FP system [6].

3 The Motion of Two Pedestrians

In this section, we illustrate a FP approach to model interaction between two pedestrians and, for this purpose, we need to clarify the meaning of 'interaction'. We have that the assumption of a physical interaction by attractive or repulsive forces stems very much from our viewing the pedestrians as particles subject to forces. This mechanistic approach can be found in many works on multiple agents [3, 32, 34, 49, 75], and it requires to prescribe how the dynamics should be. From the FP point of view, this approach leads to consider a system of coupled SDEs, and results in a FP equation whose space dimensionality equals dN, where d is the space where the pedestrians move ($d = 1, 2, 3$) and N is the number of pedestrians. It is clear that, in this setting, solving the FP problem becomes prohibitive also for a relatively small number of pedestrians. On the other hand, a setting where independent pedestrians aim at solving a unique optimization problem or multiple ones determines another form of interaction that allows to consider N uncoupled FP problems in d dimensions. In particular, one can consider the case of N pedestrians with a common cost functional to be minimized, which may model cooperative motion. However, we can also consider the case where each pedestrian aims at optimizing its own functional, possibly in competition with the others, thus defining a competition game. In the latter situation, we do not have a solution concept of optimality, but one of equilibria with respect to the competitive tasks, and this appears to be the case of two pedestrians (at least) that have planned to go along paths that cross each other and would lead to collision. Therefore we have the problem of designing an avoidance strategy that allows the non-cooperative pedestrians to deviate from their original route as less as possible and at a minimal cost.

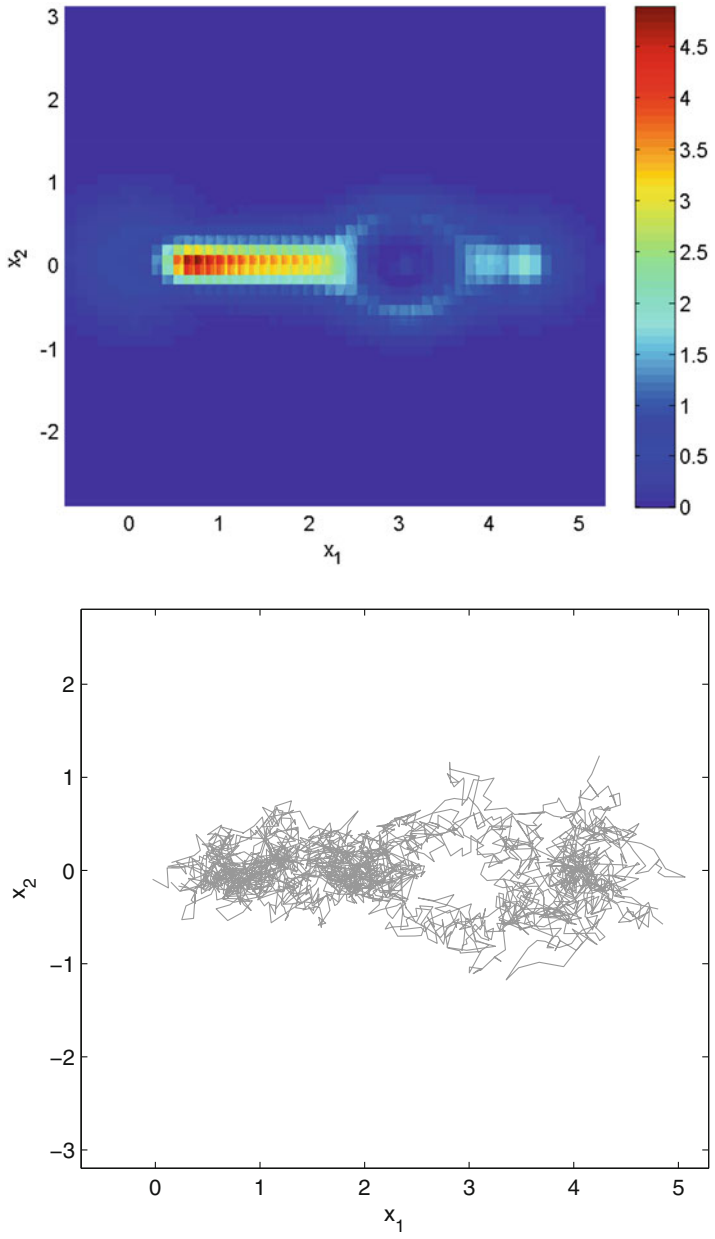

Fig. 1 Motion of a pedestrian along the desired trajectory $\bar{x}(t) = (1.5t, 0)$ with a soft obstacle (a cylinder). Top: the evolution of the PDF; bottom: different stochastic realization of the pedestrian's trajectories

The problem of avoidance is one of the important and challenging features in pedestrians' motion [41]. It involves non-cooperative behaviour and possibly non-local interactions, and the understanding of the avoidance mechanism has attracted much attention in behavioural sciences; see, e.g., [59, 73, 88]. Thus the problem of avoidance represents a benchmark for the mathematical modeling of the motion of two pedestrians in some situation where they come close.

As already mentioned, we can approach the avoidance problem from a mechanistic point of view. In fact, in this framework the setting of left-hand traffic and right-hand traffic can be considered two solutions of the avoidance problem in bidirectional traffic. On the other hand, the approach presented in [57, 58, 79] represents an alternative point of view that formulates the avoidance problem as a Nash game such that the avoidance dynamics arises as a Nash equilibrium of the game and is not assigned a priori. Specifically, in [79] the concept of Nash equilibrium is central for modeling the decision-making control, and is based on the formulation of an open-loop Nash game governed by FP equations, where the controls are included in the drifts of the stochastic equation of motion of the two pedestrians, and objective functionals are assigned that include a cost of the control and a collision-penalizing term as illustrated below.

Consider two pedestrians, $p = 1, 2$, whose position is denoted with $X^{(p)} \in \Omega \subset \mathbb{R}^2$. We assume that Ω represents a convex room limited by walls; thus the motion of the pedestrians is subject to reflecting barriers. The evolution of $X^{(p)}$ is governed by

$$\begin{cases} dX^{(p)}(t) = b^{(p)}(X^{(p)}(t), t, u^{(p)}(t))\, dt + \sigma\, dW^{(p)}(t) \\ X^{(p)}(0) = X_0^{(p)}, \qquad p = 1, 2, \end{cases} \tag{18}$$

where the drifts $b^{(p)}(X^{(p)}(t), t, u^{(p)}(t))$ have the following structure:

$$b^{(p)}(X^{(p)}(t), t, u^{(p)}(t)) = v^{(p)}(X^{(p)}(t), t) + u^{(p)}(t). \tag{19}$$

The velocity fields $v^{(p)}$, $p = 1, 2$, represent the deterministic dynamics of the single pedestrian in the absence of interaction with others (the planned motion). On the other hand, the time-dependent control functions $u^{(p)}$ represent the strategy that the pedestrians choose as an additional velocity field to avoid collision. The Brownian process is included to model dispersal due to external physical forces (e.g., in a crowd) or other perturbation to the deterministic motion. Notice that the two SDEs given in (18) are uncoupled. Therefore, corresponding to each stochastic model, we can associate a FP equation with the corresponding drift and diffusion coefficient. In the following, we denote with $f^{(p)}(x, t)$, $p = 1, 2$, the solution PDFs of the corresponding evolution FP problems in correspondence to the given controls $u^{(p)}(t)$, $p = 1, 2$, respectively.

In the FP framework, the pedestrians' objectives for the avoidance game are formulated as follows:

$$J_p(u^{(1)}, u^{(2)}) = \alpha \int_\Omega V(x - x_T^{(p)})\, f^{(p)}(x, T)dx + \frac{\nu}{2}\|u^{(p)}\|^2_{H^1(0,T;\mathbb{R}^2)}$$
$$+ \rho \int_\Omega f^{(1)}(x, t)\, f^{(2)}(x, t)\, dx, \qquad p = 1, 2. \tag{20}$$

Notice that we omit to write the PDFs as arguments of these (reduced) functionals since we already assume that the PDFs are well-defined functions of the controls. In the functional (20), the first term models the desire of the pedestrian to reach a final position at time T; this benefit term is also considered in [58]. The second term represents the H^1-cost of the control. Notice that, by embedding, we obtain control functions that are continuous. The third term penalizes collision since in this situation the two PDFs would 'overlap' and the integral would take a large value.

Now, let $U^{(p)}$ be the space of admissible controls, $u^{(p)} \in U^{(p)}$. Then a Nash equilibrium (NE) is defined as a pair of control strategies $(\bar{u}^{(1)}, \bar{u}^{(2)}) \in U^{(1)} \times U^{(2)}$ such that the following holds

$$(\bar{u}^{(1)}, \bar{u}^{(2)}) = arg \min_{u^{(1)} \in U^{(1)}} J_1(u^{(1)}, \bar{u}^{(2)}) \tag{21}$$
$$= arg \min_{u^{(2)} \in U^{(2)}} J_2(\bar{u}^{(1)}, u^{(2)}). \tag{22}$$

Notice that reduced functional objectives are non-convex and this fact prevents the application Nash's theorem [71] to prove existence of a Nash equilibrium. However, by exploiting the structure of the present problem a proof of existence of a NE is given in [79] along the following line.

Let us define

$$G_p(u^{(p)}) = \alpha \int_\Omega V(x - x_T^{(p)}) f^{(p)}(x, T)dx + \frac{\nu}{2}\|u^{(p)}\|^2_{H^1(0,T;\mathbb{R}^2)}.$$

Thus, we can write the pedestrians' objectives as follows:

$$J_p(u^{(1)}, u^{(2)}) = G_p(u^{(p)}) + W(u^{(1)}, u^{(2)}). \tag{23}$$

Therefore we have a separable game. Next, we define the following composite cost functional:

$$\hat{\mathcal{J}}(u^{(1)}, u^{(2)}) = G_1(u^{(1)}) + G_2(u^{(2)}) + W(u^{(1)}, u^{(2)}), \tag{24}$$

and consider the optimal control problem

$$\min \hat{\mathcal{J}}(u^{(1)}, u^{(2)}), \qquad (u^{(1)}, u^{(2)}) \in U^{(1)} \times U^{(2)}.$$

In [79], the following theorem is proved stating that a solution to this optimal control problem is a Nash equilibrium of our game.

Theorem 1 *Assume that $\hat{\mathcal{J}}$ has a minimum $\bar{u} = (\bar{u}^{(1)}, \bar{u}^{(2)})$. Then $(\bar{u}^{(1)}, \bar{u}^{(2)})$ is a Nash equilibrium of the game* (21)–(22).

This theorem states that the existence of a minimum of $\hat{\mathcal{J}}$ is a sufficient condition for a Nash equilibrium. However, this condition is not necessary, and there can be Nash equilibria that are not minima of $\hat{\mathcal{J}}$.

Furthermore, the result of Theorem 1 states that we can determine the NE by applying well-known tools from computational optimization to the following FP control problem:

$$\begin{aligned}
&\min \mathcal{J}(f^{(1)}, f^{(2)}, u^{(1)}, u^{(2)}) := G_1(f^{(1)}, u^{(1)}) + G_2(f^{(2)}, u^{(2)}) + W(f^{(1)}, f^{(2)}) \\
&\partial_t f^{(1)}(x,t) - \tfrac{\sigma^2}{2} \Delta f^{(1)}(x,t) + \nabla \cdot \left(b^{(1)}(x,t,u^{(1)}(t))\, f^{(1)}(x,t)\right) = 0 \\
&\partial_t f^{(2)}(x,t) - \tfrac{\sigma^2}{2} \Delta f^{(2)}(x,t) + \nabla \cdot \left(b^{(2)}(x,t,u^{(2)}(t))\, f^{(2)}(x,t)\right) = 0,
\end{aligned}$$

with initial conditions given by the distributions of the initial positions of the pedestrians, $f^{(1)}(x,0) = f_0^{(1)}(x)$ and $f^{(2)}(x,0) = f_0^{(2)}(x)$, and flux-zero boundary conditions. We refer to [79] for the proof of existences of a solution to this FP optimal control problem and for its characterization by a FP optimality system.

In [79], the validity of the FP Nash game approach to model avoidance is successfully benchmarked with results of real experiments in the field of cognitive psychology studies involving experiments with humans [59, 73, 88]. For illustration, we report results for the experiment '1C-A3' presented in [88].

We set the initial position density of the pth pedestrian as the following normalized Gaussian:

$$f_0^{(p)}(x) = \hat{C} e^{-\{(x_1 - D_1^{(p)})^2 - (x_2 - D_2^{(p)})^2\}/0.5}, \qquad p = 1, 2, \tag{25}$$

where $D^{(p)} = (D_1^{(p)}, D_2^{(p)})$ represents the Cartesian coordinates of the departure point. The terminal potential for the pth pedestrian is given by

$$V(x - x_T^{(p)}) = (x - A^{(p)})^2, \qquad p = 1, 2,$$

where the arrival point $A^{(p)} = (A_1^p, A_2^p)$ represents the desired terminal position of the pth pedestrian.

In the experiment [88], two pedestrian P1 and P2 are asked to walk from given initial to final points. In the present case, P1 goes from '1 to C', and the other goes from 'A to 3' as shown in Fig. 2 (right). In our computational setting, this motion is considered in the square domain $\Omega = [-1, 8] \times [-1, 8]$ for a time interval $[0, T]$ with $T = 5$. Pedestrian P1 starts its motion from the departure point $D^{(1)} = (1, 1)$, and pedestrian P2 starts its motion from the point $D^{(2)} = (6, 1)$. The arrival position of P1 is $A^{(1)} = (6, 4)$ and for P2 is $A^{(2)} = (1, 4)$. In the numerical setting, the spatial and temporal domains are divided into 50 uniformly distributed subintervals, and we

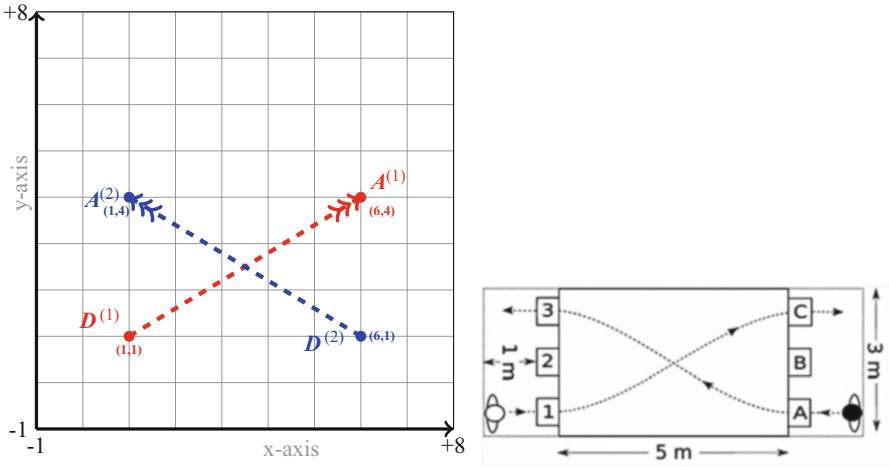

Fig. 2 Settings for the experiment '1C-A3': (left) the computational setting; (right) the experimental setting excerpt from [88]

choose $\alpha = 100$ and $\nu = 1$. The geometrical setting for the pedestrians' avoidance is shown in Fig. 2.

Solving the FP optimal control problem given above, we have the results shown in Fig. 3. Figure 3a and b depict the zoomed-in plots of the mean of the resulting PDFs obtained choosing $\rho = 0.01$ and $\rho = 200$, respectively. That is, the case of almost no penalization of collision and the case of large penalization. We notice that for $\rho = 0.01$, the two pedestrians collide at time $t = 2.5$, as denoted by the black dot. In the case of $\rho = 200$, the pedestrians P1 and P2 avoid each other as is shown by their positions at time $t = 2.5$ with a black dot. In fact, we see that the pedestrian P1 apparently slows down, while P2 accelerates; see the discussion in [59]. However, it is clear that this is one possible NE solution, since by symmetry of the experimental setting, we could exchange P1 with P2 and obtain another NE point, which can be obtained with the same numerical scheme using a different initialisation. Notice that this multitude of NE solutions reflects the output of real experiments and our own experience.

4 The Motion of Many Pedestrians

In the literature, the modeling of the motion of many pedestrians usually refers to the case of a crowd, a large group of people that are close to each other. (We may refer to swarms in the case of animals and robots.) In this case, it is the emergence of a collective behaviour and its control that are subject of mathematical investigation. With the assumption of a large number of individuals, the indeterminacy in the individual motion can be considered as a local fluctuation of a mean behaviour.

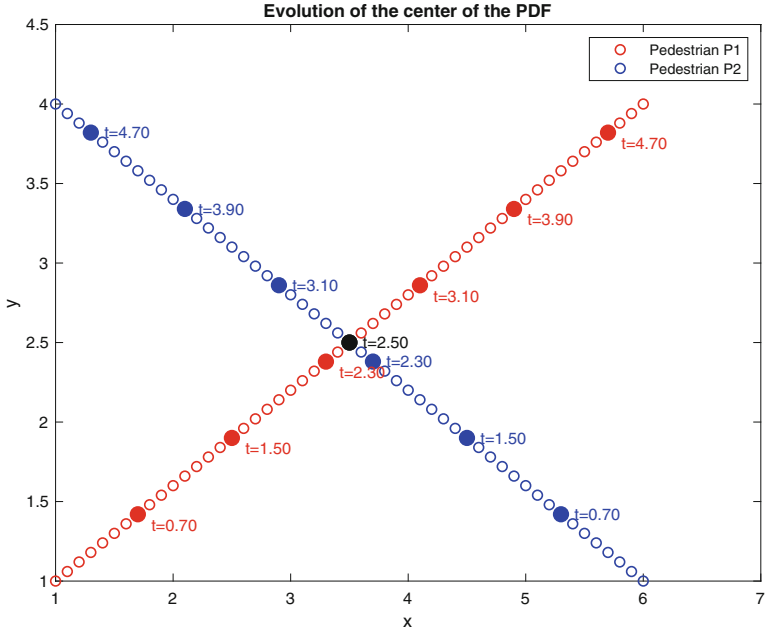

(a)

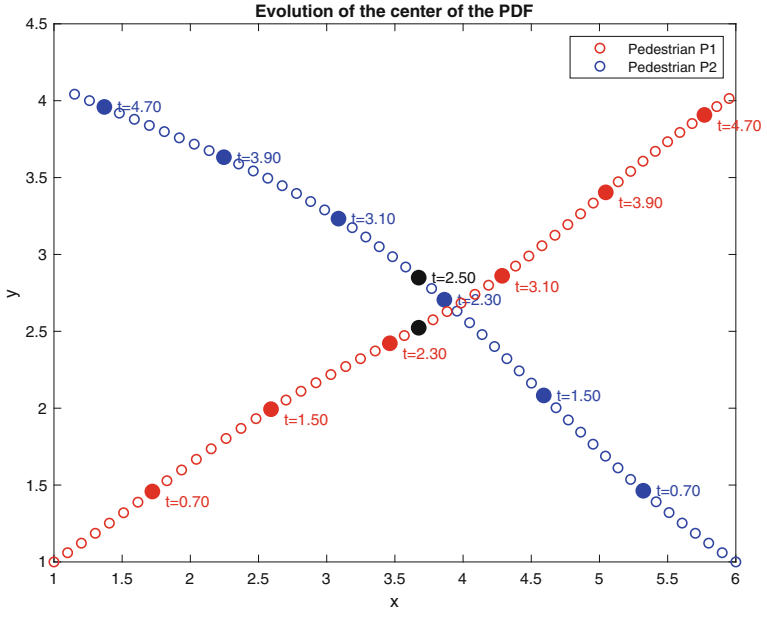

(b)

Fig. 3 Zoomed-in plots of the mean positions with $\rho = 0.01$ (**a**) and $\rho = 200$ (**b**)

Thus, a reliable description of crowd motion becomes appropriate at mesoscopic and macroscopic scales [3]. On the other hand, from the application point of view, we would like to determine efficient crowd management tools that are required, for example, in emergency evacuation procedures [11, 74], and in this context, one can identify at least three different mechanisms: the control via leadership, the concept of sparse control, and the distributed action. However, the distributed action of a controller can certainly be implemented in a swarm of robots or satellites, but it is in contrast with the concept of crisis, e.g., panic situation. For this purpose, the control exerted on a small group of agents having leadership on the crowd seems more realistic. Recently, the leadership-based controllability and optimal control of (microscopic) multi-agent systems has been proposed in [90] for a first-order model, in [18] for a second-order model, and in [91] for evolving social networks. At the mesoscopic scale, the control by leadership has been investigated in, e.g., [33].

On the other hand, in the framework of sparse controls acting on a microscopic model, in [27, 28] an efficient control mechanism is proposed that is acting only on the smallest number of agents, thus introducing sparse controllability problems. The sparse controllability of a kinetic alignment model is considered in, e.g., [76].

Now, in this general framework, we can put the FP equation into the class of mesoscopic models together with other continuity equations like the Liouville equation and the Boltzmann equation. However, the lifting of a (coupled) microscopic model at the level of a density representation is viable under appropriate assumptions. The easiest of these assumptions is to focus on a unique representative agent of the system and interpret the action of the other agents on it as a background noise. This is our working assumption in the previous two sections, which actually requires to see the chosen pedestrian as being much more 'massive' than the others. Notice that a similar assumption appears in the derivation of the FP equation starting from the Boltzmann equation [69]. In fact, Boltzmann-like kinetic models are considered in many works concerning the modeling of collective motion of pedestrians; see, e.g., [1, 50, 54, 56]. On the other hand, it appears that an appropriate working assumption to model crowd motion is to focus on mean-field theory.

Now, we illustrate the mean-field approach in the case where the motion of pedestrians in the crowd is modeled by a SDE similar to (1). For this purpose, consider a system of N identical pedestrians whose motion is given as follows:

$$dX^i(t) = \frac{1}{N}\sum_{j=1}^{N} b(X^i(t), X^j(t))\,dt + \frac{1}{N}\sum_{j=1}^{N} \sigma(X^i(t), X^j(t))\,dW^i(t) \tag{26}$$

$$X^i(0) = X_0^i, \qquad i = 1, \ldots, N, \tag{27}$$

where $X^i(t) \in \mathbb{R}^d$ denotes the position of the ith pedestrian. Notice that the structure of (26) assumes that in the drift and dispersion coefficients an average of 'interactions' appears.

Next, assume that the velocity field of the ith pedestrian is made of an 'external' field function u and a component that results from the presence of all other pedestrians. We have

$$b(x^i, x^j) = u(x^i, t) + \theta\,(x^i - x^j),$$

where θ is a function of the distance between any two pedestrians.

Now, in correspondence to (26)–(27), the following dN-dimensional FP equation results

$$\partial_t f_N - \frac{1}{2}\sum_{i=1}^{N} \Delta_i \left[\left(\frac{1}{N}\sum_{j=1}^{N} \sigma(x^i, x^j) \right)^2 f_N \right] + \sum_{i=1}^{N} \nabla_i \cdot \left[\left(\frac{1}{N}\sum_{j=1}^{N} b(x^i, x^j) \right) f_N \right] = 0 \tag{28}$$

where $f_N = f_N(x,t)$, $x = (x^1, \ldots, x^N)$, $x^i \in \mathbb{R}^d$. We denote with Δ_i, resp. ∇_i, the $\mathbb{R}^d$ Laplacian, resp. the $\mathbb{R}^d$ gradient for the variable coordinates of the ith pedestrian. With (28), one can formulate an evolution problem specifying the initial PDF $f_N(x,0) = f_{0N}(x)$, with $f_{0N}(x) \geq 0$ with $\int_{\mathbb{R}^{dN}} f_{0N}(x)\,dx = 1$.

Nevertheless, the high dimensionality of (28) makes its solution practically impossible, and it is only thanks to the mean-field strategy [20, 38, 60] that we can circumvent this problem by considering (26)–(27) in the limit of $N \to \infty$ such that

$$\frac{1}{N}\sum_{j=1}^{N} b(x^i, x^j) \to \mathbb{E}(b(x^i, \cdot)), \tag{29}$$

and similarly for σ we have $\frac{1}{N}\sum_{j=1}^{N} \sigma(x^i, x^j) \to \mathbb{E}(\sigma(x^i, \cdot))$. If these limits hold, then the stochastic differential equations (26) appear as decoupled and equivalent to each other in the sense that any of the X^i represents the same pedestrian.

Notice that the validity of (29) has been rigorously discussed in, e.g., [19, 38, 85]. In particular, the empirical measure process $X_N(A,t) := \frac{1}{N}\sum_{j=1}^{N} \mathbb{1}_A(X_t^j)$ where A denotes any Borel set of $\mathbb{R}^d$ and $\mathbb{1}_A(\cdot)$ is the indicator function of A, is proved to converge to a unique deterministic measure $\mu_t(A)$.

We remark that the above results are valid under the condition of indistinguishability, which means that the probability law above is invariant under exchange of particles. This is possible if the initial conditions X_0^i are independently and identically distributed and all the drift and dispersion functions are the same and symmetric under exchange of indices; see, e.g., [85].

Based on these considerations, in the limit $N \to \infty$, we obtain the following model of motion, where X denotes any of the X^i. We have

$$dX(t) = \mathbb{E}_{\mu_t}\left[b(X(t), \cdot)\right] dt + \mathbb{E}_{\mu_t}\left[\sigma(X(t), \cdot)\right] dW(t) \tag{30}$$

$$X(0) = X_0. \tag{31}$$

As in [19] and under suitable conditions on b and σ, the measure μ becomes absolutely continuous and we can write $\mu_t(dx) = f(\cdot, t)\, dx$, where f is the time-dependent PDF of (30)–(31), which is governed by the following mean-field FP model:

$$\partial_t f(x,t) - \frac{1}{2}\Delta\left[f(x,t)\left(\int_{\mathbb{R}^d}\sigma(x,y)f(y,t)dy\right)^2\right] + \nabla\cdot\left[f(x,t)\left(\int_{\mathbb{R}^d} b(x,y)f(y,t)dy\right)\right] = 0,$$

where Δ, resp. ∇, represent the Laplacian, resp. the gradient, in $\mathbb{R}^d$.

We see that the mean-field strategy allows to effectively model very large (ideally infinite) crowds and makes possible to reconsider the control and games approaches discussed in the previous sections also in this context. In this context, we would like to mention the framework of mean-field games [65] and related control schemes [7, 13], which have been already successfully applied to model pedestrian motion in particular situation; see [25, 63] and the references therein.

Notice that the mean-field strategy applies to many different models of motion [2, 29, 35]; see also the review [3, 10]. On the other hand, similar nonlinear (and nonlocal) models of swarms, called aggregation models, are also applied to model collective motion [14, 15, 40].

5 Closing Remarks

In this review, we have illustrated the FP control framework and related techniques to model the motion of pedestrians in some particular situation. In doing this, we have bypassed all issues concerning the numerical solution of the resulting problems. However, a few comments on this topic are in order to complete this review. Thus, we would like to point out that an appropriate numerical approximation of any continuity equation should guarantee, together with the necessary property of stability and accuracy, the non-negativity of the solution (the density) and conservation of the total mass or probability. For this purpose, the work in [68] proves these properties for the Chang-Cooper (CC) scheme [31], which is a second-order accurate finite volume scheme for the linear (parabolic) FP equation; see also [24, 64, 78, 80]. Further, in [77] similar properties are discussed for a scheme applied to the Liouville equation due to Sanders [81]. For a review of numerical methods for solving aggregation-diffusion equations see [30].

On the other hand, from the point of view of numerical optimization, we are concerned with the accurate determination of the optimization gradient and its use in gradient-based optimization techniques [17], and for the former problem, a convenient strategy is the so-called discretize-before-optimize method. This approach plays a central role in some works on FP control problems [5, 78], and in

the optimal control of multi-agent systems; see, e.g., [18, 90, 91] and the references therein. However, much less is available on the numerical analysis of nonlinear optimal control problems related to crowds and mean-field models.

Acknowledgments I would like to thank very much Mario Annunziato, Abdou Habbal, and Souvik Roy for our successful collaboration on the topics of this paper. I am also very grateful to the many Colleagues that have supported this work with fruitful discussions.

References

1. G. Albi, L. Pareschi, Binary interaction algorithms for the simulation of flocking and swarming dynamics. Multiscale Model. Simul. **11**, 1–29 (2013)
2. G. Albi, M. Fornasier, D. Kalise, A Boltzmann approach to mean-field sparse feedback control. IFAC-PapersOnLine **50**, 2898–2903 (2017)
3. G. Albi, N. Bellomo, L. Fermo, S.-Y. Ha, J. Kim, L. Pareschi, D. Poyato, J. Soler, Traffic, crowds, and swarms. From kinetic theory and multiscale methods to applications and research perspectives. Math. Models Methods Appl. Sci. **29**, 1901–2005 (2019)
4. M. Annunziato, A. Borzì, Optimal control of probability density functions of stochastic processes. Math. Model. Anal. **15**, 393–407 (2010)
5. M. Annunziato, A. Borzì, A Fokker-Planck control framework for multidimensional stochastic processes. J. Comput. Appl. Math. **237**, 487–507 (2013)
6. M. Annunziato, A. Borzì, Optimal control of a class of piecewise deterministic processes. Eur. J. Appl. Math. **25**, 1–25 (2014)
7. M. Annunziato, A. Borzì, A Fokker–Planck control framework for stochastic systems. EMS Surv. Math. Sci. **5**, 65–98 (2018)
8. M. Annunziato, A. Borzì, F. Nobile, R. Tempone, On the connection between the Hamilton-Jacobi-Bellman and the Fokker-Planck control frameworks. Appl. Math. **5**, 2476–2484 (2014)
9. J. Bartsch, A. Borzì, F. Fanelli, S. Roy, A theoretical investigation of Brockett's ensemble optimal control problems. Calc. Var. Partial Differ. Equ. **58**(5), 162 (2019). https://doi.org/10.1007/s00526-019-1604-2
10. N. Bellomo, C. Dogbe, On the modeling of traffic and crowds: a survey of models, speculations, and perspectives. SIAM Rev. **53**, 409–463 (2011)
11. N. Bellomo, D. Clarke, L. Gibelli, P. Townsend, B.J. Vreugdenhil, Human behaviours in evacuation crowd dynamics: from modelling to big data toward crisis management. Phys. Life Rev. **18**, 55–65 (2016)
12. N. Bellomo, L. Gibelli, N. Outada, On the interplay between behavioral dynamics and social interactions in human crowds. Kinet. Relat. Models **12**, 397–409 (2019)
13. A. Bensoussan, J. Frehse, P. Yam, *Mean Field Games and Mean Field Type Control Theory* (Springer, Berlin, 2013)
14. A.J. Bernoff, C.M. Topaz, Nonlocal aggregation models: a primer of swarm equilibria. SIAM Rev. **55**, 709–747 (2013)
15. A.L. Bertozzi, D. Slepčev, Existence and uniqueness of solutions to an aggregation equation with degenerate diffusion. Commun. Pure Appl. Anal. **9**, 1617–1637 (2010)
16. A.L. Bertozzi, J. Rosado, M.B. Short, L. Wang, Contagion shocks in one dimension. J. Stat. Phys. **158**, 647–664 (2015)
17. A. Borzì, V. Schulz, *Computational Optimization of Systems Governed by Partial Differential Equations*. SIAM Book Series on Computational Science and Engineering 08 (SIAM, Philadelphia, 2012)
18. A. Borzì, S. Wongkaew, Modeling and control through leadership of a refined flocking system. Math. Models Methods Appl. Sci. **25**, 255–282 (2015)

19. M. Bossy, D. Talay, A stochastic particle method for the McKean-Vlasov and the Burgers equation. Math. Comput. **66**, 157–192 (1997)
20. J.L. Boudec, D. McDonald, J. Mundinger, A generic mean field convergence result for systems of interacting objects, in *Fourth International Conference on the Quantitative Evaluation of Systems (QEST 2007)*, Edinburgh (2007), pp. 3–18
21. R.W. Brockett, Optimal control of the Liouville equation, in *Proceedings of the International Conference on Complex Geometry and Related Fields*. AMS/IP Studies in Advanced Mathematics, vol. 39 (American Mathematical Society, Providence, 2007), pp. 23–35
22. R.W. Brockett, Notes on the control of the Liouville equation, in *Control of Partial Differential Equations* (Springer, Berlin, 2012), pp. 101–129
23. L. Bruno, F. Venuti, Crowd-structure interaction in footbridges: modelling, application to a real case-study and sensitivity analyses. J. Sound Vib. **323**, 475–493 (2009)
24. C. Buet, S. Cordier, P. Degond, M. Lemou, Fast algorithms for numerical, conservative, and entropy approximations of the Fokker–Planck–Landau equation. J. Comput. Phys. **133**, 310–322 (1997)
25. M. Burger, M. Di Francesco, P.A. Markowich, M.-T. Wolfram, Mean field games with nonlinear mobilities in pedestrian dynamics. Discrete Contin. Dynam. Syst. B **19**, 1311–1333 (2014)
26. D. Canter (ed.), *Fires and Human Behaviour*, 2nd edn. (David Fulton Publishers, London, 1990)
27. M. Caponigro, M. Fornasier, B. Piccoli, E. Trélat, Sparse stabilization and optimal control of the Cucker-Smale model. Math. Control Relat. Fields **3**, 447–466 (2013)
28. M. Caponigro, M. Fornasier, B. Piccoli, E. Trélat, Sparse stabilization and control of alignment models. Math. Models Methods Appl. Sci. **25**, 521–564 (2015)
29. J.A. Carrillo, S. Martin, M.-T. Wolfram, An improved version of the Hughes model for pedestrian flow. Math. Models Methods Appl. Sci. **26**, 671–697 (2016)
30. J.A. Carrillo, K. Craig, Y. Yao, Aggregation-diffusion equations: dynamics, asymptotics, and singular limits, in *Active Particles, Volume 2. Modeling and Simulation in Science, Engineering and Technology*, ed. by N. Bellomo, P. Degond, E. Tadmor (Birkhäuser, Cham, 2019)
31. J.S. Chang, G. Cooper, A practical difference scheme for Fokker-Planck equations. J. Comput. Phys. **6**, 1–16 (1970)
32. A. Colombi, M. Scianna, Modelling human perception processes in pedestrian dynamics: a hybrid approach. R. Soc. Open Sci. **4**, 160561 (2017)
33. R.M. Colombo, N. Pogodaev, Confinement strategies in a model for the interaction between individuals and a continuum. SIAM J. Appl. Dynam. Syst. **11**, 741–770 (2012)
34. R.M. Colombo, P. Goatin, G. Maternini, M.D. Rosini, Macroscopic models for pedestrian flows, in *Big Events and Transport: The Transportation Requirements for the Management of Large Scale Events* (IUAV-TTL Research Unit, 2010), pp. 11–22
35. R.M. Colombo, M. Garavello, M. Lécureux-Mercier, A class of non-local models for pedestrian traffic. Math. Models Methods Appl. Sci. **22**, 1150023 (2012)
36. E. Cristiani, B. Piccoli, A. Tosin, *Multiscale Modeling of Pedestrian Dynamics* (Springer, Berlin, 2014)
37. F. Cucker, E. Mordecki, Flocking in noisy environments. J. Math. Pures Appl. **89**, 278–296 (2008)
38. D.A. Dawson, Critical dynamics and fluctuations for a mean-field model of cooperative behavior. J. Stat. Phys. **31**, 29–85 (1983)
39. A. Deutsch, G. Theraulaz, T. Vicsek, Collective motion in biological systems. Interface Focus **2**, 689–692 (2012)
40. L. Edelstein-Keshet, Mathematical models of swarming and social aggregation, in *Proceedings of the 2001 International Symposium on Nonlinear Theory and Its Applications (NOLTA 2001)*, Miyagi, Oct 28–Nov 1, 2001
41. A. Festa, M.-T. Wolfram, Collision avoidance in pedestrian dynamics, in *Decision and Control (CDC), 2015 IEEE 54th Annual Conference* (IEEE, Piscataway, 2015)

42. A. Fleig, L. Grüne, L^2-tracking of Gaussian distributions via model predictive control for the Fokker-Planck equation. Vietnam J. Math. **46**, 915–948 (2018)
43. A. Fleig, R. Guglielmi, Optimal control of the Fokker–Planck equation with space-dependent controls. J. Optim. Theory Appl. **174**, 408–427 (2017)
44. W. Fleming, M. Soner, *Controlled Markov Processes and Viscosity Solutions* (Springer, Berlin, 2006)
45. H. Frantzich, Study of movement on stairs during evacuation using video analysing techniques. Technical report, Department of Fire Safety Engineering, Lund Institute of Technology, Lund University (1996)
46. J. Gautrais, F. Ginelli, R. Fournier, S. Blanco, M. Soria, H. Chateé, G. Theraulaz, Deciphering interactions in moving animal groups. PLoS Comput. Biol. **8**, e1002 (2012)
47. B. Gaviraghi, M. Annunziato, A. Borzì, Analysis of splitting methods for solving a partial-integro differential Fokker-Planck equation. Appl. Math. Comput. **294**, 1–17 (2016)
48. B. Gaviraghi, A. Schindele, M. Annunziato, A. Borzì, On optimal sparse-control problems governed by jump-diffusion processes. Appl. Math. **7**, 1978–2004 (2016)
49. P. Goatin, M. Mimault, A mixed system modeling two-directional pedestrian flows. Math. Biosci. Eng. **12**, 375–392 (2015)
50. S. Göttlich, A. Klar, E. Ragavendar, S. Tiwari, Particle methods for pedestrian flow models: from microscopic to non-local continuum models. Math. Models Methods Appl. Sci. **24**, 2503 (2014)
51. L. Grüne, J. Pannek, *Nonlinear Model Predictive Control, Theory and Algorithms* (Springer, Berlin, 2011)
52. B. Hankin, R. Wright, Passenger flow in subways. Oper. Res. Soc. **9**, 81–88 (1958)
53. D.A. Helbing, A mathematical model for the behavior of pedestrians. Behav. Sci. **36**, 298–310 (1991)
54. D.A. Helbing, Fluid dynamic model for the movement of pedestrians. Complex Syst. **6**, 391–415 (1992)
55. L.F. Henderson, On the fluid mechanics of human crowd motion. Transp. Res. **8**, 509–515 (1974)
56. M. Herty, L. Pareschi, Fokker-Planck asymptotics for traffic flow models. Kinet. Relat. Models **3**, 165–179 (2010)
57. S. Hoogendoorn, P.H.L. Bovy, Simulation of pedestrian flows by optimal control and differential games. Optim. Control Appl. Methods **24**, 153–172 (2003)
58. S. Hoogendorn, P.H.L. Bovy, Pedestrian route choice and activity scheduling theory and models. Transp. Res. B **28**, 169–190 (2004)
59. M. Huber, Y.H. Su, M. Krüger, K. Faschian, S. Glasauer, J. Hermsdörfer, Adjustments of speed and path when avoiding collisions with another pedestrian. PLoS One **9**, e89589 (2014)
60. L.P. Kadanoff, More is the same; phase transitions and mean field theories. J. Stat. Phys. **137**, 777–797 (2009)
61. H. Klüpfel, T. Meyer-König, Simulation of the evacuation of a football stadium, in *Pedestrian and Evacuation Dynamics* (Springer, Berlin, 2002), pp. 423–428
62. H. Klüpfel, M. Schreckenberg, T. Meyer-König, Models for crowd movement and egress simulation, in *Traffic and Granular Flows* (Springer, Berlin, 2003), pp. 357–372
63. A. Lachapelle, M.-T. Wolfram, On a mean field game approach modeling congestion and aversion in pedestrian crowds. Transp. Res. B **45**, 1572–1589 (2011)
64. E.W. Larsen, C.D. Levermore, G.C. Pomraning, J.G. Sanderson, Discretization methods for one-dimensional Fokker-Planck operators. J. Comput. Phys. **61**, 359–390 (1985)
65. J.M. Lasry, P.L. Lions, Mean field games. Jpn. J. Math. **2**, 229–260 (2007)
66. J.L. Lions, *Optimal Control of Systems Governed by Partial Differential Equations* (Springer, Berlin, 1971)
67. A.J. Mayne, Some further results in the theory of pedestrians and road traffic. Biometrika **41**, 375–389 (1954)
68. M. Mohammadi, A. Borzì, Analysis of the Chang-Cooper discretization scheme for a class of Fokker-Planck equations. J. Numer. Math. **23**, 271–288 (2015)

69. D. Montgomery, Brownian motion from Boltzmann's equation. Phys. Fluids **14**, 2088–2090 (1971)
70. D. Morale, V. Capasso, K. Oelschlaeger, An interacting particle system modelling aggregation behavior: from individuals to populations. J. Math. Biol. **50**, 49–66 (2005)
71. J. Nash, Non-cooperative games. Ann. Math. **54**, 286–295 (1951)
72. G. Naldi, L. Pareschi, G. Toscani (eds.), *Mathematical Modeling of Collective Behavior in Socio-Economic and Life Sciences* (Springer Science & Business Media, Berlin, 2010)
73. A.H. Olivier, A. Marin, A. Crétual, J. Pettré, Minimal predicted distance: a common metric for collision avoidance during pairwise interactions between walkers. Gait Posture **36**, 399–404 (2012)
74. M. Pelé, C. Bellut, E. Debergue, C. Gauvin, A. Jeanneret, T. Leclere, L. Nicolas, F. Pontier, D. Zausa, C. Sueur, Cultural influence of social information use in pedestrian road-crossing behaviours. R. Soc. Open Sci. **4**, 160739 (2017)
75. B. Piccoli, A. Tosin, Time-evolving measures and macroscopic modeling of pedestrian flow. Arch. Ration. Mech. Anal. **199**, 707–738 (2011)
76. B. Piccoli, F. Rossi, E. Trélat, Control to flocking of the kinetic Cucker-Smale model. SIAM J. Math. Anal. **47**, 4685–4719 (2015)
77. S. Roy, A. Borzì, Numerical investigation of a class of Liouville control problems. J. Sci. Comput. **73**, 178–202 (2017)
78. S. Roy, M. Annunziato, A. Borzì, A Fokker-Planck feedback control-constrained approach for modeling crowd motion. J. Comput. Theoret. Transp. **45**, 442–458 (2016)
79. S. Roy, A. Borzì, A. Habbal, Pedestrian motion modelled by Fokker-Planck Nash games. R. Soc. Open Sci. **4**, 170648 (2017)
80. S. Roy, M. Annunziato, A. Borzì, C. Klingenberg, A Fokker-Planck approach to control collective motion. Comput. Optim. Appl. **69**, 423–459 (2018)
81. R. Sanders, A third order accurate variation nonexpansive difference scheme for single nonlinear conservation law. Math. Comput. **51**, 535–558 (1988)
82. Z. Schuss, *Theory and Applications of Stochastic Processes: An Analytical Approach* (Springer, Berlin, 2010)
83. N. Sepúlveda, L. Petitjean, O. Cochet, E. Grasland-Mongrain, P. Silberzan, V. Hakim, Collective cell motion in an epithelial sheet can be quantitatively described by a stochastic interacting particle model. PLoS Comput. Biol. **9**, e1002944 (2013)
84. A. Strandburg-Peshkin, D.R. Farine, I.D. Couzin, M.C. Crofoot, Shared decision-making drives collective movement in wild baboons. Science **348**, 1358–1361 (2015)
85. A.-S. Sznitman, Topics in propagation of chaos, in *Ecole d'Eté de Probabilités de Saint-Flour XIX - 1989*, vol. 1464, ed. by P.L. Hennequin. Lecture Notes in Mathematics (Springer, Berlin, 1991), pp. 165–251
86. E. Tadmor, C. Tan, Critical thresholds in flocking hydrodynamics with nonlocal alignment. Proc. R. Soc. A **372**, 20130401 (2014)
87. F. Tröltzsch, *Optimal Control of Partial Differential Equations* (AMS, Providence, 2010)
88. A. Turnwald, D. Althoff, D. Wollherr, M. Buss, Understanding human avoidance behavior: interaction-aware decision making based on game theory. Int. J. Soc. Rob. **8**, 331–351 (2016)
89. L. Wang, M.B. Short, A.L. Bertozzi, Efficient numerical methods for multiscale crowd dynamics with emotional contagion. Math. Models Methods Appl. Sci. **27**, 205–230 (2017)
90. S. Wongkaew, M. Caponigro, A. Borzì, On the control through leadership of the Hegselmann–Krause opinion formation model. Math. Models Methods Appl. Sci. **25**, 565–585 (2015)
91. S. Wongkaew, M. Caponigro, K. Kułakowski, A. Borzì, On the control of the Heider balance model. Eur. Phys. J. Spec. Top. **224**, 3325–3342 (2015)
92. A. Zienkiewicz, D.A.W. Barton, M. Porfiri, M. di Bernardo, Data-driven stochastic modelling of zebrafish locomotion. J. Math. Biol. **71**, 1081–1105 (2015)

Recent Developments in Controlled Crowd Dynamics

M. K. Banda, M. Herty, and T. Trimborn

Abstract We survey recent results on controlled particle systems. The control aspect introduces new challenges in the discussion of properties and suitable mean field limits. Some of the aspects are highlighted in a detailed discussion of a particular controlled particle dynamics. The applied techniques are shown on this simple problem to illustrate the basic methods. Computational results confirming the theoretical findings are presented and further particle models are discussed.

1 Introduction

Large-scale interacting particle systems have recently generated interest in the description of phenomena beyond classical statistical mechanics and we refer to the recent book on active particles [11] and furthermore to [36, 67] for some examples and further references. A major difference to mathematical descriptions in continuum and statistical mechanics is the fact that particles are no longer passively interacting. This enables analysis of new pattern formation mechanisms, but also allows to introduce control actions within the interacting particle system. Among the examples of controlled particle systems are economic models for price formation, wealth accumulation, trading or formation of consensus behavior. We refer to the references [3, 8, 12, 21, 23, 24, 44, 67, 74] as well as the references therein for some examples. Typically, control actions might be applied to drive systems towards a desired state using either an open loop [6, 16, 53, 62], a closed loop [1–3, 3, 5, 7, 25, 38, 55], or a competitive game setup [13, 17, 22, 24, 28–30, 39–

M. K. Banda
Department of Mathematics and Applied Mathematics, University of Pretoria, Hatfield, South Africa
e-mail: mapundi.banda@up.ac.za

M. Herty (✉) · T. Trimborn
IGPM, RWTH Aachen, Aachen, Germany
e-mail: herty@igpm.rwth-aachen.de; herty@mathc.rwth-aachen.de; trimborn@igpm.rwth-aachen.de

L. Gibelli (ed.), *Crowd Dynamics, Volume 2*, Modeling and Simulation in Science, Engineering and Technology, https://doi.org/10.1007/978-3-030-50450-2_7

41, 50, 57–59, 63]. Those directions have been explored recently for interacting particle systems described by ordinary differential equations with the question of control actions prevailing in the mean field limit of infinitely many particles. Those limits have been well-explored in the context of classical statistical mechanics, see, for example, [33, 34, 70]. The limit allows derivations of time-continuous descriptions of qualitative properties independent of the number of particles. In the case of finitely many interacting agents subject to control, the control problem can be solved using Pontryagin's maximum principle, dynamic programming, or Hamilton–Jacobi Bellman equations. Those techniques are well-established in the context of ordinary differential equations but pose, in view of the desired mean field limit, interesting and challenging analytical and numerical problems.

The major obstacle, for example, has been the fact that the size of the system of associated Hamilton-Jacobi Bellman equations is proportional to the number of particles. So far, different approaches have been explored to address possible issues mostly based on an approximation of the control, for example, by a restriction to short (instantaneous) time horizon controls [3, 26, 54], or by implementing the control on a binary interaction scale [2] or by solving approximate Hamilton–Jacobi equations [7]. Those approaches typically aim to derive a (suboptimal) closed loop control. On the level of open loop control problems only few and mostly theoretical results could be achieved, for example, in the game theoretic setting [63], using Riccati control [55] or using a mean field approach for both adjoint and primal variables [6, 47, 53].

Another aspect in dealing with the open loop control problem is a suitable notion of differentiability [15, 27, 53, 56] that leads to consistent optimality systems for both the large-scale particle system and the mean field optimal control problem. Here, choices regarding differentiability in the sense of Frechet as well as differentiability in metric spaces with respect to Wasserstein distance are possible and an analysis of properties and possible connections is given in [15, Section 2] or [56, Appendix], among many examples.

Suitable numerical methods for the full control problem on the mean field level are still sparse due to the complexity of solving successively forward and backward partial differential equations. Besides the mean field limit, the hydrodynamic limit of particle systems is of interest for a qualitative study of long-term behavior of solutions. For controlled particle systems, this direction is currently largely unexplored.

In this chapter, we would like to illustrate the main steps undertaken in controlled particle systems by presenting, on a simplistic particle model, challenges and approaches in mean field limits as well as on the hydrodynamic limit. The focus will be on the control action and, therefore, we present results in a simple linear setting in Sect. 2. This setup has also been used to illustrate basic properties of mean field games [27] and served as a guiding example for many previously presented techniques [56]. The linear setting enables use of a closed loop strategy based on

the Riccati equation on the level of finitely many agents. It is also well-known that in the case of linear–quadratic open loop control problems, the Riccati control is optimal. Besides the investigation of the interplay between the Riccati control and the mean field limit, we also discuss here the corresponding hydrodynamic limit in Sect. 2.3. The analytical findings are illustrated by numerical simulations of the closed loop control system in Sect. 3. Extensions to a nonlinear setting and other perspectives are discussed in Sect. 4.

2 Multiscale Riccati Control for Linear Particle Systems

The main purpose of this section is to illustrate control concepts and mean field limits. We, therefore, restrict ourselves to a simplistic setting for interacting particle systems. Consider $i = 1, \dots, N$ particles with a state $(x_i(t), v_i(t)) \in \mathbb{R}^2$ driven by the dynamics

$$\frac{d}{dt}x_i = v_i, \quad \frac{d}{dt}v_i = q_i^*, \quad (x_i, v_i)(0) = (x_{i,0}, v_{i,0}) \tag{1}$$

for initial data $(x_{i,0}, v_{i,0})$ and where each particle is subject to a control $q_i^* = q_i^*(t)$ modeling an individual strategy. The control is chosen in order to minimize a joint objective

$$\boldsymbol{q}^* := \arg\min_{q \in \mathbb{R}^N} \int_0^T \frac{1}{N} \sum_{i=1}^N \left(\frac{1}{2} v_i^2 + \frac{\alpha}{2} q_i^2 \right) dt, \tag{2}$$

where $\boldsymbol{q} = (q_i)_{i=1}^N$. The parameter $\alpha > 0$ is a weight to balance the cost of all controls and the desired state. The latter is chosen here to be $v_i \equiv 0$ for all particles $i = 1, \dots, N$ for simplicity. Clearly, other desired states may be considered and they may be dependent on further parameters and costs at terminal time $t = T$ may be added to problem (2). The terminal time $T > 0$ is fixed but can be replaced by $T = +\infty$ provided a suitable weight $\exp(-rt)$ is added towards the cost with discount $r > 0$.

At this point it is important to note that there is a major difference in discussing the case of whether or not all particles try to minimize a joint objective or their individual objective. In the latter case the problem turns into a differential game and concepts of optimality have to be discussed. We refer to [48] for a careful discussion as well as to [13], for example, for mean field limits of games. Here, we will focus on the case of a single joint objective (2).

2.1 Closed Loop Control for Particle System

The problems (2) and (1) are linear–quadratic optimal (convex) control problems. It is well-known that in this case the unique solution $\boldsymbol{q}^*$ is given by a state feedback involving a symmetric matrix $K \in \mathbb{R}^{2N\times 2N}$ which is a solution of the (matrix) Riccati equation. In order to derive this equation, it is advantageous to introduce the following vectors and matrices:

$$w := \left((x_i)_{i=1}^N, (v_i)_{i=1}^N\right)^T \in \mathbb{R}^{2N}, \tag{3}$$

$$A := \begin{pmatrix} 0 & \mathrm{Id} \\ 0 & 0 \end{pmatrix} \in \mathbb{R}^{2N\times 2N}, \quad B := \begin{pmatrix} 0 \\ \mathrm{Id} \end{pmatrix} \in \mathbb{R}^{2N\times N}, \quad M := \begin{pmatrix} 0 & 0 \\ 0 & \mathrm{Id} \end{pmatrix} \in \mathbb{R}^{2N\times 2N}, \tag{4}$$

where $\mathrm{Id} \in \mathbb{R}^{N\times N}$ denotes the identity matrix. Solving problem (1), (2) is equivalent to solving

$$\min_{q\in\mathbb{R}^N} \int_0^T \frac{1}{2N} w^T(t) M w(t) + \frac{\alpha}{2N} q(t)^T (\mathrm{Id}) q(t)\, dt \tag{5}$$

subject to (6)

$$\frac{d}{dt} w(t) = Aw(t) + Bq(t), \quad w(0) = \left((x_{i,0})_{i=1}^N, (v_{i,0})_{i=1}^N\right)^T \tag{7}$$

which necessary optimality conditions yield the following expression for $q \in \mathbb{R}^N$

$$q(t) = -\frac{2N}{\alpha} B^T K(t) w(t), \tag{8}$$

where $K(t) = K(t)^T$ fulfills the matrix Riccati equation [69]:

$$-\frac{d}{dt} K(t) = \frac{1}{2N} M + K(t)A + A^T K(t) - \frac{2N}{\alpha} K(t) B B^T K(t), \quad K(T) = 0. \tag{9}$$

Note that in the nonlinear case a state feedback or closed loop control of the type (8) is in general impossible to obtain and gives rise to the suboptimal control strategies mentioned in the introduction.

In view of the mean field limit for $N \to \infty$ particles, it is advantageous to exploit the particular structure of the matrices A and M to obtain further information on the matrix K. We split K according to the state space as follows:

$$K = \begin{pmatrix} K_{11} & K_{12} \\ K_{21} & K_{22} \end{pmatrix},$$

with $K_{ij} \in \mathbb{R}^{N\times N}$ for $i, j = 1, 2$. Direct computation yields a simplified form of Eq. (9) as follows:

$$-\frac{d}{dt}K(t) = \frac{1}{2N}\begin{pmatrix}0 & 0\\ 0 & \mathrm{Id}\end{pmatrix} + \begin{pmatrix}0 & K_{11}\\ 0 & K_{21}\end{pmatrix} + \begin{pmatrix}0 & 0\\ K_{11} & K_{12}\end{pmatrix} - \frac{2N}{\alpha}\begin{pmatrix}K_{12}K_{21} & K_{12}K_{22}\\ K_{22}K_{21} & K_{22}K_{22}\end{pmatrix}, \tag{10}$$

or

$$-\frac{d}{dt}K_{11} = -\frac{2N}{\alpha}K_{12}K_{21}, \quad K_{11}(T) = 0, \tag{11}$$

$$-\frac{d}{dt}K_{12} = K_{11} - \frac{2N}{\alpha}K_{12}K_{22}, \quad K_{12}(T) = 0, \tag{12}$$

$$-\frac{d}{dt}K_{21} = K_{11} - \frac{2N}{\alpha}K_{22}K_{21}, \quad K_{21}(T) = 0, \tag{13}$$

$$-\frac{d}{dt}K_{22} = \frac{1}{2N}Id + K_{12} + K_{21} - \frac{2N}{\alpha}K_{22}K_{22}, \quad K_{22}(T) = 0. \tag{14}$$

This nonlinear system of ordinary differential equations has a differentiable and locally Lipschitz right-hand side. Therefore, a unique solution exists and by direct computation, we obtain the assertion of the following Lemma.

Lemma 1 *The system of ordinary differential equations* (9) *has a unique differentiable solution* $K = K(t) \in C^1(\mathbb{R}^{2N\times 2N})$ *given by*

$$K(t) = \begin{pmatrix}0 & 0\\ 0 & K_{22}(t)\end{pmatrix},$$

where $K_{22}(t)$ *is given as a solution to the equation*

$$-\frac{d}{dt}K_{22}(t) = \frac{1}{2N}\mathrm{Id} - \frac{2N}{\alpha}K_{22}(t)K_{22}(t), \quad K_{22}(T) = 0. \tag{15}$$

Again, the particular structure of Eq. (15) allows the derivation of the following result for the structure of K_{22}, that is in fact, diagonal with the same entry.

Lemma 2 *The system of ordinary differential equations* (15) *has a unique differentiable solution*

$$(K_{22}(t))_{i,i} = d(t), \text{ and } (K_{22}(t))_{i,j} = 0, \ i, j = 1, \ldots, N, \ i \neq j, \tag{16}$$

where $d(\cdot)$ *is the unique solution to the (scalar) ordinary differential equation*

$$-\frac{d}{dt}d(t) = \frac{1}{2N} - \frac{2N}{\alpha}d(t)^2, \quad d(T) = 0.$$

The proof of the Lemma follows the verification that K_{22} given by Eq. (16) is in fact a solution to Eq. (15) which is also the unique solution. The ordinary differential equation for d allows for an explicit solution given by

$$d(t) = \frac{1}{2N}\sqrt{\alpha}\tanh\left(\frac{T-t}{\sqrt{\alpha}}\right).$$

However, it is not necessary to use the explicit form in the following. Having $d(t)$ available, we obtain the (optimal) closed loop control

$$\mathbf{q}^*(t) = -\frac{2N}{\alpha}B^T K(t)w(t) = -\frac{2N}{\alpha}(0, K_{22}(t))w(t) = -\frac{2N}{\alpha}d(t)v(t). \tag{17}$$

Hence, we introduce $y(t) := Nd(t)$ that satisfies

$$-\frac{d}{dt}y(t) = \frac{1}{2} - \frac{2}{\alpha}y(t)^2, \quad y(T) = 0 \tag{18}$$

and $\mathbf{q}^*(t) = -\frac{2}{\alpha}y(t)v(t)$. Summarizing, the problem (1), (2) is solved by $\mathbf{q}^*$ which is the closed loop control. The controlled particle dynamics for $i = 1, \ldots, N$ is then given by

$$\frac{d}{dt}x_i = v_i, \ \frac{d}{dt}v_i = -\frac{2}{\alpha}y(t)v_i(t), \ -\frac{d}{dt}y(t) = \frac{1}{2} - \frac{2}{\alpha}y(t)^2, \tag{19}$$

$$\text{with limit conditions} \quad (x_i, v_i)(0) = (x_{i,0}, v_{i,0}), \ y(T) = 0. \tag{20}$$

The system (19) allows for a mean field limit in the number of agents as shown in the following paragraph.

Furthermore, we note that the decay of $v_i(t)$ towards the desired zero state can be quantified using a Lyapunov function. The following result holds true.

Lemma 3 *Consider N particles with dynamics given by Eq. (19) and arbitrary initial conditions $(x_{i,0}, v_{i,0})$ for $i = 1, \ldots, N$. Let y be the solution to (18). Then, the differentiable function*

$$L(t) := w^T(t)K(t)w(t),$$

where K is given by Eq. (9) is bounded from above as

$$L(t) \leq L(0)\exp(-r(t))$$

for $t \in [0, T]$ and the rate $r(t)$ is given by

$$r(t) = \int_0^t \frac{2y(s)}{\alpha}ds \geq 0. \tag{21}$$

Proof We observe that due to Lemma 2 $d(t) \geq 0$ for $t \in [0, T]$ and therefore $K(t)$ is positive semi-definite. Hence, $L(t) \geq 0$ for all $t \in [0, T]$. According to Lemmas 1 and 2, we have $L(t) = \sum_{i=1}^{N} v_i(t)^2 d(t) = \frac{1}{N} \sum_{i=1}^{N} v_i^2(t) y(t)$. Thus

$$\begin{aligned}\frac{d}{dt} L(t) &= \frac{1}{N} \frac{d}{dt} y(t) \sum_{i=1}^{N} v_i(t)^2 - \frac{4}{N\alpha} y^2(t) \sum_{i=1}^{N} v_i^2(t) \\ &= -\frac{1}{2} \frac{1}{N} \sum_{i=1}^{N} v_i(t)^2 + \left(\frac{2}{\alpha} - \frac{4}{\alpha} \right) y(t) L(t) \leq -\frac{2y(t)}{\alpha} L(t).\end{aligned}$$

The assertion follows by Gronwall's inequality and since $y \geq 0$ the rate is non-positive.

2.2 Mean Field Limit of Controlled Particle System

We illustrate the mean field limit of the particle system (19). For more details and a detailed discussion of the mean field limit for linear systems, we refer to [49, 60]. The following formal calculation exhibits the main idea: Denote by $\mu^N(t, \cdot) \in \mathcal{P}(\mathbb{R}^2)$ the empirical measure at time t associated with the state $(x_i(t), v_i(t))_{i=1}^N \in \mathbb{R}^{2N}$ by

$$\mu^N(t, x, v) := \frac{1}{N} \sum_{i=1}^{N} \delta(x - x_i(t)) \delta(v - v_i(t)), \tag{22}$$

where δ denotes the Dirac measure on $\mathbb{R}$ and $\mathcal{P}(\mathbb{R}^2)$ is the space of probability measures on $\mathbb{R}^2$. Let ψ be any smooth compactly supported function, i.e., $\psi(x, v) \in C_0^\infty(\mathbb{R}^2)$. In the following formal computation, we neglect the time-dependence of the corresponding functions for readability.

$$\begin{aligned}\frac{d}{dt} \int_{\mathbb{R}^2} \psi(x, v) d\mu^N(x, v) &= \frac{1}{N} \sum_{i=1}^{N} \partial_x \psi(x_i, v_i) \frac{d}{dt} x_i + \partial_v \psi(x_i, v_i) \frac{d}{dt} v_i \\ &= \frac{1}{N} \sum_{i=1}^{N} \partial_x \psi(x_i, v_i) v_i - \frac{2}{\alpha} y \partial_v \psi(x_i, v_i) v_i \\ &= \int_{\mathbb{R}^2} \partial_x \psi(x, v) v d\mu^N(x, v) - \frac{2}{\alpha} y \int_{\mathbb{R}^2} \partial_v \psi(x, v) v d\mu^N(x, v).\end{aligned}$$

Hence, the measure μ^N fulfills a partial differential equation in the sense of distributions. In the following, we will assume that the measure $d\mu(t, x, v)$ has a density $f = f(t, x, v)$, i.e., $d\mu(t, x, v) = f(t, x, v)dxdv$, then the previous equality is the weak form of the mean field equation for $(x, v) \in \mathbb{R}^2$ and $t \in [0, T]$

$$\partial_t f(t, x, v) + \partial_x (v f(t, x, v)) - \frac{2}{\alpha} y(t) \partial_v (v f(t, x, v)) = 0. \tag{23}$$

Equation (23) has to be solved subject to initial conditions

$$f(0, x, v) = f_0(x, v) \tag{24}$$

, where the initial (non-negative) probability density $f_0(x, v)$ is an approximation to the empirical measure μ_0^N associated with the initial conditions

$$\mu_0^N = \frac{1}{N} \sum_{i=1}^{N} \delta(x - x_{i,0}) \delta(v - v_{i,0}).$$

Furthermore, y fulfills, as before,

$$-\frac{d}{dt} y(t) = \frac{1}{2} - \frac{2}{\alpha} y(t)^2, \quad y(T) = 0. \tag{25}$$

In order to show that the particle dynamics converges to the mean field limit, the Wasserstein distance and Dobrushin's inequality have been used as a theoretical tool. We follow the presentation in [49] and references therein for further details. The convergence is obtained in the space of probability measures $\mathcal{P}(\mathbb{R}^2)$ using the Wasserstein distance. This distance measures the space of probability measures and we refer to [9] for more details. For the following presentation it suffices to consider the 1-Wasserstein distance defined as follows.

Definition 1 Let μ and ν be two probability measures on $\mathbb{R}^2$. Then, the 1-Wasserstein distance is defined by

$$W(\mu, \nu) := \inf_{\pi \in \mathcal{P}^*(\mu, \nu)} \int_{\mathbb{R}^2} \int_{\mathbb{R}^2} |\xi - \eta| d\pi(\xi, \eta), \tag{26}$$

where $\mathcal{P}^*(\mu, \nu)$ is the space of probability measures on $\mathbb{R}^2 \times \mathbb{R}^2$ such that the marginals of π are μ and ν, respectively, i.e., $\int_{\mathbb{R}^2} d\pi(\cdot, \eta) = d\mu(\cdot)$ and $\int_{\mathbb{R}^2} d\pi(\xi, \cdot) = d\nu(\cdot)$.

Furthermore, we introduce the push-forward notion for a measureable map $g : \mathbb{R}^2 \to \mathbb{R}^2$ and a measure $\mu \in \mathcal{P}(\mathbb{R}^2)$. A measure $\nu \in \mathcal{P}(\mathbb{R}^2)$ is denoted by $\nu = g\#\mu$, if

$$\nu(A) = \mu(g^{-1}(A))$$

for any set $A \subset \mathbb{R}^2$ such that $g^{-1}(A)$ is μ-measurable. Let y be the unique solution to Eq. (25). Introduce now $\xi = (x, v) \in \mathbb{R}^2$ and rewrite Eq. (23) for a probability measure $\mu(t, \xi) := f(t, x, v)dxdv$ as

$$\partial_t \mu(t, \xi) + \nabla_\xi \cdot \left((\xi_2, -\frac{2}{\alpha} y(t)\xi_2)^T \mu(t, \xi) \right) = 0, \ \mu(0, \xi) = \mu_0 := f_0(x, v)dxdv, \tag{27}$$

which is understood in the sense of distributions. Associated with the mean field equation (27) and the initial datum, there is a system of characteristics $t \to \Xi(t, \bar{\xi}) \in \mathbb{R}^2$ emanating from $\bar{\xi} \in \mathbb{R}^2$ by

$$\frac{d}{dt}\Xi_1(t, \bar{\xi}) = \Xi_2(t, \bar{\xi}), \ \ \Xi_1(0, \bar{\xi}) = \bar{\xi}_1, \tag{28}$$

$$\frac{d}{dt}\Xi_2(t, \bar{\xi}) = -\frac{2}{\alpha} y(t)\Xi_2(t, \bar{\xi}), \ \ \Xi_2(0, \bar{\xi}) = \bar{\xi}_2. \tag{29}$$

For any $t \geq 0$ the measure $\mu(t, \cdot)$ is then obtained as

$$\mu(t, \cdot) = \Xi(t, \cdot)\#\mu_0. \tag{30}$$

The latter equation follows by integral transformation formula applied to Eq. (27). The relation (30) is now the starting point for developing the Dobrushin estimate. Let measures $\mu = \mu(t, \cdot)$ and $\nu = \nu(t, \cdot)$ in $\mathcal{P}(\mathbb{R}^2)$ be two solutions to (27) such that $t \to \mu(t, \cdot)$ and $t \to \nu(t, \cdot)$ are continuous. Then, we have

$$W(\mu(t, \cdot), \nu(t, \cdot)) \leq W(\mu_0, \nu_0)C_1, \ \ t \in [0, T] \tag{31}$$

for some constant $C_1 \geq 0$. The inequality (31) is established using the following computation. Let $\pi_0 \in \mathcal{P}^*(\mu, \nu)$ and for $(\xi, \eta) \in \mathbb{R}^4$ define $\pi(t, \cdot)$ as the measure under the image of $(\xi, \eta) \to (\Xi(t, \xi), \Xi(t, \eta))$ by

$$\pi(t, (\xi, \eta)) := \pi_0(\Xi(t, \xi), \Xi(t, \eta)).$$

Then, we have $\pi(t, \cdot) \in \mathcal{P}^*\left(\mu(t, \cdot), \nu(t, \cdot)\right)\right)$. Further, denote by $R(t)$ the distance computed at the measure $\pi(t, \cdot)$ as

$$R(t) := \int_{\mathbb{R}^4} \|\xi - \eta\| d\pi(t, (\xi, \eta)) = \int_{\mathbb{R}^4} \|\Xi(t, \xi) - \Xi(t, \eta)\| d\pi_0(\xi, \eta)$$

$$= \int_{\mathbb{R}^4} \|\xi - \eta + \int_0^t (\Xi_2(s, \xi) - \Xi_2(s, \eta), -\frac{2}{\alpha} y(s)(\Xi_2(s, \xi) - \Xi_2(s, \eta))^T ds \| d\pi_0(\xi, \eta).$$

Note that the solution to (25) fulfills $0 \leq y(t) \leq \frac{\sqrt{\alpha}}{2}$ for $t \in [0, T]$. Furthermore, the right-hand side of the system (28)–(29) is Lipschitz with constant $C_L := \max\{1, \frac{1}{\sqrt{\alpha}}\}$ and therefore we have, for any fixed T, using Gronwall's inequality:

$$\|\Xi(s, \xi) - \Xi(s, \eta)\|^2 \leq \exp(C_L T)\|\xi - \eta\|^2, \ \forall s \in [0, T]. \tag{32}$$

Hence, we estimate

$$R(t) \leq \int_{\mathbb{R}^4} \left(\|\xi - \eta\| + 4T \exp(\frac{1}{2} C_L T)\|\xi - \eta\| \right) ds d\pi_0(\xi, \eta) \leq C_1 R(0)$$

for a constant $C_1 = \max\{1, 4T \exp(\frac{1}{2} C_L T)\}$. Next, we take the infimum for both sides over all $\pi_0 \in \mathcal{P}^*(\mu_0, \nu_0)$ and obtain the Dobrushin type inequality (31), i.e.,

$$W(\mu(t, \cdot), \nu(t, \cdot)) \leq R(t) \leq C_1 W(\mu_0, \nu_0).$$

This inequality is a key estimate to show convergence of the particle dynamics towards the mean field equation: consider ν_0^N to be the empirical measure associated with initial data $\xi_{0,i} = (x_{0,i}, v_{0,i})$ for $i = 1, \ldots, N$, i.e.

$$\nu_0^N(\xi) := \frac{1}{N} \sum_{i=1}^{N} \delta(\xi - \xi_{0,i}). \tag{33}$$

Then, (30) implies that the measure at time t is given by the empirical measure

$$\nu^N(t, \xi) := \frac{1}{N} \sum_{i=1}^{N} \delta(\xi - \Xi^i(t)), \tag{34}$$

where $\Xi^i(t) = \Xi(t, \xi_{0,i})$ is the solution to the system (28)–(29) with initial data $\xi_{0,i} = (x_{0,i}, v_{0,i})$, i.e.,

$$\frac{d}{dt} \Xi_1^i(t) = \Xi_2^i(t), \ \ \Xi_1^i(0) = x_{i,0}, \tag{35}$$

$$\frac{d}{dt} \Xi_2^i(t) = -\frac{2}{\alpha} y(t) \Xi_2^i(t), \ \ \Xi_2^i(0) = v_{i,0}. \tag{36}$$

Recalling that $\xi = (x, v)$, the system (35)–(36) is equivalent to the controlled particle system (19). Let $\mu = \mu(t, \xi)$ be another solution to the mean field equation (27). Then, Dobrushin's inequality shows that

$$W(\mu(t, \cdot), \nu^N(t)) \to 0$$

provided that $W(\mu_0, \nu_0^N) \to 0$. Hence, we have shown that the limit of the particle system converges in Wasserstein towards a weak solution to the mean field equation.

Finally, we also prove the decay of the mean field Lyapunov function by extending the results of Lemma 3. For the empirical measure (22) and its density, f, we obtain as in the proof of Lemma 3.

$$L(t) = w^T K(t) w = \frac{1}{N} \sum_{i=1}^{N} v_i^2(t) y(t) = \int_{\mathbb{R}^2} v^2 y(t) d\mu^N(t, x, v)$$
$$= \int_{\mathbb{R}^2} v^2 y(t) f(t, x, v) dx dv. \tag{37}$$

The following Lemma shows that the mean field limit inherits the decay properties of the particle system and the same rate.

Lemma 4 *Consider sufficiently smooth initial conditions $f_0(x, v) \in \mathcal{P}(\mathbb{R}^2)$ with integrable second moment $\int_{\mathbb{R}^2} v^2 f_0(x, v) dx dv < \infty$. Assume that there exists a non-negative $C^1([0, T] \times \mathbb{R}^2)$ solution $f = f(t, x, v)$ vanishing as $\|(x, v)\| \to \infty$ to the dynamics given by Eq. (23) with integrable second moment $\int_{\mathbb{R}^2} v^2 f(t, x, v) dx dv < \infty$. Let y be the solution to (25). Then, the differentiable function*

$$\mathbf{L}(t) := \int_{\mathbb{R}^2} v^2 y(t) f(t, x, v) dx dv$$

is bounded from above by

$$\mathbf{L}(t) \leq \mathbf{L}(0) \exp(-r(t))$$

for $t \in [0, T]$ and rate, $r(t)$, given by Eq. (21).

Proof The (strong) assumptions allow for a pointwise evaluation of the partial differential equations. Furthermore, since $y \geq 0$ and f is assumed to be non-negative, $\mathbf{L} \geq 0$. A direct computation of the derivative of $\mathbf{L}$ yields

$$\begin{aligned}
\frac{d}{dt}\mathbf{L}(t) &= \int_{\mathbb{R}^2} v^2 y(t) \left(-\partial_x (v f(t, x, v)) + \frac{2}{\alpha} y(t) \partial_v (v f(t, x, v)) \right) dx dv + \\
&\quad + \frac{d}{dt} y(t) \int_{\mathbb{R}^2} v^2 f(t, x, v) dx dv \\
&\leq - y(t) \int_{\mathbb{R}} \partial_x \left(\int_{\mathbb{R}} v^3 f(t, x, v) dv \right) dx - \int_{\mathbb{R}^2} \frac{2}{\alpha} y^2(t) 2 v^2 f(t, x, v) dx dv \\
&\quad + \frac{2}{\alpha} y(t) \mathbf{L}(t),
\end{aligned}$$

where we used integration by parts in the v derivative and, since f is non-negative, could estimate $\frac{d}{dt}y$ using Eq. (25). Further, we obtain

$$\frac{d}{dt}\mathbf{L}(t) \leq \left(-\frac{4}{\alpha}+\frac{2}{\alpha}\right) y(t)\mathbf{L}(t) = -\frac{2}{\alpha}y(t)\mathbf{L}(t).$$

Using Gronwall's inequality the same rate $r(t)$ as in Lemma 3 is obtained. This shows that the basic properties of the controlled system are transferred from particle to mean field limit.

2.3 *Hydrodynamic Approximation to Controlled Particle System*

As the final scale of description, we consider a hydrodynamic formulation of the particle system. The procedure to derive hydrodynamic equations from kinetic or mean field equations is by now standard and a detailed discussion of the validity and its properties could be found in the references such as [34, 64]. In view of Eq. (23), we define the quantities $\rho(t,x)$ as local particle density as well as the flux $(\rho u)(t,x)$ at time t and position x by

$$\rho(t,x) := \int_{\mathbb{R}} f(t,x,v)dv, \;\; (\rho u)(t,x) := \int_{\mathbb{R}} vf(t,x,v)dv. \tag{38}$$

Here, $u = u(t,x)$ is the hydrodynamic velocity. Further, we introduce the pressure $p[f]$ as

$$p[f](t,x) = \int_{\mathbb{R}} (v-u(t,x))^2 f(t,x,v)dv. \tag{39}$$

Formally, evolution equations for the density and flux are found by integration of the mean field equation (23) with respect to dv and vdv. The quantities (38) are also referred to as the zeroth and first moments of the probability density f with respect to v. The partial differential equations obtained by integration with respect to $x \in \mathbb{R}$ and $t \in [0,T]$ are given by

$$\partial_t \rho(t,x) + \partial_x(\rho u)(t,x) = 0, \tag{40}$$

$$\partial_t(\rho u)(t,x) + \partial_x\left((\rho u^2)(t,x) + p[f](t,x)\right) + \frac{2}{\alpha}y(t)(\rho u)(t,x) = 0. \tag{41}$$

The equation for y is unchanged and given by Eq. (25). Initial conditions for the previous system are obtained by successive integration of the initial condition, i.e.,

$$\rho(0,x) = \rho_0(x) := \int_{\mathbb{R}} f_0(x,v)dv, \ \ (\rho u)(0,x) = (\rho u)_0(x) := \int_{\mathbb{R}} v f_0(x,v)dv. \tag{42}$$

The system (40)–(41) is not closed since p cannot be expressed explicitly in terms of $(\rho, \rho u)$ directly. This problem is known as a closure problem and it is due to the fact, that f is projected to a lower dimensional subspace given by density and flux and p accounts for the projection error. Several possibilities exist to overcome the problem. Further equations for the moments of the type $m^j(t,x) = \int_{\mathbb{R}} v^j f(t,x,v)dv$ of f can be derived shifting the closure problem to equations for higher moments and thereby improving the approximation of f in terms of $(\rho, \rho u, m^3, \dots)$. However, the problem in principle persists. A possibility to close the hierarchy of equations is to assume that f is close to a (known) equilibrium distribution for higher moments. We illustrate this approach by approximating

$$p[f] \approx p[\delta(\cdot - u(t,x))] \tag{43}$$

known as mono-kinetic closure. Equation (43) states that at the level of the pressure the particles propagate with the hydrodynamic speed, instead of their individual velocity v. Formally, replacing $p[f]$ by the mono-kinetic closure in Eqs. (40)–(41) leads to the system similar to pressureless gas dynamics of the form:

$$\partial_t \rho(t,x) + \partial_x(\rho u)(t,x) = 0, \tag{44}$$

$$\partial_t(\rho u)(t,x) + \partial_x(\rho u^2)(t,x) + \frac{2}{\alpha} y(t)(\rho u)(t,x) = 0. \tag{45}$$

Another used closure in gas dynamics is the Grad-closure [34]. Here, we assume that

$$p[f] \approx C_1 \rho^{C_2} \tag{46}$$

for some known constants $0 \le C_1, C_2$. In the case of isentropic gas $1 < C_2 \le 3$ and for isothermal gas, we have $C_2 = 1$. Other closure options, for example, based on entropy principles also exist, see e.g. [43].

Based on the moments of the mean field f, we obtain

$$\mathbf{L}(t) = \int_{\mathbb{R}^2} v^2 y(t) f(t,x,v)dxdv = \tag{47}$$

$$y(t) \int_{\mathbb{R}} \left(\int_{\mathbb{R}} (v - u(t,x))^2 f(t,x,v)dv \right) + (\rho u^2)(t,x)dx = \tag{48}$$

$$y(t) \int_{\mathbb{R}} p[f](t,x) + (\rho u^2)(t,x)dx. \tag{49}$$

For the closure (43), we are able to also prove decay of the corresponding Lyapunov function at the hydrodynamic scale.

Lemma 5 *Consider sufficiently smooth initial conditions* $\rho_0(x), (\rho u)_0(x)$ *such that* $\int_{\mathbb{R}} (\rho u^2)_0(x)dx < \infty$. *Assume that there exists a* $C^1([0,T] \times \mathbb{R})$ *solution* $(\rho, \rho u)(t,x)$ *vanishing at* $\|x\| \to \infty$ *and with* $\rho \geq 0$ *to the dynamics given by Eqs.* (44)–(45) *with integrable momentum* $\int_{\mathbb{R}} (\rho u^2)(t,x)dx < \infty$ *for any time* t. *Let* y *be the solution to* (25). *Then, the differentiable function*

$$\mathcal{L}(t) := \int_{\mathbb{R}} y(t)(\rho u^2)(t,x)dx$$

is bounded from above by

$$\mathcal{L}(t) \leq \mathcal{L}(0) \exp\left(-r(t)\right)$$

for $t \in [0,T]$ *and the rate,* $r(t)$, *is given by Eq.* (21).

Proof The (strong) assumptions allow for a pointwise evaluation of the partial differential equations. Note that Eqs. (44) and (45) lead to an equation for $u = u(t,x)$ as

$$\partial_t u(t,x) + u(t,x)\partial_x u(t,x) + \frac{2}{\alpha} u(t,x) = 0.$$

Furthermore, a direct computation yields

$$\begin{aligned}
\frac{d}{dt}\mathcal{L}(t) &= \frac{d}{dt} y(t) \int_{\mathbb{R}} (\rho u^2)(t,x)dx \\
&\quad + y(t) \int_{\mathbb{R}} (-\partial_x(\rho u)(t,x)) u^2(t,x)dx + 2(\rho u)(t,x)\partial_t u(t,x)dx \\
&\leq \frac{2}{\alpha} y^2(t) \int_{\mathbb{R}} (\rho u^2)(t,x)dx + y(t) \int_{\mathbb{R}} 2(\rho u)(t,x)\left(u(t,x)\partial_x u(t,x) + \partial_t u(t,x)\right)dx,
\end{aligned}$$

where we used the equation for y and the non-negativity of $\rho(t,x)$. Further, using the equation for $u(t,x)$, we obtain

$$\frac{d}{dt}\mathcal{L}(t) \leq \frac{2}{\alpha} y(t)\mathcal{L}(t) - y(t) \int_{\mathbb{R}} 2(\rho u)(t,x)\frac{2}{\alpha} u(t,x)dx = \frac{-2y(t)}{\alpha}\mathcal{L}(t).$$

Using Gronwall's inequality we obtain the assertion. The obtained rate is the same as on the particle and mean field scale.

Remark 1 Using Grad's closure a similar estimate is not possible due to the particular structure of the hydrodynamic equations and the form of the Lyapunov function.

3 Numerical Tests and Results for the Linear Control Problem

Numerical experiments will be undertaken to demonstrate the theoretical properties discussed in the previous sections. The first set of numerical tests will consider the particle system. The theoretical results are presented in Sect. 2.1. The decay of Lyapunov function will be investigated and presented in Sect. 3.1 below. Similarly, the hydrodynamic limit discussed in Sect. 2.3 will be numerically investigated and presented in Sect. 3.2.

3.1 Numerical Results for the Particle System

In these tests, we consider a system with a total of $N = 250$ particles. The initial spatial positions of these particles, $x_{i,0}$, are uniformly distributed in the interval $[0, 1]$. The initial velocities are given by $v_{i,0} = \exp(x_{i,0}) \sin(2\pi x_{i,0}) + \xi_i$ where ξ_i is a random variable uniformly distributed in $[0, 0.2]$. The dynamics are described by Eq. (19). Time marching of this dynamic system is undertaken using an embedded explicit Runge–Kutta method of orders 2 and 3 with four stages (with local error control). The control $y(t)$ is computed by piecewise constant discretization of the exact solution to Eq. (25) on the same grid used for the integration of the system of ordinary differential equations (19).

The Lyapunov function $L(t)$ in Lemma 3 is also evaluated on the same grid. For comparisons the theoretical decay rate, $r(t)$, is also computed by a midpoint integration of equation (21) using the exact solution to the ordinary differential equation (25). The terminal time for these computations has been set to $T = 1$.

In Fig. 1 computational results for the particle system are presented. The decay of the Lyapunov function, $L(t)$, with the estimate of the decay provided by Lemma 3 for different values of α is computed. We consider $\alpha \in \{10^{-2}, 10^{-3}, 10^{-4}\}$. Recall that α weighs the control cost compared to the cost associated with the quadratic deviation of particle velocities from zero. Larger values of α are related to higher control costs and lead to slower decay rates which is also observed numerically. Furthermore, we observe that the theoretical estimate is an upper bound on the observed decay in all cases. This confirms the theoretical findings.

3.2 Numerical Results for the Hydrodynamic Limit

Similar computations as above are repeated for the hydrodynamic approach in Sect. 2.3. Note that formally the equations are the so-called pressureless gas dynamics—however damped by the control in ρu. Without the control the equations may exhibit Dirac-solutions for initial values in the velocity field that lead to

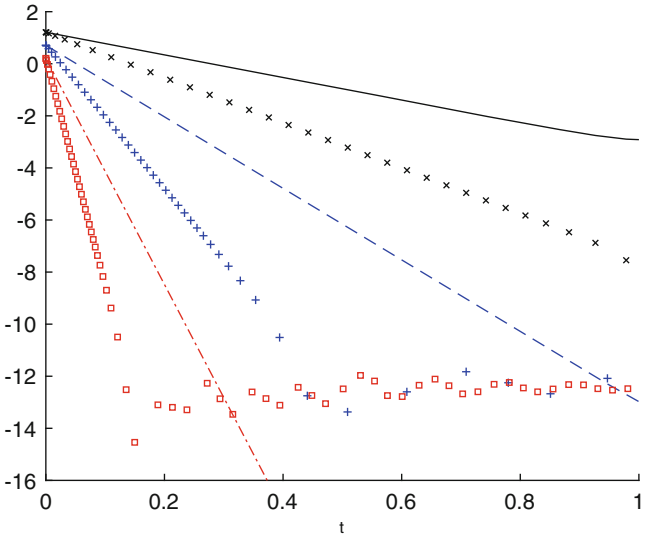

Fig. 1 Semi-logarithmic plot for the decay of the Lyapunov function $t \to L(t)$ over time. The crossed lines correspond to the numerical integration of system (19) for different values of α. The solid line shows the theoretical expected decay $L(0)\exp(-r(t))$ where the rate r is obtained by numerical integration of equation (21). The red, blue, and black lines correspond to $\alpha = 10^{-4}$, $\alpha = 10^{-3}$ and $\alpha = 10^{-2}$, respectively

concentration phenomena. This case is not present for the initial data considered here due to the strong damping and the smooth initial datum. The initial data of the particle system translates to the following initial data for the hydrodynamic simulation

$$\rho_0(x) = 1 \text{ and } (\rho u)_0(x) = \exp(x)\sin(2\pi x) + \xi(x), \tag{50}$$

where $x \to \xi(x)$ is spatially distributed random noise. Periodic boundary conditions in space are imposed.

A second-order relaxed finite-volume scheme for the spatial and temporal discretization of equation (40) as proposed in [61] is employed. The spatial domain is discretized using an equal-distant grid with center points $x_i = i\Delta x$ with $i = 1, \ldots, N_x$ grid points. We choose $N_x = 250$ spatial points. The temporal grid is chosen using a CFL condition with a CFL number of 0.9. Terminal time is set to $T = 1$. The noise is pointwise equally distributed in $[0, 0.2]$. As in the case of the particle system the control $y(t)$ is computed by piecewise constant discretization of the exact solution to Eq. (25) on the grid used for the solution of partial differential equations (40).

It is appropriate to remark at this point that in [18] a first-order version of the relaxed finite-volume scheme also referred to as the Rusanov scheme was discussed. For a system of conservation laws:

$$\partial_t U + \partial_x F(U) = 0$$

the numerical flux takes the form:

$$F_{i+1/2} = \frac{F(U_i) + F(U_{i+1})}{2} - c\frac{U_{i+1} - U_i}{2}.$$

The subcharacteristic condition needs to be satisfied i.e. the eigenvalues of the physical system to be solved must lie between the eigenvalues of the relaxation system. It was proved that for isentropic gas dynamics systems with pressure $p = p(\rho)$ the choice of

$$c = \max\left(|u_i| + \sqrt{p'(\rho_i)}, |u_{i+1}| + \sqrt{p'(\rho_{i+1})}\right),$$

is appropriate, where u is the velocity gives a scheme that preserves positivity of density as well as resolves solutions with vacuum since c does not blow up at vacuum. For relaxation schemes that can handle delta-shocks, we refer to [71]. For other numerical approaches for pressureless gas, we refer to [19, 20, 35].

The Lyapunov function $\mathcal{F}(t)$ in Lemma 5 is evaluated on the same temporal grid and the integral in space is discretized using a midpoint scheme.

In Fig. 2, we compare the decay of the Lyapunov function $\mathcal{L}(t)$ with the estimate of the decay provided by Lemma 5 for different values of α. As in the case of the particle system, the theoretical findings are confirmed by the numerical simulation.

4 Results on Nonlinear Interacting Particle Systems

In this section we briefly review some existing research directions for controlled particle systems.

4.1 One-Dimensional State Space Models

Many recent publications focus on simple models with a phase state that is one-dimensional, i.e., each particle i has a state $y_i \in \mathbb{R}$. Such models are popular in the description of opinion formation and wealth distributions [52, 66] to name just two.

Many contributions [1, 3, 5] introduce novel control strategies based on opinion formation models of the type

$$y_i' = \frac{1}{N}\sum_{j\neq i}^{N} P(y_i, y_j)(y_j - y_i) + q_i, \;\; y_i(0) = y_{i,0}, \tag{51}$$

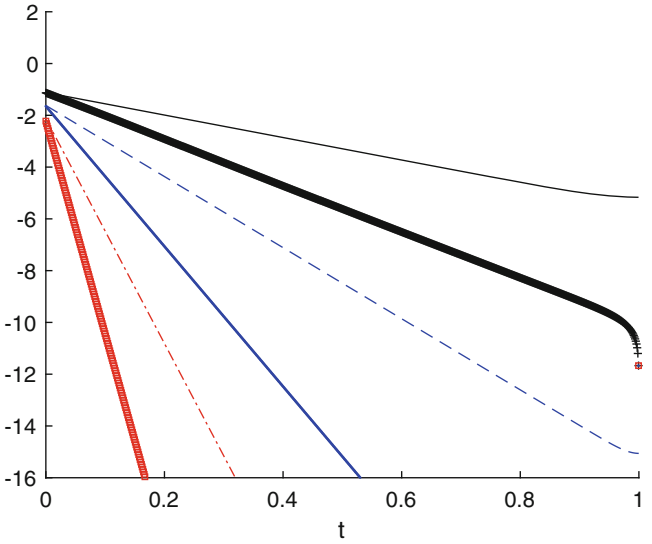

Fig. 2 Semi-logarithmic plot for the decay of the Lyapunov function $t \to \mathcal{L}(t)$ over time. The crossed lines correspond to the numerical integration of system (19) for different values of α. The solid line shows the theoretical expected decay $\mathcal{L}(0)\exp(-r(t))$ where the rate r is obtained by numerical integration of equation (21). The red, blue, and black lines correspond to $\alpha = 10^{-4}$, $\alpha = 10^{-3}$, and $\alpha = 10^{-2}$, respectively

where $y_i \in I \subset \mathbb{R}$ and the dynamics are driven by an alignment process due to pairwise interaction and weighted by a function $P(\cdot,\cdot)$. In the case of wealth models, we have $I = \mathbb{R}_+$ denoting the available money for each particle while for opinion formation, we have $I = [-1, 1]$ denoting extreme opinions. For traffic flow applications the interval I is $I = [0, v_{\max}]$ where $v_{\max}$ is the maximal speed allowed on a road. Other examples are $I = [0, 2\pi]$ in the case of one-dimensional Kuramoto-type models or $I = \mathbb{R}$ in the case of the one-dimensional Cucker–Smale model.

For constant P, the model (51) is still linear and a similar analysis as in Sect. 2 is possible. For nonlinear P, most of the research has focused on suboptimal control based on instantaneous or short time horizon control. The mean field limit of (51) and the corresponding controlled system, using a suboptimal control, has also been established. Due to the one-dimensional phase space the extension to the hydrodynamic equation is not relevant. However, moments of the kinetic distribution as well as equilibrium conditions have been studied.

A further extension to the models has been the addition of stochasticity to the dynamics. In [6] white noise, dW, is added to the dynamics leading to a problem of the form:

$$q^* = \text{argmin}_{v\in\mathbb{R}} \frac{1}{2}\int_0^T \mathbb{E}\left(\left(\frac{1}{N}\sum_{j=1}^N g(y_i)\right)^2 + \frac{\beta}{2}v^2\right)dt,$$

$$\text{subject to } dy_i = \left(\frac{1}{N}\sum_{j\neq i}^N P(y_i, y_j)(y_j - y_i) + v\right)dt + dW_i,\ y_i(0) = y_{i,0},$$

where P is a given interaction kernel and g a given cost functional. Also, in [4] a stochastic parameter, W, is included in the collision operator, P, to account for modeling errors. Thus the resulting problem reads

$$u = \text{argmin}_{v\in\mathbb{R}} \frac{1}{2}\int_0^T \mathbb{E}\left(\left(\frac{1}{N}\sum_{j=1}^N g(y_i)\right)^2 + \frac{\beta}{2}v^2\right)dt \text{subject to (51)}.$$

Using instantaneous control and polynomial chaos expansion the problem is reduced to a closed loop problem for suboptimal control q.

Additional structural requirements on the control could be considered. For example, some application might require sparse control. An existing approach modifies the cost functional to treat this case [46]:

$$q^* = \text{argmin}_{v\in\mathbb{R}} \frac{1}{2}\int_0^T \frac{1}{N}\sum_{j=1}^N y_i^2 dt + \beta\|v\|_L,$$

for $L = L_p(0, T)$ where $0 < p \leq 1$ is studied. This term promotes sparsity of the control in time. Another type of sparsity is introduced in [7] where sparsity is introduced in the number of controllable particles leading to a problem of the following type:

$$y_i' = \frac{1}{N}\sum_{j\neq i}^N P(y_i, y_j, W)(y_j - y_i) + b_i v,\ y_i(0) = y_{i,0},$$

where $b_i \in \{0, 1\}$, fixed, with $\|b\|_{\ell^1}$ sufficiently small. A further example of sparse control in the case of the Hegselmann–Krause model is given in [68].

4.2 Controlled Particle Systems in High-Dimensional State Space

Typical crowd dynamic models [10, 36, 73] have a state space that at least contains the velocity v_i and the position of the particle x_i. However, the field of control

for such models and its associated mean field equations is largely unexplored. So far, results on instantaneous control approaches applied to second-order alignment models are available in [1]. The basic model for $i = 1, \ldots, N$ particles is given by the following dynamics:

$$\frac{d}{dt}x_i(t) = v_i(t), \tag{52}$$

$$\frac{d}{dt}v_i(t) = \frac{1}{N}\sum_{j=1}^{N} P(x_i(t), x_j(t))(v_j(t) - v_i(t)) + q^*(t) \tag{53}$$

subject to initial conditions and for a given function P. The instantaneous control approach has been used to find a suboptimal explicit closed loop control for $q^*(t)$ by minimizing

$$q^*(t) = \text{argmin}_{q\in\mathbb{R}} \frac{1}{2}\int_t^{t+\Delta t} \frac{1}{N}\sum_{j=1}^{N}(v_i(s) - v_d(s))^2 + \frac{\beta}{2}q^2(s)ds, \tag{54}$$

on a small time horizon $\Delta t > 0$. The parameter $\beta > 0$ is again the regularization parameter and v_d is a desired velocity, piecewise constant on the receding horizon $(t, t + \Delta t)$. To illustrate this point, we consider for parameters $K > 0, \gamma > 0, \delta \geq 0$

$$P(x_i, x_j) = \frac{K}{(\gamma^2 + \|x_i - x_j\|^2)^\delta}. \tag{55}$$

These dynamics are known as the Cucker–Smale model. We refer to [32, 37] for more details on properties as well as motivation. Another example of P is introduced in [65] given by

$$P(x_i, x_j) = \frac{H(|x_i - x_j|)}{\frac{1}{N}\sum_{j=1}^{N} H(|x_i - x_j|)}, \tag{56}$$

where H could be given by (55), i.e., $H = H(r) = \frac{K}{(\gamma^2+r^2)^\delta}$. An extension of the instantaneous control approach to this system is straightforward.

A further class of crowd models where, to the best of our knowledge no control results are available for now, are models of the type [42]

$$\frac{d}{dt}x_i(t) = v_i(t), \tag{57}$$

$$\frac{d}{dt}v_i(t) = -\frac{1}{N}\sum_{j=1}^{N} P(x_i(t) - x_j(t)) + (\beta - \gamma|v_i|^2)v_i, \tag{58}$$

where $P(x, y)$ is given as a gradient of a potential, U, modeling interactions, $P(x_i, x_j) = \nabla_{x_i} U(|x_j - x_i|)$ and $\beta, \gamma \geq 0$ are parameters modeling the self-propulsion of particles.

Even more detailed models which have been recently introduced such as in [32] introduce, on the particle level, the concept of a visual cone, restricting the possible interaction of particle i with particles $j \neq i$ by geometric conditions. So far, no control results for those models are known.

In applications in finance, there only exist a few results on control of wealth or financial market models. For wealth models of the type (51) subject to (54), an instantaneous control approach has been introduced in [45]. The objective function intends to reduce the variance of wealth among agents and thus the objective function in (54) needs to be replaced by the empirical variance. Furthermore, the control of binary wealth interactions leading to a Boltzmann type description has been investigated in [45].

In a game theoretic setting wealth models have been studied as well. A second-order model of the type

$$\dot{x}_i = V(x_i, y_j), \tag{59}$$

$$dy_i = q_i^* \, dt + y_i \, dW_i \tag{60}$$

has been discussed in [38]. Here $V(\cdot, \cdot)$ models the speed of change in the economic configuration $x_i \in \mathbb{R}$. The control q_i^* has been computed as best reply to a cost functional of the type

$$q_i^*(t) = \text{argmin}_{q \in \mathbb{R}} \frac{1}{2} \int_t^{t+\Delta t} \mathbb{E}\Big(\frac{1}{N} \sum_{j=1}^{N} P(x_i(s), x_j(s)) \, \Phi(y_j(s) - y_i(s)) + \frac{\beta}{2} q^2(s) \Big) ds, \tag{61}$$

where $\Phi(\cdot)$ models the trading interaction of agents with different wealth levels $x_i > 0$. A portfolio model of similar structure to (59)–(61) has been discussed in [72], where additionally the dynamics are coupled to a stock price equation modeled by a stochastic differential equation.

An example of a wealth model which has been studied in the game theoretic setting without any suboptimal strategies is presented in [51]. The structure of the model is as follows:

$$dx_i = q_i^* \, dt + dW_i, \tag{62}$$

$$q_i^*(t) = \text{argmin}_{q \in \mathbb{R}} \frac{1}{2} \int_t^{\infty} \mathbb{E}\left(F(x_1, \ldots, x_N, q_i) \, e^{-r(s-t)} \right) ds. \tag{63}$$

In the mean field limit the system (62) reduces to a Hamilton–Jacobi–Bellman equation. These models are known as mean field games and have been extensively studied in the past decade, see [14, 31].

5 Summary

In summary the chapter presents some developments in controlled crowd dynamics. A discussion of the multisclae control of particle systems which culiminates in the mean field of the controlled particle system is presented. In addition, the ensuing control system for the hydrodynamic model is derived from the particle system. To demonstrate the practical application of the approaches, numerical tests are undertaken on the linear models. The behavior predicted in the theoretical discussions is clear in the numerical results. Further a discussion of work that has been done on nonlinear models is also discussed in the last section of the chapter. This includes applications in opinion formation, stochastic control, crowd models as well as wealth models among others.

Acknowledgments We acknowledge the support by the National Research Foundation of South Africa (Grant number: 93099 and 93476), DFG HE5386/14,15, 18, BMBF ENets 05M18PAA, Cluster of Excellence Internet of Production (ID 390621612) and NSF RNMS grant No. 1107291 (KI-Net).

References

1. G. Albi, Kinetic approximation, stability and control of collective behaviour in self-organized systems. PhD thesis, Università degli Studi di Ferrara (2014). http://eprints.unife.it/894/
2. G. Albi, L. Pareschi, M. Zanella, Boltzmann-type control of opinion consensus through leaders. Philos. Trans. R. Soc. Lond. Ser. A Math. Phys. Eng. Sci. **372**(2028), 20140138, 18 (2014)
3. G. Albi, M. Herty, L. Pareschi, Kinetic description of optimal control problems and applications to opinion consensus. Commun. Math. Sci. **13**(6), 1407–1429 (2015)
4. G. Albi, L. Pareschi, M. Zanella, Uncertainty quantification in control problems for flocking models. Math. Probl. Eng. **2015**, Art. ID 850124, 14pp. (2015)
5. G. Albi, M. Bongini, E. Cristiani, D. Kalise, Invisible control of self-organizing agents leaving unknown environments. SIAM J. Appl. Math. **76**(4), 1683–1710 (2016)
6. G. Albi, Y.-P. Choi, M. Fornasier, D. Kalise, Mean field control hierarchy. Appl. Math. Optim. **76**(1), 93–135 (2017)
7. G. Albi, M. Fornasier, D. Kalise, A Boltzmann approach to mean-field sparse feedback control, in *20th IFAC World Congress*, vol. 50, ed. by D.P.D. Dochain, D. Henrion (2017), pp. 2898–2903
8. G. Aletti, G. Naldi, G. Toscani, First-order continuous models of opinion formation. SIAM J. Appl. Math. **67**(3), 837–853 (electronic) (2007)
9. L. Ambrosio, N. Gigli, G. Savare, *Gradient Flows in Metric Spaces of Probability Measures*. Lectures in mathematics (Birkhäuser, Basel, 2008)
10. N. Bellomo, G. Ajmone Marsan, A. Tosin, *Complex Systems and Society. Modeling and Simulation*. SpringerBriefs in mathematics (Springer, Berlin, 2013)

11. N. Bellomo, P. Degond, E. Tadmor, *Active Particles, Volume 1 : Advances in Theory, Models, and Applications*. Modeling and simulation in science, engineering and technology (Birkhäuser, Basel, 2017)
12. E. Ben-Naim, Opinion dynamics, rise and fall of political parties. Europhys. Lett. **69**, 671 (2005)
13. A. Bensoussan, J. Frehse, P. Yam, *Mean Field Games and Mean Field Type Control Theory*. SpringerBriefs in mathematics (Springer, New York, 2013)
14. A. Bensoussan, J. Frehse, P. Yam et al., *Mean Field Games and Mean Field Type Control Theory*, vol. 101 (Springer, Berlin, 2013)
15. A. Bensoussan, J. Frehse, S.C.P. Yam, On the interpretation of the master equation. Stoch. Process. Appl. **127**(7), 2093–2137 (2017)
16. M. Bongini, M. Fornasier, D. Kalise, (Un)conditional consensus emergence under perturbed and decentralized feedback controls. Discrete Contin. Dyn. Syst. **35**(9), 4071–4094 (2015)
17. A. Borzì, S. Wongkaew, Modeling and control through leadership of a refined flocking system. Math. Models Methods Appl. Sci. **25**(2), 255–282 (2015)
18. F. Bouchut, *Nonlinear Stability of Finite Volume Methods for Hyperbolic Conservation Laws: And Well-balanced Schemes for Sources* (Springer Science and Business Media, Berlin, 2004)
19. F. Bouchut, S. Jin, X. Li, Numerical approximations of pressureless and isothermal gas dynamics. SIAM J. Numer. Anal. **41**(1), 135–158 (2003)
20. L. Boudin, J. Mathiaud, A numerical scheme for the one-dimensional pressureless gases system. Numer. Methods Partial Differ. Equ. **28**(6), 1729–1746 (2012)
21. L. Boudin, F. Salvarani, A kinetic approach to the study of opinion formation. ESAIM: Math. Model. Numer. Anal. **43**, 507–522 (2009)
22. L.M. Briceño Arias, D. Kalise, F.J. Silva, Proximal methods for stationary mean field games with local couplings. SIAM J. Control Optim. **56**(2), 801–836 (2018)
23. M. Burger, L. Caffarelli, P.A. Markowich, M.-T. Wolfram, On a Boltzmann-type price formation model. Proc. R. Soc. Lond. Ser. A Math. Phys. Eng. Sci. **469**(2157), 20130126, 20 (2013)
24. M. Burger, M. Di Francesco, P.A. Markowich, M.-T. Wolfram, Mean field games with nonlinear mobilities in pedestrian dynamics. Discrete Contin. Dyn. Syst. Ser. B **19**(5), 1311–1333 (2014)
25. M. Caponigro, M. Fornasier, B. Piccoli, E. Trélat, Sparse stabilization and optimal control of the Cucker-Smale model. Math. Control Relat. Fields **3**(4), 447–466 (2013)
26. M. Caponigro, M. Fornasier, B. Piccoli, E. Trélat, Sparse stabilization and control of alignment models. Math. Models Methods Appl. Sci. **25**(3), 521–564 (2015)
27. P. Cardaliaguet, Notes on mean field games (from P.-L. Lions lectures at the College de France) (2010)
28. P. Cardaliaguet, The convergence problem in meanfield games with local coupling. Appl. Math. Optim. **76**, 177–215 (2017)
29. P. Cardaliaguet, J.-M. Lasry, P.-L. Lions, A. Poretta, Long time average of mean field games with nonlocal coupling. SIAM J. Control Optim. **51**, 3358–3591 (2013)
30. R. Carmona, F. Delarue, Probabilistic analysis of mean field games. SIAM J. Control Optim. **51**, 2705–2734 (2013)
31. R. Carmona, F. Delarue, *Probabilistic Theory of Mean Field Games with Applications I-II* (Springer, Berlin, 2018)
32. J.A. Carrillo, M. Fornasier, G. Toscani, F. Vecil, Particle, kinetic, and hydrodynamic models of swarming, in *Mathematical Modeling of Collective Behavior in Socio-Economic and life sciences*. Model. Simul. Sci. Eng. Technol. (Birkhäuser, Boston, 2010), pp. 297–336
33. C. Cercignani, *The Boltzmann Equation and Its Applications* (Springer, New York, 1988)
34. C. Cercignani, R. Illner, M. Pulvirenti, *The Mathematical Theory of Dilute Gases*. Number 106 in applied mathematical sciences (Springer, New York, 1994)
35. C. Chalons, D. Kah, M. Massot, Beyond pressureless gas dynamics: quadrature-based velocity moment models. Commun. Math. Sci. **10**(4), 1241–1272 (2012)

36. E. Cristiani, B. Piccoli, A. Tosin, *Multiscale Modeling of Pedestrian Dynamics*. MS&A. Modeling, simulation and applications, vol. 12 (Springer, Cham, 2014)
37. F. Cucker, S. Smale, Emergent behavior in flocks. IEEE Trans. Automat. Contr. **52**, 852–862 (2007)
38. P. Degond, J.-G. Liu, C. Ringhofer, Evolution of the distribution of wealth in an economic environment driven by local Nash equilibria. J. Stat. Phys. **154**(3), 751–780 (2014)
39. P. Degond, J.-G. Liu, C. Ringhofer, Evolution of wealth in a nonconservative economy driven by local Nash equilibria. Philos. Trans. R. Soc. A **372** (2014). https://doi.org/10.1098/rsta.2013.0394
40. P. Degond, J.-G. Liu, C. Ringhofer, Large-scale dynamics of mean-field games driven by local Nash equilibria. J. Nonlinear Sci. **24**, 93–115 (2014)
41. P. Degond, M. Herty, J.-G. Liu, Meanfield games and model predictive control. Commun. Math. Sci. **5**, 1403–1422, 12 (2017)
42. M. D'Orsogna, Y.-L. Chuang, A. Bertozzi, L. Chayes, Self-propelled particles with soft-core interactions. Patterns, stability, and collapse. Phys. Rev. Lett. **96**, 104302 (2006)
43. B. Dubroca, J.L. Feugeas, Entropic moment closure hierarchy for the radiative transfer equation. C. R. Acad. Sci. Paris Ser. I **329**, 915–920 (1999)
44. B. Düring, P. Markowich, J.-F. Pietschmann, M.-T. Wolfram, Boltzmann and Fokker-Planck equations modelling opinion formation in the presence of strong leaders. Proc. R. Soc. A **465**, 3687–3708 (2009)
45. B. Düring, L. Pareschi, G. Toscani, Kinetic models for optimal control of wealth inequalities. Eur. Phys. J. B **91**(10), 265 (2018)
46. M. Fornasier, F. Solombrino, Mean-field optimal control. ESAIM Control Optim. Calc. Var. **20**(4), 1123–1152 (2014)
47. M. Fornasier, B. Piccoli, F. Rossi, Mean-field sparse optimal control. Philos. Trans. R. Soc. Lond. Ser. A Math. Phys. Eng. Sci. **372**(2028), 20130400, 21 (2014)
48. A. Friedman, *Differential Games* (American Mathematical Society, Providence, 1974). Expository lectures from the CBMS Regional Conference held at the University of Rhode Island, Kingston, R.I., June 4–8, 1973, Conference Board of the Mathematical Sciences Regional Conference Series in Mathematics, No. 18
49. F. Golse, On the dynamics of large particle systems in the mean field limit, in *Macroscopic and Large Scale Phenomena: Coarse Graining, Mean Field Limits and Ergodicity* (Springer, Berlin, 2016)
50. D. Gomes, R.M. Velho, M.-T. Wolfram, Socio-economic applications of finite state mean field games. Philos. Trans. R. Soc. Lond. Ser. A Math. Phys. Eng. Sci. **372**(2028), 20130405, 18 (2014)
51. O. Guéant, J.-M. Lasry, P.-L. Lions, Mean field games and applications, in *Paris-Princeton Lectures on Mathematical Finance 2010* (Springer, Berlin, 2011), pp. 205–266
52. R. Hegselmann, U. Krause, Opinion dynamics and bounded confidence, models, analysis and simulation. J. Artif. Soc. Soc. Simul. **5**(3), 2 (2002)
53. M. Herty, C. Ringhofer, Consistent mean field optimality conditions for interacting agent systems. Commun. Math. Sci. **17**, 1095–1108 (2019)
54. M. Herty, M. Zanella, Performance bounds for the mean-field limit of constrained dynamics. Discrete Contin. Dyn. Syst. **37**(4), 2023–2043 (2017)
55. M. Herty, S. Steffensen, L. Pareschi, Mean-field control and Riccati equations. Netw. Heterog. Media **10**(3), 699–715 (2015)
56. M. Herty, S. Steffensen, L. Pareschi, Control strategies for the dynamics of large particle systems, in *Active Particles*, ed. by P.D.N. Bellomo, E. Tadmor. Advances in theory, models, and applications, vol. 2. Model. Simul. Sci. Eng. Technol. (Birkhäuser, Basel, 2019)
57. M. Huang, R.P. Malhame, P.E. Caines, Large population stochastic dynamic games: closed-loop McKean-Vlasov systems and the Nash certainty equivalence principle. Commun. Inf. Syst. **6**, 221–252 (2006)
58. M. Huang, P.E. Caines, R.P. Malhame, An invariance principle in large population stochastic dynamic games. J. Syst. Sci. Complex. **20**, 162–172 (2007)

59. M. Huang, P.E. Caines, R.P. Malhame, The NCE mean field principle with locality dependent cost interactions. IEEE Trans. Automat. Contr. **55**, 2799–2805 (2010)
60. P. Jabin, A review of the mean fields limits for Vlasov equations. Kinet. Relat. Models **7**, 661–711 (2014)
61. S. Jin, Z.P. Xin, The relaxation schemes for systems of conservation laws in arbitrary space dimensions. Commun. Pure Appl. Math. **48**(3), 235–276 (1995)
62. D. Kalise, K. Kunisch, Z. Rao, Infinite horizon sparse optimal control. J. Optim. Theory Appl. **172**(2), 481–517 (2017)
63. J.-M. Lasry, P.-L. Lions, Mean field games. Jpn. J. Math. **2**(1), 229–260 (2007)
64. C. D. Levermore, Moment closure hierarchies for kinetic theories. J. Stat. Phys. **83**, 1021–1065 (1996)
65. S. Motsch, E. Tadmor, Heterophilious dynamics enhances consensus. SIAM Rev. **4**, 577–621 (2014)
66. G. Naldi, L. Pareschi, G. Toscani, *Mathematical Modeling of Collective Behavior in Socio-Economic and Life Sciences*. Modeling and simulation in science, engineering and technology (Birkhauser, Boston, 2010)
67. L. Pareschi, G. Toscani, *Interacting Multi-Agent Systems. Kinetic Equations & Monte Carlo Methods* (Oxford University Press, Oxford, 2013)
68. B. Piccoli, N.P. Duteil, E. Trélat, Sparse control of Hegselmann–Krause models: black hole and declustering. SIAM J. Control Optim. **57**(4), 2628–2659 (2019)
69. E.D. Sontag, *Mathematical Control Theory: Deterministic Finite-Dimensional Systems, Texts in Applied Mathematics*, vol. 6, 2nd ed. (Springer, New York, 1998)
70. H. Spohn, *Large Scale Dynamics of Interacting Particles* (Springer, Berlin, 1991)
71. T. Trimborn, L. Pareschi, M. Frank, A relaxation scheme for the approximation of the pressureless Euler equations. Numer. Methods Partial Differ. Equ. Int. J. **22**(2), 484–505 (2006)
72. T. Trimborn, L. Pareschi, M. Frank, Portfolio optimization and model predictive control: a kinetic approach. Discrete Contin. Dyn. Syst. B **24**(11), 6209–6238 (2019)
73. T. Vicsek, A. Zafeiris, Collective motion. Phys. Rep. **517**, 71–140 (2012)
74. M.-T. Wolfram, Opinion formation in a heterogeneous society, in *Econophysics of Order-Driven Markets*. New Econ. Windows (Springer, Milan, 2011), pp. 277–288

Mathematical Models and Methods for Crowd Dynamics Control

Giacomo Albi, Emiliano Cristiani, Lorenzo Pareschi, and Daniele Peri

Abstract In this survey we consider mathematical models and methods recently developed to control crowd dynamics, with particular emphasis on egressing pedestrians. We focus on two control strategies: the first one consists in using special agents, called *leaders*, to steer the crowd towards the desired direction. Leaders can be either hidden in the crowd or recognizable as such. This strategy heavily relies on the power of the *social influence* (herding effect), namely the natural tendency of people to follow group mates in situations of emergency or doubt. The second one consists in modify the surrounding environment by adding in the walking area multiple obstacles optimally placed and shaped. The aim of the obstacles is to naturally force people to behave as desired. Both control strategies discussed in this paper aim at reducing as much as possible the intervention on the crowd. Ideally the natural behavior of people is kept, and people do not even realize they are being led by an external intelligence. Mathematical models are discussed at different scales of observation, showing how macroscopic (fluid-dynamic) models can be derived by mesoscopic (kinetic) models which, in turn, can be derived by microscopic (agent-based) models.

G. Albi
Dipartimento di Informatica, Università di Verona, Verona, Italy
e-mail: giacomo.albi@univr.it

E. Cristiani · D. Peri
Istituto per le Applicazioni del Calcolo, Consiglio Nazionale delle Ricerche, Rome, Italy
e-mail: e.cristiani@iac.cnr.it; d.peri@iac.cnr.it

L. Pareschi (✉)
Dipartimento di Matematica e Informatica, Università di Ferrara, Ferrara, Italy
e-mail: lorenzo.pareschi@unife.it

L. Gibelli (ed.), *Crowd Dynamics, Volume 2*, Modeling and Simulation in Science, Engineering and Technology, https://doi.org/10.1007/978-3-030-50450-2_8

1 Introduction

This paper aims at presenting a brief survey of some recent developments in the mathematical modeling and control techniques for human crowd dynamics. Here, we define *crowd dynamics control* as the art of steering large masses of people in the desired direction, minimizing verbal directives to individuals and preserving as much as possible their natural behavior. In the extreme case, we get methods to steer crowds along predefined paths without the crowd being aware of it, i.e., individuals do not even perceive that their (apparently) natural decisions are guided. Such control techniques are expected to be effective in all situations characterized by the impossibility of directly communicating with the crowd (e.g., in case of very large groups, emergencies, violent crowds reluctant to follow directions indicated by event organizers or police).

Crowd control stems on different research topics and benefits from a multidisciplinary approach. First, physics and psychology are called upon to point out the main behavioral aspects which represent the constitutive ingredients of mathematical models. Models will then be used to create a digital twin of the moving crowd. After a careful choice of the scale of observation (mainly depending on the size of the crowd and computing resources), numerical analysis is used to solve the equations and get a reproduction of virtual crowds, while real observations and data acquisition are crucial to calibrate the models. Calibration is particularly challenging, considering the high variability among persons and the difficulty of measuring some parameters like pushiness, degree of rationality, knowledge of the surrounding environment, etc. After that, we have to set up the control problem, defining the *control (design) variables*. Roughly speaking, this means that we need to identify which part of the system is subject to modifications and which part is instead left to the natural state. Then, we must define the *objective function*, i.e., the goal of the optimization procedure. Here optimization techniques come into play to solve the control problem and get the optimal strategy to apply to steer the crowd as desired. Finally, experiments with real crowds are desirable to check the effectiveness of the strategy found in virtual environments.

Curiously, some metaheuristic optimization techniques like the one adopted in Sect. 4.2 are inspired precisely by models for collective behavior: many agents spread in the abstract space of control variables hunting for the optimal strategy of the crowd. This creates a surreal parallelism between the physical space, where people move, and the space of control variables, where people's behavior lies. In the two spaces, the same abstract mathematical methods can be then used to make agents reach their goals.

1.1 Scale of Observation, Models, and Degree of Rationality

Pedestrian dynamics can be observed at different *scales*, and the choice of the point of view drastically changes the modeling framework. A *nanoscopic* approach consists in tracking every single agent, including the position of torso and head [12, 25]. A *microscopic* approach consists instead in tracking every single agent assuming s/he is a 0-dimensional point or a small circle. A *mesoscopic* approach is based on the description of average quantities like the density of people, but it keeps the possibility to distinguish one-to-one interactions. Finally, the *macroscopic* approach describes only average quantities loosing any kind of granularity.

Multiscale approaches are also possible: one can adopt different scales of observation in different parts of the domain (passing information across an interface) or one can employ two or more scales at the same time and space, to get a fully hybridized description, as in [35, 36].

Concerning *pedestrian modeling*, many kinds of models have been investigated so far and several reviews and books are available. For a quick introduction, we refer the reader to the surveys [16, 51] and the books [36, 61, 67]. Some papers deal specifically with egressing/evacuating pedestrians: a very good source of references is the paper [1], where evacuation models both with and without optimal planning search are discussed. The paper [1] itself proposes a cellular automata model coupled with a genetic algorithm to find a top-down optimal evacuation plan. Evacuation problems were studied by means of lattice models [26, 47], social force models [53, 72, 81], cellular automata models [1, 79], mesoscopic models [2, 8, 43], and macroscopic models [23]. Limited visibility issues were considered in [23, 26, 47]. Real experiments involving people can be found in [8, 47].

It can be useful to recall here that pedestrians can show different *degrees of rationality*, depending on the situation and their knowledge of the surrounding environment. In an unknown environment with limited visibility we expected people to follow basically a full instinctive behavior, being impossible to make predictions. Conversely, an ideal rational pedestrian with a specific target and full knowledge of the environment can compute her/his path in an optimal manner, is able to forecast the behavior of other pedestrians (even for long time), and is able to understand the impact of the presence of the others at any time along her/his path. In this case dynamics of people are fully coupled in space and time, and a competition among pedestrians naturally arises. Nash equilibria or similar concepts help to find the strategy eventually adopted by the participants. For a deep discussion in this direction we refer the reader to the book [36, Sect. 4.4] and papers [34, 37].

1.2 Crowd Dynamics Control

The problem of controlling crowds falls in the larger line of research dedicated to *self-organizing agents*. For this, a vast mathematical literature is available and first principles as well as the most important qualitative results are already known. The toy model for such investigations is the Cucker–Smale model [38], introduced in 2007. Controlled versions of the model are widely studied, see, e.g., [5, 7, 15, 17, 20, 44, 56]. Let us also mention the seminal paper [31], where the authors pointed out that in a group of individuals with tendency to move together, a small percentage of informed individuals is able to steer the whole group in the desired direction.

In this paper we focus on two control strategies:

- The first one consists in using special agents, called *leaders*, to steer the crowd towards the desired direction. Leaders can be either *hidden* in the crowd [8, 31, 39, 49, 50] or *recognizable* as such [6, 9, 10, 18, 40, 66, 81]. This strategy heavily relies on the power of the social influence (or herding effect), namely the natural tendency of people to follow group mates in situations of emergency or doubt. *En passant*, let us stress that the term "herding" is largely ambiguous in the literature, as pointed out in the recent paper [48].
- The second one consists in modify the surrounding environment by adding in the walking area multiple *obstacles* optimally placed and shaped. The aim of the obstacles is to smoothly force people to behave as desired, changing surrounding conditions in such a way that the modified behavior of people naturally matches the optimal one. This approach can be seen as an inverse application of the Braess's paradox [19, 58], originally proposed in the context of traffic flow on network. In that case it was noted that adding a new road (i.e., a new connection) in the network can lead to a higher degree of congestion. In our framework, an additional constraint leads paradoxically to an improvement of the pedestrian flow. Several papers investigate numerically the effectiveness of the Braess's paradox by means of both microscopic models (e.g., Helbing's social force model) and macroscopic models. Some papers report the effect of additional obstacles manually placed in the walking area, see, among others, [41, 45, 54, 57, 64, 77]. Other papers, instead, employ optimization algorithms, see [32, 33, 37, 59, 60, 75, 80]. Note that the resulting optimization problem typically is non-convex and high dimensional. Efficient optimization algorithms, including Particle Swarm Optimization (PSO), genetic algorithms, differential evolution, and random compass search, were used.

1.3 Manuscript Organization

The rest of the manuscript is organized as follows. In Sect. 2 we introduce the mathematical model for egressing pedestrians which will serve as a guideline for the rest of the paper. Main ingredients are introduced and three scales of observation

(microscopic, mesoscopic, macroscopic) are discussed. In addition, we discuss methods to manage obstacles in models, i.e., how to prevent pedestrians from entering forbidden zones of the walking area. In Sect. 3 we present crowd control techniques based on the use of leaders, either visible (i.e., recognizable from the crowd as such) or not. In Sect. 4 we analyze crowd control techniques based on the use of smart obstacles suitably located in the walking area to modify the perception of the environment and suitably modify the optimal paths. Finally, in Sect. 5 we sketch some conclusions and future research directions.

2 Different Levels of Description

In this section we describe the model at a general level. In particular we will focus on the different levels of description: microscopic, mesoscopic, and macroscopic.

2.1 Preliminary Notions

Hereafter, we divide the population between *leaders*, which are the controllers and behave in some optimal way (to be defined), and *followers*, which represent the mass of agents to be controlled. Followers typically cannot distinguish between followers and leaders. Our approach consists in describing leaders by a *first-order* model (positions are the only state variables), while followers are described by a *second-order* model (both positions and velocities are state variables). In the latter case, the small inertia typical of pedestrian motion is obtained by means of a fast relaxation towards the target velocity.

Concerning the way interactions between individuals are modeled, we adopt a mixed approach, assuming short-range interactions to be metrical and long-range ones to be topological. We recall that, the individual interactions are said to be *metrical* if they involve only mates within a predefined sensory region, regardless of the number of individuals which actually fall in it. Interactions are instead said *topological* if it involves a predefined number of group mates regardless their distance from the considered agent.

We assume here that pedestrians have a target to reach in minimal time, but the environment is in general unknown. Therefore, since individuals have no idea of the location of their target, we expect that they often look around to explore the environment and see the behavior of the others. This is why we prefer to adhere to isotropic (all-around) interactions.

Next, before introducing the details of the model, let us briefly describe the social forces acting on the agents.

- *Leaders.*
  - Leaders are subject to an isotropic metrical short-range *repulsion force* directed against all the others, translating the fact that they want to avoid collisions and that a maximal density exists.
  - Leaders are assumed to know the environment and the self-organizing features of the crowd. They respond to an *optimal force* which is the result of an offline optimization procedure, defined as to minimize some cost functional.
- *Followers.*
  - Similarly to leaders, followers respond to an isotropic metrical short-range *repulsion force* directed against all the others.
  - Followers tend to a *desired velocity* which corresponds to the velocity that would follow if they were alone in the domain. Since they do not know the environment, we assume that followers describe a *random walk* if the exit is not visible (exploration phase) or a sharp motion toward the exit if the exit is visible (evacuation phase).
  - If the exit is not visible, followers are subject to an isotropic topological *alignment force* with all the others, including leaders, i.e., they tend to have the same velocity of the group mates (herding effect). We will distinguish in the sequel between *visible* (recognized by the followers) and *invisible* (not recognized by the followers) leaders.

2.2 The Microscopic Leader-Follower Model

In this section we introduce the microscopic model for followers and leaders. We denote by d the dimension of the space in which the motion takes place (typically $d = 2$), by N^{F} the number of followers, and by $N^{\mathrm{L}} \ll N^{\mathrm{F}}$ the number of leaders. We also denote by $\Omega \equiv \mathbb{R}^d$ the walking area and by $x^\tau \in \Omega$ the target point. To define the target's visibility area, we consider the set Σ, with $x^\tau \in \Sigma \subset \Omega$, and we assume that the target is completely visible from any point belonging to Σ and completely invisible from any point belonging to $\Omega \backslash \Sigma$.

For every $i = 1, \ldots, N^{\mathrm{F}}$, let $(x_i(t), v_i(t)) \in \mathbb{R}^{2d}$ denote position and velocity of the agents belonging to the population of followers at time $t \geq 0$ and, for every $k = 1, \ldots, N^{\mathrm{L}}$, let $(y_k(t), w_k(t)) \in \mathbb{R}^{2d}$ denote position and velocity of the agents among the population of leaders at time $t \geq 0$. Let us also define $\mathbf{x} := (x_1, \ldots, x_{N^{\mathrm{F}}})$ and $\mathbf{y} := (y_1, \ldots, y_{N^{\mathrm{L}}})$.

Finally, let us denote by $B_r(x)$ the ball of radius $r > 0$ centered at $x \in \Omega$ and by $\mathcal{B}_{\mathcal{N}}(x; \mathbf{x}, \mathbf{y})$ the *minimal* ball centered at x encompassing at least $\mathcal{N}$ agents, and by $\mathcal{N}^*$ the actual number of agents in $\mathcal{B}_{\mathcal{N}}(x; \mathbf{x}, \mathbf{y})$. Note that $\mathcal{N}^* \geq \mathcal{N}$.

Remark 1 The computation of $\mathcal{B}_{\mathcal{N}}(x; \mathbf{x}, \mathbf{y})$ requires the knowledge of the positions of all the agents, since all the distances $|x_i - x|$, $i = 1, \ldots, N^{\mathrm{F}}$, and $|y_k - x|$, $k = 1, \ldots, N^{\mathrm{L}}$ must be evaluated in order to find the $\mathcal{N}$ closest agents to x.

The microscopic dynamics described by the two populations is given by the following set of ODEs: for $i = 1, \dots, N^{\mathrm{F}}$ and $k = 1, \dots, N^{\mathrm{L}}$,

$$\begin{cases} \dot{x}_i = v_i, \\ \dot{v}_i = A(x_i, v_i) + \sum_{j=1}^{N^{\mathrm{F}}} H^{\mathrm{F}}(x_i, v_i, x_j, v_j; \mathbf{x}, \mathbf{y}) + \sum_{\ell=1}^{N^{\mathrm{L}}} H^{\mathrm{L}}(x_i, v_i, y_\ell, w_\ell; \mathbf{x}, \mathbf{y}), \\ \dot{y}_k = w_k = \sum_{j=1}^{N^{\mathrm{F}}} K^{\mathrm{F}}(y_k, x_j) + \sum_{\ell=1}^{N^{\mathrm{L}}} K^{\mathrm{L}}(y_k, y_\ell) + u_k. \end{cases} \tag{1}$$

We assume that

- A is a self-propulsion term, given by the relaxation toward a random direction or the relaxation toward a unit vector pointing to the target (the choice depends on the position), plus a term which translates the tendency to reach a given characteristic speed $s \geq 0$ (modulus of the velocity), i.e.,

$$A(x, v) := \theta(x) C_z (z - v) + (1 - \theta(x)) C_\tau \left(\frac{x^\tau - x}{|x^\tau - x|} - v \right) + C_s (s^2 - |v|^2) v, \tag{2}$$

  where $\theta : \mathbb{R}^d \to [0, 1]$ is the characteristic function of $\Omega \backslash \Sigma$, $\theta(x) = \chi_{\Omega \backslash \Sigma}(x)$, z is a d-dimensional random vector with normal distribution $\mathcal{N}(0, \sigma^2)$, and C_z, C_τ, C_s are positive constants.
- The interactions follower-follower and follower-leader are defined as

$$\begin{aligned} H^{\mathrm{F}}(x, v, x', v'; \mathbf{x}, \mathbf{y}) &:= - C_r^{\mathrm{F}} R_{\gamma, r}(x, x') + \theta(x) \frac{C_{al}^{\mathrm{F}}}{\mathcal{N}^*} (v' - v) \chi_{\mathcal{B}_{\mathcal{N}}(x; \mathbf{x}, \mathbf{y})}(x'), \\ H^{\mathrm{L}}(x, v, y, w; \mathbf{x}, \mathbf{y}) &:= - C_r^{\mathrm{F}} R_{\gamma, r}(x, y) + \theta(x) \frac{C_{al}^{\mathrm{L}}}{\mathcal{N}^*} (w - v) \chi_{\mathcal{B}_{\mathcal{N}}(x; \mathbf{x}, \mathbf{y})}(y) \\ &\quad + \theta(x) C_{at} \frac{y - x}{|y - x|}, \end{aligned} \tag{3}$$

  for given positive constants C_r^{F}, C_{al}^{F}, C_{al}^{L}, C_{at}, r, and γ.

  In the first equation of (3) the term,

$$R_{\gamma, r}(x, x') = \begin{cases} e^{-|x' - x|^\gamma} \frac{x' - x}{|x' - x|}, & \text{if } x' \in B_r(x) \backslash \{x\}, \\ 0, & \text{otherwise}, \end{cases}$$

  models a (metrical) repulsive force, while the second term accounts for the (topological) alignment force, which vanishes inside Σ. Note that the interaction with the leaders, defined by the second equation in (3), accounts the previous forces with an additional attraction towards the leaders' position. With the choice $C_{at} = 0$, $C_{al}^{\mathrm{F}} = C_{al}^{\mathrm{L}}$ we have $H^{\mathrm{F}} \equiv H^{\mathrm{L}}$ and, therefore, the leaders are not recognized by the followers as special. This feature opens a wide range of new

applications, including the control of crowds not prone to follow authority's directives.
- The interactions leader-follower and leader-leader reduce to a mere (metrical) repulsion, i.e., $K^{\mathrm{F}} = K^{\mathrm{L}} = -C_r^{\mathrm{L}} R_{\zeta,r}$, where $C_r^{\mathrm{L}} > 0$ and $\zeta > 0$ are in general different from C_r^{F} and γ, respectively.
- $u_k : \mathbb{R}^+ \to \mathbb{R}^{dN^{\mathrm{L}}}$ is the control variable, to be chosen in a set of admissible control functions. Except for the short-range repulsion forces, the behavior of the leaders is entirely characterized by the control term u. More details on the control term will be given in Sect. 3.

Remark 2 As a further generalization of the above modeling, the population of leaders can be separated into two populations $(y_k^{\mathrm{V}}(t), w_k^{\mathrm{V}}(t))$, $k = 1, \ldots, N^{\mathrm{L,V}}$ and $(y^{\mathrm{I}}(t)_k, w_k^{\mathrm{I}}(t))$, $k = 1, \ldots, N^{\mathrm{L,I}}$ with $N^{\mathrm{L}} = N^{\mathrm{L,V}} + N^{\mathrm{L,I}}$, depending on whether they are recognized by the followers (visible) or not (invisible). In the first case, the corresponding interaction function $H^{\mathrm{L,V}} \neq H^{\mathrm{F}}$ since followers will have the tendency to align with greater intensity towards leaders, whereas in the second case we simply have $H^{\mathrm{L,I}} = H^{\mathrm{F}}$. In the sequel, for the sake of simplicity, we present our analysis in the case of system (1), where all leaders are either visible or invisible, leaving to a straightforward generalization of the extension of simultaneous coexistence of visible and invisible leaders.

2.3 Boltzmann Modeling

As already mentioned, our main interest in (1) lies in the case $N^{\mathrm{L}} \ll N^{\mathrm{F}}$, that is, the population of followers exceeds by far the one of leaders. When N^{F} is very large, a microscopic description of both populations is no longer a viable option. We thus consider the evolution of the distribution of followers at time $t \geq 0$, denoted by $f(t, x, v)$, together with the microscopic equations for the leaders (whose number is still small). To this end, we denote with m^{F} the total mass of followers, i.e.,

$$m^{\mathrm{F}}(t) = \int_{\mathbb{R}^{2d}} f(t, x, v)\, dx\, dv,$$

which we shall eventually require to be equal to N^{F}. We introduce, for symmetry reasons, the distribution of leaders g and their total mass

$$g(t, x, v) = \sum_{k=1}^{N^{\mathrm{L}}} \delta_{(y_k(t), w_k(t))}(x, v), \qquad m^{\mathrm{L}}(t) = \int_{\mathbb{R}^{2d}} g(t, x, v)\, dx\, dv = N^{\mathrm{L}}. \tag{4}$$

The evolution of f can be then described by a Boltzmann-type dynamics, derived from the above microscopic formulation, which is obtained by analyzing the binary interactions between a follower and another follower and the same follower with

a leader. The application of standard methods of binary interactions, see [24, 71], shall yield a mesoscopic model for the distribution of followers, to be coupled with the previously presented ODE dynamics for leaders.

To derive the Boltzmann-type dynamics, we assume that, before interacting, each agent has at his/her disposal the values $\mathbf{x}$ and $\mathbf{y}$ that s/he needs in order to perform its movement: hence, in a binary interaction between two followers with state parameter (x, v) and $(\hat{x}, \hat{v})$, the value of $H^{\mathrm{F}}(x, v, \hat{x}, \hat{v}; \mathbf{x}, \mathbf{y})$ does not depend on $\mathbf{x}$ and $\mathbf{y}$. In the case of H^{F} of the form (3), this means that the ball $B_{\mathcal{N}}(x; \mathbf{x}, \mathbf{y})$ and the value of $\mathcal{N}^*$ have been already computed before interacting.

Moreover, since we are considering the distributions f and g of followers and leaders, respectively, the vectors $\mathbf{x}$ and $\mathbf{y}$ are derived from f and g by means of the first moments of f and g, $\pi_1 f$ and $\pi_1 g$, respectively, which give the spatial variables of those distribution. Hence, we write $H^{\mathrm{F}}(x, v, \hat{x}, \hat{v}; \pi_1 f, \pi_1 g)$ in place of $H^{\mathrm{F}}(x, v, \hat{x}, \hat{v}; \mathbf{x}, \mathbf{y})$ to stress the dependence of this term on f and g.

We thus consider two followers with state parameter (x, v) and $(\hat{x}, \hat{v})$, respectively, and we describe the evolution of their velocities after the interaction according to

$$\begin{cases} v^* = v + \eta^{\mathrm{F}} \left[\theta(x) C_z \xi + S(x, v) + m^{\mathrm{F}} H^{\mathrm{F}}(x, v, \hat{x}, \hat{v}; \pi_1 f, \pi_1 g) \right], \\ \hat{v}^* = \hat{v} + \eta^{\mathrm{F}} \left[\theta(\hat{x}) C_z \xi + S(\hat{x}, \hat{v}) + m^{\mathrm{F}} H^{\mathrm{F}}(\hat{x}, \hat{v}, x, v; \pi_1 f, \pi_1 g) \right], \end{cases} \tag{5}$$

where η^{F} is the strength of interaction among followers, ξ is a random variables whose entries are i.i.d. following a normal distribution with mean 0, variance ς^2, taking values in a set $\mathcal{B}$, and S is defined as the deterministic part of the self-propulsion term (2),

$$S(x, v) = -\theta(x) C_z v + (1 - \theta(x)) C_\tau \left(\frac{x^\tau - x}{|x^\tau - x|} - v \right) + C_s (s^2 - |v|^2) v. \tag{6}$$

We then consider the same follower as before with state parameters (x, v) and a leader agent $(\tilde{x}, \tilde{v})$; in this case the modified velocities satisfy

$$\begin{cases} v^{**} = v + \eta^{\mathrm{L}} m^{\mathrm{L}} H^{\mathrm{L}}(x, v, \tilde{x}, \tilde{v}; \pi_1 f, \pi_1 g), \\ \tilde{v}^* = \tilde{v}, \end{cases} \tag{7}$$

where η^{L} is the strength of the interaction between followers and leaders. Note that (7) accounts only the change of the followers' velocities, since leaders are not evolving via binary interactions.

The time evolution of f is then given by a balance between bilinear gain and loss of space and velocity terms according to the two binary interactions (5) and (7), quantitatively described by the following Boltzmann-type equation

$$\partial_t f + v \cdot \nabla_x f = \lambda^{\mathrm{F}} Q(f, f) + \lambda^{\mathrm{L}} Q(f, g), \tag{8}$$

where λ^{F} and λ^{L} stand for the interaction frequencies among followers and between followers and leaders, respectively. The interaction integrals $Q(f, f)$ and $Q(f, g)$ are defined as

$$Q(f,f)(t) = \mathbb{E}\left(\int_{\mathbb{R}^{4d}} \left(\frac{1}{J_{\mathrm{F}}} f(t, x_*, v_*) f(t, \hat{x}_*, \hat{v}_*) - f(t, x, v) f(t, \hat{x}, \hat{v})\right) d\hat{x}\, d\hat{v}\right),$$

$$Q(f,g)(t) = \mathbb{E}\left(\int_{\mathbb{R}^{4d}} \left(\frac{1}{J_{\mathrm{L}}} f(t, x_{**}, v_{**}) g(t, \tilde{x}_*, \tilde{v}_*) - f(t, x, v) g(t, \tilde{x}, \tilde{v})\right) d\tilde{x}\, d\tilde{v}\right),$$

where the couples (x_*, v_*) and $(\hat{x}_*, \hat{v}_*)$ are the pre-interaction states that generate (x, v) and $(\hat{x}, \hat{v})$ via (5), and J_{F} is the Jacobian of the change of variables given by (5). Similarly, (x_{**}, v_{**}) and $(\tilde{x}_*, \tilde{v}_*)$ are the pre-interaction states that generate (x, v) and $(\tilde{x}, \tilde{v})$ via (7), and J_{L} is the Jacobian of the change of variables given by (7). Moreover, the expected value $\mathbb{E}$ is computed with respect to $\xi \in \mathcal{B}$.

In what follows, for the sake of compactness, we shall omit the time dependency of f and g, and hence of $Q(f, f)$ and $Q(f, g)$ too. In conclusion, we have the following combined ODE-PDE system for the dynamics of microscopic leaders and mesoscopic followers

$$\begin{cases} \partial_t f + v \cdot \nabla_x f = \lambda^{\mathrm{F}} Q(f, f) + \lambda^{\mathrm{L}} Q(f, g), \\ \dot{y}_k = w_k = \displaystyle\int_{\mathbb{R}^{2d}} K^{\mathrm{F}}(y_k, x) f(x, v)\, dx\, dv + \sum_{\ell=1}^{N^{\mathrm{L}}} K^{\mathrm{L}}(y_k, y_\ell) + u_k. \end{cases} \tag{9}$$

Remark 3 If we would have opted for a description of agents as hard-sphere particles, the arising Boltzmann equation (8) would be of Enskog type, see [76]. The relationship between the hard- and soft-sphere descriptions (i.e., where repulsive forces are considered, instead) has been deeply discussed, for instance, in [11]. In our model, the repulsive force $R_{\gamma,r}$ is not singular at the origin for computational reasons, therefore the parameters γ and r have to be chosen properly to avoid arbitrary high density concentrations.

2.4 Mean-Field Modeling

A different level of modeling is obtained by considering directly the limit for large N^{F} of the dynamic described by (1) where all individuals in principle are allowed to interact with all others. This kind of models are typically described by Fokker–Planck equations and can also be obtained directly from (8) in the quasi-invariant limit [71]. This technique, analogous to the so-called grazing collision limit in plasma physics, has been thoroughly studied in [78] and allows, as pointed out in [71], to pass from the binary Boltzmann description introduced in the previous section to the mean-field limit.

In what follows, we shall assume that our agents densely populate a small region but weakly interact with each other. Formally, we assume that the interaction strengths η^{F} and η^{L} scale according to a parameter ε, the interaction frequencies λ^{F} and λ^{L} scale as $1/\varepsilon$, and we let $\varepsilon \to 0$. In order to avoid losing the diffusion term in the limit, we also scale the variance of the noise term ς^2 as $1/\varepsilon$. More precisely, we set

$$\eta^{\mathrm{F}} = \varepsilon, \qquad \eta^{\mathrm{L}} = \varepsilon, \qquad \lambda^{\mathrm{F}} = \frac{1}{\varepsilon m^{\mathrm{F}}}, \qquad \lambda^{\mathrm{L}} = \frac{1}{\varepsilon m^{\mathrm{L}}}, \qquad \varsigma^2 = \frac{\sigma^2}{\varepsilon}. \tag{10}$$

Under the above scaling assumptions, the weak form of Eq. (8), i.e.,

$$\frac{\partial}{\partial t}\langle f, \varphi\rangle + \langle f, v \cdot \nabla_x \varphi\rangle = \lambda^{\mathrm{F}} \langle Q(f, f), \varphi\rangle + \lambda^{\mathrm{L}} \langle Q(f, g), \varphi\rangle, \tag{11}$$

for a compactly supported test function φ, where

$$\langle Q(f, f), \varphi\rangle = \mathbb{E}\left(\int_{\mathbb{R}^{4d}} \big(\varphi(x, v^*) - \varphi(x, v)\big) f(x, v) f(\hat{x}, \hat{v})\, dx\, dv\, d\hat{x}\, d\hat{v}\right), \tag{12}$$

$$\langle Q(f, g), \varphi\rangle = \mathbb{E}\left(\int_{\mathbb{R}^{4d}} \big(\varphi(x, v^{**}) - \varphi(x, v)\big) f(x, v) g(\tilde{x}, \tilde{v})\, dx\, dv\, d\tilde{x}\, d\tilde{v}\right), \tag{13}$$

reduces to the following Fokker–Planck equation (see [71] for more details)

$$\frac{\partial}{\partial t}\langle f, \varphi\rangle + \langle f, v \cdot \nabla_x \varphi\rangle = \left\langle f, \nabla_v \varphi \cdot \mathcal{G}[f, g] + \frac{1}{2}\sigma^2 (\theta C_z)^2 \Delta_v \varphi \right\rangle, \tag{14}$$

where

$$\mathcal{G}[f, g] = S + \mathcal{H}^{\mathrm{F}}[f] + \mathcal{H}^{\mathrm{L}}[g]$$

with

$$\mathcal{H}^{\mathrm{F}}[f](x, v) = \int_{\mathbb{R}^{2d}} H^{\mathrm{F}}(x, v, \hat{x}, \hat{v}; \pi_1 f, \pi_1 g) f(\hat{x}, \hat{v})\, d\hat{x}\, d\hat{v},$$

$$\mathcal{H}^{\mathrm{L}}[g](x, v) = \int_{\mathbb{R}^{2d}} H^{\mathrm{L}}(x, v, \tilde{x}, \tilde{v}; \pi_1 f, \pi_1 g) g(\tilde{x}, \tilde{v})\, d\tilde{x}\, d\tilde{v}.$$

Since φ has compact support, Eq. (14) can be recast in strong form by means of integration by parts. Coupling the resulting PDE with the microscopic ODEs for the leaders $k = 1, \ldots, N^{\mathrm{L}}$, we eventually obtain the system

$$\begin{cases} \partial_t f + v \cdot \nabla_x f = -\nabla_v \cdot (\mathcal{G}[f, g] f) + \frac{1}{2}\sigma^2(\theta C_z)^2 \Delta_v f, \\ \dot{y}_k = w_k = \displaystyle\int_{\mathbb{R}^{2d}} K^{\mathrm{F}}(y_k, x) f(x, v)\, dx\, dv + \sum_{\ell=1}^{N^{\mathrm{L}}} K^{\mathrm{L}}(y_k, y_\ell) + u_k. \end{cases} \tag{15}$$

2.5 Macroscopic Modeling

In terms of model hierarchy one could imagine to compute the moments of (15) to further reduce complexity. Let us stress that deriving a consistent macroscopic system from the kinetic equation is in general a difficult task, since equilibrium states are difficult to obtain, therefore no closure of the moments equations is possible. For self-organizing models similar to (15), in the noiseless case (i.e., $\sigma \equiv 0$), a standard way to obtain a closed hydrodynamic system is to assume the velocity distribution to be mono-kinetic, i.e., $f(t, x, v) = \rho(t, x)\delta(v - V(t, x))$, and the fluctuations to be negligible, thus computing the moments of (15) leads to the following macroscopic system for the density ρ and the bulk velocity V,

$$\begin{cases} \partial_t \rho + \nabla_x \cdot (\rho V) = 0, \\ \partial_t (\rho V) + \nabla_x \cdot (\rho V \otimes V) = \mathcal{G}_m \left[\rho, \rho^{\mathrm{L}}, V, V^{\mathrm{L}}\right] \rho, \\ \dot{y}_k = w_k = \displaystyle\int_{\mathbb{R}^d} K^{\mathrm{F}}(y_k, x) \rho(t, x)\, dx + \sum_{\ell=1}^{N^{\mathrm{L}}} K^{\mathrm{L}}(y_k, y_\ell) + u_k, \end{cases} \tag{16}$$

where $\rho^{\mathrm{L}}(x, t)$, $V^{\mathrm{L}}(x, t)$ represent the leaders' macroscopic density and bulk velocity, respectively, and $\mathcal{G}_m$ the macroscopic interaction operator, see [4, 22] for further details. For $\sigma > 0$, the derivation of a macroscopic system depends highly on the scaling regime between the noise and the interaction terms, see, for example, [21, 22, 62]. Furthermore, the presence of diffusion operator in model (15) depends on the spatial domain, therefore the derivation of a reasonable macroscopic model is not trivial and it is left for further studies.

2.6 Interaction with Obstacles

So far we have considered pedestrians influenced by the leaders' action but free to move in any direction of the space. In practical applications, however, dynamics are often constrained by walls or other kind of obstacles. Including obstacles in mathematical models is not as trivial as one can imagine. We refer the reader to [32, Sect. 2] for a review of obstacles' handling techniques proposed in the literature.

Here we recall just the three most common procedures, the first is the one we use in the numerical tests presented in this paper.

Cut Off of the Velocity Field An easy method to deal with obstacles is obtained by computing the velocity field first neglecting the presence of the obstacles, then nullifying the component of the velocity vector which points inside the obstacle. This method is used in, e.g., [8, 35, 37]. The method requires to pay attention that pedestrians do not stop walking completely because both components of the velocity vector vanish. This can happen around corners, stair-shaped obstacles, and when obstacles are very close to each other (i.e., the distance is comparable with the spatial resolution of the numerical grid). A similar but more sophisticated approach can be found in [32, Sect. 3].

Repulsive Obstacles Another easy method used to manage obstacles is obtained assuming that they generate a repulsive (social) force, exactly as pedestrians themselves do. In other words, obstacles are treated as frozen pedestrians. In this way one can use a repulsion function of the same kind to model both the interactions with group mates and with obstacles. This method is extensively used in microscopic models, see, e.g., [28, 45, 52, 63, 68–70] and also in macroscopic and multiscale models, see, e.g., [29, 30, 42, 74], with or without the pre-evaluation of the distance-to-obstacle function. The main drawback of this approach is that it is quite difficult to tune the strength of the repulsion force in such a way that the resulting behavior is both admissible and realistic. Indeed, if the force is too small there is the risk that pedestrians enter the obstacles, while if it is too large pedestrians bypass the obstacles excessively far away. The paper [29] proposes a method to tune automatically the strength of the repulsion.

Rational Turnaround In more sophisticated models which take into account the rationality and predictive ability of pedestrians, obstacles can be managed including them into the decision-making process. For example, in the Hughes's model [57] pedestrians move, at each given time, along the fastest path toward the target, considering that crowded regions slow down the walking speed. In this framework, obstacles are easily included assuming that inside them the speed is null, so that the computation of the fastest path will circumvent them automatically.

3 Crowd Controls Through Leaders

As discussed in the previous section, in order to steer the crowd towards a desired direction or target position, we want to exploit the tendency of people to follow group mates in situations of emergency or doubt (social influence or herding effect). In particular by controlling few leaders and their trajectories we want to drive the whole system of followers. In this section, we will formulate this problem in the context of optimal control theory and discuss its numerical solution. The main challenge is represented by the complexity induced by the non-linearities, and the

high-dimensionality of models (1) and (9). Hence, we are interested in efficient methods to solve this optimization problem, synthesizing strategies scalable at various levels: from micro to macro.

3.1 Optimal Control Framework

The functional to be minimized can be chosen in several ways, the effectiveness mostly depends on the optimization method which is used afterwards. The most natural functional to be minimized for a crowd of egressing pedestrian is the *evacuation time*, which can be defined as follows:

$$\min\{t > 0 \mid x_i(t) \notin \Omega \quad \forall i = 1, \dots, N^{\mathrm{F}}\}, \tag{17}$$

subject to (1) or (9) and with $u(\cdot) \in U_{\mathrm{adm}}$, where U_{adm} is the set of admissible controls (including, for instance, box constraints to avoid excessive velocities). Such functional can be extremely nonregular, therefore the search of local minima is particularly difficult. Moreover the evacuation of the total mass in many situations cannot completely be reached, in particular for the mesoscopic model where we account for a diffusion term.

In the sequel we propose two alternative optimal control problems, both designed to improve the evacuation time, and associated with different optimization methods for their solution.

3.1.1 Quadratic Cost Functional and Model Predictive Control

A first approximation of (17) can be designed introducing a quadratic cost as follows:

$$\ell(\mathbf{x}, \mathbf{y}, u) = C_1 \sum_{i=1}^{N^{\mathrm{F}}} \|x_i - x^{\tau}\|^2 + C_2 \sum_{i=1}^{N^{\mathrm{F}}} \sum_{k=1}^{N^{\mathrm{L}}} \|x_i - y_k\|^2 + C_3 \sum_{k=1}^{N^{\mathrm{L}}} \|u_k\|^2, \tag{18}$$

for some positive constants C_1, C_2, and C_3. The first term promotes the fact that followers have to reach the exit, the second forces leaders to keep contact with the crowd, and the last term penalizes excessive velocities. This minimization is performed along a fixed time frame $[0, T]$

$$\min_{u(\cdot) \in U_{\mathrm{adm}}} \int_0^T \ell(\mathbf{x}(t), \mathbf{y}(t), u(t))\, dt, \qquad \text{subject to (1) or (9).} \tag{19}$$

For this type of problem optimal solutions are typically out of reach, therefore we have to rely on suboptimal strategies. A computationally efficient way to address the optimal control problem (19) is by Model Predictive Control (MPC) [65], the method works as follows.

Algorithm 1 (MPC)

1. Set the time step Δt with $\bar{n} = 0, \dots, N_T$ such that $T = N_T \Delta t$, and the predictive parameter $N_{\mathtt{mpc}}$, where $N_{\mathtt{mpc}} \ll N_T$.
2. `while` $\bar{n} < N_T$
   a. Solve the reduced minimization problem

$$\min_{u(\cdot)\in U_{\text{adm}}} \sum_{n=\bar{n}}^{\bar{n}+N_{\mathtt{mpc}}-1} \ell(\mathbf{x}(n\Delta t), \mathbf{y}(n\Delta t), u(n\Delta t)) \tag{20}$$

   subject to a discretization of the dynamics (1).
   b. Generate an optimal sequence of controls $\{u(\bar{n}\Delta t), \dots, u((\bar{n}+N_{\mathtt{mpc}}-1)\Delta t)\}$.
   c. Evolve the dynamics of (1) for a time step Δt with $u(\bar{n}\Delta t)$.
   d. Update $\bar{n} \leftarrow \bar{n} + 1$.

   `repeat`

□

Note that for $N_{\mathtt{mpc}} = T/\Delta t$ the MPC approach solves the full time frame problem (19), whereas for $N_{\mathtt{mpc}} = 2$, it recovers an instantaneous controller. Such flexibility is complemented with a robust behavior, as the optimization is re-initialized every time step, allowing to address perturbations along the optimal trajectory.

3.1.2 Evacuated Mass Functional and Compass Search

Complete evacuation of the crowd is not always feasible; therefore, we consider as milder request to maximize the evacuated mass at final time T, minimizing the total mass inside the domain Ω as follows:

$$\min_{u(\cdot)\in U_{\text{adm}}} \left\{ m^{\text{F}}(T|u) = \int_{\mathbb{R}^d} \int_{\Omega} f(T, x, v)\, dx\, dv \right\}, \qquad \text{subject to (9)}, \tag{21}$$

where in the microscopic case the integral over the density $f(T, x, v)$ has to be interpreted in the empirical sense as sum of Dirac masses, namely

$$m^{\text{F}}(T|u) = \frac{1}{N^{\text{F}}} \sum_{i=1}^{N^{\text{F}}} \delta(x_i(t), v_i(t)) \chi_{\Omega}(x_i(t)).$$

In order to minimize such functional we move towards random methods as compass search (see [14] and the references therein), alternative methods are genetic algorithms, or particle swarm optimization which will be discussed in more details in Sect. 4.

First of all, we consider only piecewise constant trajectories, introducing suitable *switching times* for the leaders' controls. More precisely, we assume that leaders move at constant velocity for a given fixed time interval and when the switching time is reached, a new velocity vector is chosen. Therefore, the control variables are the velocities at the switching times for each leader. In order to optimize such strategy we define the following Compass Search (CS) algorithm.

Algorithm 2 (CS)

1. Select a discrete set of sample times $S_M = \{t_1, t_2, \dots, t_M\}$, the parameters $k = 0$, $k_{\max}$ and m_E.
2. Select an initial strategy u^* piecewise constant over the set S_M, e.g., constant direction and velocity speed towards the target x^τ (*go-to-target*)

$$u_j^*(t) = -\frac{y_j(0) - x^\tau}{\|y_j(0) - x^\tau\|}, \quad j = 1, \dots, N^{\mathrm{L}},$$

   compute the functional $m(T|u^*)$.
3. Perform a perturbation of the piecewise constant $u^*(t)$ with small random variations over the time-set S_M

$$u^{(k)}(t_m) = u^*(t_m) + B_m, \quad m = 1, \dots, M, \tag{$\mathcal{P}$}$$

   where B_m is a random perturbation of the velocity at time t_m. Finally compute $m(T|u^{(k)})$.
4. `while` $k < k_{\max}$ AND $m(T|u^*) < m_E$

   a. Update $k \leftarrow k + 1$.
   b. Perform the perturbation ($\mathcal{P}$) and compute $m(T|u^{(k)})$
   c. `If` $m(T|u^{(k)}) \le m(T|u^*)$
      set $u^* \leftarrow u^{(k)}$ and $m(T|u^*) \leftarrow m(T|u^{(k)})$.

   `repeat`

□

Remark 4 In the following some remarks concerning the above control settings.

- Both MPC and CS approaches produce suboptimal controls, but they offer a good compromise in terms of computational efficiency.
- Controlling directly the velocities rather than the accelerations makes the optimization problem much simpler because minimal control variations have an immediate impact on the dynamics.
- In the mesoscopic scale, both functionals (17) and (18) can be considered, however, the major difficulty to reach a complete evacuation of the continuous

density is mainly due to the presence of the diffusion term and to the invisible interaction with respect to the leaders. Indeed the action of the Laplacian outside the visibility area causes the followers' density to spread overall the domain. Hence without any further assumptions such non-linear diffusion, boundary conditions, or stronger interaction terms exist among followers and followers-leaders. Thus, in order to deal with the optimal control of the mean-field model, we will consider functional (21), namely the mass evacuated at the final time T.

3.2 Numerical Experiments

In this section, we present some numerical tests to validate our modeling framework at the microscopic and mesoscopic level. We explore three different scenarios for pedestrians: in Setting 1 (S#1) we discuss the difference between visible and invisible leaders; in Setting 2 (S#2) and 3 (S#3) we explore situation without and with obstacles, respectively.

The dynamics at microscopic level (1) is discretized by means of the explicit Euler method with a time step $\Delta t = 0.1$. The evolution of the kinetic density in (15) is approximated by means of binary interaction algorithms, which approximates the mesoscopic model (9) simulating the Boltzmann dynamics (8) with a Monte Carlo method for small values of the parameter ε, as presented in [3]. We choose $\varepsilon = 0.02$, $\Delta t = 0.01$, and a sample of $N_s = O(10^4)$ particles to reconstruct the kinetic density for Setting 0 and 1, and $N_s = O(4 \times 10^3)$ for S#2. This type of approach is inspired by numerical methods for plasma physics and it allows to solve the interaction dynamics with a reduced computational cost compared with mesh-based methods, and an accuracy of $O(N_s^{-1/2})$. For further details on this class of binary interaction algorithms see [3, 71].

Concerning optimization, in the microscopic case we adopt either the compass search with functional (17) or MPC with functional (19). In the mesoscopic case we adopt the compass search with functional (21).

In S#2 and S#3 we set the compass search switching times every 20 time steps, and in S#3 every 50, having fixed the maximal random variation to 1 for each component of the velocity. In S#1, the inner optimization block of the MPC procedure is performed via a direct formulation, by means of the `fmincon` routine in MatLab, which solves the optimization problem via an SQP method.

In Table 1 we report the various parameters used for the different settings.

Table 1 Model parameters for the different scenarios

Setting	N^{L}	N^{F}	$\mathcal{N}$	C_r^{F}	C_r^{L}	C_{al}^{L}	C_{al}^{F}	C_{at}	C_z	C_τ	C_s	s^2	$r = \zeta$	γ
#1	3	150	10	2	1.5	3	3	0.01/0	–	1	0.5	0.4	1	1
#2	0–3	150	10	2	1.5	3	3	0	1	1	0.5	0.4	1	1
#3	0–2	150	10	2	1.5	3	3	0	1	1	0.5	0.4	1	1

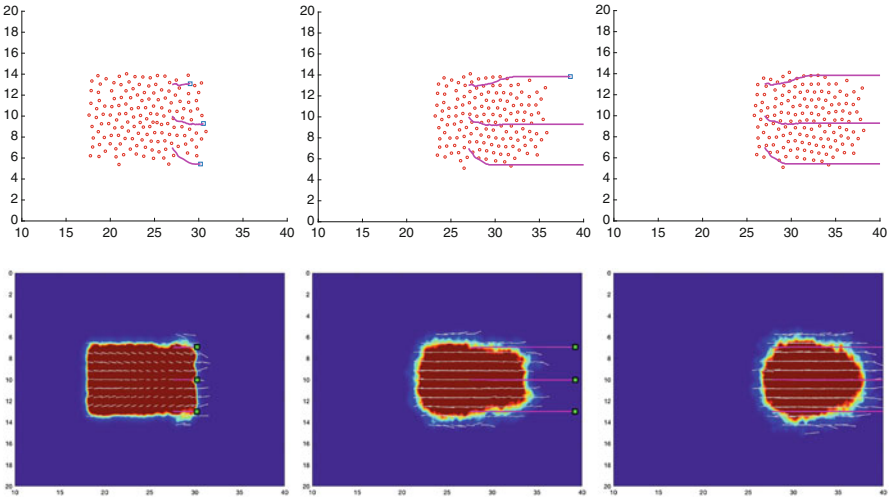

Fig. 1 *S#1- Visible leaders*. Evolution of microscopic density guided by three visible leaders. Top row shows the microscopic system, bottom row the mesoscopic system

3.2.1 S#1. Visible vs Invisible Leaders

We investigate numerically the difference among invisible and visible leaders, namely we distinguish situations where leaders are undercover with respect to cases where leaders act as an attractor of the crowd.

In this first setting the crowd of followers is distributed uniformly in the space domain with initial velocity randomly distributed with zero average, the leaders are positioned on the far right side of the crowd moving with fixed velocity $w_\ell = (|\mathrm{v}|, 0)^T$ for every $\ell = 1, 2, 3$, and no target is visible.

In Fig. 1 we observe the evolution of microscopic and mesoscopic models density for visible leaders and speed $\mathrm{v} = 1.5$. In both cases it is evident that the visibility plays a central role in attracting the whole crowd in the direction of leaders' movement.

In Fig. 2 we observe the same situation with invisible leaders reducing the speed to $\mathrm{v} = 0.5$, in order to let the leaders interact for longer time with the followers. Indeed, in this case the followers are only partially influenced by the leaders, and only the mass close to them is driven towards the right direction, the remaining part spreads in the domain.

These experiments confirm that the action of invisible leaders is in general more subtle on the crowd influence, and determining effective strategies poses an additional challenge to the crowd control.

Moreover we can also infer that for the invisible case the initial positioning of leaders is of paramount importance to maximize their impact on the crowd dynamics.

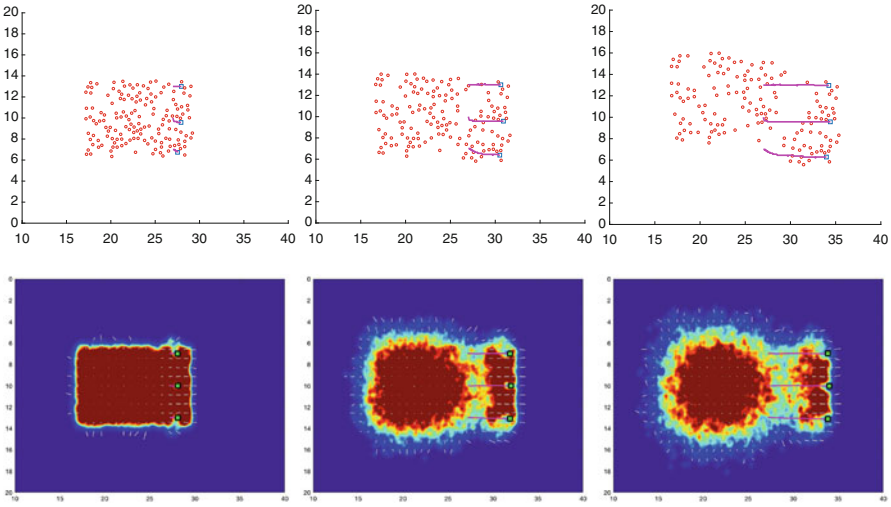

Fig. 2 *S#1- Invisible leaders*. Evolution of microscopic density guided by three invisible leaders. Top row shows the microscopic system, bottom row the mesoscopic system

3.2.2 S#2. Invisible Leaders Guiding a Crowd

We consider now the case of invisible leaders. We compare microscopic and mesoscopic framework and the evolution of the followers according to three strategies of the leaders:

- no action (leaders behave as normal followers);
- go-to-target (leaders point straight at the target);
- optimized strategy (an optimization algorithm is used to find the optimal strategy with respect to some criterion).

Differently from S#1 the crowd is now placed between the leaders and the exit. In this way leaders, moving to the exit, break more easily the initial uncertainty and trigger the crowd of followers toward the correct direction.

Microscopic Model

Figure 3 (first row) shows the evolution of the agents computed by the microscopic model, without leaders. Followers having a direct view of the exit immediately point towards it, and some group mates close to them follow thanks to the alignment force. On the contrary, farthest people split in several but cohesive groups with random direction and never reach the exit.

Figure 3 (second row) shows the evolution of the agents with three leaders. The leaders' strategy is defined manually. More precisely, at any time the control is equal

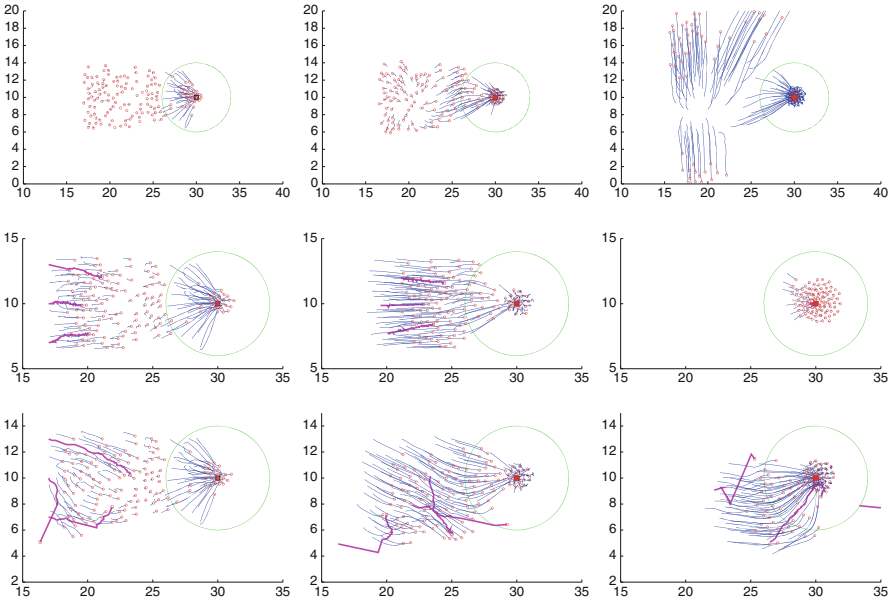

Fig. 3 *S#2- Microscopic dynamics*. First row: no leaders. Second row: three leaders, go-to-target strategy. Third row: three leaders, optimal strategy (compass search)

to the unit vector pointing towards the exit from the current position (go-to-target strategy).

The initial position of the leaders plays a central role. Indeed having placed them on the left-side of the crowd, their motion generates a larger influence into the followers' dynamics. This is in contrast with the behavior observed in Fig. 1: where only a small portion of the pedestrians was triggered by the leaders positioned on the right-hand side of the crowds.

Note also that the final leaders' trajectories are not straight lines because of the additional repulsion force. As it can be seen, the crowd behavior changes completely since, this time, the whole crowd reaches the exit. However, followers form a heavy congestion around the exit. It is interesting to note that the shape of the congestion is circular: this is in line with the results of other social force models as well as physical observation, which report the formation of an "arch" near the exits. The arch is correctly substituted here by a full circle due to the absence of walls. Note that the congestion notably delays the evacuation. This suggests that the strategy of the leaders is not optimal and can be improved by an optimization method.

Figure 3 (third row) shows the evolution of the agents with three leaders and the optimal strategy obtained by the compass search algorithm. Surprisingly enough, the optimizator prescribes that leaders *divert* some pedestrians from the right direction, so as not to steer the whole crowd to the exit at the same time. In this way congestion is avoided and pedestrian flow through the exit is increased.

In this test we have also run the MPC optimization, including a box constraint $u_k(t) \in [-1, 1]$. We choose $C_1 = 1$, and $C_2 = C_3 = 10^{-5}$. MPC results are consistent in the sense that for $N_{\mathtt{mpc}} = 2$, the algorithm recovers a controlled behavior similar to the application of the instantaneous controller (or go-to-target strategy). Increasing the time frame up to $N_{\mathtt{mpc}} = 6$ improves both congestion and evacuation times, but results still remain non-competitive if compared to the whole time frame optimization performed with a compass search.

In Fig. 4 we compare the occupancy of the exit's visibility zone as a function of time for go-to-target strategy and optimal strategies (compass search, 2-step, and 6-step MPC). We also show the decrease of the value function as a function of attempts (compass search) and time (MPC). Evacuation times are compared in Table 2. It can be seen that only the long-term optimization strategies are efficient, being able to moderate congestion and clogging around the exit.

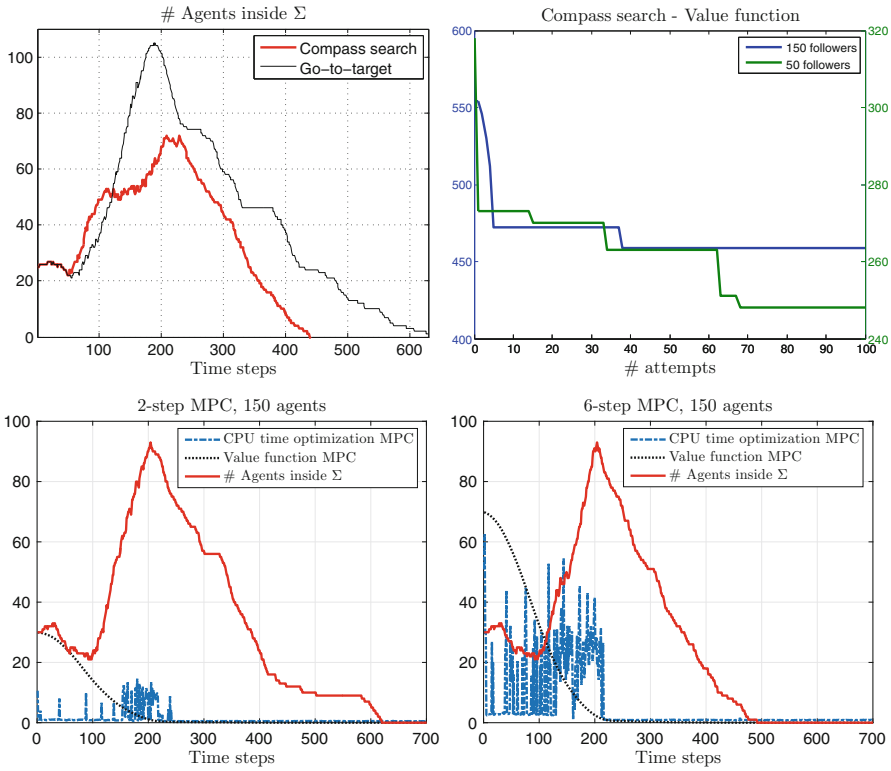

Fig. 4 *S#2-Microscopic dynamics*. Optimization of the microscopic dynamics. Top-left: occupancy of the exit's visibility zone Σ as a function of time for optimal strategy (compass search) and go-to-target strategy. Top-right: decrease of the value function (17) as a function of the iterations of the compass search (for 50 and 150 followers). Bottom: MPC optimization. occupancy of the exit's visibility zone Σ as a function of time, CPU time of the optimization call embedded in the MPC solver, and the evolution of the corresponding value (2-step and 6-step)

Table 2 S#1. Evacuation times (time steps)

	No leaders	Go-to-target	2-MPC	6-MPC	CS (IG)
$N^F = 50$	335	297	342	278	248 (318)
$N^F = 150$	∞	629	619	491	459 (554)

CS compass search, *IG* initial guess

This suggests a quite unethical but effective evacuation procedure, namely misleading some people to a false target and then leading them back to the right one, when exit conditions are safer. Note that in real-life situations, most of the injuries are actually caused by overcompression and suffocation rather than urgency.

Mesoscopic Model

We consider here the case of a continuous density of followers. Figure 5 (first row) shows the evolution of the uncontrolled system of followers. Due to the diffusion term and the topological alignment, large part of the mass spreads around the domain and is not able to reach the target exit.

In Fig. 5 (second row) we account the action of three leaders, driven by a go-to-target strategy defined as in the microscopic case. It is clear that also in this case the action of leaders is able to influence the system and promote the evacuation, but the presence of the diffusive term causes the dispersion of part of the continuous density. The result is that part of the mass is not able to evacuate, unlike the microscopic case.

In order to improve the go-to-target strategy we rely on the compass search, where, differently from the microscopic case, the optimization process accounts the objective functional (21), i.e., the total mass evacuated at final time. Figure 5 (third row) sketches the optimal strategy found in this way: on the one hand, the two external leaders go directly towards the exit, evacuating part of the density; on the other hand the central leader moves slowly backward, misleading part of the density and only later it moves forwards towards the exit. The efficiency of the leaders' strategy is due in particular by the latter movement of the last leader, which is able to gather the followers' density left behind by the others, and to reduce the occupancy of the exit's visibility area by delaying the arrival of part of the mass.

In Fig. 6 we summarize, for the three numerical experiments, the evacuated mass and the occupancy of the exit's visibility area Σ as functions of time. In the right plot the occupancy of the exit's visibility area shows clearly the difference between the leaders' action: for the go-to-target strategy, the amount of mass occupying Σ concentrates and the evacuation is partially hindered by the clogging effect, as only 66.3% of the total mass is evacuated. The optimal strategy (obtained after 30 iterations) is able to better distribute the mass arrival in Σ, and a higher efficiency is reached, evacuating up to 84.1% of the total mass.

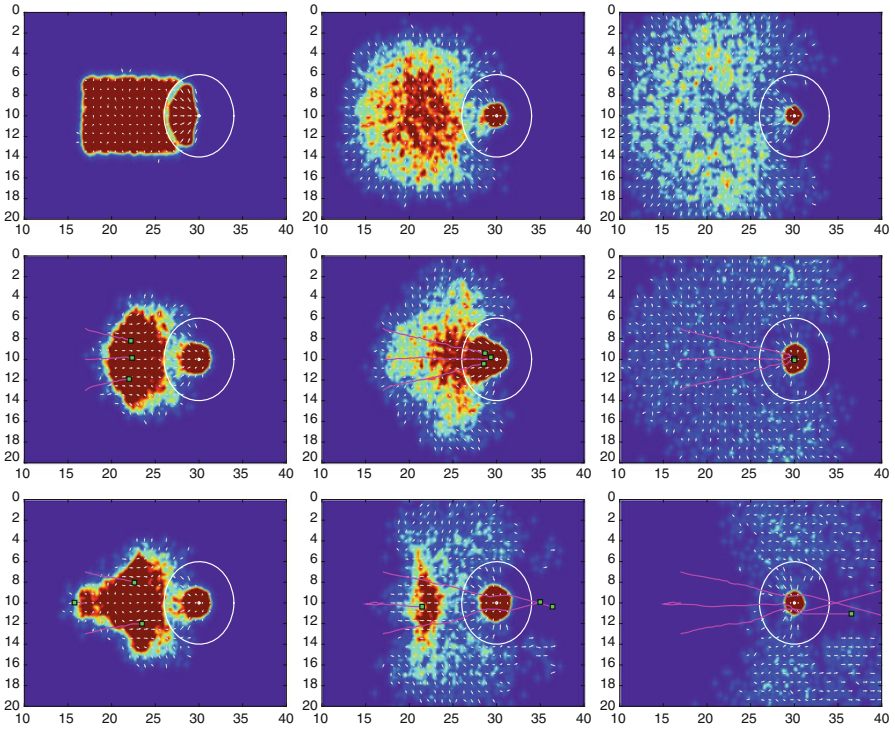

Fig. 5 *S#2-Mesoscopic dynamics*. First row: no leaders. Second row: three leaders, go-to-target strategy. Third row: three leaders, optimal strategy (compass search)

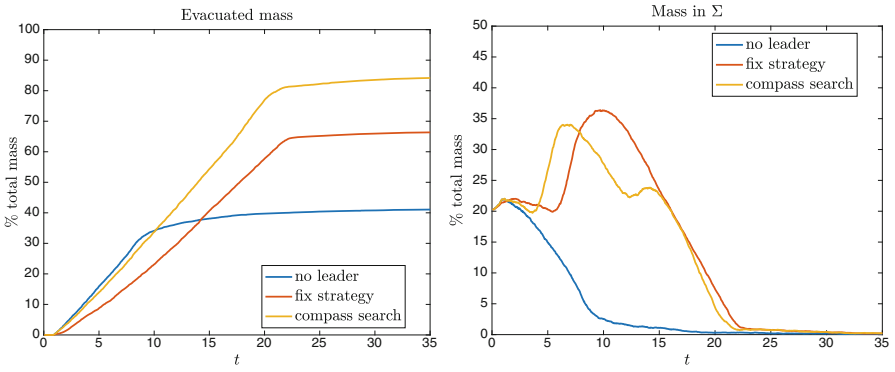

Fig. 6 *S#2. Invisible leaders' control*. On the left: percentage of mass evacuated in time. On the right: occupancy of the visibility area in terms of total mass percentage

3.2.3 S#3. Invisible Leaders in Presence of Obstacles

Finally we test the microscopic and mesoscopic model in presence of obstacles. The crowd is initially confined in a rectangular room with three walls. In order to evacuate, people must first leave the room and then search for the exit point. We assume that walls are not visible, i.e., people can perceive them only by physical contact. This corresponds to an evacuation in case of null visibility (but for the exit point which is still visible from within Σ). Walls are handled as in [35].

Microscopic Model

In Fig. 7 (first row) we observe the case where no leaders are present: the crowd splits in several groups and most of the people hit the wall. After some attempts the crowd finds the way out, and then it crashes into the right boundary of the domain. Finally, by chance people decide, *en cascade*, to go upward. The crowd leaves the domain in 1162 time steps.

If instead we hide in the crowd two leaders who point fast towards the exit (Fig. 7 (second row)), the evacuation from the room is completed in very short time, but after that, the influence of the leaders vanishes. Unfortunately, this time people decide to go downward after hitting the right boundary, and nobody leaves

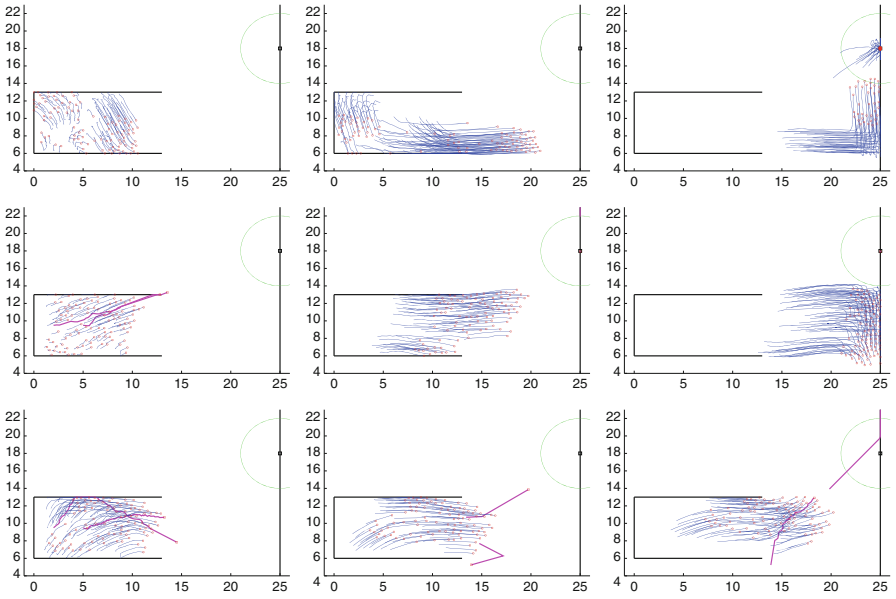

Fig. 7 *S#3-Microscopic simulation*. First row: no leaders. Second row: two leaders and go-to-target strategy. Third row: two leaders and best strategy computed by the compass search

the domain. Slowing down the two leaders helps keeping the leaders' influence for longer time, although it is quite difficult to find a good choice.

Compass search optimization finds (after 30 iterations) a nice strategy for the two leaders which remarkably improves the evacuation time, see Fig. 7 (third row). One leader behaves similarly to the previous case, while the other diverts the crowd pointing SE, then comes back to wait for the crowd, and finally points NE towards the exit. This strategy allows to bring everyone to the exit in 549 time steps, without bumping anyone against the boundary, and avoiding congestion near the exit.

Mesoscopic Model

In Fig. 8 we report the evolution of the mesoscopic density of followers. First row shows the evolution of the uncontrolled case, contrary to the microscopic in this case evacuation is not reached: the mass slowly diffuse outside the corridor and move in the opposite direction with respect the target exit, only a small percentage of the mass is able to evacuate.

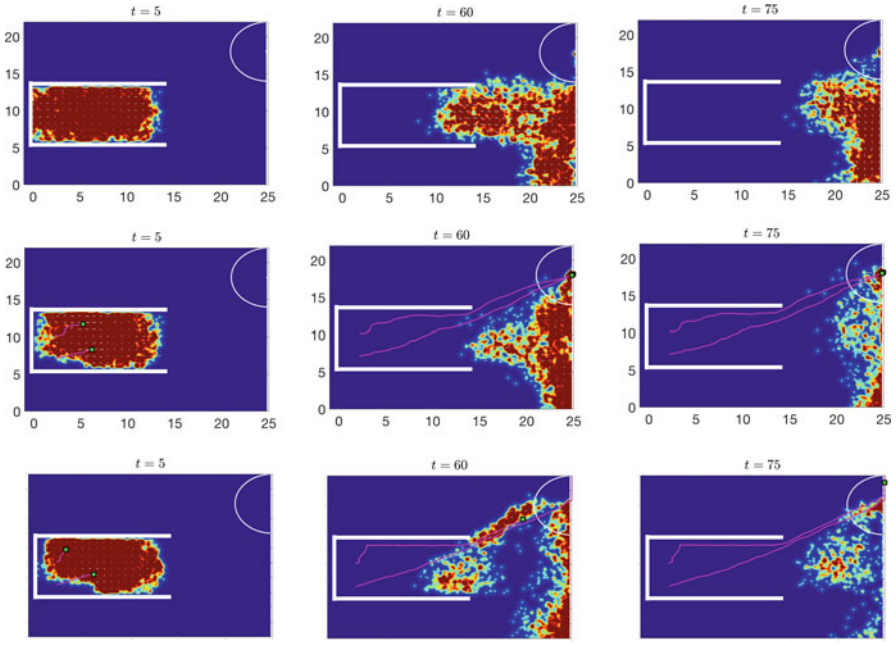

Fig. 8 *S#3-Mesoscopic dynamics*.Top row: uncontrolled setting. Middle row: two invisible leaders with go-to-target strategy. Bottom row: two invisible leaders with optimized strategy (compass search)

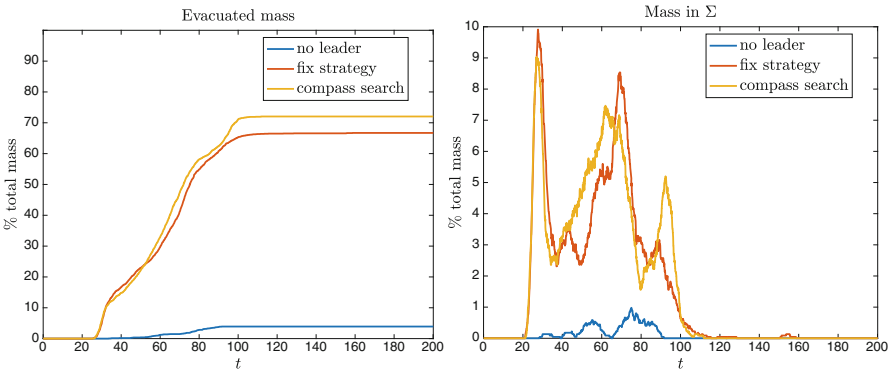

Fig. 9 *S#3. Invisible leaders' control*. On the left: percentage of mass evacuated in time. On the right: occupancy of the visibility area in terms of total mass percentage

Second rows depict the case with two leaders and a go-to-target strategy, positioned at the end of the corridor. Their movements are able to influence large part of the crowd, at final time 67.2% of the mass is evacuated.

Employing the compass search method we show in the bottom row of Fig. 8 an improvement of the go-to-target strategy (after 9 iterations). In this case evacuation of the 72.4% of the total mass is reached: one of the two leaders deviates from the original direction, slowing down part of the mass. Similarly to the optimal strategy retrieved in S#2, the optimization suggests to avoid congestion around the exit.

We compare in Fig. 9 the outcomes of the three different situations. The left plot reports the percentage of evacuated mass as a function of time, On the right we depict the occupancy of the visibility area. We observe that also in this case the optimal strategy suggests to decrease the congestion around the exit in order to increase the total mass evacuated.

4 Crowd Controls Through Smart Obstacles

The exploration activity of an unknown environment by a group of pedestrians may become crucial if the time of egress represents a critical variable. This could not be only connected with a specific state of danger, like in case of fire or earthquake, because even staying too long into an environment can be undesirable. For this reason, several signals and other indications need to be accurately located in order to correctly address a crowd entering a room. Unfortunately, in case of low visibility, the classical signage cannot be perceived, and other devices can be adopted to this aim, like lighting and sound effects.

Also the shape of the room can be designed to facilitate the egress. Walls or obstacles can be shaped in order to operate a guidance of the crowd, and several studies gave evidence of the usefulness of this strategy [32, 33]. On the other hand,

the number of obstacles cannot be too large, in order to preserve the original purpose of the room. As an extreme situation, if we lock every useless passage of a maze, we are minimizing the egress time, but we have no longer a maze.

In the following, we are illustrating the activity of optimization of the position of a number of fixed walls to minimize the egress time of a crowd from a simple square room with four entrance and four exit. The simulation of the crowd movement is performed by means of the *micro-scale* model previously described in Sect. 2.

4.1 Selection of the Objective Function

Due to the presence of a random component in the speed of the single pedestrian, the final egress time of the crowd estimated by the numerical model is a stochastic outcome. If we want to utilize this quantity as the objective function of an optimization problem, a statistical approach is essential. We can compute the expected value if we repeat the simulation a large number of times, but this data is, in our opinion, still not sufficiently representative. In fact, the variability of the egress time is also fundamental. For this reason, we are here considering as objective function the sum of expected value plus their variance,

$$\mathcal{F} = EV(x) + \sigma(x).$$

With this definition, we can assure with a probability of 80.15% that the egress time is lower than $\mathcal{F}$ (if the egress time follows a normal distribution).

Now we need to have an estimate of the number of times we need to repeat the simulation in order to have a stable value of the statistical indicators. To do that, some numerical tests have been produced. The simulator has been run for a number M of times, and this block of M simulations have been repeated for 256 times. For each block, we can compute the expected value and the variance: after that, we can also analyze statistically the 256 blocks, computing the effective value and variance of the elementary expected value. Results are reported in Fig. 10.

The experimental probability distribution (EPD) of the expected value for the different blocks of simulations is reported in Fig. 11. From this picture, it is evident that a stable value of the expected value cannot be obtained if the number of simulations for each block is lower than 128. This information is also deducible observing the right sub-graph of Fig. 10: the expected value becomes stable for the indicated number of simulations. As a consequence, in the following 256 simulations will be applied in order to evaluate the qualities of a room configuration.

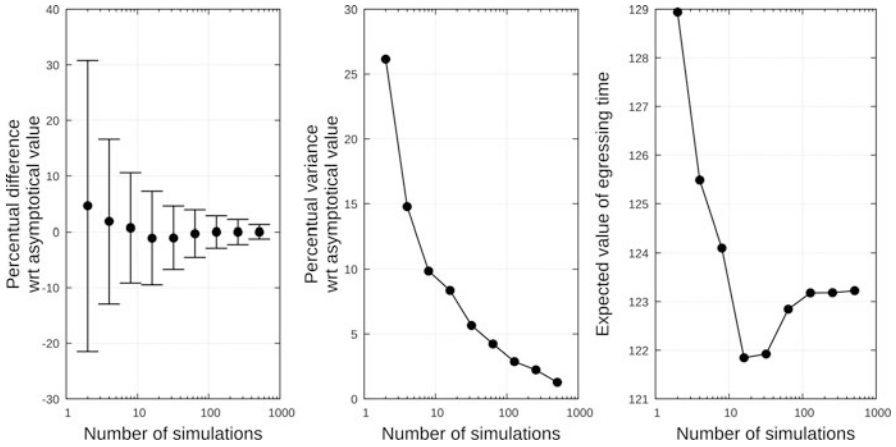

Fig. 10 Expected value and variance as a function of the number of simulations

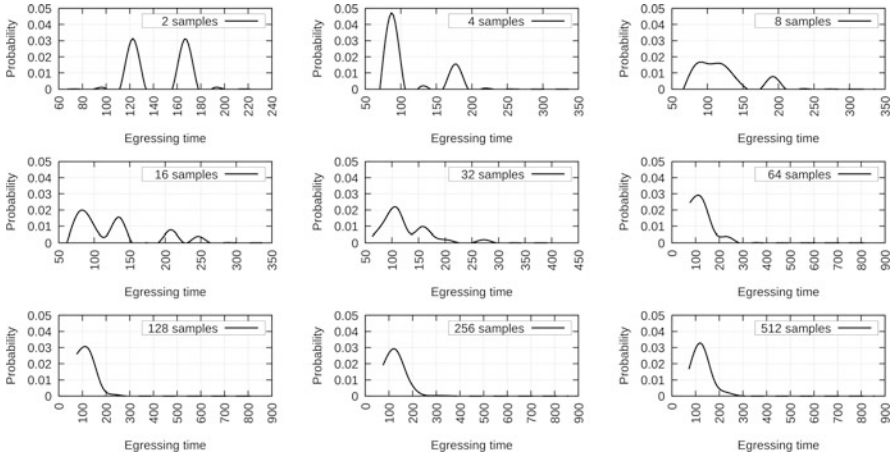

Fig. 11 Experimental probability distribution of the expected value for the different blocks of simulations

4.2 Optimization Algorithm

In this study, a heuristic optimization algorithm is adopted, namely the Imperialist Competitive Algorithm (`ICA`). In its original formulation [13], the `ICA` is described as an evolutionary algorithm. A number of trial vectors of parameters, each defining a different configuration of the system (*county*), are distributed onto the design space and assigned to different groups: each group is called *empire*. The *county* presenting the most convenient value of the objective function inside an *empire* is called *imperialist*, and each *county* is placed under the control of a single *imperialist*. Since here we are referring to a minimization problem, the *most convenient value*

is represented by the lower value of the objective function. More details about the algorithm can be found in [13]. In the original formulation, the initialization of the *counties* is performed randomly. The *counties* are then assigned to an *imperialist* on the base of their relative power, so that, at the beginning, the most powerful *imperialist* have the control of a larger *empire*. At each iteration, three main actions are performed:

- **Shifting the *counties*:** each *county* is moved toward the *imperialist* according to the equation

$$\mathbf{X}_{t+1}^k = \mathbf{X}_t^k + r\beta(\mathbf{X}^i - \mathbf{X}_t^k), \tag{22}$$

  where $\mathbf{X}$ is the generic vector of the coordinates of a point in the design variable space, $\mathbf{X}^i$ is the position of the (fixed) *imperialist* controlling the moving k^{th} *county* $\mathbf{X}^k$, t is the current iteration, k is identifying the *county*, β is the so-called *assimilation coefficient*, controlling the attractive action of the *imperialist* on the *county*, and r is a random number in between 0 and 1. If the product $r\beta$ is greater than the unit value, the *county* will overpass the *imperialist*, changing the side from which the *county* observes the *imperialist*. The displacement vector $(\mathbf{X}_{t+1}^k - \mathbf{X}_t^k)$ is further deviated from the indicated direction by a random angle in between $-\theta$ and $+\theta$, θ to be fixed.
- **Change of the *imperialist*:** if a *county* finds a value of the objective function smaller than the value owned by the referenced *imperialist*, the positions of the *county* and the *imperialist* are swapped.
- **Imperialistic competition:** the power of each *empire* is computed as the power of the *imperialist* plus a fraction ξ of the sum of the powers of the single *counties* of the *empire*. The worst *county* of the worst *empire* is re-assigned to the best *empire*. In a minimization process, the average value of the power of the *counties* is summed up to the power of the *imperialist*: lower value means higher power.
- ***Empire* elimination:** if, after the *Imperialistic Competition*, an *Imperialist* has no more *counties* under his control, the *empire* is eliminated.

Looking at Eq. (22), we can observe the full equivalence with the one dimensional, first-order, autonomous, linear differential equation that governs the evolution of a state variable

$$y_{t+1} = ay_t + b. \tag{23}$$

In fact, Eq. (23) is absolutely equivalent to Eq. (22) once we rewrite it in the reference frame of the *imperialist*. Since the value of the state variables is assigned at the beginning, that is, the relative position of the *county* with respect to the *imperialist*, at the first step we have

$$y_1 = ay_0 + b. \tag{24}$$

Applying Eq. (23), we have that at step t

$$y_t = a^t y_0 + b \sum_{i=0}^{t-1} a^i. \tag{25}$$

If $b = 0$, we can demonstrate that, if $0 < a < 1$, the series converges to the zero value (the origin of the reference frame) [46]. Since the local reference frame of an *Empire* coincides with an *imperialist*, each *county* converges toward the corresponding *imperialist*. To be more explicit, we can simplify Eq. (22) by rewriting it in the reference frame of the *imperialist*: the term $\mathbf{X^i}$ disappears, and the equation now reads

$$\mathbf{X}_{t+1} = \mathbf{X}_t - r\beta \mathbf{X}_t = (1 - r\beta)\mathbf{X}_t.$$

We are clearly in the case of Eq. (23) where $b = 0$ and $a = (1 - r\beta)$. The motion is developing along the direction connecting the initial position of the *county* and the origin of the reference frame (that is, the *imperialist*). The *county* is converging on the corresponding *imperialist*: convergence is monotone or not depending on the value of β. Since the coefficient a needs to be positive and smaller than the unit value in order to have convergence [46], we have convergence if

$$0 < 1 - r\beta < 1 \Rightarrow \beta < \frac{1}{r}; \quad r\beta > 0.$$

The different terminology adopted for the description of the algorithm is hiding a substantial similarity between `ICA` and the multi-swarm Particle Swarm Optimization (`PSO`) formulation [55]. With respect to the original formulation of `PSO`, the `ICA` has not a personal memory, so that the new position of a *county* is not influenced by the positions previously visited by itself, while `PSO` is using this information. Conversely, both `PSO` and `ICA` show a limited interaction with the other elements of the *empire*: in fact, the *Imperialist* is the equivalent of the best element of `PSO`, that is, the best visit of the whole swarm/*empire*. The great difference with `PSO` is the aforementioned proof of convergence of `ICA`, while for `PSO` an incomplete proof of convergence can be obtained [27].

An improvement of the original `ICA` is proposed in [73], namely `hICA`, and this version of the algorithm is here applied. The improvements obtained by `ICA` can be addressed mainly to the following modifications:

1. The initial distribution of the *counties* is not random, but it is produced using a Uniformly Distributed Sequence.
2. The coefficients in Eq. (22) have been optimized.
3. The *empires* are re-initialized if only a single *empire* is survived.
4. A local search algorithm (Simplex method) is applied if we have no improvements of the current best solution after a certain number of iterations. This is surely one of the main improvements of the algorithm.

4.3 Test Case

In order to empathize the ability of a fixed obstacle to efficiently redirect the flow of a group of pedestrians, such that the evacuation time is minimized, a very simple test case has been designed. Four entrance and four exit are symmetrically placed in a square room. The entrances are at the corners, the exit at the center of each side of the room. The role of the obstacle(s), in this case, is to break the symmetry of the flow, avoiding indecision (and the subsequent dead time) when different sub-groups are colliding, exploiting also all the exits.

The full number of pedestrians has been fixed to 100, in order to have a good balance between interactions and computational time. Simulation has been repeated 256 times for each configuration of the room in order to derive statistical variables, as from the indications collected previously (Fig. 10).

The only constraint is related to the distance between the wall and the obstacle, in order to avoid blockage effects (and also the exclusion of an exit or an entrance).

Regarding the selection of the obstacle(s), two different cases have been considered: one or two linear walls. A single wall is defined using four variables: two for the barycentre of the wall, one for its full length and one for the orientation (in between 0 and 90°). The width of the wall is fixed. As a consequence, we have four design variables for a single wall and eight design variables for a couple of walls. The design variables are selected in order to reduce the possibility of violation of the constraint, so that the barycentre of the wall cannot stay on the border of the room. Minimum and maximum length of the walls are also fixed.

Stopping criterion for the optimization algorithm is represented only by the full number of evaluations of the objective function: in order to balance the opportunities of the two optimization problems, in accordance with [73], the maximum number has been fixed at $1000 \times NDV$, where NDV is the number of design variables. Consequently, the problem with more design variables takes longer to complete.

Due to the symmetry of entrance and exit, the solution of the problem is cyclical, since four configurations can be obtained by a rotation of 90° around the center of the room.

4.4 Numerical Results

In Fig. 12, the convergence history of the two optimization problems is reported. The rate of convergence of the two problems is very similar as soon as, in the case of two walls, the optimizer is able to identify a new solution improving largely the egress time, further refined in the last part of the optimization problem solution. On the contrary, the identification of the optimal solution for the problem with a single wall appears to be pretty fast, and only marginal improvements are obtained after a couple of iterations: this is probably connected with the simplicity of the shape of the obstacle, unable to create a great variety of convenient situations.

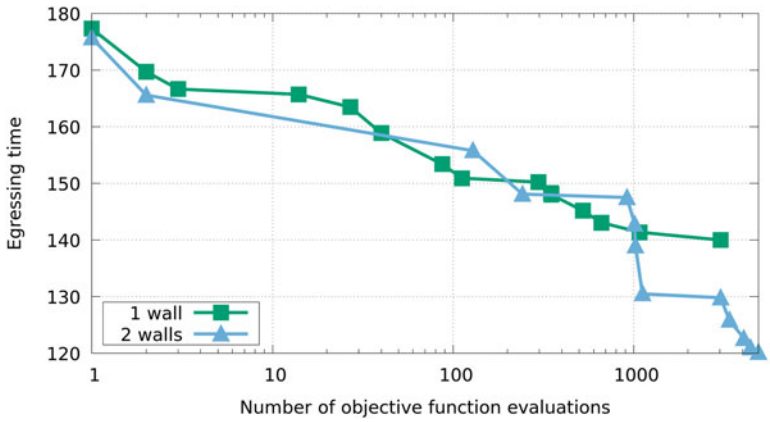

Fig. 12 Convergence history of the optimization problems: case of the room with one obstacle and room with two obstacles

Table 3 Expected value, most probable value, variance, and objective function for the different optimal configurations plus the case of empty room

	EV	$\Delta\%$	Most probable	$\Delta\%$	σ	$\Delta\%$	$EV + \sigma$	$\Delta\%$
Empty	133.22		114.43		39.99		173.21	
1 Obs.	114.66	−14.10%	100.73	−12.28%	36.94	−7.63%	151.60	−12.48%
2 Obs.	93.50	−29.82%	59.71	−48.00 %	37.22	−6.93%	130.72	−24.53%

Statistics are obtained performing 100,000 simulations

The expected value, the most probable egress time, the variance of the egress time and the objective function value for the original and for the optimal room configurations are reported in Table 3. One might therefore imagine that the regularization of the pedestrian flow, obtained through the obstacles, would also reduce the variability of the dwell time into the room. The reason of the small reduction of the variance can be linked with the constraint on the distance between the wall and the sides of the room: there is still a quite large gap between the obstacles and the borders. This gap has been introduced considering the fact the main function the room is designed for must be preserved after the insertion of the walls, so that their impact on the environment should be limited. As a consequence, the pedestrians, although driven toward the exit, have still a quite large space to explore, and the random component of the individual speed plays a not negligible role. As a consequence, the variance of the egress time is substantially not changing.

It is really interesting to compare the EPD of the egress times for the case of empty room with the ones of the optimized solutions. For these three configurations, 100,000 simulations have been produced in order to increase the stability and credibility of the statistic indicators. The most probable value of the egress time is shifted to the lower values passing from empty room to one obstacle to two obstacles, as it is also evident from Table 3. In this last case, the higher probability

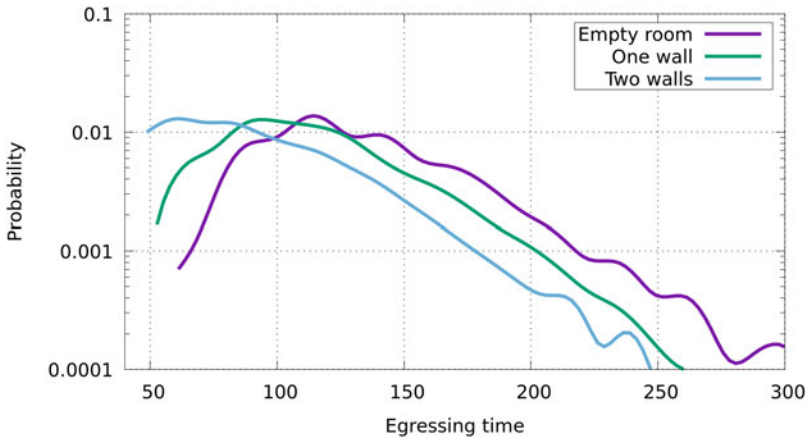

Fig. 13 Experimental probability distribution of the egress time in the case of empty room, room with one obstacle and room with two obstacles

is very close to the minimum egress time, representing a very good feature of the optimal configuration (Fig. 13).

In Fig. 14, the trajectories of the pedestrians are reported: from top to bottom the number of walls is increasing, while the time of the simulation is running from left to right. Best solution among 100,000 simulations is reported, and this is particularly advantageous for the case of the empty room, since the probability of the reported configuration is relatively small. The final outcome from this study is that a single wall is redirecting a single group of pedestrians. Naturally, if no wall is adopted, all the pedestrians are converging at the center of the room. This is connected with this specific configuration: in fact, when a pedestrian is entering the room, in order not to hit the boundaries s/he moves toward the center of the room following the bisector of the corner. The following pedestrians have a further attraction, that is, the trajectory of the preceding pedestrian(s), so that typically all the groups are moving (on average) along the bisector of the angle between the walls. The elimination of one or more groups from this path is facilitating the deviation of the converging part of the group to one of the exits. When a single obstacle is used, one group is segregated, and it moves toward the closest exit. If two obstacles are utilized, two groups are eliminated from the central area and the remaining two groups are moving together toward the opposite exit. In the particular case reported in Fig. 14, the tail of the right upper group is shifted to the top by a subset of the group entering from the lower right corner: this way, all the exits are exploited, and the congestion at the exits is reduced, also lowering the overall egress time.

We can then conclude that the use of an optimizer for the determination of the best configuration is essential for at least two distinct reasons. Firstly, although the final configuration appears to be logical, it is not easy to be identified without an aid (the paradox of the egg of Columbus). Secondly, the fine tuning of the general layout of the walls is providing an advantage impossible to obtain by a simple

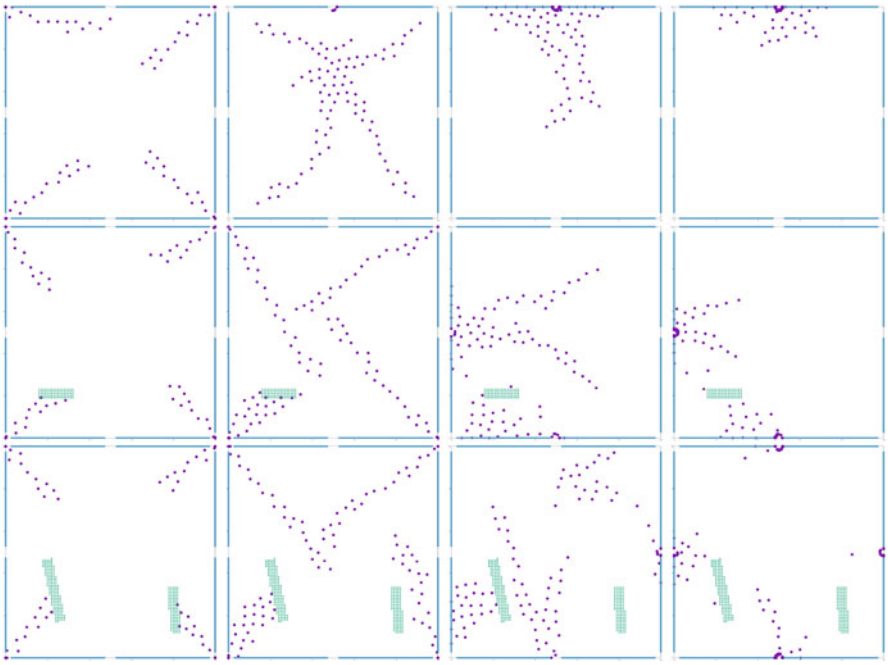

Fig. 14 Flow of the pedestrian in the case of empty room, room with a single wall and room with two walls

manual positioning. Finally, these two aspects have been pointed out in the case of a relatively simple room geometry: a much more complex geometry would include more and more difficulties in the determination of the optimal configuration, and the use of an optimization algorithm becomes vital.

5 Conclusions and Research Directions

This survey has been devoted to present some recent results in the mathematical modeling and control of crowd dynamics. We discussed the various level of modeling, from the microscopic scale of agent-based systems to the macroscopic scale of the crowd density and bulk velocity, through the mesoscopic scale based on a statistical description of the system. Several corresponding control problems, aimed at minimizing the escape time of the crowd from a given environment, have been illustrated and solved by numerical methods.

These results allow us to draw some conclusions. First of all, we can say that while the *modeling* (i.e., the mathematical description) of pedestrian flows has now reached a stage of maturity, the same cannot be said for the *optimization* of

pedestrian flows. In this field there is still room for many experiments, both virtual and real.

In the case of control through leaders, their impact on the crowd is not yet completely understood. In particular, in crowd management it is of paramount importance to be able to secure crowd evacuation through minimal intervention in order to avoid adversarial behaviors against authorities, and de-escalate tensions. Indeed, we have shown that few agents may change completely the behavior of the whole system, breaking initial uncertainties. A further research direction concerns the optimal positioning and amount of leaders within the crowd at the time of the first movement.

In the case of optimization through obstacles, basically no experiment was conducted on real people (we do not consider here the experiments investigating the effect of small obstacles in front of exit doors). Although the simulations suggest the existence of multiple optimal configurations of the obstacles, and it is therefore not easy to choose which to put into practice, virtual experiments all lead in the same, clear direction: *breaking of symmetry* is beneficial to pedestrian flows. This means, e.g., that clogging can be avoided by redirecting people through asymmetric paths, which lead people at exits at different times. Moreover, the perception of the walking area can be completely upset by using smart obstacles, in such a way that naturally chosen exit paths are rebuilt for a more efficient exit usage.

Acknowledgments Authors would like to thank the Italian Ministry of Instruction, University and Research (MIUR) to support this research with funds coming from PRIN Project 2017 (No. 2017KKJP4X entitled "Innovative numerical methods for evolutionary partial differential equations and applications").

References

1. A. Abdelghany, K. Abdelghany, H. Mahmassani, W. Alhalabi, Modeling framework for optimal evacuation of large-scale crowded pedestrian facilities. Eur. J. Oper. Res. **237**(3), 1105–1118 (2014). https://doi.org/10.1016/j.ejor.2014.02.054
2. J.P. Agnelli, F. Colasuonno, D. Knopoff, A kinetic theory approach to the dynamic of crowd evacuation from bounded domains. Math. Models Methods Appl. Sci. **25**(1), 109–129 (2015). https://doi.org/10.1142/S0218202515500049
3. G. Albi, L. Pareschi, Binary interaction algorithms for the simulation of flocking and swarming dynamics. Multiscale Model. Simul. **11**(1), 1–29 (2013). https://doi.org/10.1137/120868748
4. G. Albi, L. Pareschi, Modeling of self-organized systems interacting with a few individuals: from microscopic to macroscopic dynamics. Appl. Math. Lett. **26**, 397–401 (2013)
5. G. Albi, L. Pareschi, Selective model-predictive control for flocking systems. Commun. Appl. Ind. Math. **9**(2), 4–21 (2018). https://doi.org/10.2478/caim-2018-0009
6. G. Albi, L. Pareschi, M. Zanella, Boltzmann-type control of opinion consensus through leaders. Philos. Trans. R. Soc. A **372**, 20140138/1–18 (2014). https://doi.org/10.1098/rsta.2014.0138
7. G. Albi, M. Herty, L. Pareschi, Kinetic description of optimal control problems and applications to opinion consensus. Commun. Math. Sci. **13**(6), 1407–1429 (2015). https://doi.org/10.4310/CMS.2015.v13.n6.a3

8. G. Albi, M. Bongini, E. Cristiani, D. Kalise, Invisible control of self-organizing agents leaving unknown environments. SIAM J. Appl. Math. **76**(4), 1683–1710 (2016). https://doi.org/10.1137/15M1017016
9. G. Albi, N. Bellomo, L. Fermo, S.Y. Ha, J. Kim, L. Pareschi, D. Poyato, J. Soler, Vehicular traffic, crowds, and swarms: from kinetic theory and multiscale methods to applications and research perspectives. Math. Models Methods Appl. Sci. **29**(10), 1901–2005 (2019). https://doi.org/10.1142/S0218202519500374
10. G. Albi, L. Pareschi, M. Zanella, Boltzmann games in heterogeneous consensus dynamics. J. Stat. Phys. **175**(1), 97–125 (2019). https://doi.org/10.1007/s10955-019-02246-y
11. H.C. Andersen, J.D. Weeks, D. Chandler, Relationship between the hard-sphere fluid and fluids with realistic repulsion force. Phys. Rev. A **4**(4), 1597–1607 (1971)
12. G. Arechavaleta, J.P. Laumond, H. Hicheur, A. Berthoz, An optimality principle governing human walking. IEEE Trans. Robot. **24**(1), 5–14 (2008)
13. E. Atashpaz-Gargari, C. Lucas, Imperialist competitive algorithm: an algorithm for optimization inspired by imperialistic competition, in *IEEE Congress on Evolutionary Computation* (IEEE, 2007), pp. 4661–4667. https://doi.org/10.1109/CEC.2007.4425083
14. C. Audet, K.C. Dang, D. Orban, Optimization of algorithms with OPAL. Math. Prog. Comp. **6**(3), 233–254 (2014). https://doi.org/10.1007/s12532-014-0067-x
15. R. Bailo, M. Bongini, J.A. Carrillo, D. Kalise, Optimal consensus control of the Cucker-Smale model. IFAC-PapersOnLine **51**(13), 1–6 (2018)
16. N. Bellomo, C. Dogbé, On the modeling of traffic and crowds: a survey of models, speculations, and perspectives. SIAM Rev. **53**, 409–463 (2011)
17. M. Bongini, M. Fornasier, D. Kalise, : (Un)conditional consensus emergence under perturbed and decentralized feedback controls. Discrete Contin. Dyn. Syst. **35**(9), 4071–4094 (2015). https://doi.org/10.3934/dcds.2015.35.4071
18. A. Borzì, S. Wongkaew, Modeling and control through leadership of a refined flocking system. Math. Models Methods Appl. Sci. **25**(2), 255–282 (2015). https://doi.org/10.1142/S0218202515500098
19. D. Braess, A. Nagurney, T. Wakolbinger, On a paradox of traffic planning. Transp. Sci. **39**(4), 446–450 (2005)
20. M. Caponigro, M. Fornasier, B. Piccoli, E. Trélat, Sparse stabilization and optimal control of the Cucker-Smale model. Math. Control Relat. Fields **3**(4), 447–466 (2013). https://doi.org/10.3934/mcrf.2013.3.447
21. J.A. Carrillo, M.R. D'Orsogna, V. Panferov, Double milling in self-propelled swarms from kinetic theory. Kinet. Relat. Models **2**(2), 363–378 (2009)
22. J.A. Carrillo, M. Fornasier, G. Toscani, F. Vecil, Particle, kinetic, and hydrodynamic models of swarming, in *Mathematical Modeling of Collective Behavior in Socio-economic and Life Sciences* (Springer, New York, 2010), pp. 297–336
23. J.A. Carrillo, S. Martin, M.T. Wolfram, An improved version of the Hughes model for pedestrian flow. Math. Models Methods Appl. Sci. **26**(4), 671–697 (2016). https://doi.org/10.1142/S0218202516500147
24. C. Cercignani, R. Illner, M. Pulvirenti, *The Mathematical Theory of Dilute Gases* (Springer, New York, 1994)
25. Y. Chitour, F. Jean, P. Mason, Optimal control models of goal-oriented human locomotion. SIAM J. Control Optim. **50**(1), 147–170 (2012)
26. E.N.M. Cirillo, A. Muntean, Dynamics of pedestrians in regions with no visibility - a lattice model without exclusion. Physica A **392**, 3578–3588 (2013)
27. M. Clerc, J. Kennedy, The particle swarm - explosion, stability, and convergence in a multidimensional complex space. IEEE Trans. Evol. Comput. **6**(1), 58–73 (2002). https://doi.org/10.1109/4235.985692
28. A. Colombi, M. Scianna, A. Alaia, A discrete mathematical model for the dynamics of a crowd of gazing pedestrians with and without an evolving environmental awareness. Comput. Appl. Math. 1–29 (2016). https://doi.org/10.1007/s40314-016-0316-x

29. R.M. Colombo, M. Garavello, M. Lecureux-Mercier, A class of nonlocal models of pedestrian traffic. Math. Models Methods Appl. Sci. **22**, 1150023/1–34 (2012)
30. V. Coscia, C. Canavesio, First-order macroscopic modelling of human crowd dynamics. Math. Models Methods Appl. Sci. **18**(Suppl. 01), 1217–1247 (2008)
31. I.D. Couzin, J. Krause, N.R. Franks, S.A. Levin, Effective leadership and decision-making in animal groups on the move. Nature **433**, 513–516 (2005)
32. E. Cristiani, D. Peri, Handling obstacles in pedestrian simulations: models and optimization. Appl. Math. Model. **45**, 285–302 (2017)
33. E. Cristiani, D. Peri, Robust design optimization for egressing pedestrians in unknown environments. Appl. Math. Model. **72**, 553–568 (2019)
34. E. Cristiani, F.S. Priuli, A destination-preserving model for simulating Wardrop equilibria in traffic flow on networks. Netw. Heterog. Media **10**, 857–876 (2015)
35. E. Cristiani, B. Piccoli, A. Tosin, Multiscale modeling of granular flows with application to crowd dynamics. Multiscale Model. Simul. **9**, 155–182 (2011)
36. E. Cristiani, B. Piccoli, A. Tosin, Multiscale modeling of pedestrian dynamics, in *Modeling, Simulation & Applications* (Springer, New York, 2014)
37. E. Cristiani, F.S. Priuli, A. Tosin, Modeling rationality to control self-organization of crowds: an environmental approach. SIAM J. Appl. Math. **75**(2), 605–629 (2015). https://doi.org/10.1137/140962413
38. F. Cucker, S. Smale, Emergent behavior in flocks. IEEE Trans. Autom. Contr. **52**(5), 852–862 (2007)
39. H. Duan, C. Sun, Swarm intelligence inspired shills and the evolution of cooperation. Sci. Rep. **4**, 5210 (2014)
40. B. Düring, P. Markowich, J.F. Pietschmann, M.T. Wolfram, Boltzmann and Fokker-Planck equations modelling opinion formation in the presence of strong leaders. Proc. R. Soc. A **465**, 3687–3708 (2009)
41. R. Escobar, A. De La Rosa, Architectural design for the survival optimization of panicking fleeing victims, in *ECAL 2003*. LNAI, vol. 2801, ed. by W. Banzhaf, T. Christaller, P. Dittrich, J.T. Kim, J. Ziegler (Springer, Berlin, Heidelberg, 2003), pp. 97–106
42. R. Etikyala, S. Göttlich, A. Klar, S. Tiwari, Particle methods for pedestrian flow models: from microscopic to nonlocal continuum models. Math. Models Methods Appl. Sci. **24**, 2503–2523 (2014). https://doi.org/10.1142/S0218202514500274
43. A. Festa, A. Tosin, M.T. Wolfram, Kinetic description of collision avoidance in pedestrian crowds by sidestepping. Kinet. Relat. Models **11**(3), 491–520 (2018). https://doi.org/10.3934/krm.2018022
44. M. Fornasier, F. Solombrino, Mean-field optimal control. ESAIM Control Optim. Calc. Var. **20**(4), 1123–1152 (2014). https://doi.org/10.1051/cocv/2014009
45. G.A. Frank, C.O. Dorso, Room evacuation in the presence of an obstacle. Physica A **390**, 2135–2145 (2011). https://doi.org/10.1016/j.physa.2011.01.015
46. O. Galor, *Discrete Dynamical Systems* (Springer, Berlin, Heidelberg, 2007)
47. R.Y. Guo, H.J. Huang, S.C. Wong, Route choice in pedestrian evacuation under conditions of good and zero visibility: experimental and simulation results. Transp. Res. B **46**(6), 669–686 (2012). https://doi.org/10.1016/j.trb.2012.01.002
48. M. Haghani, E. Cristiani, N.W.F. Bode, M. Boltes, A. Corbetta, Panic, irrationality, and herding: three ambiguous terms in crowd dynamics research. J. Adv. Transp. **2019**. Article ID 9267643 (2019). https://doi.org/10.1155/2019/9267643
49. J. Han, L. Wang, Nondestructive intervention to multi-agent systems through an intelligent agent. PLoS One **8**(5), e61542 (2013). https://doi.org/10.1371/journal.pone.0061542
50. J. Han, M. Li, L. Guo, Soft control on collective behavior of a group of autonomous agents by a shill agent. J. Syst. Sci. Complexity **19**(1), 54–62 (2006). https://doi.org/10.1007/s11424-006-0054-z
51. D. Helbing, Traffic and related self-driven many-particle systems. Rev. Mod. Phys. **73**, 1067–1141 (2001)

52. D. Helbing, P. Molnár, Social force model for pedestrian dynamics. Phys. Rev. E **51**, 4282–4286 (1995)
53. D. Helbing, I. Farkas, T. Vicsek, Simulating dynamical features of escape panic. Nature **407**, 487–490 (2000)
54. D. Helbing, L. Buzna, A. Johansson, T. Werner, Self-organized pedestrian crowd dynamics: experiments, simulations, and design solutions. Transp. Sci. **39**(1), 1–24 (2005)
55. T. Hendtlass, Wosp: a multi-optima particle swarm algorithm, in *Proceedings of the 2005 IEEE Congress on Evolutionary Computation*, ed. by IEEE (IEEE, New York, 2005), pp. 727–734
56. M. Herty, L. Pareschi, S. Steffensen, Mean-field control and Riccati equations. Netw. Heterog. Media **10**(3), 699–715 (2015). https://doi.org/10.3934/nhm.2015.10.699
57. R.L. Hughes, A continuum theory for the flow of pedestrians. Transp. Res. Part B **36**, 507–535 (2002)
58. R.L. Hughes, The flow of human crowds. Annu. Rev. Fluid Mech. **35**, 169–182 (2003)
59. L. Jiang, J. Li, C. Shen, S. Yang, Z. Han, Obstacle optimization for panic flow - reducing the tangential momentum increases the escape speed. PLoS One **9**(12), e115463 (2014). https://doi.org/10.1371/journal.pone.0115463
60. A. Johansson, D. Helbing, Pedestrian flow optimization with a genetic algorithm based on Boolean grids, in *Pedestrian and Evacuation Dynamics 2005*, ed. by N. Waldau, P. Gattermann, H. Knoflacher, M. Schreckenberg (Springer, Berlin, Heidelberg, 2007), pp. 267–272
61. P. Kachroo, S.J. Al-nasur, S.A. Wadoo, A. Shende, Pedestrian dynamics. Feedback control of crowd evacuation, in *Understanding Complex Systems* (Springer, Berlin, Heidelberg, 2008)
62. T.K. Karper, A. Mellet, K. Trivisa, Hydrodynamic limit of the kinetic Cucker–Smale flocking model. Math. Models Methods Appl. Sci. **25**(01), 131–163 (2015). https://doi.org/10.1142/S0218202515500050
63. R. Löhner, On the modeling of pedestrian motion. Appl. Math. Model. **34**, 366–382 (2010)
64. T. Matsuoka, A. Tomoeda, M. Iwamoto, K. Suzuno, D. Ueyama, Effects of an obstacle position for pedestrian evacuation: SF model approach, in *Traffic and Granular Flow '13*, ed. by M. Chraibi, M. Boltes, A. Schadschneider, A. Seyfried (Springer International Publishing, Cham, 2015), pp. 163–170
65. D.Q. Mayne, J.B. Rawlings, C.V. Rao, P.O.M. Scokaert, Constrained model predictive control: stability and optimality. Automatica **36**(6), 789–814 (2000). https://doi.org/10.1016/S0005-1098(99)00214-9
66. S. Motsch, E. Tadmor, A new model for self-organized dynamics and its flocking behavior. J. Stat. Phys. **144**(5), 923–947 (2011). https://doi.org/10.1007/s10955-011-0285-9
67. G. Naldi, L. Pareschi, G. Toscani, (eds.) Mathematical modeling of collective behavior in socio-economic and life sciences, in *Modeling and Simulation in Science, Engineering and Technology* (Birkhäuser Boston, Inc., Boston, MA, 2010). https://doi.org/10.1007/978-0-8176-4946-3
68. S. Okazaki, A study of pedestrian movement in architectural space, part 1: pedestrian movement by the application of magnetic model. Trans. AIJ **283**, 111–119 (1979)
69. S. Okazaki, A study of pedestrian movement in architectural space, part 2: concentrated pedestrian movement. Trans. AIJ **284**, 101–110 (1979)
70. S. Okazaki, A study of pedestrian movement in architectural space, part 3: along the shortest path, taking fire, congestion and unrecognized space into account. Trans. AIJ **285**, 137–147 (1979)
71. L. Pareschi, G. Toscani, Interacting multi-agent systems, in *Kinetic Equations & Monte Carlo Methods* (Oxford University Press, Oxford, 2013)
72. D.R. Parisi, C.O. Dorso, Microscopic dynamics of pedestrian evacuation. Physica A **354**, 606–618 (2005). http://dx.doi.org/10.1016/j.physa.2005.02.040
73. D. Peri, Hybridization of the imperialist competitive algorithm and local search with application to ship design optimization. Comput. Ind. Eng. **137**, 1–30 (2019). https://doi.org/10.1016/j.cie.2019.106069
74. B. Piccoli, A. Tosin, Pedestrian flows in bounded domains with obstacles. Contin. Mech. Thermodyn. **21**, 85–107 (2009)

75. P.K. Shukla, Genetically optimized architectural designs for control of pedestrian crowds, in *Artificial Life: Borrowing from Biology*. LNCS, vol. 5865, ed. by K. Korb, M. Randall, T. Hendtlass (Springer, Berlin, Heidelberg, 2009), pp. 22–31
76. G. Toscani, N. Bellomo, The Enskog-Boltzmann equation in the whole space $\mathbb{R}^3$: some global existence, uniqueness and stability results. Comput. Math. Appl. **13**(9–11), 851–859 (1987)
77. M. Twarogowska, P. Goatin, R. Duvigneau, Macroscopic modeling and simulations of room evacuation. Appl. Math. Model. **38**(24), 5781–5795 (2014). https://doi.org/10.1016/j.apm.2014.03.027
78. C. Villani, A review of mathematical topics in collisional kinetic theory, in *Handbook of Mathematical Fluid Dynamics*, vol. 1 (Elsevier, Amsterdam, 2002)
79. J. Wang, L. Zhang, Q. Shi, P. Yang, X. Hu, Modeling and simulating for congestion pedestrian evacuation with panic. Physica A **428**, 396–409 (2015). https://doi.org/10.1016/j.physa.2015.01.057
80. Y. Zhao, M. Li, X. Lu, L. Tian, Z. Yu, K. Huang, Y. Wang, T. Li, Optimal layout design of obstacles for panic evacuation using differential evolution. Physica A **465**, 175–194 (2017). https://doi.org/10.1016/j.physa.2016.08.021
81. M. Zhou, H. Dong, Y. Zhao, P.A. Ioannou, F.-Y. Wang, Optimization of crowd evacuation with leaders in urban rail transit stations. IEEE Trans. Intell. Transp. Syst. **20**(12) (2019)

Mixed Traffic Simulation of Cars and Pedestrians for Transportation Policy Assessment

Hideki Fujii, Hideaki Uchida, Tomonori Yamada, and Shinobu Yoshimura

Abstract In this chapter, the authors report on the construction of a new framework for simulating mixed traffic consisting of cars, trams, and pedestrians that can be used to support road management, signal control, and public transit. More specifically, a layered road structure, originally designed for car traffic simulations, was extended to interact with a one-dimensional tram model and one-/two-dimensional pedestrian models. The newly implemented pedestrian models and interaction rules were verified through simulations involving simple road environments, and the resulting simulated values were found to be in near agreement with the empirical data. The proposed framework is then used to assess the impact of a tramway extension plan for a real city. Those simulation results showed that the impact of the proposed tramway on existing car traffic would not be severe, and by extension, implied that the proposed framework could help stakeholders decide on expansion scenarios that would be agreeable to both tram users and private car owners.

1 Introduction

Road traffic is a key part of the infrastructure that supports mobility through the transportation of humans and goods. However, at the same time, it is also the cause of various types of urban and environmental issues including traffic jams, accidents, and heavy energy consumption. In addition, engine emission contributes to problems such as air pollution and global warming.

The promotion of public transportation usage is among the most effective methods for addressing such issues. Herein, the authors focus on the extension of a tramway into a rail station square, which is an important topic because the connectivity of public transportation services (such as railways and tramways) is regarded as an index for transportation service accessibility [34, 35]. Furthermore,

H. Fujii (✉) · H. Uchida · T. Yamada · S. Yoshimura
Graduate School of Engineering, The University of Tokyo, Bunkyo-ku, Tokyo, Japan
e-mail: fujii@sys.t.u-tokyo.ac.jp; uchida@sys.t.u-tokyo.ac.jp; tyamada@sys.t.u-tokyo.ac.jp; yoshi@sys.t.u-tokyo.ac.jp

L. Gibelli (ed.), *Crowd Dynamics, Volume 2*, Modeling and Simulation in Science, Engineering and Technology, https://doi.org/10.1007/978-3-030-50450-2_9

improved public transportation services can suppress excessive public dependence on private cars. However, careful consideration must be taken given the fact that policies aimed at improving tram convenience might also impair the use of the private cars that must share the same limited available road space.

Furthermore, since it is very difficult to restore a road environment to a previous condition once it has been changed, it is strongly desirable to accurately estimate the impact of transportation policies quantitatively. This is why simulations have been playing an important role in the field of traffic engineering, and why various types of traffic simulators have been developed and utilized (e.g., [6, 26]). This is also why a number of mixed traffic simulation models that can be used to support the validity of novel signal control methods or public transport planning efforts have been proposed in recent years.

In this chapter, the authors report on a multi-agent-based traffic simulator for mixed traffic of cars, pedestrians, and trams. The contents are based on the previous article [15] with some new findings. More specifically, pedestrian and tram agent models were implemented into an existing car traffic simulator and interaction rules among these agents were set. This simulator was then applied to a case study involving a tramway extension plan in an actual city.

2 Existing Simulation Models

2.1 Simulation Models for Pedestrian Traffic

Pedestrian traffic simulation models are generally classified into two categories: macroscopic and microscopic.

In the macroscopic models, partial differential equations that express pedestrian behavior as a continuous density and velocity distributions and are based on the equation of continuity, which is the law of conservation of mass in continuum mechanics, have been proposed (e.g., [20, 22, 40, 41]). Such models are solved by the finite difference method or mesh-based methods such as the discontinuous Galerkin method.

In the microscopic models, each pedestrian is modeled as a kind of particle. Microscopic models can be divided according to the road structure representation, which comes in two types: continuous and discretized. In the continuous road representation group, a base road structure is modeled as a continuous one-dimensional (1D) or two-dimensional (2D) space. In the discretized road representation group, road space is discretized by homogeneous cells.

The social force model (SFM) [18] and centrifugal force based models (CFM) [10, 45], in which pedestrian agents move in two-dimensional (2D) road space, have already been successfully used in continuous road model groups. The predictive performance of those models was enhanced by introducing the capability to anticipate pedestrian actions [4] and by adding stride adaptation mechanisms [39]. A

1D pedestrian model [42] in which the SFM spatial dimensions are compressed into one has been applied to evacuation simulations. Furthermore, the discrete choice model [2] is among the continuous road models with discretized decision-making rules for each pedestrian agent that are now in use.

Meanwhile, the floor field model (FFM) [7] and Muramatsu's lattice-gas-based model [30] belong in the discretized road representation group.

2.2 Simulation Models for Car and Mixed Traffic

Microscopic models used for car traffic simulations are classified as well. In the continuous road representation group, the behavior of car agents is often implemented by applying car-following theories (e.g., [5, 8, 16, 19, 24, 32, 36, 38, 47]). In the discretized road representation group, the behavior of car agents is expressed using transition rules such as cellar automata (e.g., [13, 25, 31, 37]).

Several researchers have proposed simulation frameworks for mixed traffic of two or more models. For example, Yang et al. [43] proposed a framework for pedestrian road crossing behavior in Chinese cities in which they determined the criteria used by pedestrians to decide whether to start crossing a road after considering vehicle flows. While the model itself was relatively simple, the simulation results (with adjusted parameters) agreed well with the observed values. In another study, Zeng et al. [46] modeled pedestrian-vehicles interactions at crosswalks by adding external force to the SFM in order to minimize pedestrian-vehicle collisions, while Anvari et al. [3] used the SFM to model mixed car and pedestrian traffic scenarios by extending the SFM for car dynamics and integrating a car-following model.

Meanwhile, Huang et al. [21] also developed a 2D car behavior model based on the SFM and integrated it with the proportional-integral-derivative (PID) control algorithm, while Huynh et al. [23] extended the SFM to model the behavior of motorcycles, passenger cars, and buses for use in a mixed traffic simulation at a signalized intersection. However, while these SFM-based car models are capable of being naturally integrated with the SFM-based pedestrian models, significant disadvantage of existing car traffic simulators based on car-following models is that they are hard to apply to this approach. Furthermore, generally speaking, the computational loads of 2D models are much higher than those of 1D models.

Additionally, Crociani and Vizzari [11] proposed an integrated simulation model by combining a 1D car-following model and a 2D floor field pedestrian model in which they employed a hierarchical road environment structure to exploit the different representations of cars and pedestrians. In this model, the specific agent types are situated in the lower level and comprehensive views of the overall situation are given at the higher level.

Furthermore, Dobler and Lämmel [12] integrated multi-modal simulation modules into the existing framework of MATSim, which is a large-scale traffic simulation framework that is based on the queueing model [9]. Their integration approach was based on locally replacing simple queue structures with continuous 2D space at

sections with higher traffic flows. The behavior rules of agents in the 2D space are based on the SFM.

Moreover, Krajzewicz et al. [28] introduced pedestrian and bicycle agent models into the Simulation of Urban Mobility (SUMO), which is a widely used traffic simulator belonging to the continuous road model group [27], and then used it to consider and verify their agents qualitatively, even though the pedestrian and bicycle agents had relatively simple behavior rules by which they moved in 1D virtual trajectories.

3 Models in Proposed Framework

In this research, mixed traffic conditions refer to those in which cars, trams, and pedestrians coexist simultaneously. Simulating such traffic conditions requires agent models for all of those travel modes. And continuous road models are suitable for simulating the precise behavior of cars, trams, and pedestrian agents. For that reason, the authors chose The multi-agent-based car-traffic simulator, which is named ADVENTURE_Mates (Mates refers to "Multi-Agent-based Traffic and Environment Simulator"), has already been published as a module of the authors' open-source software (OSS) project [44]. The simulator employs a continuous road model for car traffic and has been used as bases of various previous researches, e.g., a vehicle emissions prediction [14], an origin-destination estimation [1], and a speeding-up of dynamic route search [29].

In this chapter, mixed traffic conditions refer to those in which cars, trams, and pedestrians coexist simultaneously. Simulating such traffic conditions requires agent models for all of those travel modes. Additionally, continuous road models are suitable for simulating the precise behavior of car, tram, and pedestrian agents. Therefore, the authors chose ADVENTURE_Mates as the basis of the research.

3.1 Road Environment Representation

A three-layer road network model based on directed graphs (Fig. 1) is employed in this simulator. The virtual driving lane is the fundamental unit for modeling the actual road structure. Car agent maneuvering is restricted to movement along the lane, except when lane-shifting. Each lane is equipped with various kinds of information related to its length, connection with other lanes, speed limit, and other accompanying attributes. The road environment provides such information if the agent requests it. Two types of lane bundle objects, basic road sections and intersections, are located in the second layer. Each object consists of virtual driving lanes and their connectors. Lane bundle objects are organized as a global road network.

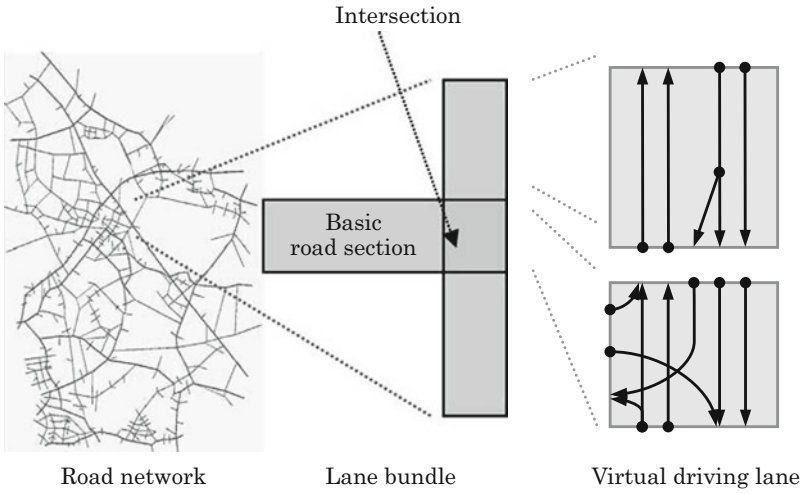

Fig. 1 Overview of layered road network

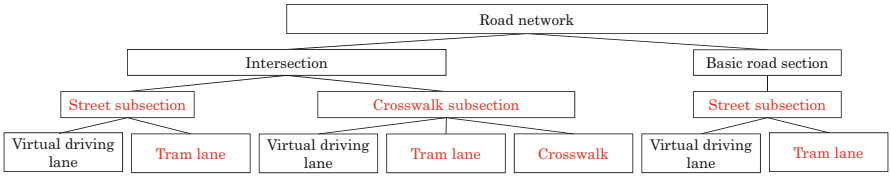

Fig. 2 New road structure (red indicates newly implemented structures for mixed traffic simulations)

A new structure that possesses a 2D domain, called a subsection, was introduced to divide lane bundles based on the access right differences for each different traffic mode. A street subsection is limited to virtual driving lanes for cars (and a tram lane if necessary), while a crosswalk subsection definition also includes a pedestrian crosswalk. Figure 2 shows the new road structure concept. In this research, since the authors were attempting to assess the impact of road policy on car traffic, pedestrians were restricted to walking on crosswalks. However, the proposed layered road network concept can be applied to general-purpose mixed traffic simulations as well.

3.2 Car Agent Definition

For driving route planning, the A* algorithm [17] is implemented in the simulator. It should be noted here that since the simulator does not include a planning process in which the origin and destination (OD) points are decided, users need to input

a proper OD matrix a priori. A search is conducted for the optimum route every time a car is generated at a terminal node, and the results are stored and reused. The route that minimizes the trip distance or the expected trip time from the origin to the destination is selected by the A* algorithm. When searching for a route that minimizes the expected trip time, the cost of each link is given as the required time average of all cars that have already passed the link, and this average is updated every 10 min.

After determining the global route on a road network, each car follows the selected route and drives from the origin to the destination. The simulator employs the generalized force model (GFM) [19] in order to determine the car agent acceleration. The model concept is shown below:

$$\frac{dV_i}{dt} = F_i^0(V_i) + F_{i,i-1}(X_i, V_i, X_{i-1}, V_{i-1}) + \xi_i, \tag{1}$$

where X_i and V_i are the position and the speed of the i-th car, respectively, $(dX_i/dt = V_i)$. The first term on the right-hand side of Eq. (1) represents the acceleration toward the driver's desired speed:

$$F_i^0(V_i) = \frac{V_i^0 - V_i}{\tau_i}, \tag{2}$$

where V_i^0 and τ_i are the desired speed and the acceleration time of car agent i, respectively. The second term of Eq. (1) represents the virtual repulsive force from interactions with the preceding $(i-1$ th) car agent:

$$F_{i,i-1} = \frac{V^{opt}(S_i, V_i) - V_i^0}{\tau_i} - \frac{\Delta V_i \Theta(\Delta V_i)}{\tau_i'} \exp\left(\frac{S(V_i) - S_i}{R_i'}\right), \tag{3}$$

with

$$V^{opt}(S_i, V_i) = V_i^0 \left\{1 - \exp\left(\frac{S(V_i) - S_i}{R_i}\right)\right\}, \tag{4}$$

$$\Delta V_i = V_i - V_{i-1}, \tag{5}$$

$$S_i = X_{i-1} - X_i - L_{i-1}, \tag{6}$$

$$S(V_i) = D_i + T_i V_i, \tag{7}$$

where $V^{opt}(S_i, V_i)$ is a distance-and-speed-dependent optimal velocity. $\Theta(\cdot)$ is the Heaviside function. ΔV_i and S_i indicate the relative speed and the distance between the i-th and its preceding car, respectively. L_i, D_i, τ_i', and T_i are the body length, the minimal car distance, breaking time, and safe time headway of car agent i, respectively. $S(v_i)$ indicates a speed-dependent safe distance. R_i and R_i' can be

interpreted as the range of the acceleration and the braking interaction, respectively. The third term of Eq. (1) is a fluctuating force that may include driver's individual variations.

The GFM is a model in which a driver determines acceleration using only the distance and the speed difference from the preceding car. However, speed determinants include not just the preceding car but also the traffic lights, the forward intersection situation, and other urban traffic conditions. Therefore, the authors expanded the GFM so that the virtual preceding cars reflect the forward road conditions, and Eq. (1) is applied to each virtual preceding car. Additionally, in order to facilitate collision avoidance between cars and pedestrians, the existence of pedestrian agents on the forward road subsection is given as a virtual preceding car to car agents. As a result, the need for modifications to the existing simulator code can be minimized, and the independence of each traffic mode simulation model is strictly maintained.

Cars are also provided with a lane-shifting function. When shifting lanes, the car agent must simultaneously consider the cars in both its current driving lane and the adjacent lane. To facilitate this, a dummy of the car agent that is going to change lanes is virtually created in the adjacent lane, appropriate speeds are evaluated for both lanes, and the slower one is selected to minimize collision risks.

3.3 Tram Agent Definition

Since the car is modeled to permit it to drive on 1D virtual driving lanes (not 2D space) on the simulator, the tram driving on 1D tracks can be easily modeled by a little extension of the car agent. More specifically, the authors created a tram lane by starting with the same structure used for the virtual driving lane for cars, modified it to prevent it from joining or branching with car lanes, and removed lane-shifting and route-searching functions from a tram agent. The tram agent attributes, such as body size (12.2–18.0 m length used in our simulation scenario, to be described later), speed limit (30–40 km/h based on Japanese law), max acceleration, and deceleration performance (2.5 km/h/s and 4.4 km/h/s, respectively), were given as parameters.

Additionally, unlike car agents that flow into the road network stochastically at the terminal nodes, tram agents flow into the network deterministically based on a given timetable. The car-following model itself is the same as that for car agents, but the scheduled departure time is added as a factor for determining the speed of the tram agents. This model was created based on information obtained during an interview with a tram operator. The actual procedure used to determine the tram's speed is described below:

Step 1 If the tram is stopped at a tram stop and its scheduled departure time is pending (considering time for passengers to embark/debark from the vehicle), the tram remains stopped. Otherwise, go to Step 2.

Step 2 The tram's speed is calculated like those of cars by applying the GFM. Go to Step 3.

Step 3 If the tram needs to stop at the next tram stop, the deceleration necessary to come to a halt at the proper position is calculated, and the speed determined in Step 2 is overwritten. To calculate the proper deceleration, a virtual preceding car is placed at the tram stop to create a situation that matches cars stopping at traffic lights.

3.4 Pedestrian Agent Definition

Since pedestrians are assumed to interact with cars and trams only in crosswalks in this research, a pedestrian agent is defined as it appears stochastically at a crosswalk endpoint and disappears when it gets to the other endpoint. Pedestrian agents have no route-searching ability.

There are two options for pedestrian behavior modeling: one is the bifurcation pedestrian model (BPM), and the other is the extended one-dimensional pedestrian model (ExOPM).

3.4.1 Bifurcation Pedestrian Model (BPM)

In this model, a pedestrian is represented by a circle with a fan-shaped view range (Fig. 3). For programmers, the use of a circle has a significant benefit when used for geometrical calculation. The circle diameter r is set to 0.49 m, which is the average width of an adult body. The view range depth R^{view} is set to 3.0 m, and the view angle θ is set to 160°.

The concept of BPM is roughly categorized into the discrete choice model group. A pedestrian agent searches for the nearest pedestrian within its view range and

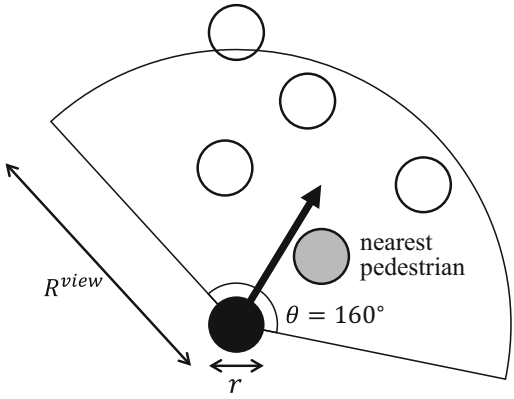

Fig. 3 Representation of pedestrian agent

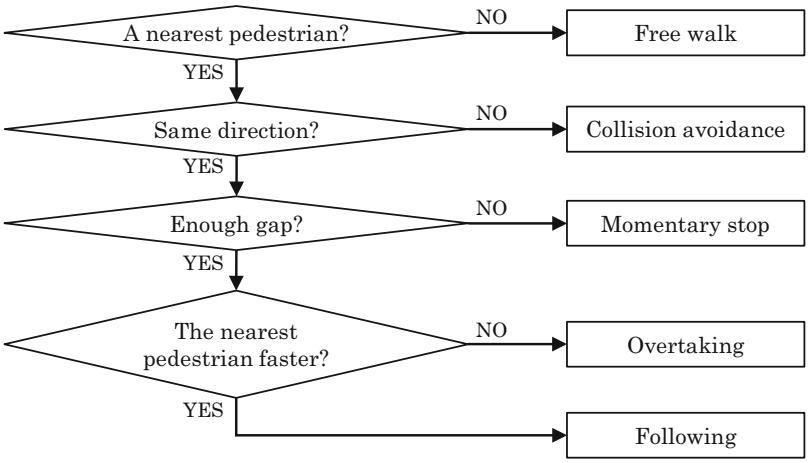

Fig. 4 Pedestrian agent decision-making flow

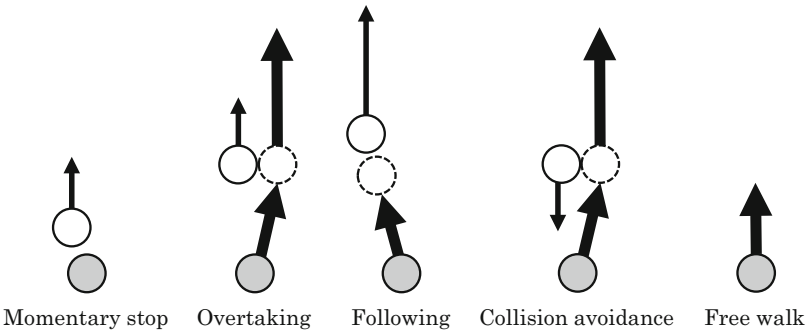

Fig. 5 Pedestrian agent movement

determines its behavior based on the walking direction, relative speed, and the position of the nearest pedestrian. Although it is understood that in the real world, a pedestrian has a continuously changing number of walking behavior choices, the authors discretized the available choices for simplification. As a result, this model is applicable to simple crosswalks but not to more complex crossings where there are more than two directions of travel to choose from.

The decision-making flow of the model is shown in Fig. 4, an overview of each movement is shown in Fig. 5. The j-th pedestrian agent needs to determine its walking speed v_j and walking direction vector $\boldsymbol{d}_j$ for every time step, the concrete methods used to compute these are listed below.

1. Free walk
   If there are no other pedestrians in the view range, agent j walks at his/her desired speed v_j^0. The walking direction $\boldsymbol{d}_j$ is set as follows:

$$\boldsymbol{d}_j = \boldsymbol{d}_j^0 = \boldsymbol{x}_j^0 - \boldsymbol{x}_j, \tag{8}$$

where $\boldsymbol{x}_j$ is the agent's current coordinate and $\boldsymbol{x}_j^0$ is the coordinate of the nearest point on the target crosswalk border.

2. Collision avoidance
   If the nearest pedestrian is walking in the opposite direction, the agent attempts to avoid collision. $v_j = v_j^0$, and $\boldsymbol{d}_j$ is set as follows:

$$\boldsymbol{d}_j = \begin{cases} \boldsymbol{d}_j^0, & \text{if } |\boldsymbol{d}_j^{np}| \sin\phi \geq c_{ps} r, \\ \boldsymbol{d}_j^{np} - c_{ps} r \boldsymbol{n}_j, & \text{otherwise,} \end{cases} \tag{9}$$

   where $\boldsymbol{d}_j^{np} = \boldsymbol{x}_j^{np} - \boldsymbol{x}_j$ ($\boldsymbol{x}_j^{np}$ is the current coordinate of the nearest pedestrian), $\boldsymbol{n}_j$ is the unit normal vector of $\boldsymbol{d}_j^0$ that satisfies $\boldsymbol{d}_j^{np} \cdot \boldsymbol{n}_j \geq 0$, ϕ is the angle between $\boldsymbol{d}_j^{np}$ and $\boldsymbol{d}_j$, and $c_{ps} (= 1.2)$ is the coefficient used to represent the personal space pedestrians need to maintain comfort.
3. Momentary stop
   If the gap to preceding pedestrian is insufficient ($|\boldsymbol{d}_j^{np}| < c_{ps} r$), the agent stops walking temporarily ($v_j = 0$).
4. Overtaking
   If the preceding pedestrian is slower, the agent tries to overtake him/her. Then $v_j = c_{ac} v_j^0$, and $\boldsymbol{d}_j$ is set according to Eq. (9). The coefficient $c_{ac} (= 1.3)$ is the pedestrian's acceleration for overtaking.
5. Following
   If the preceding pedestrian is faster, the agent follows the preceding pedestrian. $v_j = v^0$, and $\boldsymbol{d}_j$ is set as follows:

$$\boldsymbol{d}_i = \begin{cases} \boldsymbol{d}_j^{np}, & \text{if any other pedestrians are walking oppositely,} \\ \boldsymbol{d}_j^0, & \text{otherwise.} \end{cases} \tag{10}$$

Once v_j and $\boldsymbol{d}_j$ are determined for every time step ($\Delta t = 0.1$ s in the simulator), each pedestrian agent updates its position:

$$\boldsymbol{x}_j \leftarrow \boldsymbol{x}_j + v_j \frac{\boldsymbol{d}_j}{|\boldsymbol{d}_j|} \Delta t. \tag{11}$$

Here, the pedestrian's desired walking speed v_j^0 is set to 1.34 ± 0.20 m/s. Since cars are prohibited from crossing an intersection if even just one pedestrian is walking inside it, considering the slower speeds of pedestrians is quite important when dealing with mixed traffic.

3.4.2 Extended One-Dimensional Pedestrian Model (ExOPM)

In order to realize a large-scale and microscopic multi-agent crowd simulation, a 1D continuous space model with a low computational load was proposed. In the original OPM [42], the pedestrian queue is modeled as a virtual lane by utilizing the property that pedestrians moving in a passage or a room with high density tend to form lanes. Hence, walking spaces are represented as a network, and a link is composed of multiple virtual lanes. The ExOPM proposed by the authors defines sidewalks and crosswalks using the same structure as the original OPM. This is based on the following assumptions:

- In high-density environments, pedestrians tend to form queues.
- In low-density environments, pedestrian traffic volume is unaffected by whether pedestrians form queues.

Since the existing OPM targets pedestrian behavior in a high-density environment such as an evacuation, a single pedestrian cannot overtake other pedestrians except in the cases where they are passing over links of different widths (represented by the number of internal virtual lanes).

However, since this is an excessive restriction to apply to a road environment simulation in a normal situation, in the Extended OPM (ExOPM), it is assumed that the pedestrian agent receives social force from the N-th pedestrian agent ahead. Hence, the acceleration dv_j/dt of the j-th pedestrian is calculated using the following equation:

$$\frac{dv_j}{dt} = a_1(v^0 - v_j) - a_2 \exp\left(\frac{r - \left(x_{j-N} - x_j\right)}{a_3}\right), \tag{12}$$

where a_1, a_2, and a_3 are parameters, and the same values as OPM [42] are used ($a_1 = 0.962, a_2 = 0.869, a_3 = 0.214$). v_i^0 is the desired pedestrian walking speed. N is a parameter that sets the range a pedestrian agent is affected by the other pedestrian ahead.

As an example, the behavior of the fourth pedestrian in the link $\mathcal{L}_m$, which is composed of three virtual lanes (shown in Fig. 6), will be described. The pedestrian is the second one in the virtual lane ℓ_2. Here, the position of the k-th pedestrian in the virtual lane ℓ_n in the $\mathcal{L}_m$ link is expressed as $\tilde{x}_j(m, n)$.

The pedestrian at position $\tilde{x}_2(m, 2)$ confirms the front of the virtual lanes ℓ_1, ℓ_2, and ℓ_3, which are included in the same link $\mathcal{L}_m$ and obtains distances l_1, l_2, and l_3. In the case of $N = 3$, the pedestrian receives social force from the third pedestrian ahead. Since the third smallest distance is l_1, the pedestrian moves to the virtual lane ℓ_1 in the next step, and determines its acceleration using l_1.

Considering the above situation based on the positional relationship at the link rather than at the virtual lanes, the distance between pedestrians is x_1 to x_4, as shown in the lower part of Fig. 6. Next, the acceleration is calculated based on the distance to the pedestrian. In this example, since it does not interact with the first and second

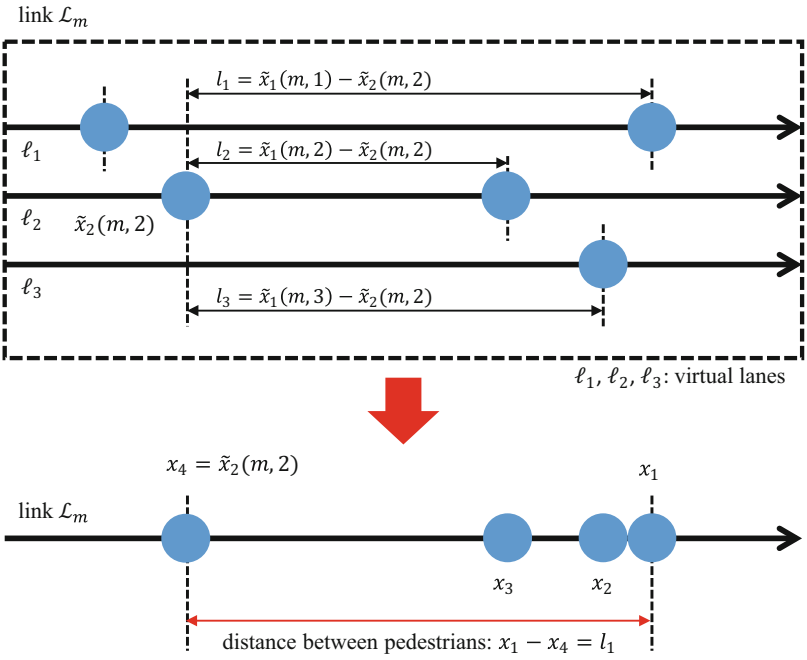

Fig. 6 Following relation in ExOPM

nearest pedestrians in front, the pedestrian's overtaking behavior can be expressed, even though it is a 1D model.

4 Verification

Prior to being applied to a real-world problem, the pedestrian models in the proposed framework along with the effects of interactions between cars and pedestrians were verified independently.

4.1 Verification of Pedestrian Models

A simple crosswalk with a length of 20 m and a width of 2.5 m (shown in Fig. 7) was created to verify the pedestrian models. Simulations using BPM (Sect. 3.4.1) and ExOPM (Sect. 3.4.2) were then conducted by varying traffic demand Q_{ped} = 1000, 1250, 1500, 1750, 2000, 2250, and 2500 ped./h at both ends and observing

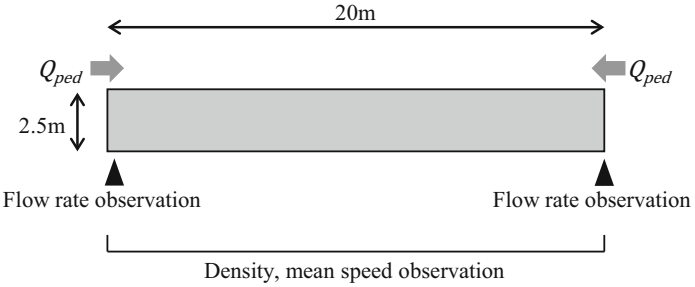

Fig. 7 Simulation environment for pedestrian model verification

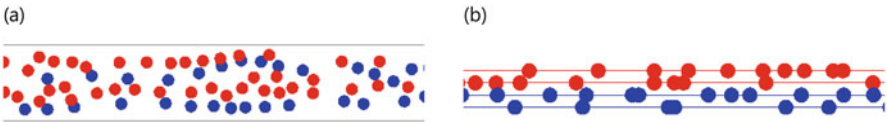

Fig. 8 Simulation screenshots of BPM (**a**) and ExOPM (**b**)

the resulting density, flow rate per unit width, and mean speed at the crosswalk. The free-flow speed of a pedestrian agent was set to 1.34 ± 0.20 m/s in both models.

Figures 8a and b show the screenshots of BPM and ExOPM, respectively. The blue dots indicate pedestrians walking from right to left, and the red dots indicate pedestrians walking from left to right. Forming walking lanes is one of the well-known emerging phenomena of crowd dynamics. Pedestrians in the ExOPM move on the walking lanes defined by the model. Meanwhile, pedestrians in the BPM form walking lanes autonomously by the effect of the behavior of following.

The quantitative results are shown in Fig. 9. Figure 9a–c show the relationships between speed-density, speed-flow, and flow-density, respectively. The output from the empirical formula at a pedestrian precinct [33] and the SFM simulation result by the SFM are also included as references. Because the mean free-flow speed is also 1.34 m/s in the empirical formula, each simulation result shows good agreement. However, since the experiment is intended for sidewalks without an obvious bottleneck, it is necessary to be careful when discussing the reproducibility of congested situations that exceed the critical density based on these results alone.

For the above-mentioned scenario, the total number of agents at each time step in the simulation and the computation time required for agent processing were also measured with each model. Figure 10 shows the results. A computer with an Intel Core i7 (2.93 GHz) CPU and 4 GB of memory was used.

In the SFM and the BPM, which are 2D models, the computational complexity is theoretically $O(mn)$ because n pedestrians search surrounding m for other pedestrians in every time step. Meanwhile, in the ExOPM, which is a 1D model, each pedestrian is affected by at most one pedestrian ahead. At this time, the pedestrian ahead can be accessed in constant time by using a sorted list in the order of distance from the link starting point of the link. Therefore, the computation

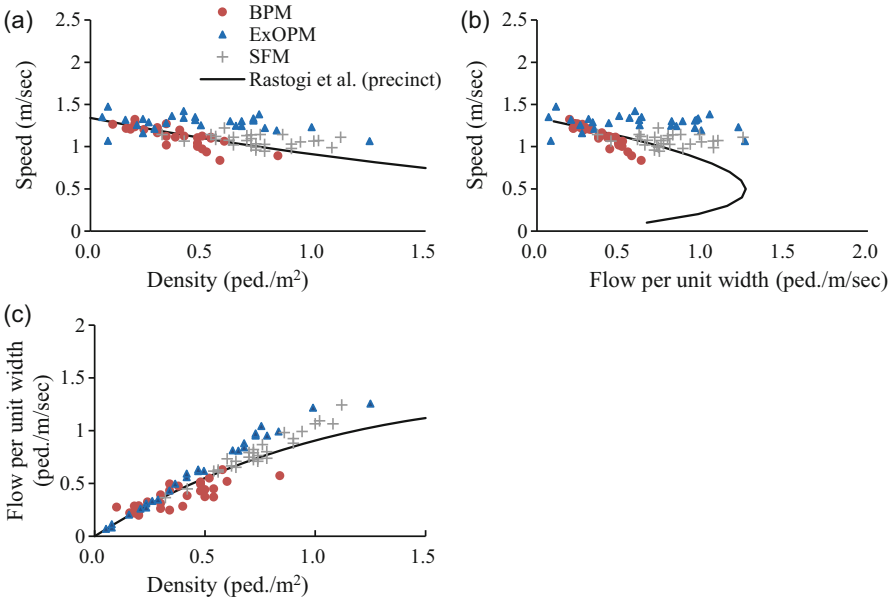

Fig. 9 Fundamental diagram of pedestrian traffic (**a**) Density - Speed, (**b**) Flow - Speed, (**c**) Density - Flow

Fig. 10 Computational time of each model

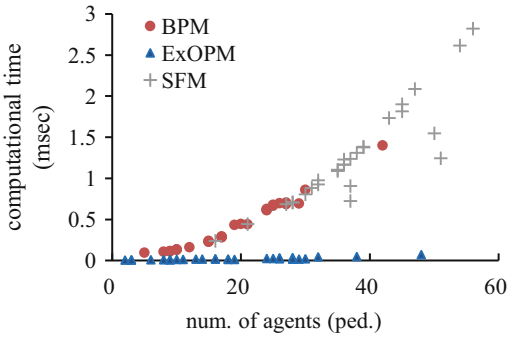

complexity is suppressed to $O(n)$. It is necessary to re-sort the list when overtaking occurs, but its frequency is sufficiently small compared to the number of agents. As a result, the ExOPM computation time is much less than that of 2D models.

4.2 Verification of Interaction Between Cars and Pedestrians

One of the impacts of pedestrians on car traffic is a drop in the volume of cars making left turns (note that cars are driven on the left side of roads in

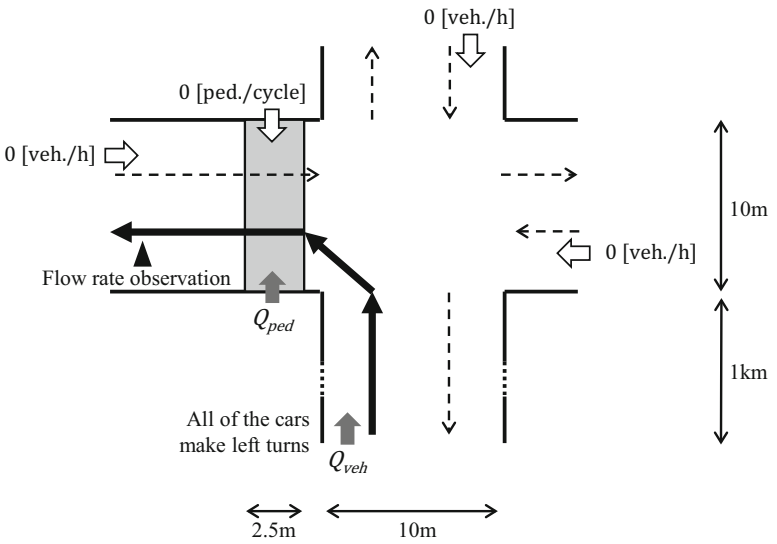

Fig. 11 Simulation environment for mixed traffic verification

Japan). To facilitate understanding, the authors created a four-way intersection where crosswalks were attached (as shown in Fig. 11). They then conducted 1-h simulations by varying the car traffic demand Q_{veh} = 50, 150, 300, and 500 veh./h and the pedestrian traffic demand Q_{ped} = 5, 20, 40, and 60 ped./cycle. Next, they counted the number of cars making left turn, and compared the simulated results with the empirical formula used in Japan. All of the cars were assigned to make left turns. The signals were set on a 120 s cycle that turned green for 60 s. The pedestrian signals were set to turn green for 50 s.

Figure 12 shows the relationship between the number of left-turn cars and the pedestrian traffic demand. When the car traffic demand was small, the simulated values were much lower than the empirical values since the traffic flow cannot reach the saturation flow rate, and all the cars have passed through the crossroad. In contrast, when the car traffic volume exceeded the saturation flow rate, it was confirmed that the simulated values were in near agreement with the empirical data.

5 Application to Real-World Problem

5.1 Simulation Target Problem

In Okayama City, which is the capital of Japan's Okayama Prefecture, many citizens have chosen private cars as their primary mode of transportation, which results in various traffic problems. Under these severe circumstances, there are two tram lines

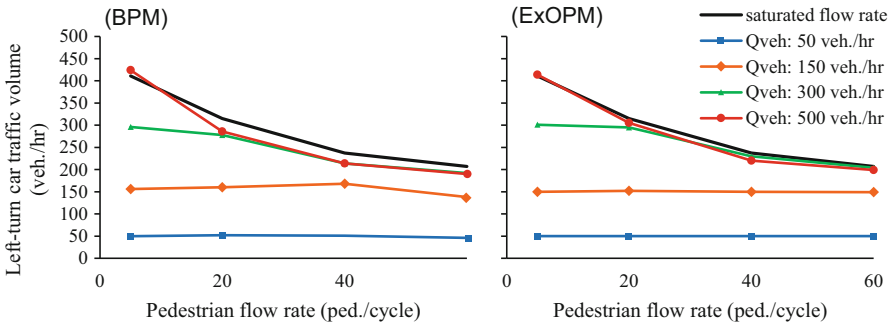

Fig. 12 Pedestrian flow and left-turn car traffic volume (left: BPM, right: ExOPM)

operating in the city. In December 2014, a large shopping center opened in the front of Okayama Station, which is located at the center of the city, and, as a result, the number of persons using Okayama Station increased significantly.

A plan to extend the tramway into the station square had been discussed in order to improve access and convenience of movement for rail users around the downtown areas. However, because the tramway crosses the large intersection in front of the rail station and since the duration of green light time for car traffic would be reduced by the project, there are concerns that the project would have a negative impact on car traffic flow. With this point in mind, the authors attempted to quantitatively assess the impact of the proposed extension by applying the mixed traffic simulation model described in Sect.3. The BPM was applied to express pedestrian movements in this simulation.

5.2 Data Preparation

The road network used in this research is shown in Fig. 13.[1] The node positions and connections were set by importing data from OpenStreetMap[2] and the precise lane configuration and signal control information were provided by the Okayama Prefectural Police.

The time period to be simulated was set as 13:00 to 14:00 on a holiday, which is one of the time periods with the highest traffic volumes. The traffic demands resulting from cars and pedestrians in this simulation area were generated from the link traffic volume observed by the prefectural police. The actual routes and timetables were provided to the bus and tram agents.

[1]The aerial photography and the road/tramway/railway center line map were created by editing Geospatial Information Authority of Japan (GSI) Maps (https://maps.gsi.go.jp/).

[2]https://www.openstreetmap.org.

Fig. 13 Target area (top: aerial photography, bottom-left: road/tramway/railway center line map, bottom-right: simulator screen)

5.3 Simulated Scenarios

In this case study, all drivers were assumed to select the route that provides them the shortest trip length and no driver was permitted to choose a detour route, even if traffic jams occurred due to the tramway extension. Although this condition imposes

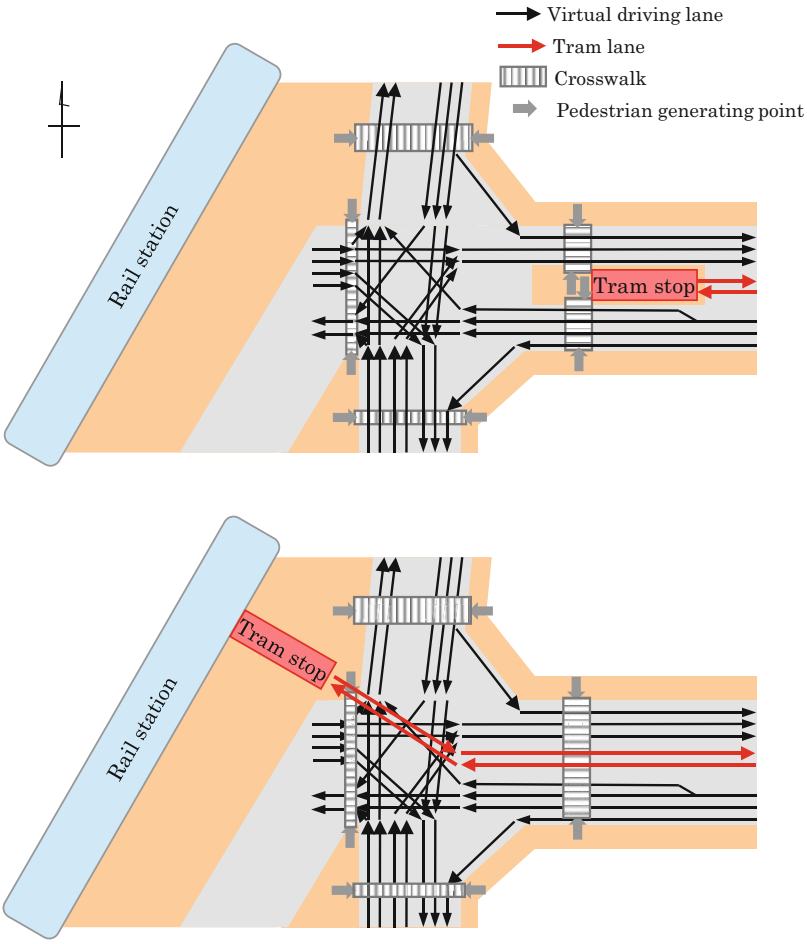

Fig. 14 Lane configuration at "Okayama-Ekimae Intersection" (intersection in front of Okayama Station) (top: without tramway extension, bottom: with tramway extension)

a severe and unrealistic assumption against the tramway extension plan, it was set in order to prevent an overly optimistic evaluation result.

The road environments around the intersection in front of Okayama Station, with and without the tramway extension, are shown in Fig. 14. The main difference is that the tram stop is relocated from the east side of the intersection to the station square. As a result, the signal aspect at the intersection needs to be changed, and it is also expected that the volume of pedestrians on the east-side crosswalk that are getting on and off of the tram will be reduced. In this research, simulations were conducted according to the four scenarios listed below. The distance from the intersection to the rearmost car agent, which is stopped by a red signal in each scenario, was evaluated as a performance index.

- Baseline scenario 1 (BASE-1):
  without tramway extension, without pedestrians
- Baseline scenario 2 (BASE-2):
  without tramway extension, with pedestrians (current status)
- Extension scenario 1 (EXT-32):
  with tramway extension (green light for tram: 32 s, 1 time per cycle), with pedestrians.
- Extension scenario 2 (EXT-64):
  with tramway extension (green light for tram: 32 s, 2 times per cycle), with pedestrians.

The signal cycle at the intersection is fixed at 150 s for all scenarios in order to maintain coordination with neighboring signals. The minimum time required for a tram to cross the intersection, based on its estimated performance, is 32 s. The specific signal control pattern is as shown in Table 1. The unit of each split is in seconds, "G", "WG", "Y", and "AR" refer to the duration of the green light for all traffic modes, the green light for pedestrians and bicycles, the yellow light, and all red (clearance time), respectively. In each split pattern, the black, blue, and red arrows indicate permitted car, pedestrian, and tram movements, respectively.

Table 1 Signal control pattern in each scenario

BASE-1&2	1ϕ G: 35(GW: 32) Y: 3	2ϕ G: 14 AR: 3	3ϕ G: 66(GW: 64) Y: 3	4ϕ G: 23 AR: 3	
	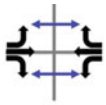	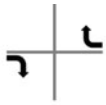	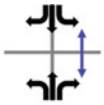		
EXT-32	1ϕ G: 25(GW: 21) Y: 3	2ϕ G:13 AR: 3	3ϕ G: 50(GW: 46) Y: 3	4ϕ G: 18 AR: 3	5ϕ G: 32(GW: 25)
	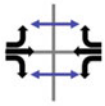		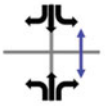	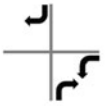	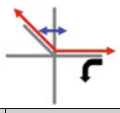
EXT-64	1ϕ G: 15(GW: 11) Y: 3	2ϕ G:9 AR: 3	3ϕ G: 32(GW: 25)	4ϕ G: 35(GW: 31) Y: 3	5ϕ G: 15 AR: 3	6ϕ G: 32(GW: 25)
	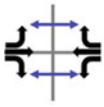	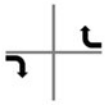	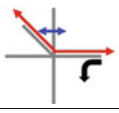		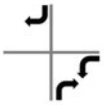	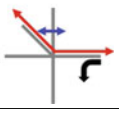

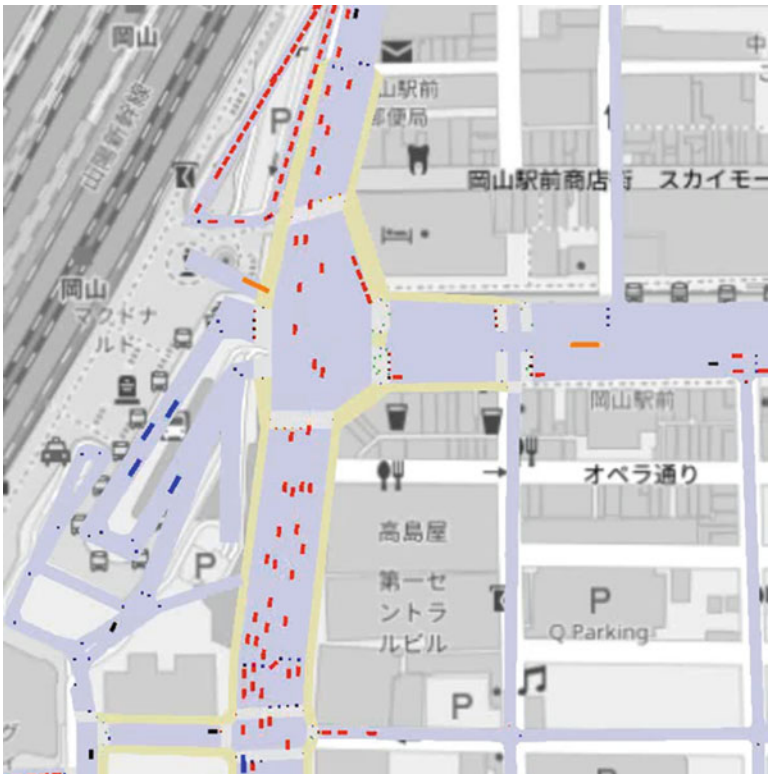

Fig. 15 Simulation screenshot showing the intersection in front of the station

5.4 Simulation Results

Figure 15 shows a simulation screenshot[3] around the intersection in front of the station for scenario EXT-32. The red, black, blue, and orange rectangles represent private cars, taxis, buses, and trams, respectively, while the green dots represent pedestrians. The small squares around intersections indicate traffic light colors or passage permissions.

As an example of the simulation results, Fig. 16 (left) shows a position comparison of the rearmost stopped car agent in the first lane (where cars are permitted to turn left or go straight) on the north-side road of the intersection in front of the station. The mean, minimum, and maximum values of the positions that were measured once per signal cycle are indicated in the figure. A comparison between BASE-1 and BASE-2 shows that the existence of pedestrians significantly affects congestion levels, thereby also implying that the influence of pedestrians must be

[3]The background image was imported from OpenStreetMap.

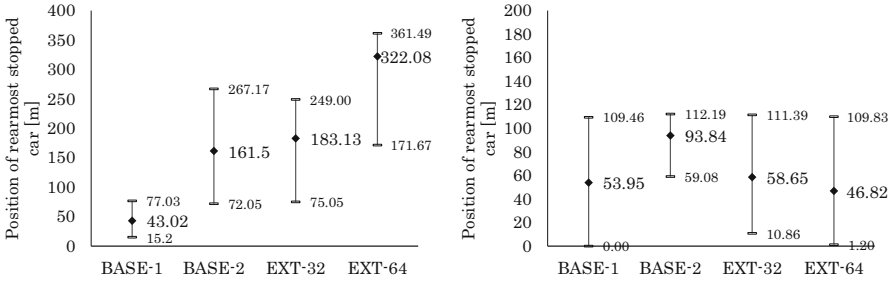

Fig. 16 Position of rearmost stopped car agent (left: in first lane of north-side road, right: in first lane of east-side road)

considered in those scenarios. On the other hand, in the comparison between BASE-2 and EXT-32, even though the average value is declining slightly, it can be seen that the change is sufficiently small compared with the daily fluctuation level. However, in EXT-64, it is understood that car traffic is significantly affected by the tramway extension since the traffic jam length is becoming much longer.

Similarly, Fig. 16 (right) shows the position of the rearmost stopped car agent in the first lane (where cars are permitted only to turn left) of the east-side road. In EXT-32 and EXT-64, the congestion length is seen to decrease compared with BASE-2, and the traffic flow is found to become moderately smooth due to the changes in the signal control patterns that accompanied the tramway extension.

6 Conclusion

In this chapter, the authors reported on the development of a simulation framework for mixed traffic that was achieved by newly implementing pedestrian and tram agents for an existing multi-agent-based car-traffic simulator. The results show that the presence of pedestrians is not negligible for the traffic policy assessment. It also indicates the importance of pedestrian modeling and pedestrian simulations. The layered road structures that the authors modified could be effectively reused in existing simulation models while maintaining their independence. This flexibility facilitates the easy implementation of new agents.

The proposed pedestrian models and interaction rules show good agreement with the observed empirical values, which implies that this multi-agent-based framework is usable as a platform for evaluating various emerging technologies and new algorithms related to mixed traffic. When assessing the impact of pedestrian crossing from the viewpoint of cars, the position of the pedestrian in the direction of crossing needs to be correctly reproduced. This is because it determines whether or not a car can pass through. Meanwhile, more detailed models that attempt to

reproduce the pedestrian position in the direction orthogonal to crossing may be too high specification for this purpose.

In this study, the authors simulated the tramway extension plan in front of Okayama Station using the proposed framework and quantitatively assessed its impact on road traffic. From the simulation results, it was confirmed that the assessment must consider the influence of pedestrians. Moreover, it was determined that there was hardly any negative influence on car traffic patterns at the intersection in front of the station in the case of EXT-32, in which the duration of the green light for the tram is 32 s $\times$ 1 time per cycle, and that the traffic situation on the east-side road of the intersection actually improved after the tramway extension because cars would be permitted to turn left during the same period the tram is crossing the intersection. It was also determined that there are no remarkable changes on the west- and south-side roads of the intersection in front of the station, or in any other subareas in the simulation locale.

Although the simulation results in this research were obtained from a limited number of scenarios, they showed that this kind of mixed traffic simulation of cars, pedestrians, and trams has the potential to provide objective data to stakeholders for use in discussions about transportation policies.

Acknowledgments This work was supported by the Japan Society for the Promotion of Science (JSPS) KAKENHI Grant Number 15H01785. The authors sincerely thank the Okayama Prefectural Police, the Nonprofit Organization "Kokyo-no-kotsu-RACDA," and the Okayama Electric Tramway Co., Ltd. for providing simulation data and helpful comments.

References

1. K. Abe, H. Fujii, S. Yoshimura, Inverse analysis of origin-destination matrix for microscopic traffic simulator. Comput. Model. Eng. Sci. **113**(1), 68–85 (2017)
2. G. Antonini, M. Bierlaire, M. Weber, Discrete choice models of pedestrian walking behavior. Transp. Res. Part B Method. **40**(8), 667–687 (2006). https://doi.org/10.1016/j.trb.2005.09.006
3. B. Anvari, W. Daamen, V.L. Knoop, S.P. Hoogendoorn, M.G.H. Bell, Shared space modeling based on social forces and distance potential field, in *Pedestrian and Evacuation Dynamics 2012* (Springer International Publishing, Cham, 2013), pp. 907–916
4. M. Asano, T. Iryo, M. Kuwahara, Microscopic pedestrian simulation model combined with a tactical model for route choice behaviour. Transp. Res. Part C Emerg. Technol. **18**(6), 842–855 (2010). https://doi.org/10.1016/j.trc.2010.01.005
5. M. Bando, K. Hasebe, A. Nakayama, A. Shibata, Y. Sugiyama, Structure stability of congestion in traffic dynamics. Jpn. J. Ind. Appl. Math. **11**(2), 203–223 (1994). https://doi.org/10.1007/bf03167222
6. J. Barceló (ed.), *Fundamentals of Traffic Simulation* (Springer, New York, 2010). https://doi.org/10.1007/978-1-4419-6142-6
7. C. Burstedde, K. Klauck, A. Schadschneider, J. Zittartz, Simulation of pedestrian dynamics using a two-dimensional cellular automaton. Physica A Stat. Mech. Appl. **295**(3–4), 507–525 (2001). https://doi.org/10.1016/s0378-4371(01)00141-8
8. R.E. Chandler, R. Herman, E.W. Montroll, Traffic dynamics: studies in car following. Oper. Res. **6**(2), 165–184 (1958). https://doi.org/10.1287/opre.6.2.165

9. D. Charypar, K.W. Axhausen, K. Nagel, Event-driven queue-based traffic flow microsimulation. Transp. Res. Rec. J. Transp. Res. Board **2003**(1), 35–40 (2007). https://doi.org/10.3141/2003-05
10. M. Chraibi, A. Seyfried, A. Schadschneider, Generalized centrifugal-force model for pedestrian dynamics. Phys. Rev. E **82**(4) (2010). https://doi.org/10.1103/physreve.82.046111
11. L. Crociani, G. Vizzari, An integrated model for the simulation of pedestrian crossings, in *11th International Conference on Cellular Automata for Research and Industry*. Lecture notes in computer science (Springer International Publishing, Cham, 2014), pp. 670–679
12. C. Dobler, G. Lämmel, Integration of a multi-modal simulation module into a framework for large-scale transport systems simulation, in *Pedestrian and Evacuation Dynamics 2012* (Springer International Publishing, Cham, 2013), pp. 739–754
13. M. Fukui, Y. Ishibashi, Traffic flow in 1d cellular automaton model including cars moving with high speed. J. Phys. Soc. Jpn. **65**(6), 1868–1870 (1996). https://doi.org/10.1143/jpsj.65.1868
14. H. Fujii, S. Yoshimura, Precise evaluation of vehicles emission in urban traffic using multi-agent-based traffic simulator mates. Comput. Model. Eng. Sci. **88**(1), 49–64 (2012)
15. H. Fujii, H. Uchida, S. Yoshimura, Agent-based simulation framework for mixed traffic of cars, pedestrians and trams. Transp. Res. Part C Emerg. Technol. **85**, 234–248 (2017). https://doi.org/10.1016/j.trc.2017.09.018
16. H. Ge, R. Cheng, Z. Li, Two velocity difference model for a car following theory. Physica A Stat. Mech. Appl. **387**(21), 5239–5245 (2008). https://doi.org/10.1016/j.physa.2008.02.081
17. P. Hart, N. Nilsson, B. Raphael, A formal basis for the heuristic determination of minimum cost paths. IEEE Trans. Syst. Sci. Cybern. **4**(2), 100–107 (1968). https://doi.org/10.1109/tssc.1968.300136
18. D. Helbing, P. Molnár, Social force model for pedestrian dynamics. Phys. Rev. E **51**(5), 4282–4286 (1995). https://doi.org/10.1103/physreve.51.4282
19. D. Helbing, B. Tilch, Generalized force model of traffic dynamics. Phys. Rev. E **58**(1), 133–138 (1998). https://doi.org/10.1103/physreve.58.133
20. L. Huang, S. Wong, M. Zhang, C.W. Shu, W.H. Lam, Revisiting Hughes' dynamic continuum model for pedestrian flow and the development of an efficient solution algorithm. Transp. Res. Part B Method. **43**(1), 127–141 (2009). https://doi.org/10.1016/j.trb.2008.06.003
21. W. Huang, M. Fellendorf, R. Schönauer, Social force based vehicle model for 2-dimensional spaces, in *91st Annual Meeting of the Transportation Research Board* (2012)
22. R.L. Hughes, A continuum theory for the flow of pedestrians. Transp. Res. Part B Method. **36**(6), 507–535 (2002). https://doi.org/10.1016/s0191-2615(01)00015-7
23. D.N. Huynh, M. Boltze, A.T. Vu, Modelling mixed traffic flow at signalized intersection using social force model. J. East. Asia Soc. Transp. Stud. **10**, 1734–1749 (2013). https://doi.org/10.11175/easts.10.1734
24. R. Jiang, Q. Wu, Z. Zhu, Full velocity difference model for a car-following theory. Phys. Rev. E **64**(1) (2001). https://doi.org/10.1103/physreve.64.017101
25. B.S. Kerner, S.L. Klenov, D.E. Wolf, Cellular automata approach to three-phase traffic theory. J. Phys. A Math. Gen. **35**(47), 9971–10013 (2002). https://doi.org/10.1088/0305-4470/35/47/303
26. R. Kitamura, M. Kuwahara (eds.), *Simulation Approaches in Transportation Analysis* (Springer, Berlin, 2005). https://doi.org/10.1007/b104513
27. D. Krajzewicz, G. Hertkorn, C. Feld, P. Wagner, SUMO (simulation of urban mobility); an open-source traffic simulation (2002), pp. 183–187
28. D. Krajzewicz, J. Erdmann, J. Härri, T. Spyropoulos, Including pedestrian and bicycle traffic into the traffic simulation SUMO, in *ITS 2014, 10th ITS European Congress* (2014)
29. N. Mita, H. Uchida, H. Fujii, S. Yoshimura, Speedup of dynamic route search for large-scale microscopic traffic simulation. J. Adv. Simul. Sci. Eng. **4**(1), 31–43 (2018). https://doi.org/10.15748/jasse.4.31
30. M. Muramatsu, T. Irie, T. Nagatani, Jamming transition in pedestrian counter flow. Physica A Stat. Mech. Appl. **267**(3–4), 487–498 (1999). https://doi.org/10.1016/s0378-4371(99)00018-7

31. K. Nagel, M. Schreckenberg, A cellular automaton model for freeway traffic. J. Phys. I **2**(12), 2221–2229 (1992). https://doi.org/10.1051/jp1:1992277
32. G. Peng, X. Cai, C. Liu, B. Cao, M. Tuo, Optimal velocity difference model for a car-following theory. Phys. Lett. A **375**(45), 3973–3977 (2011). https://doi.org/10.1016/j.physleta.2011.09.037
33. R. Rastogi, T. Ilango, S. Chandra, Pedestrian flow characteristics for different pedestrian facilities and situations. European Transport - Trasporti Europei (53) (2013). ISSN 1825-3997
34. J. Scheurer, S. Porta, Centrality and connectivity in public transport networks and their significance for transport sustainability in cities, in *World Planning Schools Congress, Global Planning Association Education Network* (2006)
35. S. Tahmasseby, N. van Oort, R. van Nes, The role of infrastructures on public transport service reliability, in *2008 First International Conference on Infrastructure Systems and Services: Building Networks for a Brighter Future (INFRA)* (2008), pp. 1–5. https://doi.org/10.1109/INFRA.2008.5439680
36. T. Tang, Y. Wang, X. Yang, Y. Wu, A new car-following model accounting for varying road condition. Nonlinear Dyn. **70**(2), 1397–1405 (2012). https://doi.org/10.1007/s11071-012-0542-8
37. O.K. Tonguz, W. Viriyasitavat, F. Bai, Modeling urban traffic: a cellular automata approach. IEEE Commun. Mag. **47**(5), 142–150 (2009). https://doi.org/10.1109/mcom.2009.4939290
38. M. Treiber, A. Hennecke, D. Helbing, Congested traffic states in empirical observations and microscopic simulations. Phys. Rev. E **62**(2), 1805–1824 (2000). https://doi.org/10.1103/physreve.62.1805
39. I. von Sivers, G. Köster, Dynamic stride length adaptation according to utility and personal space. Transp. Res. Part B Method. **74**, 104–117 (2015). https://doi.org/10.1016/j.trb.2015.01.009
40. Y. Xia, S.C. Wong, M. Zhang, C.W. Shu, W.H.K. Lam, An efficient discontinuous Galerkin method on triangular meshes for a pedestrian flow model. Int. J. Numer. Methods Eng. **76**(3), 337–350 (2008). https://doi.org/10.1002/nme.2329
41. Y. Xia, S.C. Wong, C.W. Shu, Dynamic continuum pedestrian flow model with memory effect. Phys. Rev. E **79**(6) (2009). https://doi.org/10.1103/physreve.79.066113
42. T. Yamashita, T. Okada, I. Noda, Implementation of simulation environment for exhaustive analysis of huge-scale pedestrian flow. SICE J. Control Meas. Syst. Integr. **6**(2), 137–146 (2013). https://doi.org/10.9746/jcmsi.6.137
43. J. Yang, W. Deng, J. Wang, Q. Li, Z. Wang, Modeling pedestrians' road crossing behavior in traffic system micro-simulation in China. Transp. Res. Part A Policy Pract. **40**(3), 280–290 (2006). https://doi.org/10.1016/j.tra.2005.08.001
44. S. Yoshimura, Mates: multi-agent based traffic and environment simulator - theory, implementation and practical application. Comput. Model. Eng. Sci. **11**, 17–25 (2006)
45. W.J. Yu, R. Chen, L.Y. Dong, S.Q. Dai, Centrifugal force model for pedestrian dynamics. Phys. Rev. E **72**(2) (2005). https://doi.org/10.1103/physreve.72.026112
46. W. Zeng, P. Chen, H. Nakamura, M. Iryo-Asano, Application of social force model to pedestrian behavior analysis at signalized crosswalk. Transp. Res. Part C Emerg. Technol. **40**, 143–159 (2014). https://doi.org/10.1016/j.trc.2014.01.007
47. L.J. Zheng, C. Tian, D.H. Sun, W.N. Liu, A new car-following model with consideration of anticipation driving behavior. Nonlinear Dyn. **70**(2), 1205–1211 (2012). https://doi.org/10.1007/s11071-012-0524-x